General Disclaimer

One or more of the Following Statements may affect this Document

- This document has been reproduced from the best copy furnished by the organizational source. It is being released in the interest of making available as much information as possible.

- This document may contain data, which exceeds the sheet parameters. It was furnished in this condition by the organizational source and is the best copy available.

- This document may contain tone-on-tone or color graphs, charts and/or pictures, which have been reproduced in black and white.

- This document is paginated as submitted by the original source.

- Portions of this document are not fully legible due to the historical nature of some of the material. However, it is the best reproduction available from the original submission.

JSC-11402

NASA TM X-58187
December 1976

NASA TECHNICAL MEMORANDUM

MIUS INTEGRATION AND SUBSYSTEMS TEST PROGRAM

hudmius

MODULAR INTEGRATED UTILITY SYSTEMS
improving community utility services by supplying electricity, heating, cooling, and water/ processing liquid and solid wastes/ conserving energy and natural resources/ minimizing environmental impact

NATIONAL AERONAUTICS AND SPACE ADMINISTRATION

LYNDON B. JOHNSON SPACE CENTER

HOUSTON, TEXAS 77058

1. Report No.	2. Government Accession No.	3. Recipient's Catalog No.
NASA TM X-58187		

4. Title and Subtitle	5. Report Date
MIUS INTEGRATION AND SUBSYSTEMS TEST PROGRAM	December 1976
	6. Performing Organization Code JSC-11402

7. Author(s)	8. Performing Organization Report No.
Willie S. Beckham, Jr., Gerald C. Shows, Tony E. Redding, Richard C. Wadle, Martin B. Keough, and Jerry C. Poradek	
9. Performing Organization Name and Address Lyndon B. Johnson Space Center Houston, Texas 77058	10. Work Unit No. 386-01-00-00-72
	11. Contract or Grant No.
12. Sponsoring Agency Name and Address National Aeronautics and Space Administration Washington, D.C. 20546	13. Type of Report and Period Covered Technical Memorandum
	14. Sponsoring Agency Code

15. Supplementary Notes

16. Abstract

The MIUS Integration and Subsystems Test (MIST) facility at the Lyndon B. Johnson Space Center was completed and ready in May 1974 for conducting specific tests in direct support of the Modular Integrated Utility System (MIUS) Program sponsored by the U.S. Department of Housing and Urban Development (HUD). A series of subsystems and integrated tests has been conducted since that time, culminating in a series of 24-hour dynamic tests to further demonstrate the capabilities of the MIUS Program concepts to meet typical utility load profiles for a residential area. This report presents results of the MIST Program, which achieved demonstrated plant thermal efficiencies ranging from 57 to 65 percent.

17. Key Words (Suggested by Author(s))	18. Distribution Statement
Energy conservation Thermal energy Utilities services	STAR Subject Category: 85 (Urban Technology and Transportation)

19. Security Classif. (of this report)	20. Security Classif. (of this page)	21. No. of Pages	22. Price*
Unclassified	Unclassified	152	$6.75

*For sale by the National Technical Information Service, Springfield, Virginia 22151

NASA TM X-58187

MIUS INTEGRATION AND SUBSYSTEMS TEST PROGRAM

Willie S. Beckham, Jr., Gerald C. Shows, Tony E. Redding, Richard C. Wadle,
Martin B. Keough, and Jerry C. Poradek
Lyndon B. Johnson Space Center
Houston, Texas 77058

PREFACE

The Department of Housing and Urban Development (HUD) is conducting the Modular Integrated Utility System (MIUS) Program devoted to development and demonstration of the technical, economic, and institutional advantages of integrating the systems for providing all or several of the utility services for a community. The utility services include electric power, heating and cooling, potable water, liquid-waste treatment, and solid-waste management. The objective of the MIUS concept is to provide the desired utility services consistent with reduced use of critical natural resources, protection of the environment, and minimized cost. The program goal is to foster, by effective development and demonstration, early implementation of the integrated utility system concept by the organization, private or public, selected by a given community to provide its utilities.

Under HUD direction, several agencies are participating in the HUD-MIUS Program, including the Energy Research and Development Administration, the Department of Health, Education, and Welfare, the Department of Defense, the Environmental Protection Agency, the National Aeronautics and Space Administration, and the National Bureau of Standards (NBS). The National Academy of Engineering is providing an independent assessment of the Program.

This publication is one of a series developed under the HUD-MIUS Program and is intended to further a particular aspect of the program goals.

COORDINATED TECHNICAL REVIEW

Drafts of technical documents are reviewed by the agencies participating in the HUD-MIUS Program. Comments are assembled by the NBS Team, HUD-MIUS Project, into a Coordinated Technical Review. The draft of this publication received such a review, and all comments were resolved.

CONTENTS

Section	Page
SUMMARY	1
INTRODUCTION	1
KEY MIUS DESIGN ISSUES	2
Thermal Integration Techniques	2
Mixed-Mode Air-Conditioning	2
Thermal Storage	2
Integration of Subsystems Control	2
Display Requirements	3
TEST PROGRAM	3
Phase II (Subsystems) Tests	3
Phase III (Integrated Systems) Tests	23
CONCLUDING REMARKS	30
APPENDIX—MIST FACILITY DESCRIPTION	127

TABLES

Table		Page
I	Engineering Data	31
II	Operational Data	31
III	Engine Heat Balance—Forced-Convection Mode	32
IV	Diesel Engine Noise Levels	32
V	JSC Environmental Health Services Analysis Report	33
VI	HACS Instrumentation List	34
VII	Power Ratio as a Function of Load, MIST Series II Test—Compression Chiller	36
VIII	Thermal Storage Summary Data, MIST Series IV Test—Thermal Storage Tests	
	(a) Cold thermal storage	37
	(b) Hot thermal storage	37
IX	Exchanger Thermal Effectiveness, Series V Test—Heat-Rejection/Heat-Transfer Network	
	(a) Oil aftercooler interchanger	38
	(b) Jacket-water interchanger	38
	(c) Excess-steam condenser	38
X	Exchanger Thermal Effectiveness, Series VI Test—Ancillary Exchangers	
	(a) Regenerative sewage heater	39
	(b) Sterilization regenerative heat exchanger	39
	(c) Facility heat exchanger	39
	(d) Auxiliary facility heat exchanger	39
	(e) WMS heater	40
	(f) Freshwater heater	40
	(g) Freshwater preheater	40
	(h) Water sterilization heat exchanger	40
XI	Water Management Subsystem Tests	40
XII	Physical-Chemical Test Results	41
XIII	Reverse-Osmosis Test Results	41
XIV	Biological-Physical-Chemical Test Results (Temperature Effects)	42
XV	Biological-Physical-Chemical-Overload Test Results	43

Table		Page
XVI	Engineering-Unit Conversion Table Based on Thermoelectric Curve	
	(a) Hot water (355.37 K (180° F)) (sensors T-45 and T-49)	44
	(b) Cold water (280.37 K (45° F)) (sensors T-48 and T-50)	44
XVII	Processed Data (Example)	45
XVIII	Specific Engine-Heat-Recovery Rates, Ebullient-Cooling Mode	46
XIX	Space-Heating Test Results	47
XX	Space-Cooling Test Results	50
XXI	Integrated Test Matrix	51
XXII	Series I Test Conditions	51
XXIII	Test IIA-1 Performance Summary	52
XXIV	Test IIA-2 Performance Summary	52
XXV	Test IIB-1 Performance Summary	53
XXVI	Test IIB-2 Performance Summary	53
XXVII	Test IIC-1 Performance Summary	54
A-I	Maximum Performance Parameters	130
A-II	Power Generation Subsystem Thermal Properties	130
A-III	Power Generation Subsystem Mechanical Properties	131
A-IV	Power Generation Subsystem Electrical Parameters	132
A-V	Heating, Ventilation, and Air-Conditioning Subsystem Thermal Parameters	132

FIGURES

Figure		Page
1	The MIST power generation subsystem	55
2	Power distribution simplified block diagram	56
3	Fuel consumption rate as a function of electrical load—forced-circulation-cooling mode (0.6 m^3/min (160 gal/min))	57
4	Steady-state steam rate (103 $\times 10^3$ pascals (15 psig)) as a function of electrical load—forced-circulation-cooling mode (0.6 m^3/min (160 gal/min))	58
5	Engine-exhaust heat recovery as a function of electrical load— forced-circulation-cooling mode	59
6	Fuel consumption rate as a function of electrical load—ebullient-cooling mode	60
7	Steady-state steam rate as a function of electrical load—ebullient-cooling mode	61
8	Combined engine-exhaust and jacket-water heat recovery as a function of electrical load—ebullient-cooling mode	62
9	Ebullient-cooling-mode input-output heat-flow rates	63
10	Engine heat rate as a function of electrical load	64
11	Diesel engine exhaust-gas temperatures before and after heat-recovery-unit cleaning operation (ebullient-cooling mode)	65
12	Transient response tests, MIST PGS II and III, June 12 to 14, 1974	66
13	MIST engine emissions as a function of electrical load—ebullient-cooling mode	67
14	Space-cooling-loop schematic	68
15	Cold thermal storage schematic	69
16	Space-heating-loop schematic	70
17	Cooling-water-loop schematic	71
18	Jacket-water-loop schematic	72
19	Oil-coolant-loop schematic	73
20	Steam-loop schematic	74

Figure		Page
21	MIST series I test—absorption chiller	
	(a) Steam rate as a function of unit capacity	75
	(b) Unit capacity as a function of chilled-water temperature	76
	(c) Subsystem power consumption as a function of load	77
	(d) Coefficient of performance as a function of load	78
22	MIST series II test—compression chiller	
	(a) Unit capacity as a function of chilled-water temperature, 284.26-K (52° F) sensor set point	79
	(b) Unit capacity as a function of chilled-water temperature, 285.93-K (55° F) sensor set point	80
	(c) Subsystem power consumption as a function of load	81
	(d) Coefficient of performance as a function of load	82
23	Typical recording-ammeter strip chart	83
24	MIST series III test—combined chillers	
	(a) Subsystem power consumption as a function of load	84
	(b) Coefficient of performance as a function of load	85
25	MIST series IV test—thermal storage tanks	
	(a) Cold thermal storage discharge/charge profiles	86
	(b) Hot thermal storage discharge/charge profiles	87
26	MIST series V test—heat-rejection/heat-transfer network	
	(a) Cooling-tower heat-rejection curve	88
	(b) Engine available recoverable heat as a function of output power (manufacturer's catalog data, ebullient-cooling mode)	89
	(c) Engine heat rejected to cooling loop (engine only; results based on exchanger performance)	90
	(d) MIST ambient conditions as a function of load	91
	(e) Cooling-tower makeup as a function of load	92
	(f) Heat rejection as a function of cooling-tower range	93
	(g) Condensate temperature as a function of engine load	94
27	Physical-chemical WMS	95
28	Reverse-osmosis WMS	96
29	Biological-tertiary WMS	97
30	Biological-oxygen-demand reduction	98
31	Ammonia reduction	99

Figure		Page
32	Solid-waste-management schematic	100
33	Heat-recovery unit	101
34	A DEXTIR real-time printout	102
35	MIST series I integrated tests	
	(a) Engine heat rejection/recovery as a function of engine load (time averaged)	103
	(b) Engine-oil-rejected heat as a function of engine load (time averaged)	104
	(c) Engine/incinerator-recovered high-grade heat as a function of engine load (time averaged; steam heat recovery at 103 kilopascals (15 psia))	105
	(d) Hot thermal storage charge/discharge temperature profile	106
	(e) Hot thermal storage charge/discharge rate as a function of steam-heat availability	107
	(f) Floating-split ratio as a function of steam-heat consumption	108
	(g) Domestic-hot-water preheating as a function of engine load	109
	(h) Domestic-hot-water-heating temperature as a function of time—low-grade heat and thermal storage used	110
36	MIUS power profile—less space cooling	111
37	MIUS space-heating-load profile	112
38	MIUS space-cooling-load profile	113
39	MIUS domestic-hot-water-flow profile	114
40	MIST power profile	115
41	MIST space-heating profile	
	(a) Design winter day	116
	(b) Average spring/fall day	117
42	MIST space-cooling profile	
	(a) Design summer day	118
	(b) Average spring/fall day	118
43	MIST domestic-hot-water-flow profile	119
44	Test IIA-1: summer design day with thermal storage	120
45	Test IIA-2: summer design day without thermal storage	121
46	Test IIB-1: winter design day with thermal storage	122
47	Test IIB-2: winter design day without thermal storage	123

Figure		Page
48	Test IIC-1: spring/fall average day	124
49	Domestic-hot-water-heating steam heat required as a function of flow rate	125
50	Domestic-hot-water-heating steam heat required as a function of engine load	126
A-1	Baseline MIST system	133
A-2	MIST system schematic	134
A-3	Thermal interface	135
A-4	Electrical block diagram	136
A-5	MIST heating and cooling subsystem	137
A-6	MIST wastewater management system	138
A-7	Solid-waste-interface schematic	139

ACRONYMS

BOD	biological oxygen demand
COD	chemical oxygen demand
COP	coefficient of performance
DEXTIR	trade name for data acquisition system
HACS	heating and cooling subsystem
HGF	heat-gain factor
HLF	heat-loss factor
HRU	heat-recovery unit
HSD	Hamilton-Standard Division
HUD	U.S. Department of Housing and Urban Development
HVAC	heating, ventilation, and air-conditioning
JSC	NASA Lyndon B. Johnson Space Center
LHV	lower heating value
MIST	MIUS integration and subsystems test
MIUS	modular integrated utility system
NASA	National Aeronautics and Space Administration
PC	performance coefficient
P-C	physical-chemical
PGS	power generation subsystem
RO	reverse osmosis
SFC	specific fuel consumption
SWMS	solid waste management subsystem
USPO	Urban Systems Project Office
WMS	wastewater management subsystem

MIUS INTEGRATION AND SUBSYSTEMS TEST PROGRAM

By Willie S. Beckham, Jr., Gerald C. Shows, Tony E. Redding, Richard C. Wadle, Martin B. Keough, and Jerry C. Poradek
Lyndon B. Johnson Space Center

SUMMARY

The Urban Systems Project Office at the Lyndon B. Johnson Space Center undertook the MIUS Integration and Subsystems Test (MIST) Program in support of the conceptual design work associated with the Modular Integrated Utility System (MIUS) Program sponsored by the U.S. Department of Housing and Urban Development. The MIUS Program was intended to develop and demonstrate the technical, economic, and institutional advantages of integrating the systems for providing all or several of the utility services for a community. The objective of the MIUS Program was provision of the desired services consistent with reduced use of natural resources, environmental protection, and minimized cost.

The MIST Program is the test verification of the MIUS design concepts. On a small scale, tests of full-size MIUS designs can be run to verify designs before full-scale deployment.

The test program herein described was a multiphase operation. Its initial thrust was to establish the performance characteristics of the elements that make up the facility and to compare these results to manufacturers' data. After the operational envelope was explored and understood, fully integrated tests were conducted, with the use of load profiles characteristic of different types of user facilities and weather conditions, in an attempt to demonstrate the capability of the subsystems to function in a long-term integrated fashion, to examine the overall energy balance and polluting byproducts produced, and to compare the test results with the conventional utility service experience.

Results of the integrated tests were highly encouraging. Total plant efficiencies ranged from 57 to 65 percent, an approximate doubling of the figures associated with conventional systems. Reduction of total input energy also results in fewer emissions.

INTRODUCTION

The objective of the MIUS Integration and Subsystems Test (MIST) Program was to verify in practice the conceptual design approach of integrating utility functions, with the goal of reducing energy consumption by increasing overall efficiency and reducing environmental problems associated with providing these services. This document contains the description, results, and conclusions associated with the tests.

The broad organization and objectives of the Modular Integrated Utility System (MIUS) Program are delineated in the Preface. A detailed description of the MIST facility and its operational characteristics are provided in the appendix.

The MIST facility was completed in April 1974 and was accepted by the National Aeronautics and Space Administration (NASA) in May 1974 from the prime contractor, Hamilton-Standard Division (HSD) of the United Technologies Corporation. The MIST is a laboratory test-bed for evaluation and verification of MIUS concepts and is composed of commercially available hardware, described herein. The acceptance tests served to demonstrate the MIST capability to meet the operational specifications of the contract. Details of the acceptance tests are contained in the document "MIST Acceptance Test Report," dated June 1974. Following completion of the acceptance tests, the subsystems tests and integrated-systems tests were performed.

The rationale used in developing the test program was a building block approach that began with vendor performance data on individual hardware elements and culminated in simulations of complete time cycle profiles representing a typical user facility configuration under actual environmental conditions. Design analysis for establishing the final MIST configuration was based on vendor-supplied operating data for the individual hardware components. The test profiles were constructed to

best investigate hardware components, as well as the key issues raised as a result of the analytical design studies conducted in the MIUS Program. The MIST Program was conducted in three phases, as follows.

Phase I — acceptance tests
Phase II — subsystems tests
Phase III — integrated-systems tests

The data derived from the phase II testing provided performance and calibration measurements for the individual subsystems. The data derived from the phase III testing provided performance and calibration measurements for the series I (static set points) and series II (dynamic 24-hour profile) integrated-systems tests.

As an aid to the reader, where necessary the original units of measure have been converted to the equivalent value in the Système International d'Unités (SI). The SI units are written first, and the original units are written parenthetically thereafter.

KEY MIUS DESIGN ISSUES

During early design work on the MIUS Program, several issues were raised that could not be resolved with confidence by analysis alone. The test investigation of these issues was, in fact, one of the reasons for building the MIST facility. Those issues into which insight was gained in the subsystems and integrated-systems tests are briefly described in the following subsections.

Thermal Integration Techniques

Thermal integration of MIST/MIUS subsystems requires that all thermal entities — the prime-mover/incinerator heat loop, the cooling loop, the heating loop, and the wastewater management subsystem (WMS) loop — be operated as an integrated utility system over a variety of cyclical load profiles and utilize effectively all recovered waste heat. Techniques for integrating the waste-heat recovery, transport, and utilization between subsystems were studied.

Mixed-Mode Air-Conditioning

Energy savings resulting from the use of absorption and compression chillers, with the absorption chiller carrying the baseload commensurate with the available high-grade waste heat from the prime mover and the incinerator and with the compression machine serving as the peaking chiller, were considered a potential improvement. Control of the two chillers to effectively reduce the energy used for space cooling was the key issue examined.

Thermal Storage

The efficient collection and storage of thermal energy in the MIUS at off-peak periods for utilization during peak periods as a supplementary energy source to optimize the energy savings is a prime issue. Multiple arrangements were made in the MIST to test the charging and discharging of thermal storage both upstream and downstream of the absorption and compression chillers. Generation of chilled water for storage during off-peak hours for utilization during the subsequent peak period was studied to determine electrical power "peak shaving" capability. Collection and storage of hot water for heating was accomplished in conjunction with peak electrical loading for use during periods of low electrical load and high heat demand. The incinerator was operated at full load to supplement additional high-grade-heat requirements. Charging rates and usage rates of the thermal energy tanks were determined.

Integration of Subsystems Control

A key issue in utility subsystems integration is the problem of controls integration. The MIUS will utilize waste products of one or more subsystems (water, heat, sludge for fuel, etc.) as a primary input for another subsystem, and this interdependency must be carefully controlled. The control of one subsystem process must be governed not only by the loads to be met by that process, but also by the functioning of the other processes that provide the energy input. If the product of a unit is required by

another subsystem, the unit may not automatically shut down when loads decrease below the amount required for maximum efficiency. This issue was addressed by experience gained in operating the MIST facility rather than by any specific test.

Display Requirements

The display of control and monitoring information for any one of such subsystems is quite conventional; however, because the parameters of one subsystem directly influence those of another subsystem in both the MIST and MIUS, the information must be easily related through the displays. Groupings of related parameters in various process loops were limited in the MIST; however, an MIUS installation would require either such an arrangement or monitoring displays that enable the operator to scan a given segment of the control panel to determine the status of related processes. This issue was addressed by operational experience in the same manner as controls integration.

TEST PROGRAM

The test program was conducted in three phases. The phase I tests were performed by the prime contractor as a demonstration of compliance with contract specifications, and results were reported in the MIST Facility Final Report.[1] Phase II of the test program pertained to individual subsystems tests, whereas phase III was a series of integrated tests.

Phase II (Subsystems) Tests

One objective of the phase II series of tests was to obtain performance data and operational characteristics of the individual MIST subsystems over their full range of operating capacity. These data will be used for correlation with and validation of vendor-supplied data for use in system performance computer mathematical models, and for subsystem evaluations made during the phase III integrated-systems testing. To the maximum extent practical, each subsystem was to be operated independently from the others to avoid confusion of performance data. The subsystem-level tests served to calibrate and validate the performance of the MIST electrical- and thermal-load simulators over their full operational range.

Additional objectives of the phase II tests were to obtain performance data and operational characteristics of the total MIST system and to demonstrate the capability of the system to meet a wide mix of imposed loads in an efficient manner

Power Generation Subsystem

The purpose of the power generation subsystem (PGS) test series was to determine engine fuel consumption, engine heat-production rates, and heat-recovery-unit (HRU) performance as functions of electrical load supplied by the generator. Tests were divided into three series, as follows:

Series I — forced-circulation jacket water, 355.37 K (180° F)

Series II — forced-circulation jacket water, 377.59 K (220° F)

Series III — ebullient cooling, 394.26-K (250° F) jacket water

Engine noise levels and engine exhaust emissions were also measured.

Subsystem description.—The MIST PGS generates, conditions, regulates, and controls electrical power for the other MIST subsystems and for the simulated external loads. The PGS consists of a diesel engine-generator set with heat-recovery units on the engine-exhaust stack, the engine lubrication oil/aftercooler, and the engine jacket-water coolant loops. The engine is a four-cycle, turbocharged, in-line, six-cylinder unit that operates at 1200 rpm and drives a 375-kilovolt-ampere 60-hertz, three-phase, brush-type generator. For testing purposes, the engine may be operated in either the ebullient or

[1] Lyndon B. Johnson Space Center; Hamilton-Standard Division of the United Technologies Corp., MIUS Integration and Subsystems Test, MIST Final Facility Report, 1974 (JSC internal document, restricted distribution).

the forced-circulation jacket-water cooling mode by piping-configuration changes. The electrical output ratings of the MIST diesel engine-generator are as follows.

1. Capacity — continuous rating
   a. High-temperature jacket water (377.59 to 394.26 K (220° to 250° F)) — 230 kilowatts
   b. Standard cooling (355.37 K (180° F)) — 300 kilowatts
2. Voltage — 480 volts alternating current, three-phase
3. Frequency — 60 hertz
4. Power factor — 0.8 minimum
5. Regulation
   a. Voltage — ±1 percent
   b. Frequency — ±0.05 percent.

Figure 1 is a schematic diagram of the diesel engine and its associated heat-recovery and cooling loops, showing the engine interfaces with the MIST. Also shown are the locations and designations of operational and engineering instrumentation used in the PGS testing. Figure 2 is a simplified schematic diagram of the MIST electrical system. More detailed descriptions of the MIST PGS are found in the MIST Test Requirements Document and the MIST Facility Final Report.[1]

Test description.—All three PGS test series were conducted in essentially the same manner; the only difference was that associated with the different cooling modes. The engine-generator was operated at steady-state electrical load conditions of 0 (net), 50, 100, 150, 200, and 230 kilowatts. The zero-load condition was defined as the minimum self-sustaining load; i.e., all the electrical power generated is used to drive engine auxiliary equipment. The engine-generator loading (above the zero point) was accomplished by using the electrical-load simulator. For each load test point, the engine-generator was operated at steady-state conditions, with waste-heat production and power generation, for a sufficient length of time (normally 0.5 hour) to obtain an accurate fuel consumption measurement. The fuel consumption was measured by means of the differential volume technique. The accuracy of the measurement was approximately $\pm 0.2 \times 10^{-3}$ cubic meter (±0.05 gallon). A summary of the test procedure used in each test series follows.

1. Establish/verify test configurations.
2. Start engine according to standard operating instructions and activate all ancillary equipment required for proper engine cooling.
3. Shut off supply valve to the fuel day tank and record fuel level in graduated sight glass on day tank.
4. Operate engine-generator at a steady-state zero net load to the electrical-load simulator for 30 minutes. Record data.
5. Increase electrical load on the engine-generator to 50 kilowatts, using the electrical simulator load bank. Operate for 30 minutes at constant load as observed on the engine-generator wattmeter. Record data, including fuel consumption.
6. Repeat operation of item 4 for electrical loads of 100, 150, 200, and 230 kilowatts.
7. Reduce simulated electrical load to zero.
8. Perform engine shutdown and auxiliary equipment shutdown according to standard operating instructions.

During initial PGS testing, several load-transient tests were performed to determine thermal stabilization periods between load changes. Tests were conducted for both ebullient and forced-circulation cooling. The procedures used in conducting the tests were generally as follows.

1. Load-increase transient
   a. Establish engine-generator operation at 100 kilowatts and continue operation for 1 hour or until all temperatures and flow rates have stabilized.
   b. Increase the engine load from 100 to 150 kilowatts.
   c. Simultaneously with step 1-b, begin recording system temperatures and flow rates at 15-second intervals, including measurement of steam-condensate return rate. Continue recording until condensate return rate has stabilized.

2. Load-decrease transient — Reverse the previous procedure, decreasing the load from 150 to 100 kilowatts.

[1] Lyndon B. Johnson Space Center; Hamilton-Standard Division of the United Technologies Corp., MIUS Integration and Subsystems Test, MIST Final Facility Report, 1974 (JSC internal document, restricted distribution).

Data recorded.—During each test series and for each load condition, the engineering and operational data listed in tables I and II were recorded continuously on a DEXTIR data acquisition system. The sensor numbers listed in tables I and II may be correlated with their location shown in figure 1.

The steam production rate was determined by collecting and weighing the quantity of condensate from the excess-steam condenser during a fixed-period test run. These data were recorded manually, as were the fuel consumption measurements. Key operational parameters such as jacket-water temperatures, exhaust-gas temperatures, and lubrication oil/aftercooler coolant temperature were monitored for stability during each steady-state run. These data were also manually recorded for checking against the data printouts.

Test results.—The MIST PGS test results consist primarily of diesel engine-generator thermal performance characteristics for the three PGS test series. Key parameters to be evaluated include engine fuel consumption under steady-state load conditions, engine-cooling and heat-recovery rates, and transient thermal response characteristics.

Series I and II — forced-circulation cooling: Figure 3 shows engine fuel consumption rates under a steady-state load condition for the forced-circulation jacket-cooling mode. Measurements are shown for both the 355.37 K (180° F) (series I) and 377.59 K (220° F) (series II) jacket-water inlet-temperature conditions. In both cases, the waterflow rate through the engine cylinder cooling jackets was 0.6 m^3/min (160 gal/min). Note, in figure 3, the negligible difference in fuel consumption with respect to the two different jacket-water operating temperatures. Note also the excellent agreement of the test data with fuel consumption data quoted by the engine manufacturer at 75, 150, and 225 kilowatts for the standard cooling mode (355.37 K (180° F) forced circulation).

Figure 4 shows the steam generation rate in the engine-exhaust heat-recovery unit as a function of engine load. As in the case of fuel consumption, very little difference in heat-recovery rates is observed between the 355.37 and 377.59 K (180° and 220° F) jacket-water-operating-temperature modes.

Figure 5 shows essentially the same data shown in figure 4 except that the steam production rate has been converted to a heat rate so that performance comparisons can be made with vendor data and with exhaust-gas sensible-heat transfer. The original vendor data indicated "recoverable" exhaust, based on a constant 422.04 K (300° F) final (T-5) gas temperature. Actually, the final temperature varies with engine load as would be expected, and the exit temperature was greater than 422.04 (300° F) at engine loads exceeding 80 kilowatts. Therefore, for comparison purposes, the vendor data have been corrected to the measured exit temperatures. However, this correction did not bring the vendor data in line with the measured heat recovery. This discrepancy appears to be a result of lower measured exhaust-gas flow rates and lower initial exhaust temperatures than those stated by the supplier.

The accurate determination of engine jacket-water and oil cooler/aftercooler heat-recovery rates was complicated by the relatively small inlet-to-outlet temperature difference of the cooling water in passing through the engine and heat exchanger. In general, at low engine loads, when generation rates are reduced, the error was greatest. Table III shows a heat balance for the engine operating at 150 kilowatts. Both 355.37 and 377.59 K (180° and 220° F) jacket-water-temperature cases are shown. The table shows the current trend: (1) that more heat is transferred to the jacket water at lower jacket-water temperature because of the larger gradient available and (2) that at the higher temperature, more heat is transferred to the oil cooler/aftercooler coolant loop. In both cases, approximately 75 percent of the input fuel energy (lower heating value (LHV) = 37 601.5 MJ/m^3 (135 000 Btu/gal)) was recovered. If the unrecovered exhaust heat is added to this quantity, approximately 90 percent of the total input energy is identified. The balance of the energy is attributed to radiation and convection losses from the engine and associated cooling equipment.

Series III — ebullient cooling: Figure 6 shows the engine fuel comsumption as a function of load for the ebullient-cooling mode. As in the case of forced-circulation cooling, the manufacturer's fuel consumption data agree with the measured values. Figure 7 shows the steady-state steam generation rate from engine-exhaust heat and jacket-water heat recovery as a function of engine-generator load. The equivalent heat recovery is shown in figure 8. Also shown (fig. 8) is the vendor's estimate of "recoverable" heat corrected to the measured exit temperature of the exhaust gases. As in the forced-circulation case, the measured values are lower than the corrected vendor values. A partial explanation

for this discrepancy is the lesser exhaust-gas heat recovery observed in the forced-circulation tests. Other possible reasons include lower gas-flow rates and inlet temperatures compared to the vendor data. A discussion of these parameters is provided in a subsequent section of this report.

Figure 9 shows the input heat rate and the distribution of electrical and thermal output heat rates as a function of engine load. Note that at full load (230 kilowatts), approximately 78.3 percent of the input fuel energy (LHV) is recovered in the form of electrical and thermal energy, or slightly more than in the forced-circulation-cooling-mode cases.

Figure 10 shows the heat rate or specific fuel consumption (SFC) of the engine-generator unit as a function of load. Data points shown for the two forced-circulation cases and the ebullient-cooling case indicate very little difference in SFC with respect to cooling mode except at low loads, at which the ebullient mode is slightly better. The heat rate is minimum and relatively flat with respect to load from approximately 150 kilowatts (65 percent) to full load (230 kilowatts). The full-load heat rate is 2.9 J_t/J_e (9750 Btu/kWh), which corresponds to a thermal-to-electrical conversion efficiency of 35 percent.

Engine exhaust-gas heat-recovery unit: Figure 11 shows exhaust-gas temperatures at the inlet and the exit of the heat-recovery unit as a function of engine load. Because performance of the heat-recovery unit was not in accordance with original predictions, the unit was cleaned. As indicated in the figure, the final (exit) exhaust temperature dropped approximately 55.56 K (100° F) because of the cleaning operation, a result indicating increased heat transfer from the gas to the water in the heat-recovery unit. The steam generation rate increased approximately 20 to 25 percent in the forced-convection-cooling mode. During testing, the exhaust gases were found to contain large quantities of unburned hydrocarbons, which would accumulate on the tube walls. One explanation for the carbon buildup is that the engine was operated at low loads for extended periods.

Noise data: Engine noise data were measured during the initial PGS testing with the engine set up for forced-circulation cooling. Measurements were made with a Bruel and Knaer sound-level meter, type 220S with octave band filter set. Table IV shows the sound levels in decibels at distances of 0.9, 7.0, and 15.2 meters (3, 23, and 50 feet) from the engine. Measurements were made at engine loads of 20, 50, 100, 150, 200, and 230 kilowatts. The data indicate that noise levels are almost invariant with load. The noise levels measured agree with available engine manufacturer's data (table IV).

Thermal transient tests: Figure 12 shows the steam-condensate return rate variation during the load transients. This parameter was the most responsive to load changes. From figure 12, it can be observed that the load-increase transient stabilizes within 1.5 minutes for the forced-circulation case (377.59 K (220° F) jacket water) and within 2.5 minutes for ebullient cooling. The load-reduction transient, which is shown for the ebullient-cooling mode only, stabilizes within 1.5 minutes.

Exhaust-gas analysis: An example of exhaust-gas-analysis test data is presented as table V. A summary graph of several parameters is included as figure 13. During the entire test period, stack-gas visible emission was sometimes observed to be less than 10 percent of capacity and did not exceed the permissible 20 percent of capacity at any time.

The maximum particulate emission occurred with the engine operating at 100-percent load and was calculated to 64 000 $\mu g/m^3$. On the basis of an average gas-flow rate of 17.0 m^3/min (600 ft^3/min), this particulate emission is equivalent to a pollutant mass rate of 0.07 kg/hr (0.15 lb/hr). The maximum allowable emission rate was calculated to be 1.1 kg/hr (2.5 lb/hr).

Conclusions and recommendations.— On the basis of the results of PGS testing to date, the following conclusions have been reached.

1. Engine fuel consumption data closely agree with manufacturer's data.
2. The electrical generation performance is acceptable and within specification requirements for the MIST facility.
3. The engine heat rate (fuel heat energy input per unit of electrical energy generated) was not affected by the engine operating temperature (cooling mode) within the accuracy of the measurement technique used.
4. Performance of the exhaust/jacket-water heat-recovery unit is substantially reduced by soot buildup on the inside surfaces of the boiler tubes. Reduced performance is indicated by increased final (exit) exhaust-gas temperatures and reduced steam generation under constant engine-load conditions.
5. Final exhaust-gas temperatures from the heat-recovery unit ranged from 44.44 K (80° F) to

approximately 100 K (180° F) higher than that implied by vendor data. This increase resulted in a reduction in heat recovery below the "recoverable" amounts advertised in supplier data.

6. The ebullient-cooling mode is preferable to the forced-circulation mode because (1) a jacket-water pump is not required (thus, parasitic loads are reduced), (2) the recovered jacket-water heat and exhaust heat are combined in a single, easily controllable low-pressure-steam system, and (3) slightly more energy is recoverable (78 percent compared to approximately 75 percent).

7. Engine noise data agree with supplier-furnished data.

8. The limited thermal transient testing conducted indicated that heat recovery (steam generation rate) responds quickly to engine-generator load demands. Stabilization periods are on the order of 1.5 to 2.5 minutes and should be compatible with most heat-using equipment.

9. The results obtained from exhaust-gas analysis indicated that the diesel engine was operating well within the applicable limits for particulate matter as defined by the Texas Air Control Board.

Recommendations are as follows.

1. A more detailed evaluation of the diesel engine and its exhaust silencer heat-recovery unit should be made to determine heat-recovery-performance degradation as a result of soot buildup (fouling).

2. Additional and improved instrumentation should be incorporated in the MIST PGS. Specifically, more thermocouples should be placed in the exhaust-gas duct and the steam-condensate system. Also, an improved (or more accurately calibrated) flowmeter should be placed in the exhaust-gas duct. An improved measurement technique is also needed to obtain steam flow-rate data.

Heating and Cooling Subsystem

The purpose of the heating and cooling subsystem (HACS) tests was to determine the performance characteristics and operational efficiencies of the equipment through individual equipment testing over a full range of load conditions. Performance information was collected and compared, if possible, with available manufacturer's data. Six major test series were associated with the HACS, as follows.

1. Series I — absorption chiller test. This test was conducted to study the performance of the absorption chiller during its operation within the MIST complex with an energy source generated by the heat rejected from the diesel engine exhaust and jacket water. The main purpose was to determine the chiller capacity as a function of steam rate and cooling-water temperature. Resulting data were used to determine the chiller coefficient of performance (COP), the overall energy consumption, and the subsystem efficiency.

2. Series II — compression chiller test. The scope of this test was an examination of the electrically driven compression chiller similar to that of the absorption chiller. Capacity as a function of condensing-water temperature and return-chilled-water temperature was examined; and, from the collected data, the COP, the total power used, and the subsystem efficiency were determined.

3. Series III — combined-chiller performance and control characteristics. The objectives of this test series were twofold. The foremost objective was to analyze the chillers operating together and determine their combined performance characteristics. Secondly, the test was designed to examine those techniques used to control the combined chilled-water temperature and determine what effect the location of the chilled-water temperature sensor would have on compression chiller operation and the resulting combined coefficient of performance.

4. Series IV — thermal storage tanks. The hot and cold thermal storage tanks were tested to evaluate their charging, discharging, and heat-storage characteristics for selected chilled-water flow rates. An additional effort was made to analyze temperature stratification within the tank and thus to determine whether significant thermal separation was maintained and what effect it may have had on thermal storage capacity.

5. Series V — heat rejection/heat transfer. Determination of the heat-rejection characteristics of the cooling tower while the PGS, the HACS, and the incinerator were operational was the goal of this test series. In addition, the heat-transfer characteristics of the oil aftercooler interchanger, the jacket-water interchanger, and the excess-steam condenser were to be determined, and their thermal effectiveness was to be assessed.

6. Series VI — ancillary heat exchangers. This test series enabled those heat exchangers not included in series V tests to be examined for thermal

effectiveness of heat transfer under varying load conditions. A list of that equipment follows.

Facility heat exchanger
Auxiliary facility heat exchanger
WMS heater
Freshwater preheater
Freshwater heater
Water sterilization heat exchanger
Regenerative sewage heater
Sterilization regenerative heat exchanger

Subsystem description.—The HACS provides space heating and cooling to the using facility. It has the capability to store and then utilize thermal energy recovered from the power generation subsystem and the incinerator. Cooling is provided by chilled water produced by an 87.9-kilowatt (25 ton) absorption unit using 103 × 10^3-pascal (15 psig) steam and by an 82.6-kilowatt (23.5 ton) electrically driven reciprocating compression unit. The baseline is satisfied by the absorption machine, and the peak demands are satisfied by the compression unit. Chilled water is delivered to the simulated cooling load at a temperature of 279.82 ± 1.11 K (44° ± 2° F). The cooling loop is equipped with a 9.8-cubic-meter (2600 gallon) cold-water storage tank capable of storing 297.8 megajoules (282 495 British thermal units). The total capacity of the system is dependent upon available waste-heat energy from the engine and the incinerator, but the cooling-load simulator is designed to impose loads of as much as 175.7 kilowatts (600 000 Btu/hr) on the system.

Steam and/or hot water recovered through the heat exchangers interfacing with the engine and the incinerator is used to satisfy a 146.4-kilowatt (500 000 Btu/hr) space-heating requirement at a temperature of 355.37 K (180° F), and to heat 0.01 m^3/min (2.77 gal/min) of domestic hot water from 283.15 to 344.26 K (50° to 160° F). In addition, thermal energy is used to enhance the operation of the wastewater treatment plant by increasing the temperature of the wastewater from 283.15 to 310.93 K (50° to 100° F) for process stabilization and to 373.15 K (212° F) for sterilization. The space-heating loop contains a hot-water thermal storage tank of 9.8-cubic-meter (2600 gallon) capacity, capable of storing 1378.1 megajoules (1 307 027 British thermal units) at 383.15 K (230° F).

A 615-kilowatt (175 ton) capacity wet-cooling tower is provided to reject all heat transferred into the cooling-water loop from the major equipment and heat exchangers. The blowdown water from the cooling tower can be processed in the wastewater management subsystem and returned as cooling-tower makeup water.

The HACS has a total of 11 heat exchangers. For operation of the jacket-water interchanger and the auxiliary facility heat exchanger, the engine must be configured in the forced-circulation mode. All other heat exchangers require that the engine cooling be in the ebullient mode.

Figures 14 to 20 are schematic representations of the HACS showing relative positions of the components and instrumentation.

Test description.—In general, the tests noted previously were performed by using the MIST standard operating procedures. Heating and cooling loads were controlled by maintaining a predetermined temperature difference between the inlet and outlet fluid at the HACS load simulators. With the exception of the thermal storage tests, all flow rates were set in accordance with the design requirements and were not varied during the tests. The temperature of the cooling-tower water was controlled in accordance with test requirements by manually adjusting the cooling-tower bypass valve to maintain the desired outlet temperature. Finally, each test sequence was run for a minimum of 30 minutes to ensure that a stable condition was obtained.

Figure 14 depicts the space-cooling loop, showing the absorption and compression chillers plus supporting components. In the series I tests, the diesel engine was configured in the ebullient mode and the electrical load was set at 180 kilowatts to ensure maintenance of 103 × 10^3-pascal (15 psig) steam pressure to the absorption chiller. The cooling load to the absorption machine was varied over a range from 35.2 to 87.9 kilowatts (120 000 Btu/hr (10 tons) to 300 000 Btu/hr (25 tons)), with incremental settings of 17.6 kilowatts (60 000 Btu/hr), for each of three cooling-tower water temperatures; namely, 299.82, 302.59, and 305.37 K (80°, 85°, and 90° F). On the assumption that the cooling-water temperature drops by 2.78 to 5.55 K (5° to 10° F) as the water goes through the cooling tower, these valves represent dry-bulb atmospheric temperature conditions of 302.59 to 305.37 K, 305.37 to 308.15 K, and 308.15 to 310.93 K (85° to 90° F, 90° to 95° F, and 95° to 100° F), respectively. The energy consumption (steam rate) of the chiller was determined through enthalpy differences of inlet steam

and outlet condensate. The condensate was manually weighed and its temperature recorded periodically throughout each test setup. The configuration did not include the cold thermal storage tank; therefore, the thermal control bypass valve, SV-804, was closed to the tank during the test. Finally, amperage measurements were made on all operational pumps and motors in conjunction with generator voltage and power factor recordings so that the power consumption and resulting efficiencies could be determined.

For the series II compression chiller tests, the engine remained in the ebullient mode, but the electrical power generated was the only energy input used. The engine load and resulting steam generation were minimized by setting the electrical-load simulator to 0 kilowatt. The operational set point[2] on the chiller was set at 285.93 K (55° F), and the cooling load was varied from 17.6 kilowatts (60 000 Btu/hr (5 tons)) to 87.9 kilowatts 300 000 Btu/hr (25 tons)) at 17.6-kilowatt (60 000 Btu/hr) increments. By loading the chiller in this manner, compressors (two cylinders each) could be cycled through their control steps of 40, 60, 80, and 100 percent of rated capacity. Each of these load conditions was repeated for cooling-tower-water temperatures of 299.82, 302.59, and 305.37 K (80°, 85°, and 90° F). Upon completion of this segment, the chiller set point was reset to 284.26 K (52° F) and the complete test was repeated. No thermal storage was attempted during this test. Instantaneous current readings were taken as in series I on all supporting equipment, and a continuous amperage record was made of the compression chiller motors, together with the generator voltage and power factor, so that total energy consumption and subsystem efficiency could be calculated.

To accomplish the objectives of the series III combined-chiller tests, the engine was configured in the ebullient mode with a 180-kilowatt load imposed to ensure adequate energy to drive the absorption chiller. The cooling load was varied from 70.3 to 175.8 kilowatts (240 000 Btu/hr (20 tons) to 600 000 Btu/hr (50 tons)) at 17.6-kilowatt (60 000 Btu/hr) increments. This procedure was followed to determine the capability of the compression chiller to operate in conjunction with the absorption chiller and satisfy all loads in excess of 87.9 kilowatts (25 tons). As in series II tests, loads were established so that the chiller compressors were cycled at 40, 60, 80, and 100 percent of their rated capacity. Similarly, as in series I and II tests, the temperature of the cooling-tower water to the chiller was controlled at 299.82, 302.59, and 305.37 K (80°, 85°, and 90° F) for each load setting, and thermal storage was not included.

Series III tests also included measuring the effect on power consumption of the compression chiller operational sensor location. The sensor was first placed upstream of the chiller inlet to sense return-chilled-water temperature; then it was moved downstream of both chillers to sense combined chilled-water output temperature. No change was made to the absorption chiller controls. Power measurements identical to those described previously were made during this sequence of tests.

Figures 15 and 16 are schematic representations of the thermal storage components within the respective cooling and heating loops. During series IV tests, the flow rates through the tanks were varied in an attempt to judge the relative effect on charge/discharge rates and on thermal mixing of the water in the tank with the inlet water. The engine was configured in the ebullient mode and set to generate 150 kilowatts of power. The heating and cooling loads were set at "zero" during the charge sequence and at "maximum" during discharges. The absorption chiller was operational during the cold thermal storage tests, and the facility heat exchanger was on-line during the hot thermal storage tests.

The flow rate to the cold thermal storage tank was electronically controlled through control valve SV-804 for full, three-fourths, and one-half flow. During cold-storage charge operations, the inlet, outlet, and tank temperatures were monitored every 15 minutes. When the chiller outlet and tank temperatures (TP-31 and TP-33) became equal and the tank registered a temperature of 280.37 K (45° F) or lower, the tank was considered charged and the test was terminated. For the discharge run, the chilled-water return and tank temperatures (TP-36 and TP-33) were monitored for similarity; and when the tank temperature reached 285.93 K (55° F), the test was ended.

[2]The operational set point on the chiller represents the lowest temperature of return chilled water at which the chiller will operate. The sensor will automatically signal chiller shutdown when this temperature is reached.

The hot thermal storage test was run using essentially the same techniques as noted previously. However, the flow was controlled manually by setting diverter valve SV-801 at positions of full, three-fourths, and one-half flow. The inlet, outlet, and tank temperatures were monitored as before, so that when the tank and the facility heat exchanger outlet temperatures (TP-28 and TP-30) became equal and the tank temperature reached 383.15 K (230° F) or higher, the charging was considered complete. During discharge, steam valve SO-56 to the facility heat exchanger was closed, and the thermal charge satisfied the heating load until the internal temperature registered full discharge at 349.82 K (170° F). As a final test sequence, both the hot and cold tanks were charged and allowed to stand for 24 hours. Internal tank temperatures were taken periodically to establish heat leak or heat gain relative to the atmosphere.

In the heat-rejection/heat-transfer series V tests, the waste heat recovered from the engine, the chillers, and the incinerator was transferred into the cooling-water loop and rejected through the wet-cooling tower. This configuration is shown in figure 17. During "engine only" testing, the cooling loop was configured so that only one cooling-water pump was operating to supply 0.9 m^3/min (225 gal/min). With the inclusion of the chillers and the incinerator, the cooling loop was reconfigured to bring two pumps on-line (items 510A and 510B) to supply 1.7 m^3/min (450 gal/min). The engine was configured in the ebullient-cooling mode.

Loads were imposed on the cooling tower over the full range of MIST heat-rejection capabilities by using the prime mover, the air-conditioning chillers, and the incinerator in various load combinations. The first segment of the test was performed with only the diesel engine operating through a range of 25 to 225 kilowatts at 25-kilowatt increments. The second sequence of loads was satisfied by using the engine and the chillers in combination to obtain 150 kilowatts and 105.5 kilowatts (30 tons), 175 kilowatts and 105.5 kilowatts (30 tons), 200 kilowatts and 140.7 kilowatts (40 tons), and, lastly, 225 kilowatts and 175.8 kilowatts (50 tons). Finally, to obtain the maximum heat-rejection load on the tower, the incinerator was operated — with oil used as fuel (waste incineration not operational) — in conjunction with the engine at 225 kilowatts and the chiller providing 175.8 kilowatts (50 tons) of air-conditioning. With only the engine operating, all the steam generated was condensed in the excess-steam condenser. With the addition of the air-conditioning load, part of this steam was used to drive the absorption chiller and the remainder was condensed. With the inclusion of the incinerator, all additional steam generated was condensed and the heat of condensation transferred to the cooling-water loop. Heat-transfer data were collected on the oil aftercooler interchanger and the excess-steam condenser during operation in the ebullient-cooling mode. For convenience, the jacket-water interchanger was tested during the series VI forced-circulation-cooling configuration.

The test was run over several days under varying ambient conditions, and no attempt was made to control the cooling-water temperature. The cooling-tower blowdown was accomplished as required during the interim between set points, but no attempt was made to process the blowdown water by using the facilities of the water management subsystem. This test series did not include the measurement of noise emitted from the tower or the determination of its drift characteristics.

The ancillary exchanger tests in the series VI category were run in two phases because of the necessity of placing the engine in both the forced-circulation and ebullient-cooling modes. In the forced-circulation mode, the rejected jacket-water heat was measured first through the auxiliary facility heat exchanger and then through the jacket-water interchanger. All other ancillary exchangers of series VI tests were checked during the phase II ebullient cooling. Figures 18, 19, and 20 are schematic representations of the jacket-water loop, the oil coolant loop, and the steam loop, respectively, showing the location of those exchangers included in this series.

The auxiliary facility heat exchanger and the jacket-water interchanger were tested separately when the engine was cooled in the forced-circulation mode. First, the engine jacket-water-temperature controller, SV-827, was set at a temperature of 377.59 K (220° F) to ensure a complete bypass of the jacket-water interchanger; thus, the auxiliary facility heat exchanger was left free for independent testing. The heating-load simulator was set at maximum load, and the facility heat exchanger was taken out of the space-heating loop by closing steam valve SO-56. When the jacket-water interchanger was tested, SV-827 was set to a temperature of 355.37 K (180° F) to ensure that all heat

transfer and control was performed by this exchanger. The auxiliary facility heat exchanger was taken out of the engine-cooling loop by stopping flow in the space-heating loop. Cooling-water flow through the jacket-water interchanger was maintained at 0.9 m^3/min (225 gal/min), and engine loads were varied from 25 to 225 kilowatts for both exchanger tests (fig. 18).

The engine cooling was then placed in the ebullient mode, and the cooling tower was operated at 1.7 m^3/min (450 gal/min), as depicted in figure 19. The WMS heat-transfer loop was configured to bypass the biological-disk unit, the Met-Pro unit,[3] and the reverse-osmosis (RO) unit and thereby isolate the WMS heater and supporting WMS exchangers for testing. The WMS flow was set at the upper limit (approximately 0.15×10^{-3} m^3/min (4 gal/min)), temperature controller was set at 377.59 K (220° F), and the electrical loads were varied from 50 to 225 kilowatts.

During the second sequence, in which the freshwater preheater was tested, the WMS flow was stopped, the freshwater preheater bypass valve SO-35 was closed, and the position of valve SO-809 was adjusted to ensure full flow through the preheater. Measurements of heat transfer were made at engine load settings from 50 to 225 kilowatts, with a nominal freshwater flow of 0.01 m^3/min (2.77 gal/min).

For the third segment of the test, temperature controller valves SV-809 and SV-810 were set at 327.59 K (130° F) so as to bypass the preheater. At the same time, the heating-load simulator was brought on-line, the hot thermal storage tank was placed in the bypass mode, and valve SO-35 was opened. The engine load and freshwater flow were stabilized at 175 kilowatts and 0.01 m^3/min (2.77 gal/min), respectively. In this configuration, the facility heat exchanger was tested through a range of 29.3 to 146.4 kilowatts (100 000 to 500 000 Btu/hr), at 29.3-kilowatt (100 000 Btu/hr) increments, and the heat-transfer characteristics of the freshwater heater were examined (figs. 19 and 29).

Lastly, the water sterilization heat exchanger was tested by reducing the inlet steam pressure from 103×10^3 pascals (15 psig) to 48×10^3 pascal (7 psig) at 14×10^3-pascal (2 psig) increments, to determine the effect on the sterilization capability.

Data recorded.—The continuous acquisition and recording of test data was accomplished primarily by using the DEXTIR data system. The instrumentation considered mandatory for HACS series testing is listed in table VI. This list includes both operational and engineering instruments and is categorized by type and equipment association. In some instances, the same instrument reading was used for an outlet point on one component and an inlet point for another. When instrumentation was not adequate or available, manual measurements were made (e.g., steam condensate, weight and temperature, atmospheric wet- and dry-bulb temperature, cooling-tower makeup, etc.). For measurements that were critical to the control of the test, data were manually recorded from the visual display control panel and used as the prime data source during the test. These data included such items as the load simulator temperature differences; the engine power load, voltage, and power factor; the chiller inlet and outlet chilled-water temperatures; the cooling-tower outlet temperatures; the thermal storage tank inlet, outlet, and internal temperatures; etc.

Test results.—The results of the six major test series associated with the HACS are presented in the following subsections.

Series I — absorption chiller: Figure 21(a) depicts the amount of steam consumed by the absorption chiller for three different condenser water temperature settings (cooling-tower temperature) over a full range of load conditions. An analysis of the resulting test data indicates that chiller performance was less efficient than catalog data predicated. At low loads (below 35.2 kilowatts (10 tons)), the chiller operation was erratic and became unstable below 42×10^3 pascal (6 psig) inlet steam pressure. Complete shutdown of the equipment occurred at 21×10^3 pascals (3 psig).

The steam usage rate for the rated conditions as determined from test data is higher than that from the manufacturer's data. Some difference can be expected because steam usage was measured during system operation and was based on manual measurements of chiller condensate weight and temperature that were generated during the test.

Outlet chilled-water temperature as a function of unit capacity is shown in figure 21(b). The manufacturer's rating point at 280.37 K (45° F) chilled water and 302.59 K (85° F) condensing water is 92.1 kilowatts (314 400 Btu/hr (26.2 tons)). The test capacity for the same set of conditions

[3]A physical-chemical wastewater treatment unit manufactured by the Met-Pro Company.

equals 79.1 kilowatts (270 000 Btu/hr (22.5 tons)) or is lower by 14 percent.

The power consumption of the absorption chiller was considered minimal. The catalog data indicate that approximately 0.25 kilowatt is used for control and solenoid operation; thus, no attempt was made to measure this value. The supporting power requirements are plotted in figure 21 (c). The power for item 510A represents the energy required to pump 0.9 m^3/min (225 gal/min) of cooling water through the HACS. A second pump (item 510B) supplied 0.9 m^3/min (225 gal/min) of cooling water to the engine-cooling loop and therefore is not represented. The cooling-tower fan was operated continuously, but only one-half of the power consumed was considered to be for HACS heat rejection. The sum total resulted in 20 kilowatts being required to run the subsystem for absorption chiller testing. Therefore, the average subsystem coefficient of performance — considering the total energy used for an 87.9-kilowatt (25 ton) output and each of the condenser water settings — is equal to 0.55.

The coefficient of performance for the absorption chiller (fig. 21(d)) reached a maximum of 0.65 at a rated capacity of 92.1 kilowatts (314 400 Btu/hr (26.2 tons)). However, for maximum loading conditions obtained during the test of 98.1 kilowatts (27.9 tons), with the use of 299.82-K (80° F) condensing water, the COP of the chiller reached 0.69.

Series II — compression chiller: Figures 22(a) and 22(b) present the average chilled-water temperature resulting from each loading condition for the 284.26 K (52° F) and 285.93 K (55° F) return-chilled-water sensor setting, respectively. When the chilled-water sensor was set at 284.26 K (52° F), the chiller produced chilled water at a temperature of approximately 280.37 K (45° F) when operating at its rated load of 82.6 kilowatts (282 000 Btu/hr (23.5 tons)). The results were the same for each condenser water setting; i.e., 299.82, 302.59, and 305.37 K (80°, 85°, and 90° F). At other loads, the operation remained relatively stable but the chiller produced chilled water at temperatures within a range of 279.26 to 282.04 K (43° to 48° F). Some erratic behavior was noted during the 305.37-K (90° F) condensor water setting at low loads. When the sensor was reset at 285.93 K (55° F), the chiller produced chilled water having a much wider range of temperatures and functioned less predictably. The coldest water was produced within the 52.8- to 70.3-kilowatt (15 to 20 ton) range, and the chiller became more stable operationally after the load exceeded 70.3 kilowatts (20 tons). The lowest temperature reached was 282.59 K (49° F) (with 302.59 K (85° F) cooling water used), and the highest was 285.37 K (54° F) (with 305.37 K (90° F) cooling water used).

The total subsystem power consumption for varying loads is shown in figure 22 (c). The total auxiliary power measured during the test was constant throughout the test at 21.44 kilowatts when the 284.26-K (52° F) sensor setting was used and was 20.86 kilowatts for the 285.93-K (55° F) setting. The curves include usage of both auxiliary and chiller power and represent the operational trends of the compression chiller within the HACS. It can be seen that a definite increase in power is required to meet cooling loads at a return-chilled-water-sensor setting of 285.93 K (55° F), compared with a setting of 284.26 K (52° F). Results showing the electrical power used per unit of refrigeration power for each cooling load setting are contained in table VII. Here again, an increase in the quantity of electrical power per unit of refrigeration power is required to drive the chiller when the 285.93-K (55°F) sensor setting is used instead of the 284.26-K (52°F) setting. A typical trace of chiller amperage taken from a continuous-recording ammeter is depicted in figure 23. The cycling shown is characteristic of chiller operation when the load is set at a point at which the compressor cylinders are operating intermittently. At the higher loads, for which all cylinders are functioning, the trace becomes a continuous straight line. This result explains the more stable operation noted previously at a load of approximately 70.3 kilowatts (20 tons).

The maximum coefficient of performance of the chiller was reached during use of the 284.26-K (52° F) set point, with 299.82-K (80° F) condensing water used at an 87.9-kilowatt (25 ton) load. The COP at this point was 4.28. The erratic behavior of the chiller at the 285.93-K (55° F) set point resulted in high COP values at low loads. The more stable data taken at high loads resulted in a COP of 3.80, with 299.82-K (80° F) condensing water used at 87.9 kilowatts (25 tons). The average subsystem COP — with consideration given to the auxiliary power and the compression chiller power required to meet an 87.9-kilowatt (25 ton) cooling load — is 2.00. The COP's for all conditions are shown in figure 22(d).

Series III — combined chillers: The power consumption for the combined operation of the absorp-

tion and compression chillers is shown in figure 24 (a). The results indicate that there is a definite power advantage in setting the compression chiller operational sensor downstream of the chilled-water outlets to sense combined chilled-water supply instead of sensing return-chilled water from the cooling load. The auxiliary power for pumps and motors during subsystem operation was measured at 38 kilowatts. All power used in excess of this value was required to operate the compression chiller. During maximum loading on the cooling system (i.e., 175.8 kilowatts (50 tons)), the power requirements for the compression chiller exceeded 22 kilowatts. Operational trends of the compression chiller are indicated by the change in slope of the curves and the abrupt changes in power required. The smoothest operation was noted during the 299.82-K (80° F) condenser water setting. The greatest savings in power were experienced when the cooling load exceeded 123.1 kilowatts (35 tons). Cycling of the compression chiller was not as frequent as that noted during the series II test. The compressors operated in a more continuous mode when the sensor was placed downstream of the combined chilled-water outlets. The frequency of in-rush cycling current was reduced, and a more constant engine load was the result.

The coefficient of performance for combined operation is depicted in figure 24(b). An interesting point to be made here is that the COP is lower when the combined chilled-water supply is sensed even though there is a reduction in power consumed. This reduction in power results in an increase in steam energy required by the absorption chiller. Therefore, the increased use of the absorption chiller having a much lower COP results in an overall decrease in the combined COP. The maximum COP for the return-chilled-water setting was 1.06 with 299.82-K (80° F) condenser water used. The maximum COP for the combined-chilled-water-supply setting was 1.02.

The average subsystem COP for combined-chiller operation — considering all energy used to meet the maximum load of 175.8 kilowatts (50 tons) — was 0.81 when the return-chilled-water sensor was used and was 0.83 when the sensor was moved downstream.

Series IV — thermal storage tests: Significant differences in charge and discharge rates as a function of fluid flow were noted during the running of the cold thermal storage test. The configuration and instrumentation locations are shown in figure 15. The actual test data taken during the full-flow (0.2 m^3/min (60 gal/min)) discharge/charge test are plotted in figure 25(a). These plots typify the trends obtained for the other flow rates — three-fourth and one-half flow (not shown). It can be seen that definite thermal stratification[4] was maintained within the cold-storage tank during the discharge cycle. The trace of thermal sensor TP-33 shows an upsurge in temperature between 9 and 10 p.m. Approximately 2 hours later, sensor TP-15 indicated that the stratification layer had reached the bottom of the tank. At this flow rate, to discharge the tank from 279.82 to 285.93 K (44° to 55° F) required approximately 4 hours. When the flow rate was reduced to 0.17 m^3/min (45 gal/min, almost 7 hours were required for discharge; when it was set at 0.11 m^3/min (30 gal/min); discharge was complete after 10 hours. The plots of the thermal charge cycles did not reveal similar surges of temperature that would indicate thermal layering. Test data did show that 2, 4, and 5 hours were required to charge the tank from 285.93 K (55° F) to 279.82 K (44° F) for full, three-fourths, and one-half flow, respectively. Table VIII is a tabulation of the discharge and charge rates based on these data.

The heat gained during the 24-hour soak test resulted in elevation of the tank temperature from 278.98 to 280.37 K (42.5° to 45° F). The storage capacity of the cold-storage tank was reduced by 57.4 megajoules (54 459 British thermal units). The heat-gain factor (HGF) is defined as the rate at which thermal energy is gained into the tank per unit temperature difference between the storage medium and the average ambient air. Using 280.37 K (45° F) as the average charge temperature and 302.59-K (85° F) ambient air, the HGF equals 29.9 W/K (56.7 Btu/(hr · ° F)).

The maximum ideal storage capacity of the 9.8-cubic-meter (2600 gallon) cold thermal tank is 293.8 megajoules (282 495 British thermal units). This capacity exists when the tank is considered charged at 278.71 K (42° F) and discharged at 285.93 K (55° F). The specific capacity then becomes 30.3 MJ/m^3 (108.7 Btu/gal) or 0.030 MJ/kg (13.026 Btu/lb) of fluid. The effective storage capacity, on the basis of actual test data from all three flow rates and in con-

[4]Thermal stratification is a demarcation or separation layer between a higher temperature fluid and a colder fluid.

sideration of the heat gained during a 24-hour period has an average value of 191.6 megajoules (181 749 British thermal units).

The performance coefficient (PC) for thermal storage is the ratio of the performance of a thermal energy storage system to the theoretical performance of an ideal water tank containing a specific mass of water and having perfect stratification and zero heat loss or heat gain. The average value of the PC for this test was 0.88.

The space-heating loop shown in figure 16 contains the hot thermal storage tank and the instrumentation used in this test. The hot thermal storage test results for full flow are presented in figure 25 (b). The profiles are indicative of the results obtained for the three-fourths and one-half flow rates. No differences were noted in charge or discharge rates as the setting of control valve SV-801 was manually adjusted from full flow through half flow. There was no indication of a thermal layer within the tank during any of the flow rates tested. At the end of the test series, an additional temperature probe (TP-44) was added to the outlet of the tank. During a short rerun, it was found that the TP-28 tank and TP-44 temperatures matched closely and showed no indication of thermal stratification. The significant break in plots TP-27, TP-18/34, and TP-30 at approximately 6:30 p.m. resulted when the thermal storage tank could no longer maintain the 355.37-K (180° F) supply and the system temperature thus began to drop. Normally, when the TP-28 temperature reached 349.82 K (170° F), the tank no longer be used and would be considered discharged.

During the 24-hour soak test for the hot tank, the temperature was reduced from 384.82 K (233° F) to 381.87 K (227.7° F) because of heat loss. The storage capacity was reduced by 122.6 megajoules (116 296 British thermal units). The heat-loss factor (HLF) is defined similarly to the heat-gain factor in its relation to the ambient air and the resulting rate of heat loss. Using an average charge temperature of 383.15 K (230° F) and 302.59-K (85° F) ambient air, the HLF equals 17.6 W/K (33.4 Btu/(hr • ° F)).

The maximum ideal storage capacity of the 9.8-cubic-meter (2600 gallon) hot thermal storage tank is 1378.1 megajoules (1 307 027 British thermal units). Ideal conditions exist when the maximum charge temperature of 383.15 K (230° F) is reached and a minimum discharge temperature of 349.82 K (170° F) is not exceeded. The effective storage capacity, in consideration of the heat-loss factor, had an average value of 1398.8 megajoules (1 326 699 British thermal units). This value is slightly higher than the ideal capacity because the actual charge temperature reached 388.71 K (240° F). The average performance coefficient for hot thermal storage equaled 0.92.

Series V — heat rejection/heat transfer: The data obtained during this test indicates that the amount of heat rejected by the cooling tower during specific loading conditions was less than anticipated. Figure 26(a) is a plot of cooling-tower heat rejection as a function of the load on the engine, the air-conditioning chillers, and the incinerator. The values are calculated on the basis of the cooling-water flow rate and the tower inlet- and outlet-temperature differences recorded during the test. Figure 26(b) shows the engine manufacturer's catalog data for available recoverable heat during operation in the ebullient-cooling mode. From a comparison of the two curves, it can be seen that a marked difference exists between the test results and the manufacturer's data. An examination of engine stack-gas temperatures indicated that the diesel exhaust temperature was running excessively high. In turn, the outlet from the heat-recovery unit was exceeding the design conditon of 422.04 K (300° F) (approximately 533.15 to 588.71 K (500° to 600° F)). This situation resulted in reduced steam production and explains the reduced heat transfer into the cooling-tower loop.

Figure 26(c) shows the actual quantity of heat transferred from the engine to the cooling loop through the oil aftercooler interchanger and the excess-steam condenser. The total quantity of heat rejected is the sum of the heat quantities rejected by both exchangers. The "engine only" curve in figure 26(a) and the total-heat-rejection curve in figure 26(c) followed the same trend very closely until the engine load reached 180 kilowatts. The test run on the exchangers indicates that the heat quantity transferred dropped off sharply after this load was reached. Following completion of this test, the engine was overhauled and the engine heat-recovery unit was cleaned to improve its heat-transfer capabilities. The cooling-tower test and the exchanger tests were not rerun, but the engine tests were; and reference data can be obtained from the section entitled "Power Generation Subsystem" for comparative analysis. The maintenance and rework of the engine and the recovery unit did improve the quantity of heat generated and recovered.

Figures 26(d) and 26(e) represent the ambient

conditions and the cooling-tower makeup experienced during the test. No measurement was made of the windspeed during the test, but the location of the tower would tend to minimize drift. Figure 26(f) is presented to show the calculated values of cooling-tower "range," expressed in units of temperature. The range is a measure of the heat-rejection rate compared to the water circulation rate. For this particular cooling tower operating under the MIST conditions, the calculated range values agree well with catalog data.

The analysis of heat transferred through the oil aftercooler interchanger indicates a considerable difference between actual operating characteristics and those outlined in the procurement specifications. The oil-aftercooler-interchanger specification requires 0.3 m^3/min (80 gal/min) of fluid flow on the shell side, but test data failed to show a measurable flow rate. Upon checking the design specification, it was learned that this exchanger was selected for a fail-safe condition to protect the engine from damage. It is only under a failure condition that the full flow rate would be experienced. To determine the effectiveness of this exchanger, therefore, it was necessary to calculate the flow through the shell side on the basis of the measured heat transfer on the tube side. Table IX (a) is a tabulation of the thermal effectiveness.

A similar condition exists for the jacket-water interchanger. Whereas the performance specification indicates a jacket-water flow of 0.6 m^3/min (160 gal/min) through the shell side, the actual operating flow was so low that the flowmeter could not register a value. Here again, the specification relates to a fail-safe design condition rather than to operational parameters. The jacket-water interchanger was designed to accept full flow only if a system failure occurred. Table IX (b) is a tabulation of the results — calculated by using the heat-transfer data taken on the tube side — obtained when the engine was run in the forced-circulation mode during series VI testing.

It can be shown that the excess-steam condenser actually extracts more than the latent heat of vaporization from the steam. Figure 26(g) is a plot of condensate temperature as a function of engine load. Temperatures as low as 308.15 K (95° F) occurred during low engine load; the maximum temperature was 333.15 K (140° F). Review of the excess steam-condenser specification shows the tube-side flow rate to be 454×10^{-3} m^3/min (225 gal/min). By operating with the latter flow rate, the exchanger is essentially oversized and would extract the additional heat noted. The main disadvantage to this situation is that this energy must be replaced in the saturated liquid returning to the engine before steam can be produced. Table IX (c) represents data for the thermal effectiveness of this exchanger. Specification data necessary for an effectiveness comparison were not available. The exchanger was designed to transfer 351 kilowatts (1 200 000 Btu/hr).

Series VI — ancillary heat exchangers: The calculated results from the series VI tests are presented in table X(a) to X(h). The heat-transfer characteristics and the thermal effectiveness of the auxiliary facility heat exchanger, the facility heat exchanger, the WMS heater, and the regenerative sewage heater are considered acceptable. The data from the freshwater preheater, the freshwater heater, the sterilization regenerative heat exchanger, and the water sterilization heat exchanger indicate that neither the quantity of heat transferred nor the thermal effectiveness reached expectations and thus are subject to further study. In the freshwater heater test, the facility heat exchanger was operational and supplied heat to both the space-heating load and the freshwater heater. The flow through the latter was dependent upon that modulated flow rate to the facility heat exchanger to satisfy the space-heating load. In addition, the steam pressure was 62×10^3 pascals (9 psig) instead of the 103×10^3 pascals (15 psig) normally supplied. As a result of these deviations from the design conditions, the quantity of heat transferred was considerably less than anticipated. Although results from the freshwater preheater indicated reduced heat transfer and thermal effectiveness, the temperature of the outlet freshwater was between 325.93 and 327.04 K (127° and 129° F) and is considered adequate to meet preheat requirements. The slight reduction in freshwater flow rate enabled the temperature to approach the specification. Failure to record the steam condensate during the water sterilization heat exchanger test prohibited the calculation of its thermal effectiveness. The heat-transfer rate, however, exceeded that required by design specifications; therefore, its effectiveness should be acceptable. The temperature of the sewage water reached 389.26 K (241° F) when steam at a pressure of 103×10^3 pascals (15 psig) was available and 374.82 K (215° F) when 48×10^3-pascal (7 psig) steam was used. It is obvious that a temperature adequate to sterilize the process fluid

was reached. The flow rate on both the tube and shell sides of the sterilization regenerative heat exchanger was below design specification; therefore, the expected amount of heat transfer was not reached. Temperatures of outlet fluids were adequate, however, to sustain the sterilization.

Conclusions and recommendations.—On the basis of the results presented in the preceding section, the following conclusions from the HACS tests have been reached.

1. Although performance of the absorption and compression chillers does not coincide with the manufacturer's predictions, it is adequate to meet design requirements for cooling loads under separate or combined operation.
2. Some reduction in power requirements can be realized by adjusting and properly locating the operational sensor on the compression chiller during joint chiller operation.
3. Further study is required to determine the full scope of thermal stratification within the thermal storage tanks. It is recommended that a thermocouple tree be developed and used within the tanks to gather data for a three-dimensional analysis of the fluid during operation.
4. The quantity of heat transferred from the heat-recovery unit into the cooling loop is dependent upon the maintenance of the HRV. Tubes should be cleaned periodically to remove hydrocarbon buildup.
5. The excess-steam condenser is operating as an oversized exchanger because of excessive cooling-water flow. It is recommended that a bypass arrangement be installed to reduce flow to its design requirements.
6. The exchangers associated with the WMS should be reevaluated with the design flow rates. Some reduction in heat transfer was noted, but an increase could be achieved by testing at design conditions.
7. The cooling-tower heat rejection was adequate to handle the maximum load placed on it. Its operational parameters were well within manufacturer specifications.

Wastewater Management Subsystem

All treatment processes, from primary settling to complete tertiary treatment, have problems associated with them. In addition, small treatment systems are always costly when compared to large, regional systems. The performance of MIUS-type systems, therefore, was to be evaluated with specific knowledge gained about operational characteristics, problems, and costs.

The integrated-systems concept also means interdependence of operational labor within the system. Manpower required to operate the wastewater system in an integrated utility complex, therefore, is less than that required by the same-size individually operated plant. Specific knowledge of operational and maintenance manpower requirements is required for effective MIUS evaluation.

Integration of closely coupled utility functions creates problems that are not encountered by individual utility functions. Failures of equipment in one utility more seriously affect or obstruct operation in a different utility function within the MIUS concept when compared to conventional, separate systems. The type, the magnitude, and the frequency of failures and their interutility effects must be investigated to evaluate the MIUS concept.

In summation, the purpose of this initial test program was as follows.

1. To identify process treatment effectiveness.
2. To obtain specific information on manpower requirements for process operation in a manpower-sharing integrated utility.
3. To identify the type, the magnitude, and the frequency of problems related to closely coupled utility systems.

Specific test objectives.—A large number of possible treatment processes were considered for testing. Some processes were combined into the two basic test series discussed in this report; namely, independent physical-chemical treatment and biological-physical-chemical treatment.

The objective of the tests was to identify the basic process advantages and disadvantages and thereby to define the best potential treatment processes that could be integrated into a wastewater treatment system. After this objective was accomplished, by using the purposes outlined in the previous section as the evaluation criteria, a further detailed test program could be defined.

Subsystem description.—The initial MIST wastewater treatment system (figs. 27 to 29) consisted of an inclined-screen-separator primary stage, a temperature-controlling heat exchanger, a four-stage rotating-disk aerobic biological contact

unit with clarifier, a submerged four-stage rotating-disk anaerobic denitrifying unit, an alum-coagulant upflow chemical clarifier, an expanded-bed upflow granular-carbon contact column, a chlorine contact basin, and a multimedia filter.

Because of problems in obtaining raw wastewater of domestic quality at the NASA Lyndon B. Johnson Space Center (JSC), a day tank of approximately 26.5 cubic meters (7000 gallons) capacity was filled during the early afternoon hours, when the sewage was strongest. The day tank was aerated to prevent the sewage from becoming septic. Flow through the system was constant, and the overall wastewater subsystem simulated a potential MIUS system with an aerated flow equalization basin. Flow splitting and level controllers were used to adjust the hydraulic capacity of subsequent treatment processes. The associated plumbing was designed to accommodate the adjustment in the flow schemes to bypass specific components within the overall system to achieve the level of treatment desired in each particular test.

Process operation.—The various elements of the WMS and the method of matching the different flow rates and flow paths are described.

Day tank: Sewage to be treated was pumped from a 7.9-meter (26 foot) deep manhole on the JSC main sewer line to a 26.5-cubic-meter (7000 gallon) covered day tank that was fitted with aerative piping and aerated with a minimum of 10 to 15 milligrams of oxygen per liter of air per hour from facility air lines. The raw sewage was screened to remove solids with a diameter larger than 1.3 centimeters (0.5 inch) by a coarse screen that was periodically backflushed to the sewer. The tank was filled at a rate of approximately 1.1 m^3/min (300 gal/min). At times, the tank was filled twice a day; but, in general, once a day was required. The filling process took place between 12:30 p.m. and 3 p.m. to obtain the strongest possible sewage.

Inclined-screen separator: Water was pumped, as required, at approximately 0.03 m^3/min (8 gal/min) from the day tank over the 22.9-centimeter (9 inch) wide inclined screen with a 0.040 screen size. Sludge from the screen was conveyed to the combined sludge tank, and the screened wastewater entered a level-controlled holding tank.

Holding-tank distribution: Wastewater from the holding tank could be directed to flow through or bypass the heat exchanger to either the rotating-disk processes or directly to the chemical clarifier.

Heat exchanger: The heat exchanger, a tube-in-tube unit, was designed to achieve a maximum temperature rise of 22.22 K (40° F) in incoming sewage at a temperature of 288.71 K (60° F) with a flow of 0.02 m^3/min (5 gal/min).

Rotating-biological-disk process: The rotating-disk process is a type of secondary wastewater treatment process and consists of four groups of large-diameter plastic disks mounted on a horizontal shaft. The contoured-bottom tank is partitioned into four stages, each with its own disk group. The disks are rotated slowly, with approximately 40 percent submerged in the wastewater. The biomass on the disks is very filamentous and provides a large active-biological-surface area, larger than the surface area of the disks. The biomass achieves a buildup of approximately 0.318 centimeter (0.125 inch) and is maintained at that level by the shearing forces created when the rotating disk passes through the mixed liquor. The rotation also creates a mixing action that keeps the solids in suspension as they pass through the various stages. This unit operates with separate, nearly homogeneous cultures on each disk; i.e., nitrifiers on one disk and carbonaceous bacteria operating on a different disk. Other biological systems provide only a heterogeneous environment. The initial stages, which receive the highest organic loading, develop cultures of filamentous and nonfilamentous bacteria and fungi for organic decomposition. As the concentration of organic water decreases, nitrifying bacteria appear, together with higher concentrations of rotifers, protozoans, and other predators. Because the biomass is continuously being sloughed and replaced by new growth, sludge recycling is unnecessary; hence, the system is simplified and operator attendance is reduced to a minimum.

Denitrifying process: In this test program, a rotating-disk system similar to the one just described was used for dentrification. The system is modified so that the entire disk assembly is submerged in the wastewater and thus an anaerobic condition is created. The dentrification step in this system had to be preceded by biological-oxygen-demand (BOD) removal and nitrification in the rotating-disk process previously described. A carbon source — in this case, methanol — was added to the influent flow of the denitrifier. This food source is required for development of the denitrifying bacteria on the media. To achieve a high level of nitrogen removal, a high degree of ammonia conversion to nitrate in the aerobic disk system is re-

quired, as well as the nitrate conversion to nitrogen gas.

Physical-chemical treatment system.—In addition to the screening and biological processes described, a packaged physical-chemical (P-C) system was installed in the overall system. The unit was used both as an independent P-C system without the use of the biological processes and as a tertiary system for polishing the effluent from the biological processes. The P-C process steps are as follows.

1. The untreated wastewater is pumped from the holding tank or the denitrifier, as applicable, to the flash-mix tank by a constant-rate influent pump. Coagulant chemical is added to the incoming wastewater in the flash-mix tank by a manually variable positive-displacement feed pump.

2. A motor-driven mixer mounted on the flash-mix tank provides agitation to fully contact the chemical and wastewater streams. Both the coagulant feed pump and the mixer are turned off and on with the input pump.

3. From the flash-mix tank, the chemically treated wastewater flows by gravity to the downcomer section of the clarifier. Here, the chemically treated wastewater is agitated gently by a series of flat circular disks that give the stream a downward rotation motion. The rotating stream is directed against a series of baffles located at the bottom of the downcomer that stop the rotation of the water and redirect it into an upward, linear path. The flat disks are driven by an electric motor through a variable-speed drive and a gear reducer that are mounted on top of the clarifier.

4. Sludge is withdrawn from the bottom of the clarifier by means of a positive-displacement pump. This pump is controlled by a photoelectric instrument mounted above the clarifier water surface. This instrument detects the level of sludge in the clarifier and starts and stops the sludge pump accordingly. The withdrawn sludge is pumped to the drain. From the clarifier, the water passes upward through a carbon column to which a continuous supply of air is added by a small compressor.

5. From the carbon column, the water then flows by gravity to a surge tank that acts as a holding reservoir for the pressure filter. Level-control probes in this tank operate the filter-feed/backwash pump. Disinfectant chemical, when applicable, is added to this tank by a manually variable positive-displacement feed pump. The disinfectant-chemical pump is turned off and on with the filter-feed/backwash pump. The latter pump normally drives the water through the pressure filter, which removes any residual solids from the waste stream left after the preceding treatment steps. This pump, in conjunction with proper valving, also serves to backflush the accumulated solids from the filter bed during the backwashing operation.

6. After passage through the pressure filter, the water moves through a flow control valve to drain as final effluent or to the RO unit if applicable.

Test description.—Six different test series were to be investigated in this phase of the MIST Program; however, because of certain limitations, modifications and deletions had to be made (table XI).

Independent physical-chemical testing: A schematic of the P-C system used is shown in figure 27. In the following description of flow through the system, the numbers in parentheses represent components designated in figure 27.

1. Raw wastewater is drawn into an aerated tank (1). Because of the dilute characteristics of the JSC wastewater, the water was selected during a limited time period, between 12:30 and 4:30 p.m. each day. The characteristics of the raw wastewater are shown in columns 2 and 3 of table XII.

2. Wastewater is screened through a Bauer hydrosieve for primary solids separation (2).

3. Primary treated water is delayed in a stirred holding tank.

4. Wastewater is taken from the holding tank to the P-C plant coagulant flash mixer, through two heat exchangers that control inlet temperature to ± 0.56 K ($\pm 1.0°$ F) from ambient to 302.59 and 310.93 K (85° and 100° F) (5 and 6).

5. Wastewater is delayed approximately 2 hours in an upflow flocculator clarifier; here, a heavy sludge blanket of aluminum hydroxide is produced (8).

6. Clarified effluent is passed through an aerated upflow carbon column (9).

7. Water is delayed in a chlorine contact basin for 15 minutes (10).

8. The final treatment step of the process is filtration through a multimedia filter (11).

9. Water is then sent back through the regenerative heat exchanger to reduce the temperature for discharge (5).

10. Water is sent to the surge tank and then discharged (12).

Reverse-osmosis testing: Figure 28 is a schematic diagram of the RO test setup. In the RO test series, the P-C system was used first to pretest the wastewater. The P-C outlet water then was processed in the RO unit as follows. (Numbers in parentheses represent components designated in fig. 28.)

1. Refiltered through the RO sand filter (16)
2. Acidified to proper hydrogen-ion concentration (pH) to protect the RO membrane (15)
3. Forced through the RO separation module (14)
4. Dispensed
   a. Purified component: sampled and sent to drain
   b. RO underflow component: returned to holding tank (4)

Biological-tertiary testing: Figure 29 shows the entire WMS flow schematic. The flow pattern for the biological-tertiary test series is as follows. (Parenthetic numbers represent components designated in fig. 29.)

1. Water is treated as in the P-C system, through the temperature-conditioning stage; flow rate 0.019 m^3/min (5 gal/min).
2. Wastewater is contacted in four stages by the rotating biological disks (18).
3. Wastewater is settled for 2 hours (19).
4. Flow from the settler is split, with 0.0019 to 0.0057 m^3/min (0.5 to 1.5 gal/min) flow through the denitrifier (20).
5. Flow is combined at the P-C system rapid-mix unit and proceeds through the P-C unit as previously described.

Biological overloading: The biological overload test setup was identical to that for the biological-tertiary tests. Sludge was added to the wastewater supply tank to increase BOD, chemical oxygen demand (COD), and suspended solids to approximately two and three times the normal concentration.

Biological-system poisoning: Again, the test setup for biological-system poisoning was the same as the biological-tertiary pattern. Alum was added in increasing amounts until the biomass was no longer viable enough to properly process the incoming wastewater.

Data recorded.—Water samples were taken at numerous points in the system as required for the different test series. These locations are indicated in figure 29. The points investigated and the analysis performed can be readily identified on each data sheet. Temperatures and flows were routinely recorded.

Test results.—The MIST WMS test results include graphs of several critical parameters showing daily variations in input and output and tables summarizing the overall results of the analyses performed on each test series. Several visual observations are also included.

Independent physical-chemical testing: Table XII shows the averaged results for the different parameters investigated during the P-C test series. In general, it can be seen that little difference in the removal efficiency of the system was found when the temperature was increased from 302.59 to 310.93 K (85° to 100° F). There is an apparent increase in ammonia removal at the higher temperature, but further investigation would be required to verify that conclusion. Operational difficulties with maintaining a proper sludge blanket in the clarifier were encountered at the higher temperature. Sludge-blanket upset appears to be caused by small changes in inlet water temperature. This conclusion also should be investigated further. In general, the P-C unit produced very good removal efficiencies with the exception of the ammonia.

Reverse-osmosis testing: After the wastewater was passed through the P-C system, a further reduction in pollutants was achieved by means of the RO unit. The resultant effluent is of extremely high quality and could be used for boiler purposes in the MIST system. The results of the RO tests are summarized in table XIII.

Biological-tertiary testing: Extreme cyclic influent parameters were troublesome throughout the program. Figures 30 and 31 are examples of the variation in BOD and in ammonia, respectively, during a portion of the test program. The effectiveness of the rotating biological disks and of the P-C system as a tertiary process sequence is also shown for the ammonia and BOD measured during this period. Strongest raw wastewaters were consistently found at midweek, with weak waste at the beginning and the end of the week. Data were not recorded during the weekend. Table XIV shows the results of this test series in relation to temperature effects. Operation at the controlled temperatures of 302.59 and 310.93 K (85° and 100° F) revealed no

specific temperature effect. Later, the wastewater temperature was allowed to fall to approximately 294 K (70° F) but was not controlled. Even with this lower temperature, no significant change in the biological portion or in the tertiary portion can be seen. Biomass growth on the disk, however, is much greater at warm temperatures. High-quality treatment was reliably achieved during the entire test period even though the influent water content continued to fluctuate widely.

Biological overloading: Creation of an overload condition was attempted by adding primary sludge from a nearby treatment plant to produce two and three times the normal concentration of several contaminants: BOD, COD, suspended solids, and turbidity. The results were not optimum (table XV). Only in COD, suspended solids, and turbidity were there significant changes in the influent concentration and then not the twofold and threefold changes anticipated. However, the significant result was the capability of the rotating-disk system to absorb changes of this magnitude. The tertiary system was not required to smooth out the operational surges.

Biological-system poisoning: Alum was added to the first stage of the rotating disk in an attempt to reduce the phosphates in the biological system, as well as to remove suspended solids and BOD more effectively. The addition of 100 mg/liter of alum produced a good removal of phosphate but no change in suspended solids or BOD removal. The alum dosage was increased in steps to approximately 500 mg/liter with no change in conditions. At that point, the ammonia conversion to nitrate ceased. Although no other immediate changes occurred visually or chemically in the rotating disk, a biological kill obviously had occurred. Subsequently, major sloughing of the biomass was observed.

Conclusions and recommendations.—On the basis of WMS testing results, the following conclusions have been reached.

1. Physical-chemical testing
   a. Alum as a single coagulant is excellent.
   b. The Met-Pro flocculation blanket is stable under water temperature conditions.
   c. Redesign of the P-C unit can save power.
   d. Activated carbon is not necessary in all cases with an MIUS.
   e. The P-C system produces excellent water and has reasonably low manpower requirements if it is well automated.
2. Biological testing
   a. The Bio-Surf[5] is stable under difficult water conditions.
   b. Better clarification is required to reduce suspended solids.
   c. Denitrifiers less expensive than the one used are available; however, the performance of denitrifiers is excellent.
   d. The Bio-Surf is an economical wastewater treatment system with low power and maintenance requirements.
3. General
   a. Analysis delays produce significant problems in test operation.
   b. Detailed coliform tests are required.
   c. Chemical analysis of ammonia conversion is the most rapid measure of biological toxicity.
   d. The RO process has limited use in an MIUS.
   e. System design should enable removal of water at various points in the treatment process for use when high levels of water purity are not required.

Solid Waste Management Subsystem

The solid waste management subsystem (SWMS) consists of an incinerator, with its loader equipment, that burns solid waste. The thermal energy produced is exhausted out the stack through the heat-recovery unit to produce steam. Figures 32 and 33 are schematic diagrams of the overall solid waste system and the heat-recovery unit, respectively.

The incinerator was designed to burn at a rate of 31.8 kg/hr (70 lb/hr). The thermal energy produced would be recovered with a design efficiency of 60 percent. Supplementary fuel is supplied for startup and to maintain the primary and secondary chambers at desired temperatures.

Test objectives.—Three specific tests were planned.

1. Series I, boiler mode test.
2. Series II, refuse charge-rate test.
3. Series III, sludge charging-rate tests.

[5] A biological sewage treatment unit manufactured by the Autotrol Corporation.

The first test was designed to determine heat-recovery efficiency when only fuel oil was burned. The second test was to provide incinerator performance data at various refuse charge rates. The third test was not performed.

Test description.—The boiler mode test (series I) was operated using a variable afterburner temperature controller set point ranging from 977.59 to 1144.26 K (1300° to 1600° F). Although 1310.93 K (1900° F) was the maximum test temperature planned, it was not possible to reach a temperature much in excess of 1144.26 K (1600° F).

The refuse charge-rate test (series II) was performed with charging rates ranging from 30- to 10-minute cycles.

Test results.—During the boiler mode tests, fuel consumption varied from 0.016 to 0.019 m^3/hr (4.2 to 4.9 gal/hr) for afterburner temperatures in the range of 977.59 to 1144.26 K (1300° to 1600° F). During these same tests, the feed-water flow varied from 0.057 to 0.114 m^3/hr (15 to 30 gal/hr). These values indicate heat-recovery efficiencies from 23 to 40 percent.

Results of the solid-waste charge-rate test demonstrated the capability of the incinerator to reduce refuse volume. Ten 0.2-cubic-meter (55 gallon) drums of grade 2 shredded waste (666.3 kilograms (1469 pounds)) were loaded into the incinerator during the 11 hours of operation. One 0.2-cubic-meter (55 gallon) drum of ash (137 kilograms (302 pounds)) was cleaned out after test completion and represented a weight reduction of 79 percent. However, energy recovery was small and slagging problems occurred in the primary chamber.

Conclusions and recommendations.—The incinerator performance in reducing the volume of solid waste was excellent. The slagging problems that occurred can be eliminated by charging no more than 136.1 kilograms (300 pounds) of solid waste between ash cleanout periods.

The time required to bring the incinerator up to operating conditions was excessive, more than 2 hours. The proposal to correct the problem is to shut down the main blower until solid waste is actually being burned, because the blower introduces a large volume of ambient air into the primary chamber and heat from combustion must heat this air as well as the chamber.

Another problem encountered was the exiting of smoke and flames through the charging door when the charge sequence was activated.

Control and Monitoring Subsystem

The purpose of the originally installed control and monitoring equipment for the MIST was, specifically, to maintain the operational status of the subsystems and to record data for detailed analysis after the subsystem tests had been run. Hence, there were no tests associated with evaluating the control and monitoring equipment. However, before each test, the control and monitoring equipment was checked out to determine its integrity at that time.

Subsystem description.—The MIST control and monitoring equipment provided the majority of information pertinent to most subsystem tests. The operational equipment displaying pressures, temperatures, electrical parameters, and pump and motor status information had to be functioning properly before commitment to the subsystems test. The following tests at the displays and controls were conducted before each subsystem test.

1. Operational display

a. Temperatures — The operational temperatures were displayed on a multipoint digital readout device. This unit served as the primary indicator for 48 critical subsystem temperatures. The operation of the unit and of the thermocouples associated with it was verified before each test. A multipen strip-chart recorder was also set up to monitor critical cooling- and heating-water temperatures. The signals for this recorder were provided by redundant temperature probes.

b. Pressures — Individual pressure meters were located in the control room. These meters were driven directly by the sensors in the subsystem lines. Only the most critical pressures were displayed; and because of their criticalness, they were checked before each test.

c. Motor, pump, and valve status information — Operating lights that indicated the mode of operation of pumps, motors, and valves were used to establish the appropriate configuration of the subsystem before and during its test. A lighting test verified operation of the indicators.

2. Controls — The subsystem controls for the MIST were primarily manual valve adjustments at the valves and manual control of the pump and motor operation by the use of remote switches. There were, however, nine automatic controllers that had to be verified as operational if they were to

be used in the particular test phase. One of these controllers was electronic, and the set point was adjusted in the control room. The other controllers were pneumatic; two of them were located in the control room, and the remaining six were located in the equipment area. The set-point adjustment for these controllers had to be checked out before tests involving these control loops were conducted.

With the data-recording equipment, all instrumented parameters were converted to digital signals and recorded on magnetic tape for posttest processing. The tape-recorded data served as the historical record for a detailed analysis by test engineers. The equipment that recorded the data was called the DEXTIR and was manufactured by Beckman Instruments. The data were recorded in digital counts representative of the conditioned signals with a range of −10 to +10 millivolts. A standard reference signal of 5 millivolts was included in seven different channels as a check on the multiplexing and analog-to-digital conversion equipment. The output of the DEXTIR was checked by printing a paper tape of the data or by calling up any measurement individually on the digital data readout. Since the DEXTIR output was in counts representative of the conditioned signals, the operator had to use appropriate tables to convert the DEXTIR output to the engineering-unit value anticipated.

An example of the DEXTIR paper-tape printout (fig. 34), an engineering-unit conversion table (table XVI), and a copy of the processed data from the DEXTIR magnetic-tape output (table XVII) are included.

Test results.—Several noteworthy observations were made. It should be pointed out, however, that although the actual impact of such an operation was originally unknown, it was well understood that the MIST operation could not be optimum with the manual controls and the techniques for recording and processing test data that were implemented. In that respect, there were numerous delays in test starts, retesting was necessary, and undue compromises were made to avoid such retesting or delays in starting. These problems were caused by failures that went unnoticed until the recorded data were processed by the off-line computer; and, as a result, precautions were taken to avoid such recurrences. The measures taken to alleviate the problem of testing while bad data were being recorded are summarized as follows.

1. The standard reference calibration signal of 5 millivolts in the seven channels was checked before and periodically throughout the test.
2. The magnetic tape was dumped immediately after a test procedure was shut down or completed. This dump verified the integrity of the taped data and enabled the operator to ascertain whether the data could be processed. If there were problems with the recorded data, it was necessary to adjust the data acquisition system (DEXTIR) and rerun the test.
3. If no major discrepancies in the recorded data were found, the next phase of the testing was initiated. The recorded data were sent to the NASA data-processing center, where a hard-copy tabulation and a microfilm of the tabulation were produced. Copies of the processed data were produced and made available through the NASA microfilm reproduction center.
4. The printouts of data were then distributed to those individuals or contractors primarily concerned with the test — generally, the following recipients.

a. The Urban Systems Project Office (USPO) subsystem engineer

b. The simulation program development contractor (Lockheed Electronics Company)

c. The MIST development contractor (HSD of the United Technologies Corporation)

d. The test support contractor (Northrop Services, Inc.)

A microfilm copy of the tabulated data was then filed in the USPO. Additional hard copies can be produced upon specific request.

Conclusions.—A monitoring and control system that provides display of only the "critical" parameters in real time is not sufficiently conducive to a successful testing program. Sensors not "critical" to operations (i.e., safe operations etc.) are sometimes very valuable in the analysis. If such a sensor has failed and the failure is not realized until the recorded data have been processed, the test is less than a success. Hence, evaluation testing of future subsystems should be accomplished with a monitoring and control system that provides real-time status of all measured values.

Phase III (Integrated Systems) Tests

The MIST integrated tests were conducted in two series. The series I tests were performed to demonstrate the capability of the various subsystems to function as an integrated unit at discrete set points. In the series II tests, the unit was operated to meet the demands of a 24-hour varying profile.

Series I Testing

Steady-state tests were conducted in the series I program to establish the capability of the PGS, the HACS, and the WMS to function in an integrated mode under a variety of conditions. Because of the experimental nature of the WMS, these tests were conducted independently from the remainder of the integrated tests. Specifically, the space-heating tests were conducted primarily to evaluate thermal storage use with a variety of heating-load conditions and steam energy production rates. The space-cooling tests were designed to establish the floating-split[6] characteristics of the air-conditioning chillers and the thermal storage usage at selected loads and thereby enable the system performance and control characteristics to be studied.

The test data collected, presented subsequently under "Series I Test Results," were intended to provide a confidence level before the more complex, dynamic series II tests were conducted. Because the series I tests were intended as a confidence and multipoint operation demonstration, no attempt was made to draw any major design conclusions from these data. This information does, however, serve as a cross-check at discrete points to the data obtained in the series II tests.

Test configuration and description.—To ensure the most effective thermal integration of recovered waste heat into the MIST system, the engine was configured in the ebullient-cooling mode, the incinerator was made operational, and the heating and cooling loops utilized the energy to meet the loads and/or charge the thermal storage units. The engine and incinerator heat-recovery rates (i.e., the total enthalpy difference through the heat-recovery units) were determined through measurement of the generated system pressure and the quantity and temperature of the makeup water to the units. The makeup-water measurements were necessary because collected condensate representing the steam usage was not returned to the holding tank for reuse. Although the actual quality of the steam generated was not a factor in the analysis of series I test results, the steam was assumed to have a 2-percent moisture content.

The incinerator was operated with only fuel oil as an energy source, and the configuration was such that the generated steam was integrated directly into the waste-heat-recovery manifold. Fuel-oil usage was recorded, and steam generation was determined by measuring the makeup-water requirement to the incinerator boiler.

The space-heating tests were conducted first with the engine operating independently, and secondly with the incinerator and the engine operating simultaneously. The tests were conducted by maintaining a fixed engine load and a fixed heating load until the thermal storage tank was configured in either the charge or the discharge mode to compensate for the difference between the waste thermal energy produced and the heating-load requirements. The tank was fully charged before the start of the test if the discharge configuration was required during the test. The energy usage within the heating loop was determined by the steam-condensate quantity and temperature measured at the outlet of the facility heat exchanger when the thermal storage tank was in the charge mode. When the thermal storage tank was in the discharge mode, the total heat usage was found by measuring the heat drain in the tank and the heat transfer through the facility heat exchanger. The hot thermal storage tank was considered charged when the fluid temperature reached 383.15 K (230° F); the discharge point was considered to be 349.82 K (170° F).

The space-cooling tests were configured so that the absorption and compression chillers could operate independently or in conjunction with others on the basis of cooling-load conditions and the availability of steam to drive the absorption chiller. As in the space-heating test, only the engine was operated for some load conditions, whereas both the engine and the incinerator were functioning for other conditions. The floating split between the absorption chiller and the compression chiller for

[6]The floating-split mode of chiller operation requires that all the available steam be utilized by the absorption chiller, with any remaining cooling load being carried by the compression chiller.

each electrical- and cooling-load combination was determined by measuring the percent of cooling load carried by the absorption chiller. Steam consumption was measured at the condensate outlet of the chiller, and load percentage was determined by measuring the change in temperature of the chilled water undergoing constant flow through the chiller. The split ratio resulted from the difference in total cooling load and the percent of absorption chiller load.

The cold thermal storage tank was placed in both the charge and the discharge mode to test its capability to store or provide heat energy within the cooling loop. The tank was considered charged when the internal fluid temperature reached 280.37 K (45° F) and was completely discharged at 285.93 K (55° F). For those tests requiring discharge, the tank was fully charged before the start of the test. Finally, it should be noted that no attempt was made to configure the engine in the forced-circulation-cooling mode or to run the dry-heat-rejection test as described in the MIST Test Requirements Document dated May 1974. Data from these tests were not considered critical to the series II testing.

Series I test results.—Results of the integrated-systems series I tests are presented in the following subsections.

System heat-recovery tests: Table XVIII summarizes the test data for heat recovery from the engine at the selected engine settings. Included is the specific high-grade heat recovered from the exhaust gas and the jacket water, as well as the specific low-grade heat recovered from the engine oil cooler/aftercooler coolant.

For each power load, the heat-recovery results were time averaged to normalize the test data. The time-averaged heat-recovery rate was determined by the following relationship.

Time-averaged heat-recovery rate =

$$\frac{T_1HR_1 + T_2HR_2 + \ldots T_nHR_n}{T_1 + T_2 + \ldots T_n}$$

where

T = duration of test, hours

HR = heat-recovery rate, British thermal units per hour

n denotes test number

The total engine heat rejected through the lubrication oil and recovered from the exhaust gas and the jacket water is plotted as a function of engine load in figure 35(a). The low-grade heat from the lubrication oil as a function of engine load is shown in figure 35(b). The total MIST system high-grade heat recovered from the engine and the incinerator is depicted in figure 35(c). The operational characteristics of the incinerator changed during the running of series I tests, as evidenced by its performance curve. The efficiency dropped from an average of 66 percent during the 41-kilowatt engine setting down to an average low of 41 percent during the 107-kilowatt setting. Operation became stable during the 122-kilowatt-engine-load run. A significant difference was noted between the amount of heat recovered during the subsystem tests and at the start of the series I tests. The time-averaged operating efficiency of the incinerator was determined to be 55 percent. A complete tabulation of the heat-rejection/heat-recovery information for each engine load is offered as part of the space-heating test results in table XIX.

Space-heating tests: The results shown in table XIX represent a comparison of heating load, engine load, incinerator status, and thermal storage status. If a comparison is made of the quantities of high-grade heat utilized,[7] a difference will be noted. This difference is a result of the test technique used in measuring steam condensate. All condensate was measured and dumped instead of being returned to the condensate loop. Makeup requirements were met by using lower temperature facility water. The difference noted previously is equivalent to the energy required to raise the condensate from its makeup temperature to the normal saturation temperature of condensate. Therefore, with a closed-loop configuration in which condensate was being returned to the heat-recovery unit, the actual heat available for consumption or utilization would be equal to the high-grade-heat recovery rate. This table aids in assessing the interactions and effects of changing the heating loads, the thermal storage status, and the incinerator status while the engine parameters are held constant. A typical thermal storage charge/discharge temperature profile is offered, for reference purposes only, in figure 35(d). This chart was obtained from actual computer plots of internal tank fluctuations in the heating-load-simulator operation.

[7]Recovered heat utilized is defined as the sum of heat to load and thermal charge or the difference between heat to load and thermal discharge.

Figure 35(e) represents hot thermal storage charge and discharge rates as a function of steam heat available for averaged values of space-heating loads used in the series I tests. This chart can be used to determine the quantity of thermal energy that can be stored or the quantity that must be discharged to meet a specific space-heating load, with a specific amount of steam heat available. To arrive at the amount of steam heat available, the operational status of the incinerator and the electrical load on the engine must be determined. By using the 55-percent efficiency value for the incinerator and the total heat content of the fuel used, the recovered waste heat can be calculated. By using table XVIII and extrapolating for the exact kilowatt load, the engine-recovered steam heat can be determined. The sum of these two values represents the total steam heat available. The intersection of the space-heating load and the steam-heat quantity determines the charge or discharge rate resulting from these conditions. This procedure can be followed for each hour of a 24-hour profile to estimate the total daily charge/discharge profile and waste-heat utilization.

Space-cooling tests: Table XX contains the results of the space-cooling tests and indicates the floating-split ratio of the absorption/compression chiller for each load condition. In an effort to validate test results for better correlation to theoretical system performance, the following assumptions were made.

1. Test data for absorption chiller loads of less than 35.2 kilowatts (10 tons) were considered unreliable because the units under test were not designed to operate at less than 50 percent of their 87.9-kilowatt (25 ton) rated capacity, according to the manufacturer.
2. Test data that resulted in an absorption chiller COP greater than 0.7 were questionable, and this value was used instead because it is the maximum value obtained in subsystem testing.

Because condensate measurements similar to those for the space-heating tests were made for this segment of tests, some increase in steam availability could be expected in a closed-loop configuration. This increase would result in a slightly higher percent of absorption chiller operation for all settings. Although data reliability at low load settings (less than 50 percent of rated capacity) is questionable, the data enable estimation of the floating split resulting from a specific space-cooling load condition and electrical-load profile.

Figure 35(f) is a graphical presentation of the calculated floating-split ratios plotted against theoretical performance for 70.3, 105.5, and 140.7 kilowatts (20, 30, and 40 tons). Figures 35(g) and 35(h) are discussed in the section entitled "Series II Testing."

Series II Testing

The series II integrated tests were conducted to demonstrate the MIUS concept in meeting typical residential load profiles. Several key issues discussed in the section entitled "Key MIUS Design Issues" were identified as the basis for the demonstration. The series II testing consisted of a series of five 24-hour tests for simulating different seasonal load profiles and a separate test for domestic-hot-water heating. Table XXI shows, for each test, the simulated seasonal test conditions and whether thermal storage was used.

Test configuration and procedures.—The MIST configuration used for all the series II testing was typical of that expected in an MIUS installation. The major aspects of configuration and operational procedures that are pertinent to test data analysis are presented in this section. Any deviation for a particular test is discussed in the section relating to that test.

Power generation subsystem: The ebullient-cooling mode was used throughout the series II testing. In this cooling mode, the heat recovered from the engine exhaust, the engine water jacket, and the incinerator is collected in a common steam header as saturated steam at a pressure of approximately 103×10^3 pascals (15 psig). Heat was recovered from the engine oil/aftercooler at a temperature of approximately 330.37 K (135° F). Engine loading was established by adjusting the load simulator each hour to follow the MIST electrical profile.

Heating, ventilation, and air-conditioning subsystem: The configuration of the heating, ventilation, and air-conditioning (HVAC) subsystem was varied from test to test on the basis of the requirement for thermal storage. For each test profile requiring space cooling, the absorption and compression chillers were operated in the floating-split mode used for series I testing.

The heating- and cooling-load simulators were used to establish the required loads on the HVAC subsystem by establishing a predetermined temperature difference of chilled water entering and leaving the simulator.

Domestic-hot-water loads were satisfied from the hot thermal storage tank during all of the test profiles. The tank was charged before each test with enough heat to satisfy the requirements. A constant domestic-hot-water flow of 0.008 m^3/min (2.21 gal/min) was maintained throughout each test profile for the freshwater preheater and freshwater heater heat exchangers.

Solid waste management subsystem: Because of operational problems experienced during previous testing, the incinerator was operated without trash, with fuel oil used as the only heat source throughout the series II testing. The incinerator was operated at a constant rate during all of the tests; the length of operation varied from test to test.

Wastewater management subsystem: A constant flow rate of 0.023 m^3/min (6 gal/min) was maintained throughout all the series II testing through the WMS heater.

General procedures: All the test profiles required hourly adjustments of the load values for a 24-hour period. Test data were recorded continuously on magnetic tape and manually for several parameters at 1-hour intervals. In addition, a printed copy of all the data recorded on magnetic tape was obtained hourly.

Load conditions.—The load conditions used for the integrated tests were based on the results of the NASA "MIUS Community Study," which established the power, heating, air-conditioning, and domestic-water-heating profiles of figures 36, 37, 38, and 39, respectively. In addition, the study defined incinerator burn times and heat-recovery rates. An analysis of these load conditions was performed to establish the MIST load conditions that are thermally representative of the MIUS system loads. The MIST loads were determined by duplicating the MIUS waste-heat utilization for absorption chilling (i.e., the floating split). This procedure established the air-conditioning-load profile and the power profile. The profiles for space heating and for domestic-water heating were established by maintaining the same percent of the recovered waste heat for these functions as is required by the MIUS.

Table XXII lists the eight selected engine set points used in the series I tests and also identifies the incinerator status from each run. At each test point, heating and cooling loads, as well as operating modes, were varied. The number of tests to be conducted as series I tests was minimized by determining the peak heating, air-conditioning, and domestic-water-heating loads associated with hourly power loads. These load conditions were then reviewed to eliminate duplicate and/or similar load conditions.

The series II test profiles were selected to best address the key issues identified in the section entitled "Key MIUS Design Issues." These profiles are presented in figures 40 to 43. Each test consisted of 24-hour profiles for heating and/or air-conditioning loads and domestic electrical loads. The domestic-hot-water heating loads and the wastewater-treatment heat load were assumed to be independent of season and were held at a constant level throughout each test profile. The loads were scaled down from those for much larger facilities to be consistent with MIST equipment capacities. The resulting load profiles indicated that a relatively large auxiliary electrical load was required to accommodate the scaled-down MIST equipment, compared to that for an MIUS of much larger capacities.

Heating of domestic water may be accomplished in the MIUS concept in any of the following methods and their combinations.

1. At a constant flow rate when a hot-water surge tank is used
2. At the demand flow rate when a hot-water surge tank is not used
3. With or without preheating the domestic water with the oil/aftercooler heat
4. By using high-grade waste heat directly or with the return water from the space-heating system

To determine the effects of these options on the MIUS system, additional series II tests were conducted with domestic water flows of 0.006, 0.009, 0.011, and 0.017 m^3/min (1.5, 2.25, 3.0, and 4.5 gal/min). Each of these flow conditions was tested with and without preheating and with engine loads of 75, 125, 175, and 215 kilowatts. The higher engine loads were selected to provide additional heat-recovery data.

Series II test results.—The following comments concern the series II test data analysis in general and apply to all the individual tests. Any analyses

that were peculiar to a particular test are discussed in the section pertaining to that test.

Cooling-tower test data were used to determine the incinerator heat-recovery rates. The amount of heat rejected attributable to the incinerator was taken as the increase over the engine and chiller heat observed when the incinerator was in operation. This heat-rejection rate was used as the heat-recovery rate for each hour of incinerator operation. The incinerator fuel consumption rate was then estimated from the heat-recovery rate, with a 60-percent efficiency assumed.

The heat-recovery rates from the engine water jacket, exhaust heat exchanger, and oil cooler/aftercooler were also taken from the subsystems test data. An average engine load was determined for each test profile. On the basis of this average load, the heat-recovery rates were determined from the appropriate engine data. The average rates obtained were then used in calculating energy balances for each 24-hour profile for the series II testing.

The amount of energy supplied to the space-heating-load simulator was determined from series II test data. Supply and return water temperatures and flow rates for the load simulator were used. Each measurement was averaged for each test profile, and these values were then used to calculate the total amount of heat transferred during the 24-hour period.

The amount of heat supplied to the WMS heater, the freshwater preheater, and the freshwater heater was calculated by using averaged inlet and outlet water temperatures. The flow rates were preset at the beginning of the test period and were assumed to remain constant throughout the test profile.

The quantity of electrical power delivered to the compression chiller was calculated from measured amperage values. By using the total ampere-hour value for the 24-hour profile and an average power factor of 0.9, the total compression chiller power consumption for each test profile was determined. The energy consumption for the absorption chiller was determined by using data from a steam meter on the chiller and the difference between the inlet and outlet steam enthalpy.

To estimate the COP for the chillers, the total amount of cooling delivered was assumed to be the amount required by the test procedure. By using the assumed cooling load and a COP of 0.59 for the absorption chiller, as estimated from subsystems test data, a COP of 3.0 for the compression chiller was determined. This value also agrees with subsystems test data, and these COP values were used in all chiller analyses.

The amount of heat rejected by the excess-steam condenser was calculated by collecting the condensate from the condenser. The enthalpy difference between the excess steam and the condensate was determined from measured data. An adjustment was made to compensate for replacing the condensate in the system with colder makeup water.

The system efficiency is defined as the summation of all the electricity generated and the waste heat utilized divided by the total heat content of the fuel consumed by the system. The efficiency was calculated for each 24-hour test profile on the basis of the analyses performed for the major system components.

The data for each series II test are presented in a performance summary table and an energy flow chart. The summary table shows the total services produced and the total fuel consumed for the 24-hour test profile. The energy flow chart shows the energy flow between major MIST components and the energy balance for the 24-hour test profile.

Test IIA-1: In test IIA-1, a design-summer-day load profile was simulated and cold thermal storage was used. The performance summary and the energy flow chart are shown in table XXIII and figure 44, respectively.

The quantity of high-grade heat was out of balance by 864.57 megajoules (0.82×10^6 British thermal units) for the 24-hour period, or by approximately 7 percent of the high-grade heat recovered. This disagreement is due to assumptions used in the data analysis and to inaccuracy in the total test instrumentation. The assumption that delivered cooling is equivalent to the desired cooling load, the chiller COP assumptions, the incinerator-heat-recovery assumptions, and the engine-heat-recovery assumptions all have a direct impact on heat-balance calculations. When the potential for combined errors resulting from the data analysis assumptions and procedures and from expected measurement errors is considered, the 7-percent imbalance noted in the high-grade heat values is within reasonable limits.

No measurement was made of the unused low-temperature heat that was recovered from the engine to enable a heat-balance calculation similar to that for the high-grade heat.

Test IIA-2: In test IIA-2, a design-summer-day

load profile similar to that for test IIA-1 was simulated, but no thermal storage capability was used in satisfying the loads other than for domestic-hot-water heating as previously described. The performance summary and the energy flow chart are shown in table XXIV and figure 45, respectively.

The quantity of high-grade heat is out of balance by 158.15 megajoules (0.15×10^6 British thermal units) for the 24-hour period, or by approximately 13 percent of the recovered heat. The imbalance is caused by a combination of measurement error and assumptions used in the data analysis procedure, as in test IIA-1. The imbalance noted is well within acceptable limits. No attempt was made to perform a similar energy-balance analysis on the low-temperature heat.

A comparison of the test data from tests IIA-1 and IIA-2 shows that thermal storage resulted in only insignificant changes in the system performance characteristics. The most significant benefits to be expected from the use of thermal storage are increased system efficiency through increased utilization of "free" heat by the absorption chiller and reduced peak electrical demand due to limiting compression chiller loads at times of high electrical load. Neither of these benefits is evident in the test data. The small differences noted in the two sets of data can be attributed primarily to nonrepeatability of the test profile and to measurement uncertainties. It should be noted, for example, that the difference between the high-grade-heat imbalance (7 percent for test IIA-1 compared to 13 percent for test IIA-2) could result in a detectable difference in overall system efficiency.

Test IIB-1: In test IIB-1, a design-winter-day load profile was simulated and thermal storage was used to satisfy the loads. The performance summary and the energy flow chart are shown in table XXV and figure 46, respectively.

The energy flow chart shows a net loss of 295.22 megajoules (0.28×10^6 British thermal units) from the heat contained in the storage tank for the 24-hour period. In consideration of this value, the quantity of high-grade heat is out of balance by 105.4 megajoules (0.1×10^6 British thermal units), or by approximately 1 percent of the recovered heat. This imbalance is a result of the combination of measurement uncertainties and assumptions used in the data analysis procedure and is well within acceptable limits. No attempt was made to perform a similar energy-balance analysis on the low-temperature heat recovered.

Test IIB-2: In test IIB-2, a design-winter-day load profile similar to that for test IIB-1 was simulated but no thermal storage capability was used in meeting the loads. One other significant difference between the two winter design test cases was that the incinerator was operated for 12 hours as an additional heat source rather than for 6 hours as in the previous test profiles. The performance summary and the energy flow chart are shown in table XXVI and figure 47, respectively.

The quantity of high-grade heat is out of balance by 1233.59 megajoules (1.17×10^6 British thermal units) for the 24-hour period, or by approximately 11 percent of the heat recovered. The imbalance is due to a combination of measurement uncertainties and assumptions used in the data analysis procedure. The relatively high imbalance, as compared to that for the other series II tests, is due primarily to the assumption concerning incinerator heat recovery and the increased incinerator operating time. No attempt was made to perform a similar energy-balance analysis on the low-temperature heat.

A comparison of the data for tests IIB-1 and IIB-2 shows a system efficiency of approximately seven percentage points higher in the test with thermal storage over that without thermal storage. This large difference is due, in part, to the increased incinerator operation and consequently higher quantity of unused heat in the case without thermal storage. Had the incinerator been modulated to provide only the heat required for the additional 6 hours of operation, the thermal storage case would have shown an improvement of approximately three percentage points. As noted in the case of the two summer design test cases, the uncertainties in the imbalance of the two high-grade-heat quantities could very significantly alter the comparison between the two winter design cases.

Test IIC-1: In test IIC-1, an average load profile for a spring or fall day was simulated and thermal storage was used in satisfying the loads. The performance summary and the energy flow chart are shown in table XXVII and figure 48, respectively.

A net gain of 843.5 megajoules (0.8×10^6 British thermal units) in the heat content of the thermal storage tank was noted over the 24-hour period. In consideration of this value, the quantity of high-grade heat is out of balance by 495.54 megajoules (0.47×10^6 British thermal units). The imbalance

is caused by a combination of measurement uncertainties and the assumptions used in the data analysis procedure.

It should be noted that, because the expected engine heat was sufficient to meet the loads, the incinerator was not operated. The only significant impact on the test data was in the area of plant efficiency. The 63-percent efficiency shown in table XXVII, which is approximately the same as that for the design summer and winter days, would have been reduced to 53 percent if the incinerator had been operated for 6 hours. This reduction in plant efficiency is to be expected in an MIUS application during the periods of low HVAC loads because the potential for recovered-heat utilization is reduced.

Test IID: Figure 49 indicates the amount of high-grade (steam) energy required to increase the temperature of domestic water from 308.15 to 338.71 K (95° to 150° F) when no preheating is done. If preheating is accomplished by using lubrication oil heat, the high-grade-energy savings are evidenced by the reduction in steam heat required. (See the preheat curve (fig. 49).) In figure 50, the required steam heat is plotted against the engine load for each of the flow rates tested. The results show that the amount of thermal energy provided by the low-grade heat is not significantly affected by the engine load. Figure 35(g) quantifies the amount of energy required to preheat domestic water. In the tests conducted, the low-grade heat provided 62 to 65 percent of the total energy needs for domestic water heating.

Integrated-Systems Test Conclusions

Overall results of the integrated-systems tests tend to affirm the objectives of the MIUS Program. Increased plant efficiencies, reduced prime energy input, and reduced emissions resulted when the various utility services were operated in a unified fashion.

Series I tests.—The total quantity of heat rejected and recovered from the ebulliently cooled diesel-generator set is in good agreement with the manufacturer's data for the total quantity of high-grade heat available for rejection and recovery, as shown in figure 35(a). An examination of the quantity of low-grade heat rejected from the lubrication oil (fig. 35(b)) and the quantity of steam heat made available from the heat-recovery unit (fig. 35(c)) indicates an equally good agreement with the manufacturer's data on an individual basis. These data compare favorably with subsystem heat-rejection results obtained during earlier tests. Consistency of results between heating loads for a single engine-load setting is evidenced from table XIX, where the deviation from the average quantity of heat rejected or recovered is less than 1 percent.

Space-heating loads were amply met with energy from the engine and the incinerator or with a combination of steam heat and energy from the charged hot thermal storage tank. Integration of the incinerator waste heat into the system during low electrical loads (41 kilowatts), however, was not adequate to meet the high space-heating loads. Discharge of the hot thermal storage tank was required in addition to the incinerator heat when the heating loads approached 102.5 kilowatts (350 000 Btu/hr).

Reduction in operating efficiency of the incinerator was caused by tube fouling from exhaust gases. Frequent cleaning of the tubes appears to be mandatory to maintain reasonable efficiency. With this periodic cleaning, a 60-percent efficiency can be assumed.

Although the space-cooling results compare favorably with theoretical results, some improvement could be expected in a closed-loop system in which condensate could be reused. Additional testing is required on the space-cooling loop to obtain the chiller operational set points for optimum floating-split characteristics. These tests would be followed by cold thermal storage performance and control tests.

Series II tests.—Results of the series II tests demonstrated the operational feasibility of complete utilities integration into the MIUS concept for typical residential loads. This demonstration was based on the issues described in the section entitled "Key MIUS Design Issues." The key issues relating to thermal integration techniques, mixed-mode air-conditioning, and integration of subsystem controls were resolved successfully in the series II testing. All the MIST subsystems were operated in an integrated manner during dynamic simulations of a variety of typical residential load profiles without significant problems.

The thermal storage system design and procedure used in the series II testing resulted in no appreciable benefits to support the thermal storage key design issue. The most significant benefits to be derived from the use of thermal storage are increased plant efficiency through increased utilization of "free" recovered heat for cooling and heating and the reduction of peak electrical demand

through limiting compression chiller loads during periods of high electrical load. Neither of these benefits is clearly evident in the test data; however, significant benefits could be derived through increased system control capabilities and design changes to enable independent operation of the two chillers.

Analyses of the test data were based on several basic assumptions rather than on measured test data. Examples include the procedure for determining incineration and engine heat recovery, cooling delivered to the cooling-load simulator, and assumed flow rates in several heat exchangers. The results are reasonably consistent but could be made more meaningful and conclusive with better test data and controls.

The test results confirm the technical validity of the MIUS concept and provide the basis for continued testing with the MIST as a utility system test-bed.

Because domestic water heating requires a constant amount of energy annually rather than seasonally, it is concluded that preheating of domestic water serves to improve the overall thermal efficiency of an MIUS system. Furthermore, the preheating provides a nearly fixed percentage of total water-heating needs regardless of waterflow rate and engine load. These conditions favor the use of a demand-flow domestic water system to eliminate the need for a hot-water surge tank. However, the final heating of the water would require a surge capability to prevent drastic changes to steam consumption with domestic-hot-water use. As part of the series II air-conditioning-profile tests, the hot thermal storage tank was used to provide this final heating of the domestic water. The results of this test are plotted in figure 35(h). During this 24-hour test, water at a constant flow of 0.009 m^3/min (2.28 gal/min) was heated from 294.26 to 338.71 K (70° to 150° F) by using a preheater and the thermal storage tank. All steam produced during this test was used for air-conditioning purposes and not for heating water.

The results of the domestic-water-heating tests signify that hot thermal storage tanks can be used to provide the thermal surge capability and eliminate the need for a hot-water surge tank. This use of hot thermal storage increases its effectiveness from seasonal heating applications to annual use.

Displays and controls.—Two of the identified key issues, integration of controls and data display requirements, were not addressed by specific tasks. Rather, the evaluation and testing of the MIST provided the experience in dealing with the various thermal, electrical, and water treatment loops that was necessary to associate the operating parameters in more easily recognized formats for ease of control by the test personnel. In addition, the trade-offs between automation and manual control were a direct evolvement of the initial test program.

Since completion of the integrated tests, implementation of these identified needs has proceeded and a refined data system and a limited automation of control functions are now being installed. Plans have been made to rerun a selected set of profiles upon completion of this installation, to compare the two approaches.

CONCLUDING REMARKS

An analysis of the results of the tests described herein leads to the conclusion that the technical goals of the MIUS Program are feasible; i.e., provision of utility services can be achieved by integrated systems with a reduction of prime energy consumption and a reduction in environmental impact. In the area of economics, it can be concluded that an automated control system can operate the plant with a minimum manpower level. No other firm conclusions in the economic sphere can be drawn from the experience gained from this program.

The demonstrated ability to simulate important system variables on a small scale and to thusly prove out design concepts at low cost was shown to have valid application to the urban sector.

Lyndon B. Johnson Space Center
National Aeronautics and Space Administration
Houston, Texas, December 22, 1976
386-01-00-00-72

TABLE I.—Engineering Data

Item	*Sensor number*	*Location*
Pressure	P-1	Fuel input (engine)
	P-2	Ambient air
	P-3	Engine-exhaust stack 1
	P-4	Engine-exhaust stack 2
	P-5	Exhaust silencer heat-exchanger feed water
	P-12	Oil interchanger water inlet
	P-16	Cooling-tower inlet
	P-17	Excess-steam-condenser cooling-tower water outlet
	P-18	Condensate main-line inlet
	P-31	Condenser water
	P-32	Jacket-water heat-recovery inlet
Temperature	T-1	Fuel
	T-2	Ambient air
	T-3	Engine inlet air
	T-4	Engine-exhaust stack 1
	T-5	Engine-exhaust stack 2
	T-7	Exhaust silencer heat-exchanger feed water
	T-26	Oil interchanger water inlet
	T-30	Cooling-tower water inlet
Temperature	T-31	Excess-steam condensate outlet
	T-40	Oil interchanger oil-loop outlet
Flow	F-4	Exhaust silencer heat-exchanger feed water
	F-18	Cooling-tower water inlet
	F-22	Excess-steam-condenser condensate outlet (manual)
	F-28	Oil/aftercooler interchanger cooling-tower water inlet
	F-38	Oil/aftercooler engine inlet
	F-39	Engine-exhaust gas
	F-40	Oil interchanger outlet

TABLE II.—Operational Data

Item	*Sensor number*	*Location*
Pressure	PI-1	Oil/aftercooler inlet
	PI-2	Exhaust-silencing heat-recovery backpressure
	PI-3	Engine jacket-water inlet
	PI-5	Cooling-tower water pump outlet
	PI-6	Steam pressure
Temperature	TP-1	Oil/aftercooler outlet coolant
	TP-2	Oil/aftercooler inlet coolant
	TP-3	Engine jacket-water outlet
	TP-5	Exhaust-silencing steam
	TP-6	Engine jacket-water inlet
	TP-10	Cooling-tower water pump outlet
Temperature	TP-11	Steam manifold
	TP-14	Oil/aftercooler interchanger cooling-tower water outlet
	TP-15	Excess-steam-condenser cooling-tower water outlet

TABLE III.—Engine Heat Balance—Forced-Convection Mode

[150-kilowatt electrical load]

Jacket-water inlet temperature, K (°F)	Unrecovered exhaust heat,[a] kW(Btu/hr)	Jacket-water heat recovery, kW(Btu/hr)	Oil cooler aftercooler heat rejection, kW (Btu/hr)	Exhaust heat recovery, kW(Btu/hr)	Electric power equivalent, kW(Btu/hr)	Heat input rate,[b] kW(Btu/hr)	Total Recovery, percent	Quantity accountable, percent
355.37 (180.0)	70.9 (242 000)	152.3 (520 000)	35.1 (120 000)	35.7 (122 000)	149.7 (511 000)	477.4 (1 630 000)	78.2	93.0
377.59 (220.0)	64.1 (219 000)	112.5 (384 000)	42.2 (144 000)	36.0 (123 000)	149.7 (511 000)	477.4 (1 630 000)	71.3	85.0

[a]Based on a 310.93-K (100° F) ambient temperature.

[b]LHV = 37601.6 MJ/m³ (135 000 Btu/gal).

TABLE IV.—Diesel Engine Noise Levels

Electrical load, kW	Noise level, dB at –		
	0.9 m(3 ft)	7.0 m(23 ft)	15.2 m(50 ft)
Test data			
20	104	96.5	92.0
50	106	97	91.0
100	105	97	90.5
150	104	96.5	89.0
200	105	97.5	89.5
230	105	98.0	90.5
Engine manufacturer's data			
230 (mechanical noise)	97.9	85.9	78.5
230 (exhaust with straight stack)	108.6	95.1	89.2

TABLE V.—JSC Environmental Health Services Analysis Report

[Diesel engine exhaust gas - 75 percent (173 kW) loading, MIST Project, building 32J]

Pollutant	Concentration			Average	Deviation
	Feb. 24, 1975	Mar. 5, 1975[a]	Mar. 12, 1975		
Carbon monoxide, p/m	147	130	145	141	9
Carbon dioxide, vol. %	7.5	8.5	7.5	7.8	0.6
Oxygen, vol. %	10.7	9.9	11.3	10.6	0.7
Nitrogen vol. %	81.8	81.6	81.2	81.5	0.3
Water, vol. %	3.7	5.6	6.6	5.3	1.5
Unburned hydrocarbons, p/m	7	27	28	21	12
Methane, p/m	5	11	9	8	3
Free carbon, p/m	5	16	19	13	7
Oxides of nitrogen, $\mu g/m^3$	1490×10^{-3}	1420×10^{-3}	962×10^{-3}	1291×10^{-3}	286×10^{-3}
Sulfur dioxide, $\mu g/m^3$	170×10^{-3}	184×10^{-3}	168×10^{-3}	174×10^{-3}	9×10^{-3}
Sulfur trioxide, $\mu g/m^3$	2.23×10^{-3}	2.93×10^{-3}	2.84×10^{-3}	2.67×10^{-3}	0.38×10^{-3}
Particulates, $\mu g/m^3$	43.0×10^{-3}	90.2×10^{-3}	58.8×10^{-3}	64.0×10^{-3}	24.0×10^{-3}

[a]Engine operating at 200 kW.

TABLE VI.—HACS Instrumentation List

Item	*Sensor nomenclature*	*Location*
Pressure	PI-5	Cooling-tower water pump outlet
	PI-6	Steam manifold
Temperature		General
	Sling psychrometer	Ambient wet and dry bulb
	TP-1	Engine oil coolant outlet
	TP-2	Engine oil coolant inlet
	TP-6	Engine jacket-water inlet
	TP-10	Cooling-tower water pump outlet
	TP-27	Heating-load water supply (simulator)
	TP-18/TP-34	Heating-load water return (simulator)
	TP-35	Cooling-load water supply (simulator)
	TP-24/TP-36	Cooling-load water return (simulator)
	TP-11	Steam manifold
		Absorption chiller
	Thermometer	Absorption chiller condensate outlet
	T-33	Absorption chiller chilled-water inlet
	TP-13	Absorption chiller condenser water outlet
	TP-19	Absorption chiller chilled-water outlet
	T-34	Absorption chiller condenser water inlet
		Compression chiller
	TP-25	Compression chiller condenser water outlet
	TP-26	Compression chiller chilled-water outlet
	TP-32	Compression chiller chilled-water inlet
		Combined chillers
	TP-17	Combined-chillers condenser water outlet
	TP-31	Combined-chillers chilled-water outlet
		Thermal storage
	TP-15	Cold thermal storage outlet
	TP-33	Chilled-water storage tank
	TP-28	Hot thermal storage tank
		Heat rejection/heat transfer
	TP-29	Cooling-tower water outlet
	TP-30	Cooling-tower water inlet
	TP-26	Oil-aftercooler-interchanger cooling-water inlet
	TP-14	Oil-aftercooler-interchanger cooling-water outlet
		Excess-steam condenser
	Thermometer	Excess-steam condensate outlet
	TP-22	Excess-steam-condenser cooling-tower water outlet
		Jacket-water interchanger
	T-8	Jacket-water interchanger outlet
	TP-16	Jacket-water interchanger cooling-tower water outlet
		Auxiliary facility heat exchanger
	TP-3	Engine jacket-water outlet
	TP-29	Jacket-water pump inlet
	T-9	Auxiliary facility heat exchanger water inlet

TABLE VI.—Continued

Item	*Sensor nomenclature*	*Location*
Temperature		Facility heat exchanger
	Thermometer	Facility heat exchanger condensate outlet
	TP-30	Facility heat exchanger hot-water outlet
		Freshwater preheater
	T-22	Potable water inlet
	TP-8	Freshwater preheater outlet
	TP-21	Freshwater preheater oil-loop outlet
		Freshwater heater
	T-23	Heater water outlet
	T-24	Freshwater heater heating-water inlet
	T-21	Freshwater heater heating-water outlet
		WMS heater
	T-10	WMS heat exchanger sewage inlet
	T-11	WMS heat exchanger sewage outlet
	T-28	WMS heater oil-loop outlet
		Water sterilization heat exchanger
	TP-23	Sterilized water inlet
	T-13	Sterilized water outlet
	Thermometer	Sterilizer condensate outlet
		Regenerative sewage heater
	T-25	Sewage supply inlet (biological disk)
	T-14	Sewage regenerative heater outlet
	TP-9	Regenerative sewage heater process water inlet
	T-17	Sewage regenerative water outlet
		Sterilization regenerative heat exchanger
	T-18	Sterilizer preheat outlet
	T-19	RO water outlet
	TP-12	Sterilizer outlet
Flow	F-2	Jacket-water return
	F-3	Jacket-water interchanger
	F-10	Met-Pro unit inlet
	F-11	Incinerator fuel flow rate
	F-12	Potable water inlet
	F-14	Potable water into freshwater heater
	F-15	Potable water out of freshwater heater
	F-16	Hot thermal storage/facility heat exchanger supply
	F-17	Facility heating hot-water supply
	F-18	Cooling-tower water inlet
	F-23	Compression chiller chilled-water inlet
	F-24	Absorption chiller chilled-water outlet
	F-25	Absorption chiller condenser water outlet
	F-27	Compression chiller condenser water outlet
	F-28	Oil-aftercooler-interchanger cooling-tower water inlet
	F-32	Sterilization regenerative heat exchanger inlet
	F-36	Cooling-tower water makeup
	F-38	Oil aftercooler engine inlet
	F-40	Oil interchanger outlet

TABLE VI.—Concluded

Item	*Sensor nomenclature*	*Location*
Flow	F-41	Cold thermal storage bypass
	Manual	Excess-steam-condenser condensate weight
	Manual	Absorption chiller condensate weight
	Manual	Facility heat exchanger condensate weight
	Manual	Water sterilization heat exchanger weight
Power	Ammeter	Cooling-tower fan
	Ammeter	Cooling-water pump motors
	Ammeter	Chilled-water pump motors
	Strip chart (ammeter)	Compression chiller motors
	Wattmeter	Engine
	Power factor meter	Engine

TABLE VII.—Power Ratio As A Function Of Load, MIST Series II Test—Compression Chiller

299.82 K (80° F) condenser water		*302.59 K (85° F) condenser water*		*305.37 K (90° F) condenser water*	
Cooling load, kW (ton)	*Power consumption per unit cooling load, kW/kW (kW/ton)*	*Cooling load, kW (ton)*	*Power consumption per unit cooling load, kW/kW (kW/ton)*	*Cooling load, kW (ton)*	*Power consumption per unit cooling load, kW/kW (kW/ton)*
Sensor set point = 284.26 K (52° F)					
19.20 (5.46)	0.26 (0.90)	18.46 (5.25)	0.28 (0.99)	17.44 (4.96)	0.27 (0.96)
31.69 (9.01)	.26 (.90)	36.65 (10.42)	.28 (1.00)	38.68 (11.00)	.28 (.97)
54.97 (15.63)	.25 (.87)	56.34 (16.02)	.24 (.86)	53.77 (15.29)	.30 (1.06)
73.99 (21.04)	.24 (.84)	71.78 (20.41)	.28 (.98)	74.38 (21.15)	.31 (1.09)
91.30 (25.96)	.23 (.82)	89.12 (25.34)	.26 (.93)	88.59 (25.19)	.27 (.95)
Sensor set point = 285.93 K (55° F)					
24.23 (6.89)	0.32 (1.14)	26.20 (7.45)	0.22 (0.79)	20.15 (5.73)	0.34 (1.18)
35.48 (10.09)	.31 (1.08)	40.44 (11.50)	.30 (1.04)	35.27 (10.03)	.27 (.95)
52.44 (14.91)	.31 (1.10)	54.79 (15.58)	.34 (1.20)	49.97 (14.21)	.28 (1.00)
67.98 (19.33)	.30 (1.05)	72.13 (20.51)	.32 (1.12)	73.78 (20.98)	.31 (1.10)
88.69 (25.22)	.26 (.93)	91.19 (25.93)	.26 (.92)	87.57 (24.90)	.28 (.99)

TABLE VIII.—Thermal Storage Summary Data, MIST Series IV Test—Thermal Storage Tests

(a) Cold thermal storage

Discharge rate, kW (Btu/hr), at -	
Full flow	20.7 (70 623)
Three-fourths flow	11.8 (40 356)
One-half flow	8.3 (28 250)
Charge rate, kW (Btu/hr), at -	
Full flow	41.4 (141 248)
Three-fourths flow	20.7 (70 624)
One-half flow	16.5 (56 499)
Ideal capacity, MJ (Btu)	297.8 (282 495)
Heat-gain factor, W/K (Btu/(hr • °F))	29.89 (56.7)
Effective capacity, MJ (Btu)	191.6 (181 749)
Performance coefficient	0.88

(b) Hot thermal storage

Discharge rate, kW (Btu/hr), at -	
Full flow	218.7 (746 872)
Three-fourths flow	Not applicable
One-half flow	Not applicable
Charge rate, kW (Btu/hr), at -	
Full flow	153.1 (522 810)
Three-fourths flow	Not applicable
One-half flow	Not applicable
Ideal capacity, MJ (Btu)	1378.1 (1 307 027)
Heat-loss factor, W/K (Btu/(hr • °F))	17.61 (33.4)
Effective capacity, MJ (Btu)	1398.8 (1 326 699)
Performance coefficient	0.92

TABLE IX.—Exchanger Thermal Effectiveness, Series V Test—Heat-Rejection/Heat-Transfer Network

(a) Oil aftercooler interchanger

Engine load, kW	Total heat rejection, MJh (Btuh)	Thermal effectiveness ϵ, $\frac{[a](t_i - t_e)_l}{t_{1i} - t_{2i}}$
25	100.585 (0.954 × 10^5)	0.056
50	140.756 (1.335)	.76
75	152.881 (1.450)	.85
100	163.424 (1.550)	.096
125	154.462 (1.465)	.090
150	187.885 (1.782)	.110
175	207.707 (1.970)	.120
200	219.305 (2.080)	.130
225	210.027 (1.992)	.130
Spec.	229.005 (2.172)	.120

(b) Jacket-water interchanger

Engine load, kW	Total heat rejection, MJh (Btuh)	Thermal effectiveness ϵ, $\frac{[a](t_i - t_e)_l}{t_{1i} - t_{2i}}$
25	240.392 (2.280 × 10^5)	0.028
50	271.811 (2.578)	.031
75	284.675 (2.700)	.034
125	480.784 (4.560)	.053
175	448.099 (4.250)	.053
225	595.708 (5.650)	.069
Spec.	591.490 (5.610)	.074

(c) Excess-steam condenser

Engine load, kW	Total heat rejection, MJh(Btuh)	Thermal effectiveness ϵ, $\frac{[a](t_i - t_e)_l}{t_{1i} - t_{2i}}$
25	112.815 (1.070 × 10^5)	0.99
50	114.924 (1.090)	.99
75	216.142 (2.050)	.98
100	288.892 (2.740)	.98
125	321.577 (3.050)	.97
150	375.349 (3.560)	.97
175	525.383 (4.983)	.97

Engine load, kW	Total heat rejection, MJh(Btuh)	Thermal effectiveness ϵ, $\frac{[a](t_i - t_e)_l}{t_{1i} - t_{2i}}$
200	540.882 (5.130 × 10^5)	0.97
225	548.262 (5.200)	.97
150; [b]105.5 (30)	[c]0 (0)	(d)
175; [b]105.5 (30)	[c]0 (0)	(d)
200; [b]140.7 (40)	343.718 (3.260)	.97
225; [b]175.8 (50)	134.746 (1.278)	.97
225; [b]175.8 (50); (e)	495.545 (4.700)	.97

[a]The numerator contains the difference between inlet and exit temperature for the one of the two fluids for which this difference is larger. The denominator contains the difference between the two inlet temperatures. In addition, ϵ is always taken as positive.

[b]Air-conditioner load, kilowatts (tons).

[c]Measurement in doubt.

[d]Nonoperational.

[e]Incinerator.

TABLE X.—Exchanger Thermal Effectiveness, Series VI Test—Ancillary Exchangers

(a) Regenerative sewage heater

Steam pressure, kPa (psig)	Total heat transfer, MJh (Btuh)	Thermal effectiveness ϵ, $\frac{^{a}(t_i - t_e)_l}{t_{1i} - t_{2i}}$
110.3 (16)	95.208 (0.93×10^5)	0.960
89.6 (13)	103.959 (.986)	.970
75.8 (11)	109.125 (1.035)	.980
62.1 (9)	107.544 (1.020)	.990
48.3 (7)	108.282 (1.027)	.970
Spec.	101.850 (.966)	.850

(b) Sterilization regenerative heat exchanger

Steam pressure, kPa (psig)	Total heat transfer, MJh(Btuh)	Thermal effectiveness ϵ, $\frac{^{a}(t_i - t_e)_l}{t_{1i} - t_{2i}}$
110.3(16)	155.200 (1.472×10^5)	0.590
89.6 (13)	169.645 (1.609)	.630
75.8 (11)	170.172 (1.614)	.620
62.1 (9)	169.750 (1.610)	.630
48.3 (7)	164.268 (1.558)	.630
Spec.	307.027 (2.912)	.85

(c) Facility heat exchanger

Heating load, MJh (Btuh)	Total heat transfer, MJh (Btuh)	Thermal effectiveness ϵ $\frac{^{a}(t_i - t_e)_l}{t_{1i} - t_{2i}}$
105.4 (100 000)	176.709 (1.676×10^5)	0.98
210.9 (200 000)	265.274 (2.516)	.98
316.3 (300 000)	340.028 (3.225)	.98
421.8 (400 000)	433.970 (4.116)	.98
527.2 (500 000)	519.795 (4.930)	.97
Spec.	532.447 (5.050)	.98

(d) Auxiliary facility heat exchanger

Engine load, kW	Total heat transfer, MJh (Btuh)	Thermal effectiveness ϵ, $\frac{^{a}(t_i - t_e)_l}{t_{1i} - t_{2i}}$
25	210.870 (2.000×10^5)	0.720
50	284.675 (2.700)	.780
75	298.908 (2.835)	.770
125	388.739 (3.687)	.810
175	492.442 (4.718)	.850
225	629.342 (5.969)	.870
Spec.	515.999 (4.894)	.900

[a]The numerator contains the difference between inlet and exit temperature for the one of the two fluids for which this difference is larger. The denominator contains the difference between the two inlet temperatures. In addition, ϵ is always taken as positive.

TABLE X.—Concluded

(e) WMS heater

Engine load, kW	Total heat transfer, MJh (Btuh)	Thermal effectiveness ϵ, $\frac{[a](t_i - t_e)_l}{t_{1i} - t_{2i}}$
50	40.803 (0.387 ×10^5)	0.900
75	40.803 (.387)	.910
100	37.851 (.359)	.950
150	37.535 (.356)	.920
200	36.586 (.347)	.930
225	42.596 (.404)	.950
Spec.	74.648 (.708)	.45

(f) Freshwater heater

Heating load, MJh (Btuh)	Total heat transfer, MJh (Btuh)	Thermal effectiveness ϵ, $\frac{[a](t_i - t_e)_l}{t_{1i} - t_{2i}}$
105.4 (100 000)	53.877 (0.511 ×10^5)	0.480
210.9 (200 000)	52.507 (.498)	.590
316.3 (300 000)	51.663 (.490)	.640
421.8 (400 000)	48.289 (.458)	.680
527.2 (500 000)	35.742 (.339)	.700
Spec.	163.108 (1.547)	.64

(g) Freshwater preheater

Engine load, kW	Total heat transfer, MJh (Btuh)	Thermal effectiveness ϵ, $\frac{[a](t_i - t_e)_l}{t_{1i} - t_{2i}}$
50	67.689 (0.642 ×10^5)	0.740
75	70.958 (.673)	.790
100	69.060 (.655)	.730
150	69.587 (.660)	.720
200	70.536 (.669)	.770
225	72.223 (.685)	.700
Spec.	118.087 (1.120)	.940

(h) Water sterilization heat exchanger

Steam pressure, kPa (psig)	Total heat transfer, MJh (Btuh)	Thermal effectiveness ϵ, $\frac{[a](t_i - t_e)_l}{t_{1i} - t_{2i}}$
110.3 (16)	146.660 (1.391 ×10^5)	(b)
89.6 (13)	127.682 (1.211)	(b)
75.8 (11)	108.914 (1.033)	(b)
62.1 (9)	100.585 (.954)	(b)
48.3 (7)	92.256 (.875)	(b)
Spec.	54.299 (.515)	(b)

[a]The numerator contains the difference between inlet and exit temperature for the one of the two fluids for which this difference is larger. The denominator contains the difference between the two inlet temperatures. In addition, ϵ is always taken as positive.

[b]Data not recorded.

TABLE XI.—Water Management Subsystem Tests

Test program	Completion status	Remarks
Independent physical-chemical	Partially completed	
Iron salt coagulant	Completed	Alum replaced iron because of unavailability of ferric chloride
Lime	Not completed	Lack of liming equipment and recarbonation
Reverse osmosis	Completed	
Biological-tertiary	Completed	
302.59 K (85° F)		
310.93 K (100° F)		
Hydraulic overload	Completed	Biological overload substituted; hydraulic overload could not be achieved because of pump flow limitations
Biological-system poisoning	Completed	Excess alum added
Sludge train	Not completed	Inadequate sludge conditioning equipment

TABLE XII.—Physical-Chemical Test Results[a]

[Coagulant dose: average alum, 195 mg/liter]

Test parameter	Influent, p/m, at temperature -		Effluent, p/m, at temperature -		Reduction, percent, at temperature -	
	A[b]	B[c]	A[b]	B[c]	A[b]	B[c]
BOD	135	206	6.5	11.9	95.2	94.2
Ammonia	18.5	26.7	15.0	14.7	18.9	44.9
Suspended solids	255	223	6.0	5.4	97.6	97.6
Turbidity	—	159	—	15	—	90.6
Phosphorus	6.5	4.4	.14	.2	97.8	95.5

[a]pH, unchanged, total dissolved solids, unchanged, sludge solids concentrate, 0.24 percent

[b]Temperature A = 302.59 K (85° F)

[c]Temperature B = 310.93 K (100° F)

TABLE XIII.—Reverse-Osmosis Test Results

Test Parameter	Influent	Effluent
Chloride,[a] p/m	137	13
pH	7.2	6.0
Suspended solids, p/m	3.1	< 1
Turbidity, p/m	10	< 5
Sodium,[b] p/m	154	14.6
Total dissolved solids,[c] p/m	655	46
BOD,[d] p/m	3.5	0.9
Conductance,[e] μmho/cm	920	101

[a]Reduction, 90.5 percent.

[b]Reduction, 90.5 percent.

[c]Reduction, 93.0 percent.

[d]Reduction, 74.3 percent.

[e]Reduction, 89.0 percent.

TABLE XIV.—Biological-Physical-Chemical Test Results (Temperature Effects)

Test parameter	Raw or primary	Bio-Surf						Denitrifier				Physical-chemical				
		In	1st	2d	3d	4th	Out	1st	2d	3d	4th	In	Clarifier	Carbon	Chlorine	Out
Controlled temperature (302.59 and 310.93 K (85° and 100° F))																
BOD, p/m	94	—	—	—	—	—	29	—	—	—	—	29	—	—	—	5
Ammonia, p/m	15.5	12.5	7.0	4.4	2.3	1.8	1.4	—	—	—	—	1.2	0.8	—	—	0.9
Nitrate, p/m	0.5	0.5	5.3	11.0	12.0	13.0	15.9	—	—	—	—	—	—	—	—	8.5
Suspended solids, p/m	80	81	—	—	—	—	21	—	—	—	—	9	—	—	—	2.6
Turbidity, p/m	80	65	—	—	—	—	40	—	—	—	—	—	—	—	—	20
Phosphorus, p/m	3.5	2.9	3.1	2.6	2.8	2.9	2.8	—	—	—	—	2.8	<0.1	—	—	<0.1
Random temperature ≈294 K (≈70° F))																
BOD, p/m	—	93	—	—	—	—	22	—	—	—	—	—	5	3.7	4.1	3.5
COD, p/m	—	156	—	—	—	—	60	—	—	—	—	—	15	20	—	—
Ammonia, p/m	—	16.6	10.6	5.3	3.2	3.3	—	—	—	—	—	—	—	—	—	2.6
Suspended solids, p/m	—	147	—	—	—	—	27	—	—	—	—	—	4.0	6.0	6.0	4.8
Turbidity, p/m	—	90	—	—	—	—	27	—	—	—	—	—	—	—	—	9.0
Phosphorus, p/m	—	3.9	—	—	—	—	2.1	—	—	—	—	—	—	—	—	<0.1
Dissolved oxygen, p/m	—	1.3	1.6	2.5	4.5	6.1	5.7	3.4	2.4	2.0	1.9	—	1.9	7.2	—	8.6
Sludge solids, percent	—	—	—	—	—	—	0.43	—	—	—	—	—	—	—	—	—

TABLE XV.—Biological-Physical-Chemical-Overload Test Results

[Values in parts per million]

Test parameter	Raw or primary	Bio-Surf						Denitrifier				Physical-chemical				
		In	1st	2d	3d	4th	Out	1st	2d	3d	4th	IN	Clarifier	Carbon	Chlorine	Out
Overload 1																
BOD	40	47	—	—	—	—	13	—	—	—	—	—	—	—	—	7.2
COD	146	233	—	—	—	—	47	—	—	—	—	—	28	—	—	31
Ammonia	9.0	8.2	3.3	1.1	0.5	0.4	.5	—	—	—	—	—	—	—	—	.4
Nitrate	.5	1.9	6.0	5.5	6.1	5.6	6.0	2.3	0.8	0.3	0.2	—	4.2	—	—	4.3
Suspended solids	80	277	—	—	—	—	30	—	—	—	—	—	—	—	—	7.8
Turbidity	80	131	—	—	—	—	32	—	—	—	—	—	—	—	—	9
Phosphorus	6.5	6.7	—	—	—	—	1.6	—	—	—	—	—	—	—	—	.05
Overload 2																
BOD	—	50	—	—	—	—	9	—	—	—	—	—	—	—	—	7.6
COD	—	441	—	—	—	—	74	—	—	—	—	—	46	—	—	12.5
Ammonia	—	18.1	12.0	6.8	3.2	1.9	1.6	—	—	—	—	—	—	—	—	.6
Nitrate	—	1.8	6.0	6.2	7.0	9.5	12.1	2.0	0.5	0.2	0.2	—	3.5	—	—	5.3
Suspended solids	—	303	—	—	—	—	40	—	—	—	—	—	—	—	—	7.2
Turbidity	—	227	—	—	—	—	65	—	—	—	—	—	—	—	—	5
Phosphorus	—	6.6	—	—	—	—	2.8	—	—	—	—	—	—	—	—	.05

TABLE XVI.—Engineering-Unit Conversion Table Based on Thermoelectric Curve

[Constantan thermocouple]

(a) Hot water (355.37 K (180° F)) (sensors T-45 and T-49)

Electromotive force, mV	Differential temperature, K (°F), corresponding to potential difference of -									
	0.000 mV	0.01 mV	0.02 mV	0.03 mV	0.04 mV	0.05 mV	0.06 mV	0.07 mV	0.08 mV	0.09 mV
0.0	0 (0)	0.22 (0.4)	0.44 (0.8)	0.67 (1.2)	0.94 (1.7)	1.17 (2.1)	1.39 (2.5)	1.61 (2.9)	1.83 (3.3)	2.06 (3.7)
.1	2.33 (4.2)	2.56 (4.6)	2.78 (5.0)	3.0 (5.4)	3.22 (5.8)	3.44 (6.2)	3.61 (6.5)	3.83 (6.9)	4.06 (7.3)	4.28 (7.7)
.2	4.5 (8.1)	4.72 (8.5)	4.89 (8.8)	5.11 (9.2)	5.33 (9.6)	5.56 (10.0)	5.78 (10.4)	6.0 (10.8)	6.22 (11.2)	6.5 (11.7)
.3	6.72 (12.1)	6.94 (12.5)	7.17 (12.9)	7.39 (13.3)	7.61 (13.7)	7.89 (14.2)	8.11 (14.6)	8.33 (15.0)	8.56 (15.4)	8.78 (15.8)
.4	9.0 (16.2)	9.17 (16.5)	9.39 (16.9)	9.61 (17.3)	9.83 (17.7)	10.06 (18.1)	10.28 (18.5)	10.44 (18.8)	10.67 (19.2)	10.89 (19.6)
.5	11.11 (20.0)	11.33 (20.4)	11.56 (20.8)	11.78 (21.2)	12.06 (21.7)	12.28 (22.1)	12.5 (22.5)	12.72 (22.9)	12.94 (23.3)	13.17 (23.7)
.6	13.44 (24.2)	13.67 (24.6)	13.89 (25.0)	14.11 (25.4)	14.33 (25.8)	14.56 (26.2)	14.83 (26.7)	15.06 (27.1)	15.28 (27.5)	15.5 (27.9)
.7	15.72 (28.3)	15.94 (28.7)	16.22 (29.2)	16.44 (29.6)	16.67 (30.0)	16.89 (30.4)	17.11 (30.8)	17.33 (31.2)	17.56 (31.6)	17.83 (32.1)
.8	18.06 (32.5)	18.28 (32.9)	18.5 (33.3)	18.72 (33.7)	19.0 (34.2)	19.22 (34.6)	19.44 (35.0)	19.67 (35.4)	19.89 (35.8)	20.11 (36.2)
.9	20.28 (36.5)	20.5 (36.9)	20.72 (37.3)	20.94 (37.7)	21.17 (38.1)	21.39 (38.5)	21.56 (38.8)	21.78 (39.2)	22.0 (39.6)	22.22 (40.0)

(b) Cold water (280.37 K (45° F)) (sensors T-48 and T-50)

Electromotive force, mV	Differential temperature, K (°F), corresponding to potential difference of -									
	0.00 mV	0.01 mV	0.02 mV	0.03 mV	0.04 mV	0.05 mV	0.06 mV	0.07 mV	0.08 mV	0.09 mV
0.0	0 (0)	0.28 (0.5)	0.56 (1.0)	0.83 (1.5)	1.11 (2.0)	1.39 (2.5)	1.67 (3.0)	1.94 (3.5)	2.22 (4.0)	2.5 (4.5)
.1	2.78 (5.0)	3.0 (5.4)	3.28 (5.9)	3.56 (6.4)	3.78 (6.8)	4.06 (7.3)	4.28 (7.7)	4.56 (8.2)	4.78 (8.6)	5.06 (9.1)
.2	5.28 (9.5)	5.56 (10.0)	5.78 (10.4)	6.06 (10.9)	6.33 (11.4)	6.56 (11.8)	6.83 (12.3)	7.06 (12.7)	7.33 (13.2)	7.56 (13.6)
.3	7.83 (14.1)	8.06 (14.5)	8.33 (15.0)	8.56 (15.4)	8.83 (15.9)	9.11 (16.4)	9.33 (16.8)	9.61 (17.3)	9.83 (17.7)	10.11 (18.2)
.4	10.33 (18.6)	10.61 (19.1)	10.83 (19.5)	11.11 (20.0)	11.33 (20.4)	11.61 (20.9)	11.89 (21.4)	12.11 (21.8)	12.39 (22.3)	12.61 (22.7)
.5	12.89 (23.2)	13.11 (23.6)	13.39 (24.1)	13.61 (24.5)	13.89 (25.0)	14.11 (25.4)	14.39 (25.9)	14.67 (26.4)	14.89 (26.8)	15.17 (27.3)
.6	15.39 (27.7)	15.67 (28.2)	15.89 (28.6)	16.17 (29.1)	16.39 (29.5)	16.67 (30.0)	16.89 (30.4)	17.17 (30.9)	17.44 (31.4)	17.67 (31.8)
.7	17.94 (32.3)	18.17 (32.7)	18.44 (33.2)	18.67 (33.6)	18.94 (34.1)	19.17 (34.5)	19.44 (35.0)	19.67 (35.4)	19.89 (35.8)	20.11 (36.2)
.8	20.28 (36.5)	20.5 (36.9)	20.72 (37.3)	20.94 (37.7)	21.17 (38.1)	21.39 (38.5)	21.56 (38.8)	21.78 (39.2)	22.0 (39.6)	22.22 (40.0)

TABLE XVII.—Processed Data (Example)

TAB GROUP NO.- 5 MIST BANDPASS TABS HACS1D1,4,3,1,6,STEP4-46,MKED

DAY	HR	MIN	SECS	JACKET WATER INTERCHANGER OUT T06 DEG F 025 CNT BND DATA	EXHAUST SILENCER HX FEED WATER T07 DEG F 025 CNT BND DATA	AUXILIARY HX HEATING WATER IN T09 DEG F 025 CNT BND DATA	WMS HX SEWAGE IN T10 DEG F 025 CNT BND DATA	WMS HX SEWAGE OUT T11 DEG F 025 CNT BND DATA	INCINERATOR HX FEED WATER T12 DEG F 025 CNT BND DATA
283	7	10	.000	91.4	129.4	142.8	73.7	74.7	139.1
283	7	11	.000			150.8			
283	7	13	.000						138.0
283	7	14	.000		133.3	157.9			
283	7	16	.000		130.0			76.2	
283	7	17	.000		132.5	155.5	75.0		
283	7	19	.000		134.9	157.4			136.8
283	7	21	.000		136.0	158.4		77.4	
283	7	22	.000			159.9			
283	7	24	.000			161.5			
283	7	25	.000				76.5		
283	7	27	.000					78.7	135.4
283	7	28	.000		137.1	163.1			
283	7	30	.000		134.7		74.6	76.5	132.8
283	7	31	.000			165.1			
283	7	33	.000	90.3		163.5			131.3
283	7	34	.000			165.4			
283	7	39	.000				75.7	77.9	
283	7	41	.000			166.4			
283	7	42	.000						129.9
283	7	44	.000		133.5	167.6			
283	7	45	.000		132.2			79.1	
283	7	47	.000		130.6		77.0		
283	7	48	.000		129.3	169.1			
283	7	50	.000		128.1				
283	7	52	.000		124.2		75.0	77.4	127.3
1	7	53	.000		122.4				
1	7	55	.000		121.2				
283	7	58	.000		119.2				
283	8	1	.000		117.3		76.3	78.8	
283	8	2	.000	89.1					
283	8	4	.000		115.3				
283	8	5	.000			170.4			
283	8	7	.000		113.9			79.9	
283	8	9	.000				77.6		
283	8	10	.000		112.4				
283	8	13	.000		108.5		75.6	78.2	125.1
283	8	15	.000		107.4				
283	8	18	.000		106.2				
283	8	19	.000						124.0
283	8	21	.000					79.3	
283	8	23	.000		104.9		76.8		
283	8	26	.000						122.6
283	8	27	.000		103.7			80.5	
283	8	30	.000				78.1		121.1
283	8	32	.000		102.5				

TABLE XVIII.—Specific Engine-Heat-Recovery Rates, Ebullient-Cooling Mode[a]

Engine load, kW	*Heat-recovery rate kW (Btu/hr)*	*Test time, hr*	*Specific heat-recovery rate*[b]*, J/J (Btu/kWh)*	*Specific heat-rejection rate*[c]*, J/J (Btu/kWh)*
41	42.7 (145 873)	25.07	1042×10^{-3} (3558)	598×10^{-3} (2042)
57	52.6(179 462)	26.35	922 (3148)	554 (1893)
95	83.0(283 355)	22.67	873 (2983)	429 (1466)
107	100.1(341 917)	27.70	936 (3196)	394 (1345)
122	132.4(452 023)	14.3	1085 (3705)	326 (1112)

[a]Summary data from engine-only tests (incinerator not operational).

[b]High-grade heat.

[c]Low-grade heat.

TABLE XIX.—Space-Heating Test Results

Engine load, kW	Incinerator status and value, on/off, MJ(Btu)	Thermal storage status and value, charge/discharge, MJ (Btu)	Test setting, MJh (Btuh)	Actual heat load, MJh (Btuh)	Oil aftercooler heat rejection, MJh (Btuh)	Specific oil heat-rejection rate, J/J (Btu/kWh)	High-grade-heat heat recovery rate, MJh (Btuh)	Specific high-grade-heat recovery rate, J/J (Btu/kWh)
Test series 1A-1, ebullient mode								
41	Off	Charge						
		18.8 (17 792)	52.7 (50 000)	115.6 (109 680)	86.1 (81 640)	583×10^{-3} (1991)	152.3 (144 450)	1032×10^{-3} (3523)
	Off	Discharge						
		167.1 (158 517)	263.6 (250 000)	296.5 (281 220)	86.8 (82 320)	588 (2008)	147.2 (139 580)	997 (3404)
	Off	Charge						
		26.3 (24 952)	105.4 (100 000)	112.3 (106 500)	78.6 (74 575)	533 (1819)	158.5 (150 307)	1073 (3666)
	Off	Discharge						
		122.5 (116 162)	210.9 (200 000)	241.3 (228 900)	87.9 (83 370)	595 (2033)	162.0 (153 665)	1097 (3748)
	Off	Off	52.7 (50 000)	55.4 (52 550)	102.0 (96 720)	691 (2359)	149.0 (141 365)	1010 (3448)
			38.0 (36 024)	12.6 (11 947)				
Test series 1A-2, ebullient mode								
41	On	Charge						
	209.9 (199 090)	266.3 (252 561)	52.7 (50 000)	60.5 (57 420)	119.2 (113 100)	808×10^{-3} (2759)	356.5 (338 117)	2415×10^{-3} (8248)
	On	Discharge						
	225.4 (213 822)	141.6 (134 259)	421.7 (400 000)	471.4 (447 120)	120.6 (114 405)	817 (2790)	375.5 (356 178)	2544 (8687)
	On	Charge						
	193.2 (183 196)	229.7 (217 893)	105.4 (100 000)	112.1 (106 340)	124.3 (117 900)	842 (2876)	372.9 (353 666)	2526 (8626)
	On	Discharge						
	237.8 (225 584)	80.0 (75 859)	369.0 (350 000)	405.7 (384 800)	102.0 (96 738)	691 (2359)	370.4 (351 265)	2508 (8567)
	On	Charge						
	234.3 (222 247)	137.9 (130 812)	210.9 (200 000)	213.2 (202 208)	123.2 (116 870)	834 (2850)	366.8 (347 930)	2485 (8486)
Test series 1B-1, ebullient mode								
57	Off	Charge						
		108.8 (103 199)	52.7 (50 000)	57.4 (54 470)	109.1 (103 487)	532×10^{-3} (1816)	190.7 (180 883)	929×10^{-3} (3173)
	Off	Discharge						
		206.5 (195 812)	316.3 (300 000)	357.7 (339 300)	107.5 (101 978)	524 (1789)	190.5 (180 695)	928 (3170)
	Off	Charge						
		0	158.2 (150 000)	166.0 (157 425)	112.4 (106 564)	548 (1870)	188.7 (178 936)	919 (3139)
	Off	Discharge						
		167.5 (158 889)	263.6 (250 000)	306.7 (290 925)	126.1 (119 580)	614 (2097)	187.0 (177 333)	911 (3111)

TABLE XIX.—Continued

Engine load, kW	*Incinerator status and value, on/off, MJ (Btu)*	*Thermal storage status and value, charge/discharge, MJ (Btu)*	*Test setting, MJh (Btuh)*	*Actual heat load, MJh (Btuh)*	*Oil aftercooler heat rejection, MJh (Btuh)*	*Specific oil heat-rejection rate, J/J (Btu/kWh)*	*High-grade-heat heat recovery rate, MJh (Btuh)*	*Specific high-grade-heat recovery rate, J/J (Btu/kWh)*
Test series IC-1, ebullient mode								
95	Off 180.3 (171 045)	Charge	52.7 (50 000)	63.0 (59 760)	145.9 (138 420)	427×10^{-3} (1457)	308.3 (292 365)	901×10^{-3} (3077)
	Off 235.6 (223 474)	Discharge	421.7 (400 000)	460.5 (436 720)	145.9 (138 348)	426 (1456)	285.9 (271 160)	836 (2854)
	Off 62.1 (58 853)	Charge	158.2 (150 000)	186.8 (177 205)	141.2 (133 959)	413 (1410)	288.1 (273 288)	842 (2877)
	Off 61.3 (58 158)	Discharge	316.3 (300 000)	292.2 (277 120)	154.2 (146 231)	451 (1539)	312.7 (296 607)	914 (3122)
Test series ID-1, ebullient mode								
107	Off 198.0 (187 809)	Charge	105.4 (100 000)	105.3 (99 840)	164.3 (155 805)	426×10^{-3} (1456)	347.8 (329 836)	903×10^{-3} (3083)
	Off 61.5 (58 301)	Charge	210.9 (200 000)	238.1 (225 780)	160.3 (152 057)	416 (1421)	362.1 (343 463)	940 (3210)
	Off 25.0 (23 683)	Charge	263.6 (250 000)	268.6 (254 760)	136.1 (129 114)	353 (1207)	350.8 (332 754)	911 (3110)
	Off 199.3 (189 005)	Discharge	421.8 (400 000)	479.7 (454 920)	146.3 (138 783)	380 (1297)	381.3 (361 614)	990 (3380)
Test series ID-2, ebullient mode								
107	On 155.9 (147 907)	Charge	105.4 (100 000)	127.7 (121 125)	152.2 (144 328)	395×10^{-3} (1348)	565.7 (536 551)	1468×10^{-3} (5014)
	On 144.6 (137 167)	Charge	263.6 (250 000)	343.2 (325 518)	136.3 (129 297)	346 (1180)	587.8 (557 468)	1525 (5210)
	On 180.1 (170 785)	Charge	369.0 (350 000)	419.1 (397 440)	131.9 (125 120)	342 (1169)	607.0 (575 694)	1575 (5380)

TABLE XIX.—Concluded

Engine load, kW	*Incinerator status and value, on/off, MJ(Btu)*	*Thermal storage status and value, charge/discharge, MJ (Btu)*	*Test setting, MJh (Btuh)*	*Actual heat load, MJh (Btuh)*	*Oil aftercooler heat rejection, MJh (Btuh)*	*Specific oil heat-rejection rate, J/J (Btu/kWh)*	*High-grade-heat heat recovery rate, MJh (Btuh)*	*Specific high-grade-heat recovery rate, J/J (Btu/kWh)*
Test series IE-1, ebullient mode								
122	Off	Charge 26.6 (25 247)	316.3 (300 000)	355.8 (377 472)	148.7 (140 996)	338×10^{-3} (1156)	476.0 (451 418)	1083×10^{-3} (3700)
	Off	Charge 143.0 (135 606)	158.2 (150 000)	176.7 (167 638)	137.2 (130 139)	312 (1067)	477.2 (452 627)	1086 (3710)
Test series IE-2, ebullient mode								
122	On 184.1 (174 600)	Charge 396.9 (376 439)	158.2 (150 000)	180.2 (170 910)	124.4 (118 000)	2832×10^{-3} (9673)	670.1 (635 528)	1525×10^{-3} (5209)
	On 170.0 (161 221)	Charge 347.1 (329 174)	210.9 (200 000)	233.7 (221 676)	131.2 (124 400)	299 (1020)	626.9 (595 601)	1427 (4874)
	On 146.7 (139 151)	Charge 184.7 (175 218)	369.0 (350 000)	420.5 (398 860)	139.5 (132 321)	318 (1085)	697.7 (661 699)	1588 (5424)

TABLE XX.—Space-Cooling Test Results

Engine load, kW	Incinerator status	Test setting, kW (tons)	Actual cooling load, kW (tons)	Absorption chiller load, kW (tons)	Compression chiller load, kW (tons)	Floating-split ratio, absorption/ compression percentages
Test series IA-1, ebullient mode						
41	Off	105.5 (30)	34.64 (9.85)	16.14 (4.59)	18.50 (5.26)	46.6/53.4
	Off	35.2 (10)	47.41 (13.48)	15.72 (4.47)	31.69 (9.01)	33.0/67.0
	Off	70.3 (20)	71.04 (20.20)	27.78 (7.90)	43.26 (12.30)	39.1/60.9
Test series IA-2, ebullient mode						
41	On	105.5 (30)	131.04 (37.26)	85.07 (24.19)	45.96 (13.07)	65.0/35.0
	On	87.9 (25)	110.71 (31.48)	95.16 (27.06)	15.54 (4.42)	86.0/14.0
Test series IB-1, ebullient mode						
57	Off	35.2 (10)	52.47 (14.92)	22.19 (6.31)	30.28 (8.61)	42.3/57.7
	Off	87.9 (25)	101.46 (28.85)	33.97 (9.66)	67.49 (19.19)	33.5/66.5
	Off	52.8 (15)	47.51 (13.51)	29.05 (8.26)	18.46 (5.25)	61.1/38.9
Test series IC-1, ebullient mode						
95	Off	70.3 (20)	70.37 (20.01)	35.77 (10.17)	34.61 (9.84)	50.8/49.2
	Off	105.5 (30)	132.86 (37.78)	55.00 (15.64)	77.86 (22.14)	41.4/58.6
	Off	52.8 (15)	53.24 (15.14)	44.73 (12.72)	8.51 (2.42)	84.0/16.0
Test Series ID-2, ebullient mode						
107	On	140.7 (40)	167.19 (47.54)	85.07 (24.19)	82.12 (23.35)	50.9/49.1
	On	12.31 (35)	129.42 (36.80)	70.41 (20.02)	59.01 (16.78)	54.4/45.6
Test series IE-2, ebullient mode						
122	On	140.7 (40)	136.42 (38.79)	72.73 (20.68)	63.69 (18.11)	53.3/36.7
	On	105.5 (30)	137.23 (39.02)	69.21 (19.68)	68.01 (19.34)	50.4/49.6
	On	105.5 (30)	118.48 (33.69)	51.03 (14.51)	67.45 (19.18)	43.1/56.9
	On	70.3 (20)	72.73 (20.68)	72.73 (20.68)	0 (0)	100.0/0

TABLE XXI.—Integrated Test Matrix

Test no.	*Season/test condition*	*MIST configuration*
IIA-1	Design summer day	Thermal storage
IIA-2	Design summer day	No thermal storage
IIB-1	Design winter day	Thermal storage
IIB-2	Design winter day	No thermal storage
IIC-1	Average spring/fall day/ domestic-hot-water heating	Thermal storage

TABLE XXII.—Series I Test Conditions

Test no.	*Engine load, kW*	*Incinerator status*
IA-1	41	Off
IA-2	41	On
IB-1	57	Off
IC-1	95	Off
ID-1	107	Off
ID-2	107	On
IE-1	122	Off
IE-2	122	On

TABLE XXIII.—Test IIA-1 Performance Summary

[Summer design day with thermal storage]

Electricity generated, MJ (kWh)	10 962.0 (3045)
Air-conditioning, MJ (ton-hr)	[a]10 470.2 (827)
Absorption, MJ (ton-hr)	5 355.4 (423)
Compression, MJ (ton-hr)	5 114.8 (404)
Space heating, MJ (Btu)	0 (0)
Trash incinerated (equivalent), kg (lb)	190.5 (420)
Potable water heated, m^3 (gal)	12.1 (3184)
Wastewater treated, m^3 (gal)	32.7 (8640)
Fuel consumed, m^3 (gal)	1.0 (261)
Peak electrical demand, kW	178
Equivalent energy service (electricity and heat used), MJ (Btu)	24 251.2 (23×10^6)
Plant efficiency, percent	65

[a]Excess cooling of 88.6 megajoules (7 ton-hours) was produced and remained in the storage tank at the end of the test.

TABLE XXIV.—Test IIA-2 Performance Summary

[Summer design day without thermal storage]

Electricity generated, MJ (kWh)	11 008.8 (3058)
Air-conditioning, MJ (ton-hr)	10 457.6 (826)
Absorption, MJ (ton-hr)	5 545.3 (438)
Compression, MJ (ton-hr)	4 912.3 (388)
Space heating, MJ (Btu)	0 (0)
Trash incinerated (equivalent)	Not applicable
Potable water heated, m^3 (gal)	12.0 (3182)
Wastewater treated, m^3 (gal)	32.0 (8460)
Fuel consumed, m^3 (gal)	1.0 (264)
Peak electrical demand, kW	177
Equivalent energy service (electricity and heat used), MJ (Btu)	24 251.2 (23×10^6)
Plant efficiency, percent	65

TABLE XXV.—Test IIB-1 Performance Summary

[Winter design day with thermal storage]

Electricity generated, MJ (kWh)	7 837.2 (2177)
Air-conditioning, MJ (ton-hr)	0 (0)
Absorption, MJ (ton-hr)	0 (0)
Compression, MJ (ton-hr)	0 (0)
Space heating, MJ (Btu)	8 719.89 (8.27×10^6)
Trash incinerated (equivalent), kg (lb)	190.5 (420)
Potable water heated, m^3 (gal)	12.0 (3182)
Wastewater treated, m^3 (gal)	32.7 (8640)
Fuel consumed, m^3 (gal)	0.8 (220)
Peak electrical demand, kW	136
Equivalent energy service (electricity and heat used), MJ (Btu)	20 486.99 (19.43×10^6)
Plant efficiency, percent	65.4

TABLE XXVI.—Test IIB-2 Performance Summary

[Winter design day without thermal storage]

Electricity generated, MJ (kWh)	7 473.6 (2076)
Air-conditioning, MJ (ton-hr)	0 (0)
Absorption, MJ (ton-hr)	0 (0)
Compression, MJ (ton-hr)	0 (0)
Space heating, MJ (Btu)	8 519.55 (8.08×10^6)
Trash incinerated (equivalent), kg (lb)	381.0 (840)
Potable water heated, m^3 (gal)	12.0 (3182)
Wastewater treated, m^3 (gal)	32.7 (8640)
Fuel consumed, m^3 (gal)	0.9 (240.1)
Peak electrical load, kW	140
Equivalent energy service (electricity and heat used), MJ (Btu)	19 601.30 (18.59×10^6)
Plant efficiency, percent	57.4

TABLE XXVII.—Test IIC-1 Performance Summary

[Spring/fall average day with thermal storage]

Electricity generated, MJ (kWh)	7 984.8 (2218)
Air-conditioning, MJ (ton-hr)	1 228.1 (97)
Absorption, MJ (ton-hr)	1 228.1 (97)
Compression, MJ (ton-hr)	0 (0)
Space heating, MJ (Btu)	369.04 (0.35×10^6)
Trash incinerated (equivalent), kg (lb)	0 (0)
Potable water heated, m^3 (gal)	12.0 (3182)
Wastewater treated, m^3 (gal)	32.7 (8640)
Fuel consumed, m^3 (gal)	0.7 (192)
Peak electrical demand, kW	150
Equivalent energy service (electricity and heat used), MJ(Btu)	17 292.2 (16.4×10^6)
Plant efficiency, percent	63

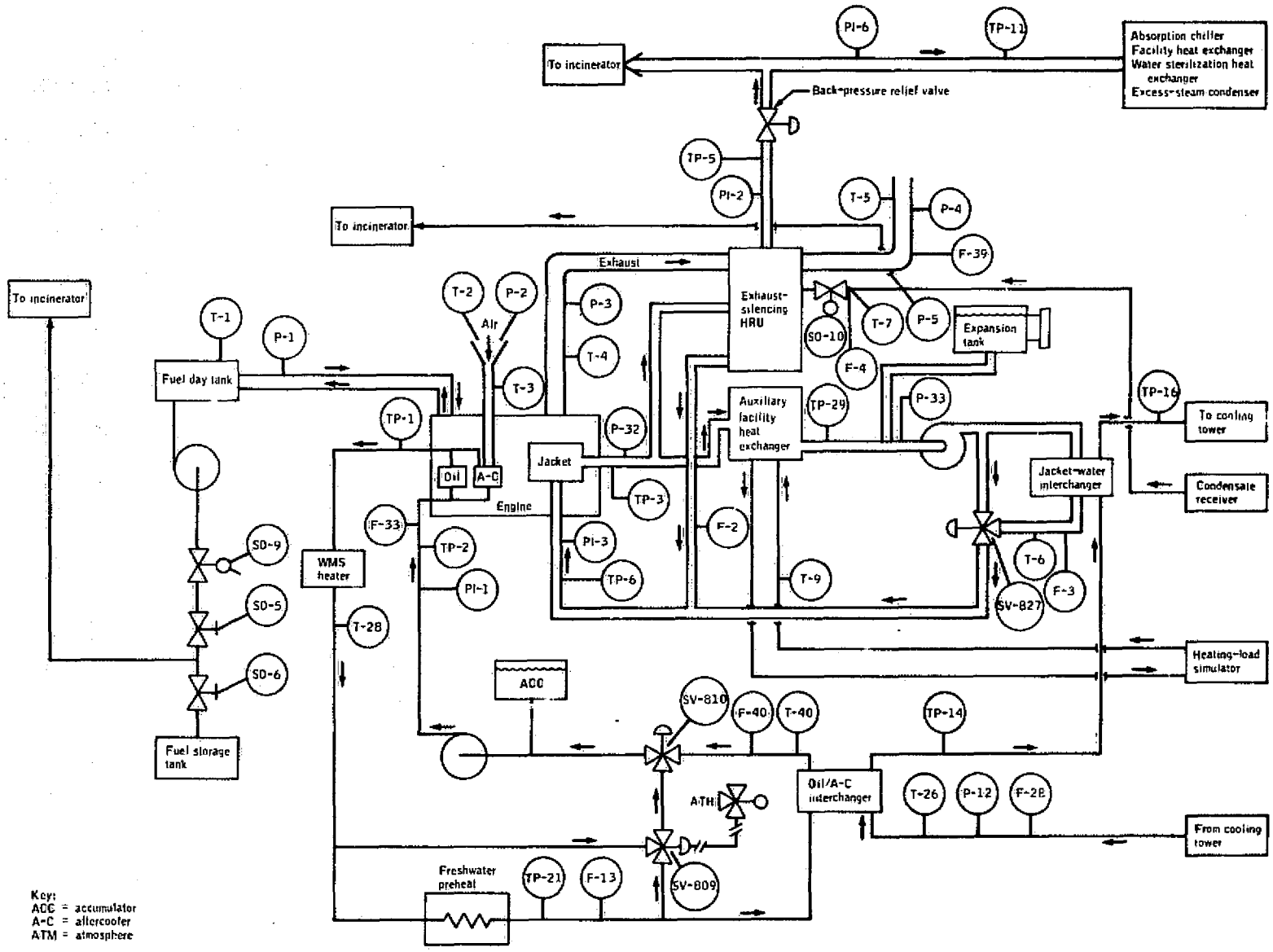

Figure 1.—The MIST power generation subsystem.

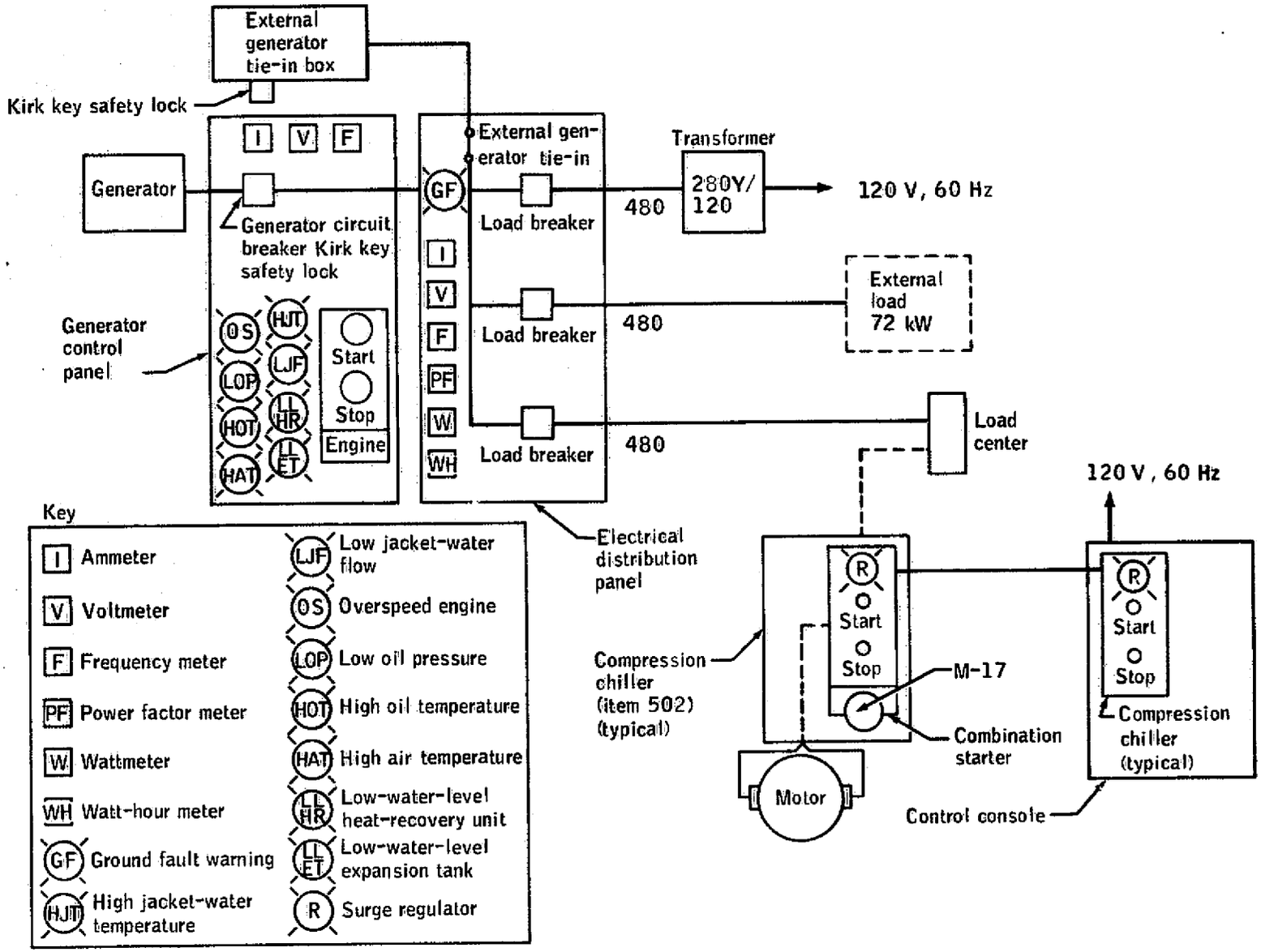

Figure 2.—Power distribution simplified block diagram.

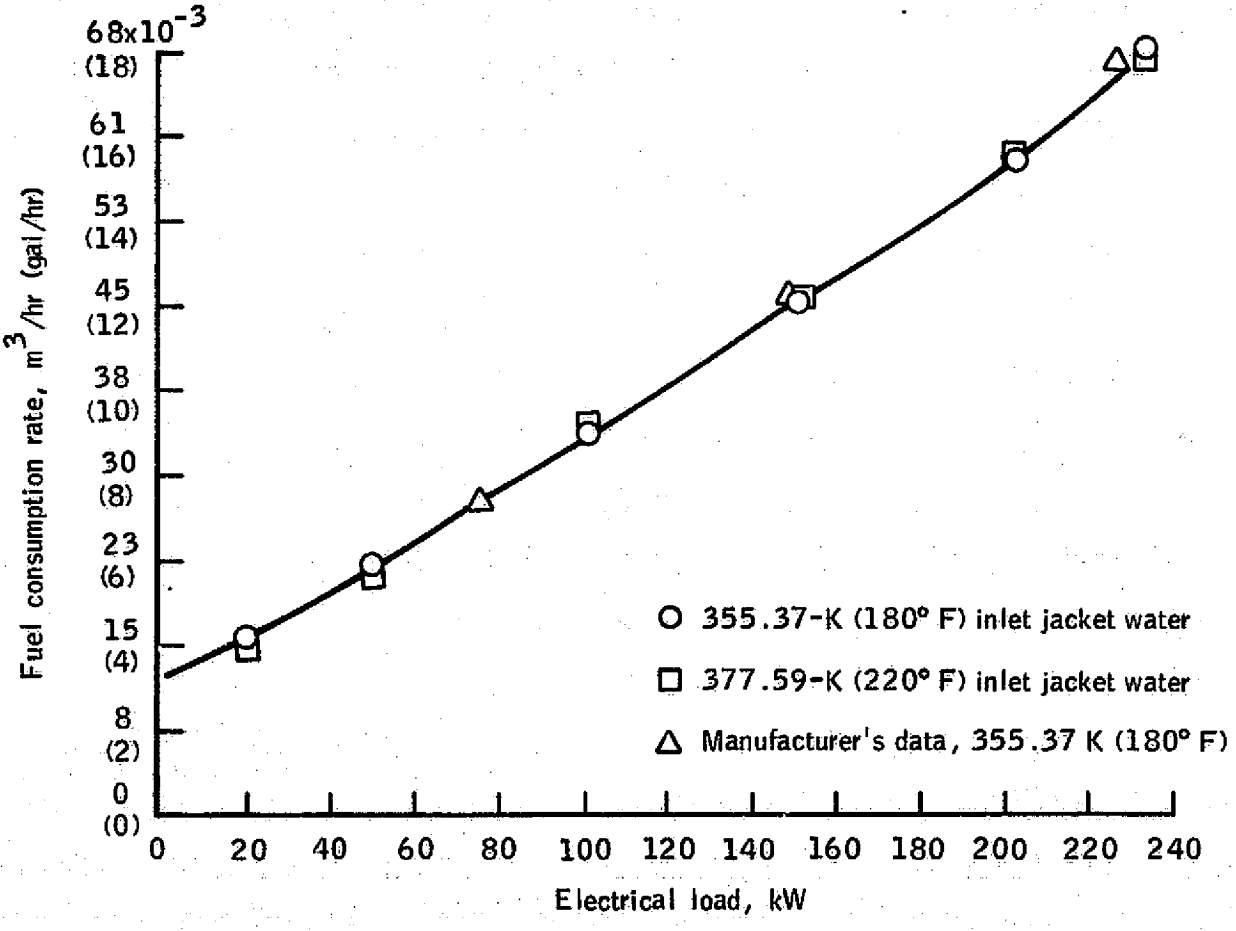

Figure 3.—Fuel consumption rate as a function of electrical load—forced-circulation-cooling mode (0.6 m^3/min (160 gal/min)).

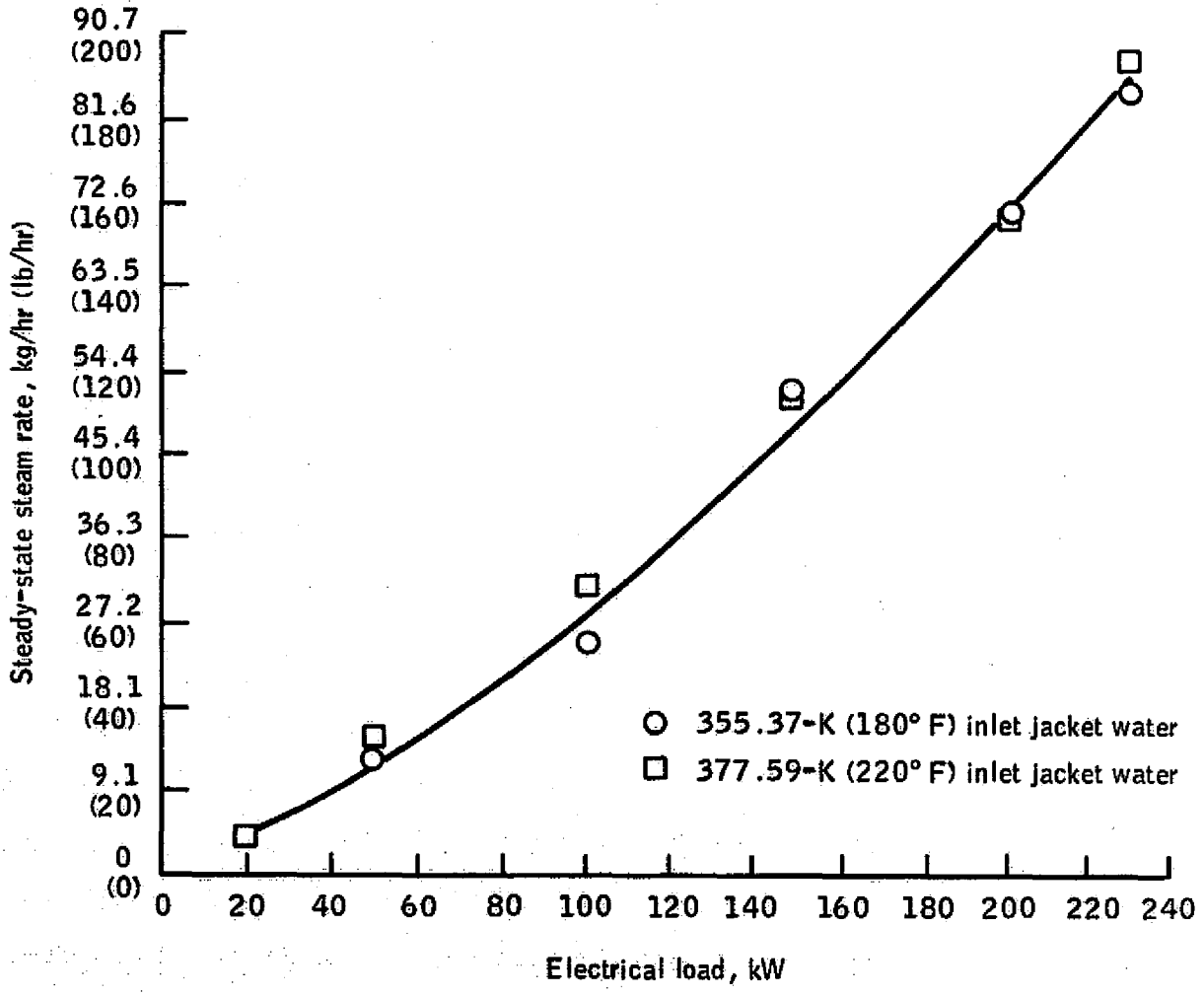

Figure 4.—Steady-state steam rate (103 $\times$ 10^3 pascals (15 psig)) as a function of electrical load—forced-circulation-cooling mode (0.6 m^3/min (160 gal/min)).

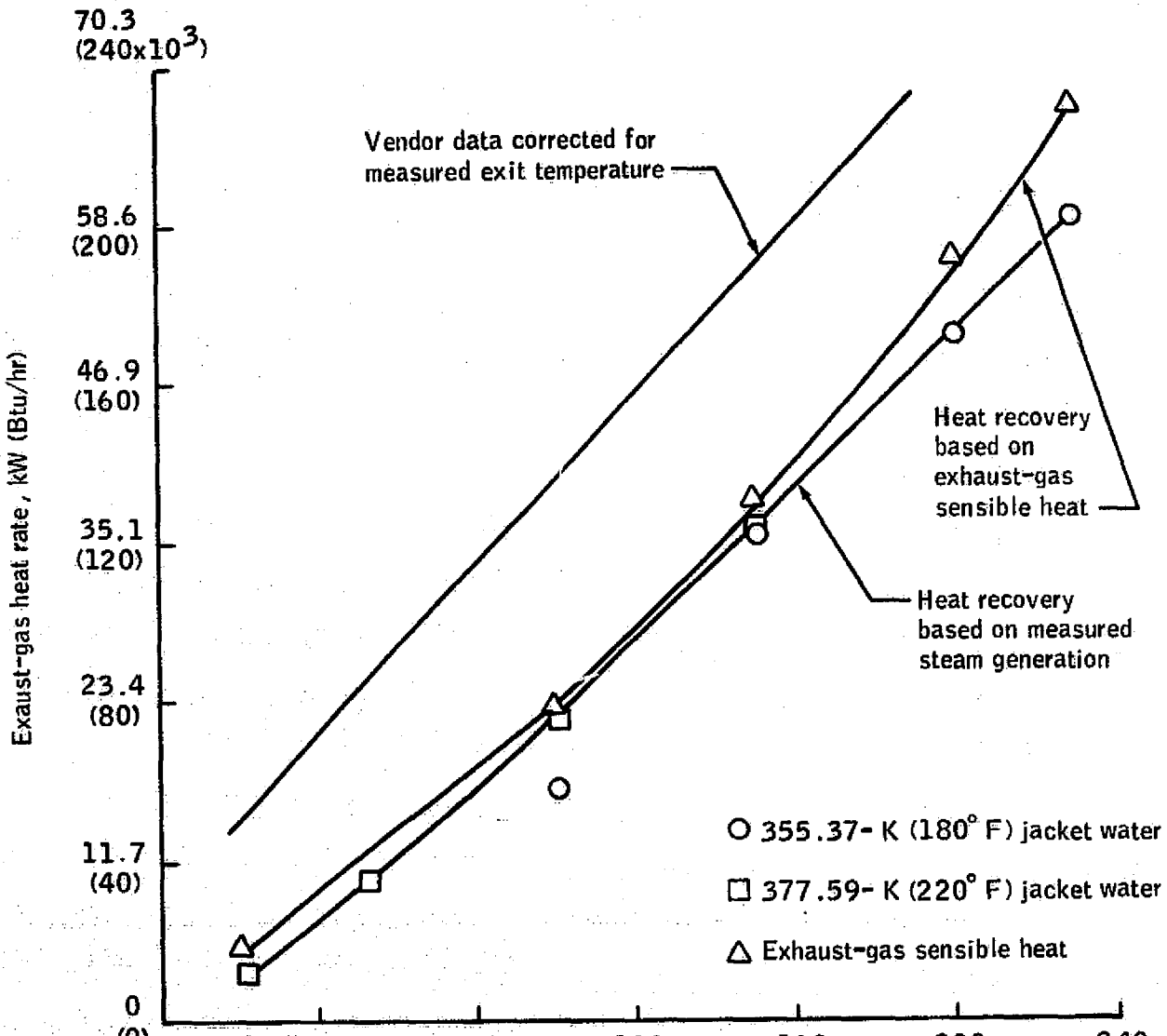

Figure 5.—Engine-exhaust heat recovery as a function of electrical load—forced-circulation-cooling mode.

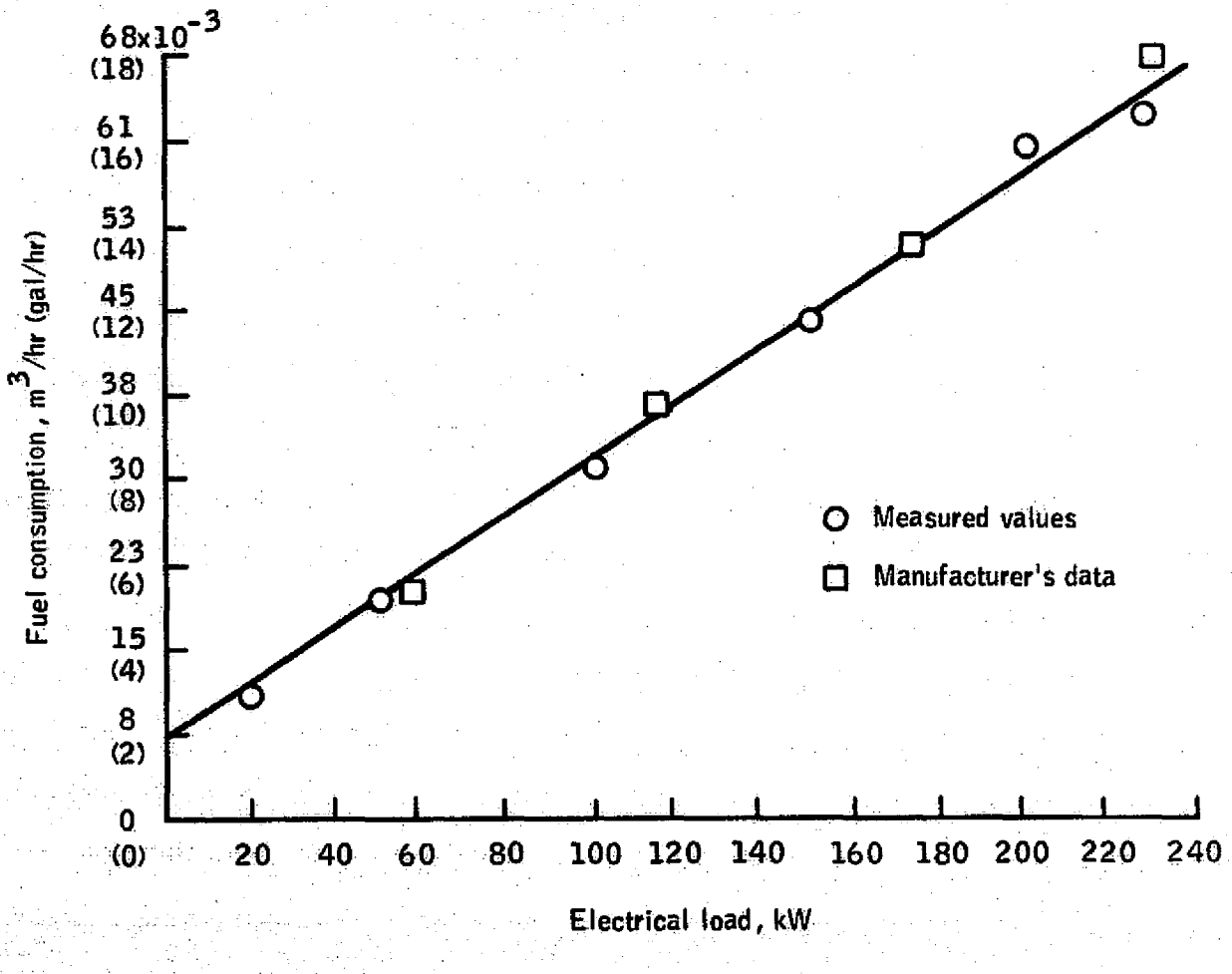

Figure 6.—Fuel consumption rate as a function of electrical load—ebullient-cooling mode.

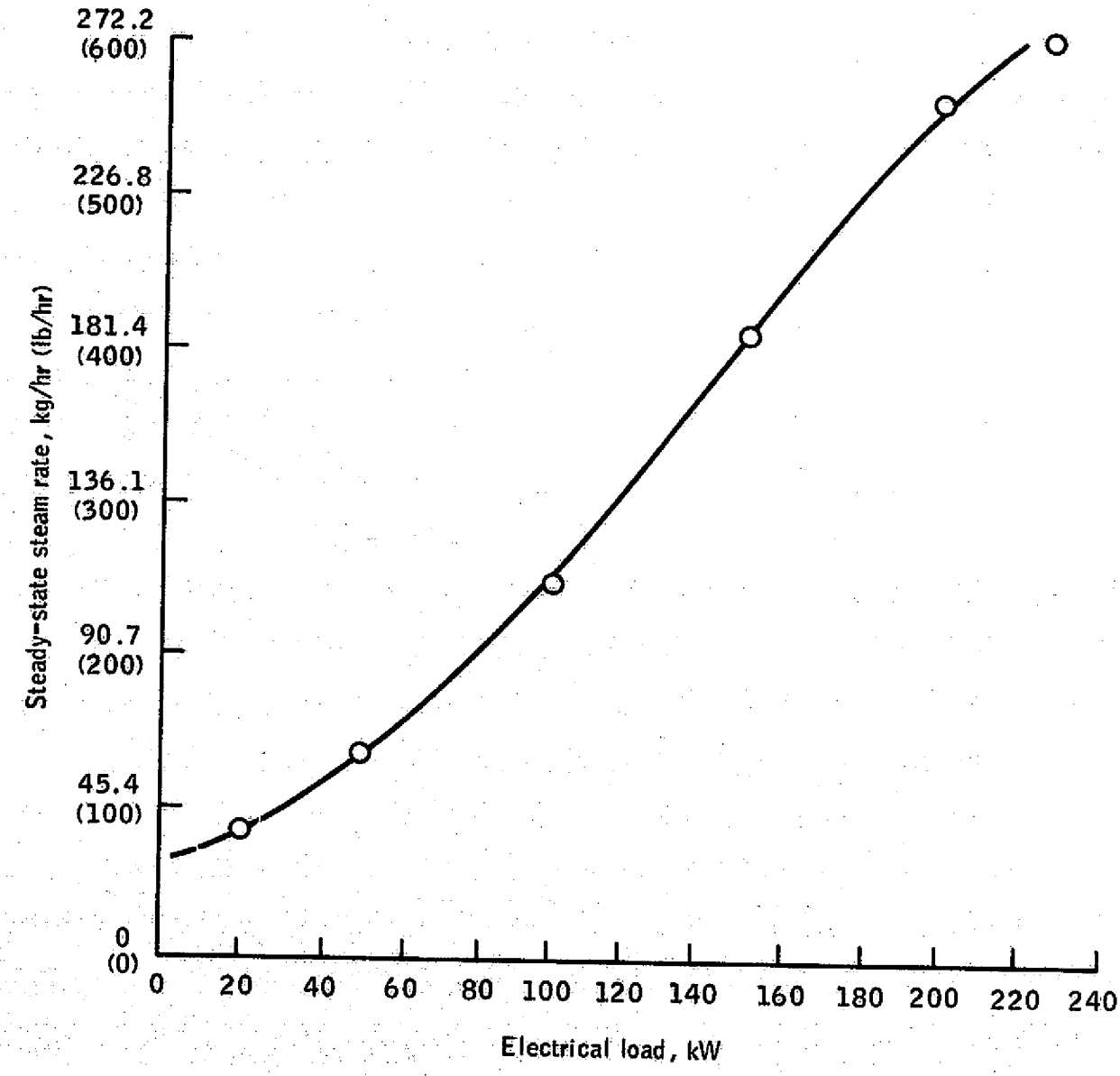

Figure 7.—Steady-state steam rate as a function of electrical load—ebullient-cooling mode.

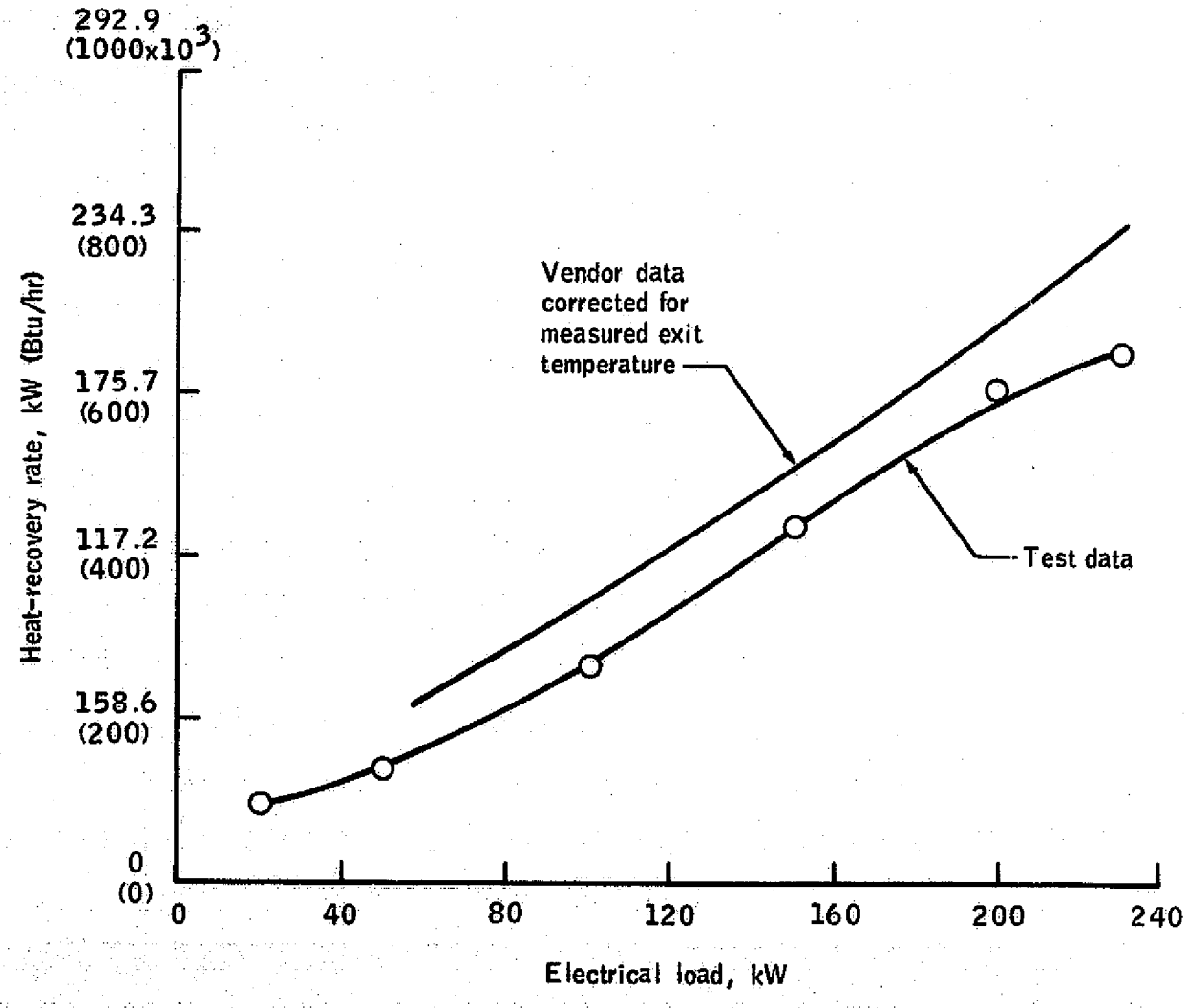

Figure 8.—Combined engine-exhaust and jacket-water heat recovery as a function of electrical load—ebullient-cooling mode.

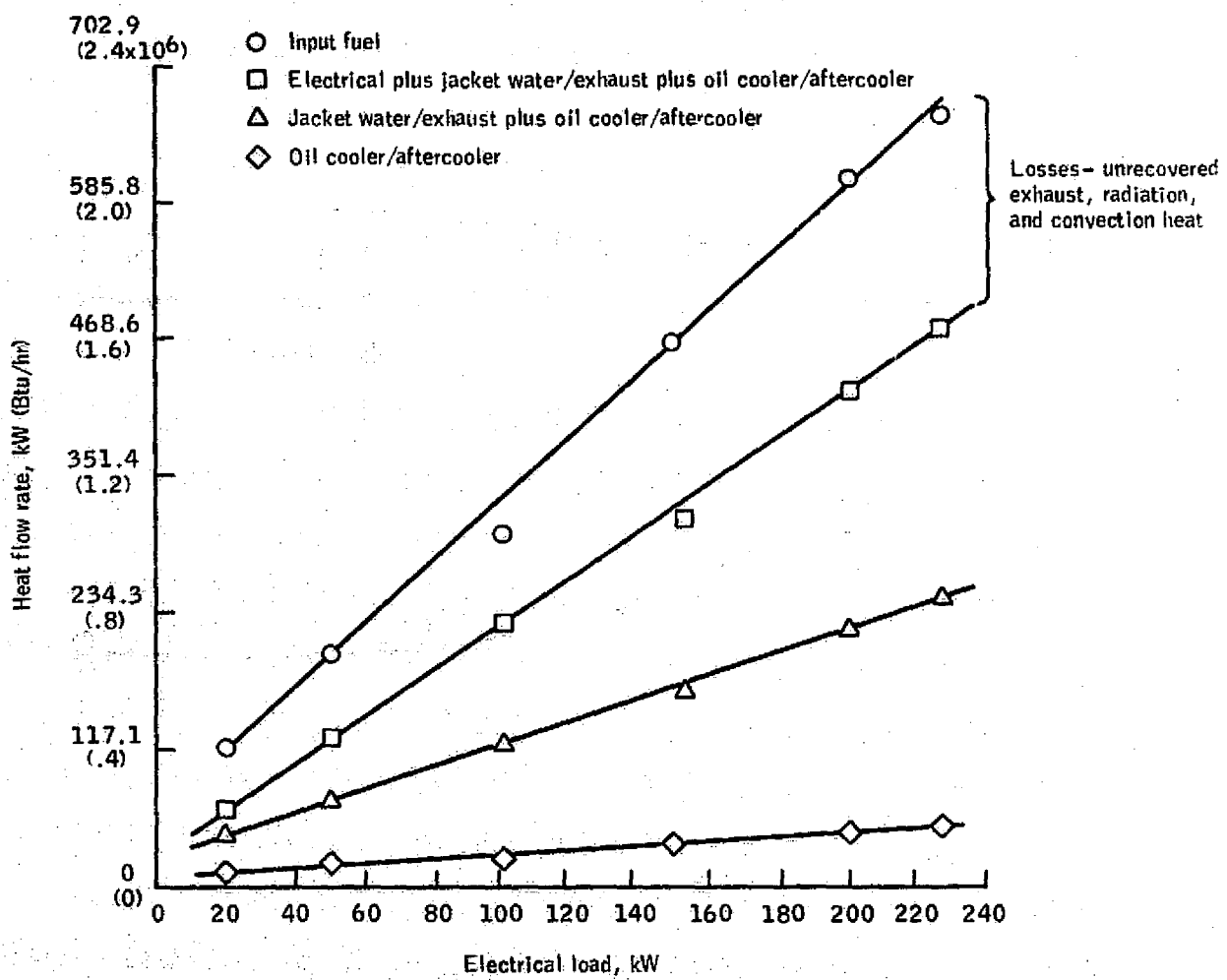

Figure 9.—Ebullient-cooling-mode input-output heat-flow rates.

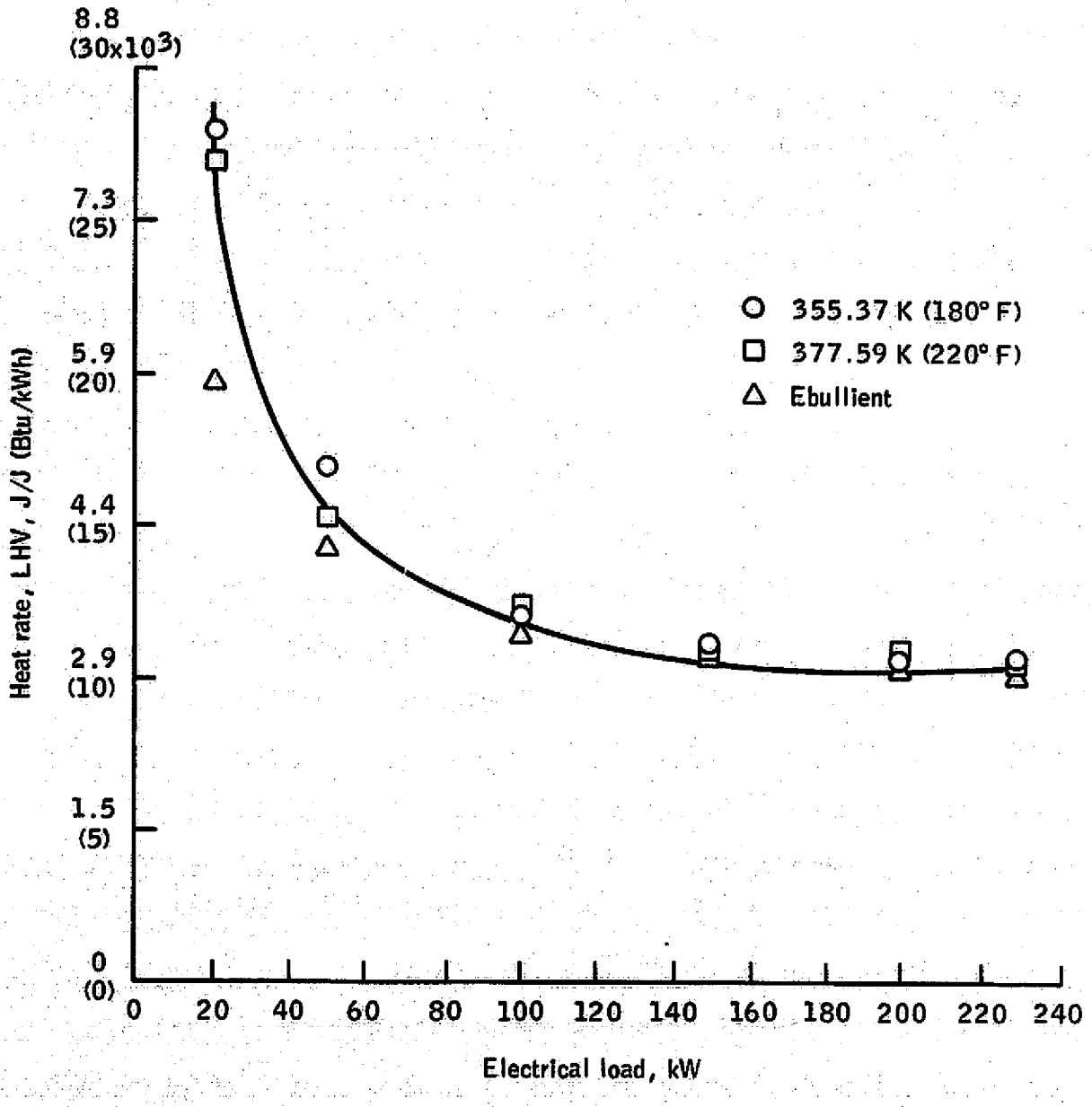

Figure 10.—Engine heat rate as a function of electrical load.

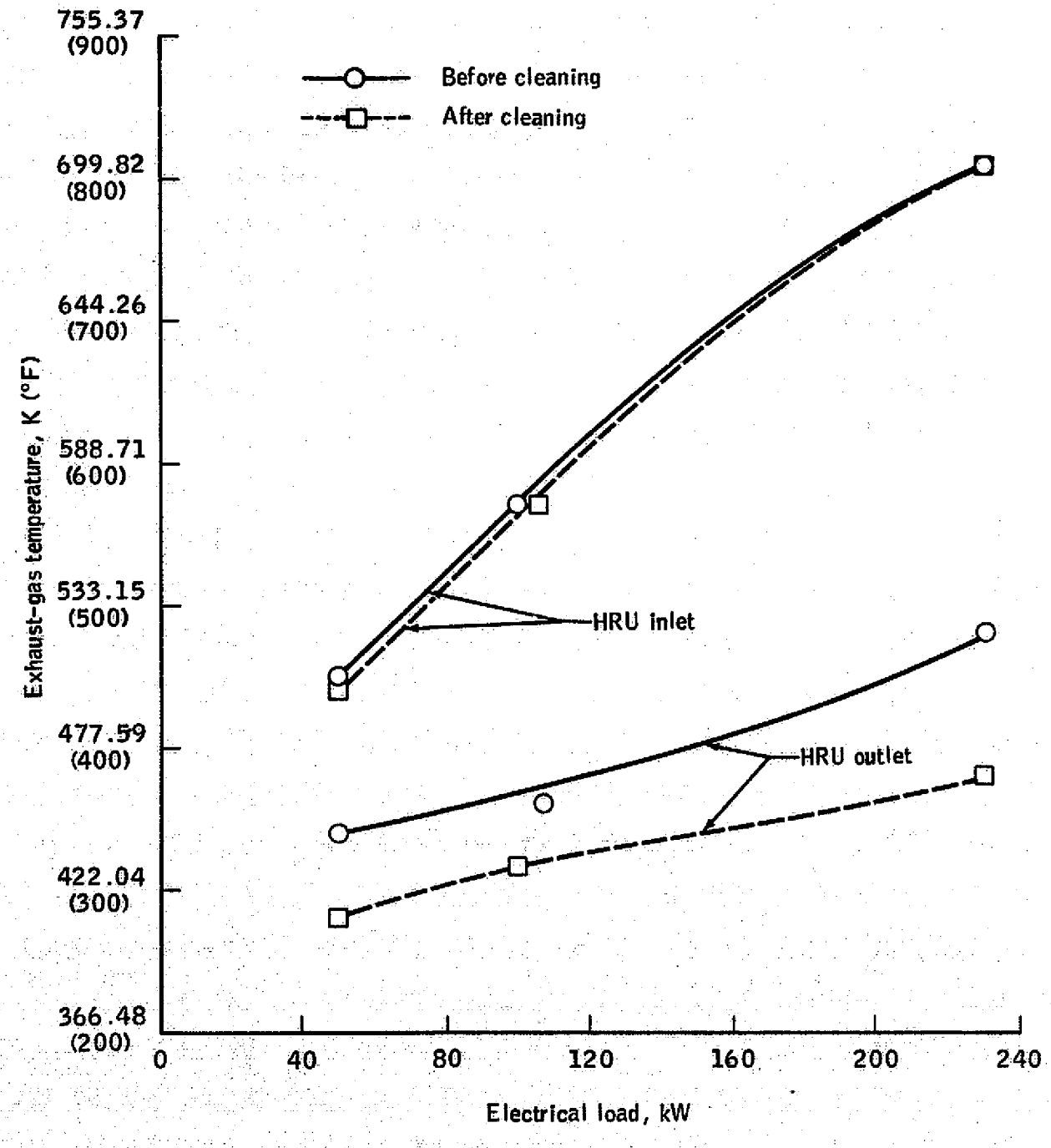

Figure 11.—Diesel engine exhaust-gas temperatures before and after heat-recovery-unit cleaning operation (ebullient-cooling mode).

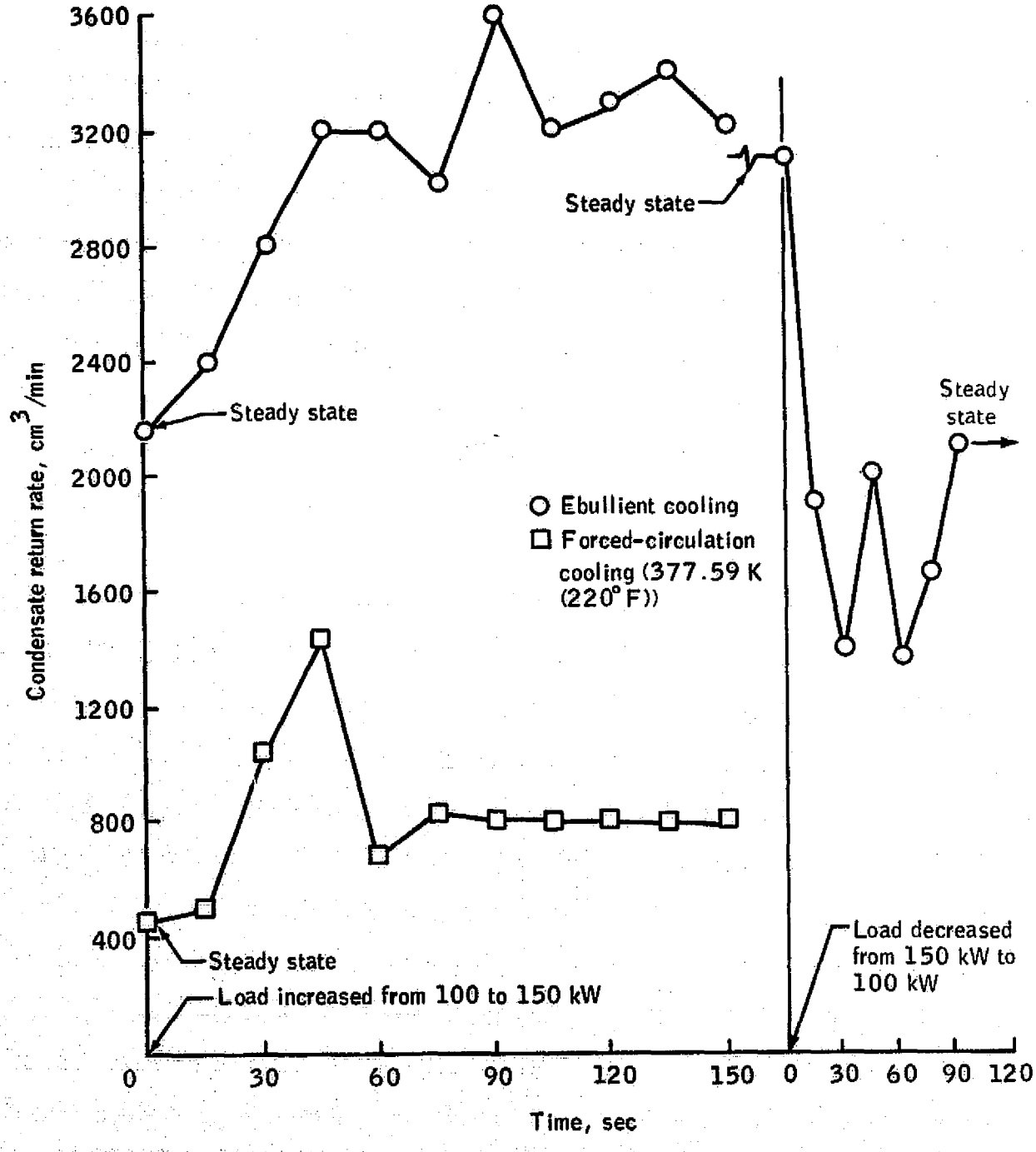

Figure 12.—Transient response tests, MIST PGS II and III, June 12 to 14, 1974.

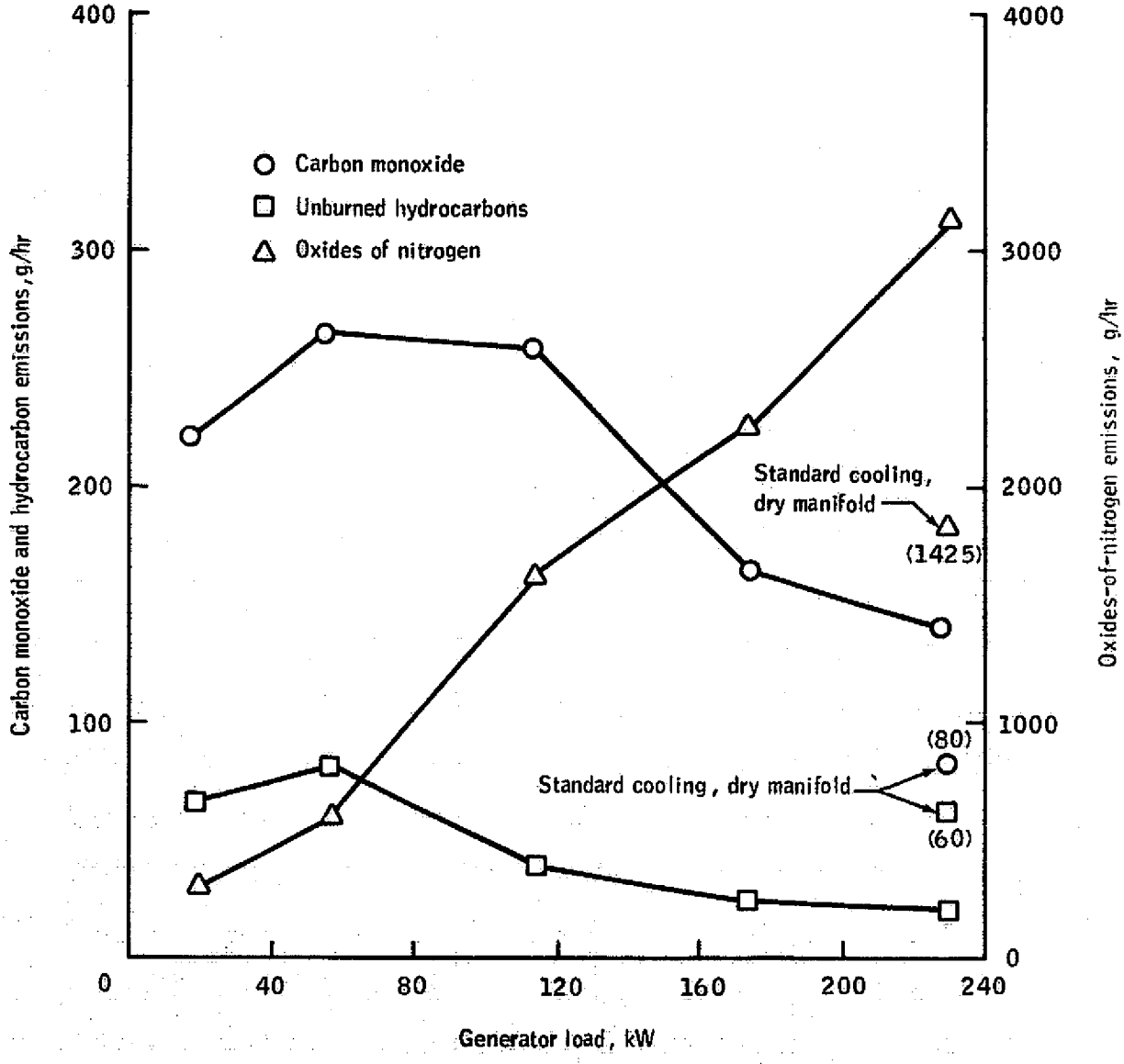

Figure 13.—MIST engine emissions as a function of electrical load—ebullient-cooling mode.

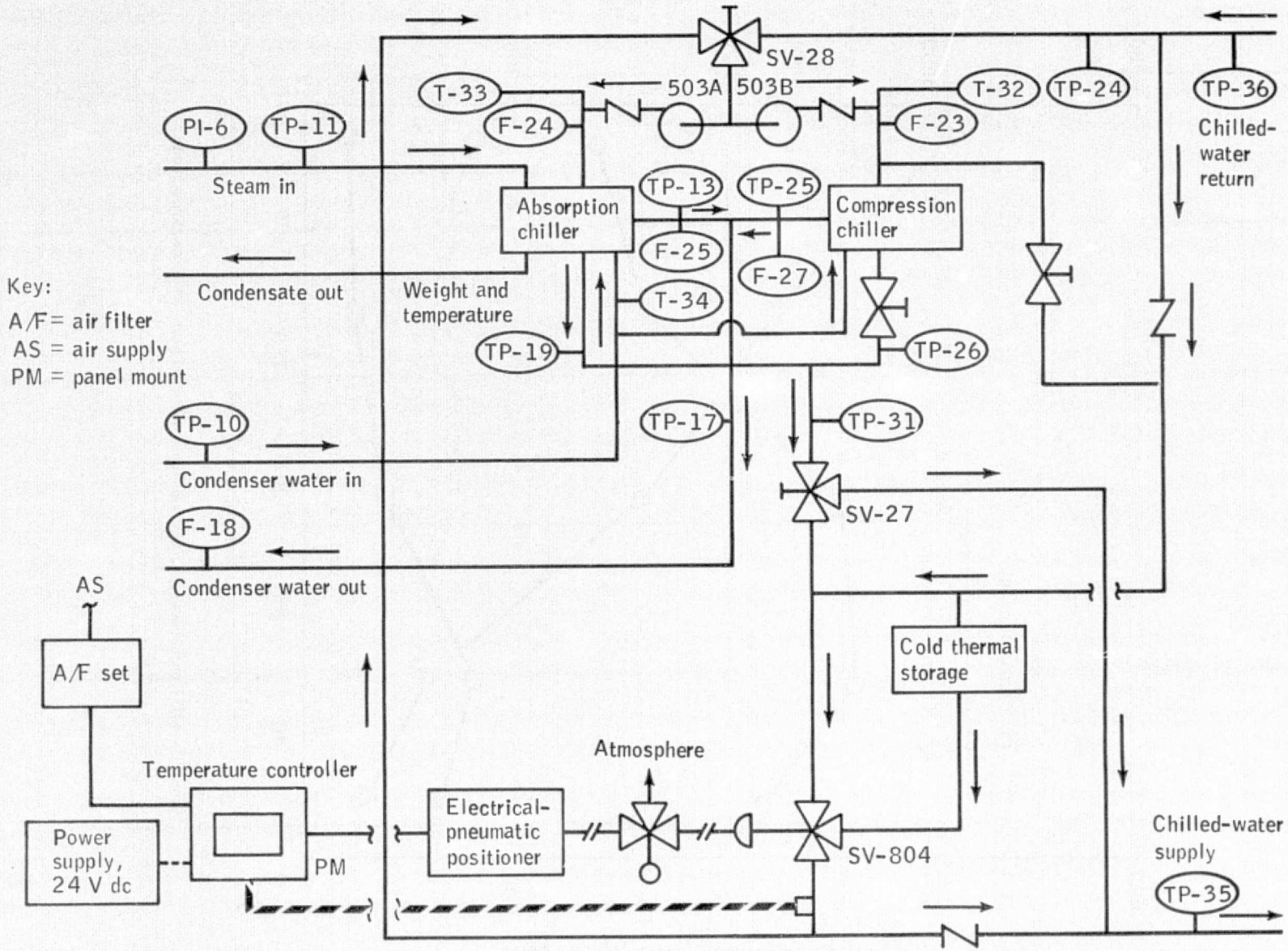

Figure 14.—Space-cooling-loop schematic.

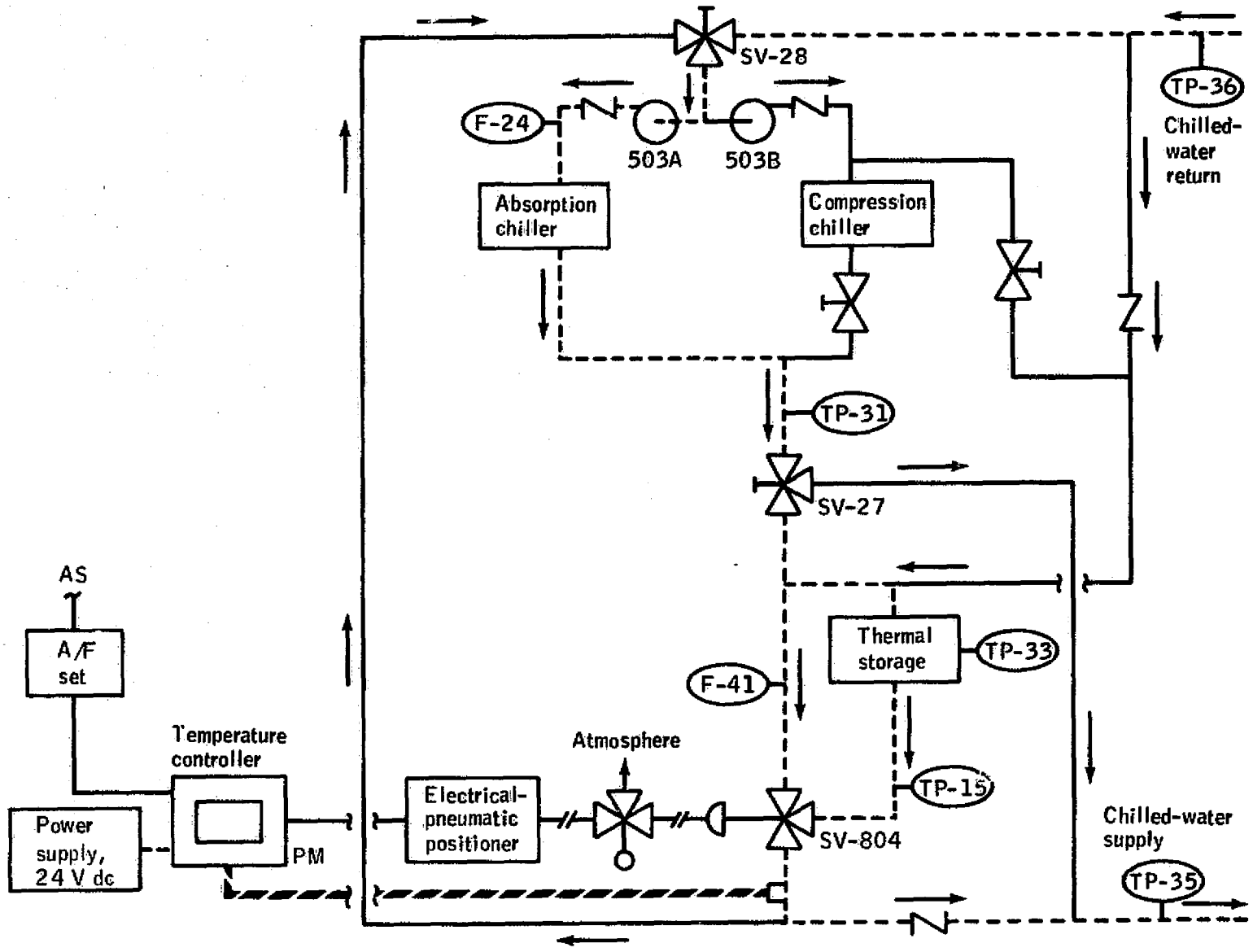

Figure 15.—Cold thermal storage schematic.

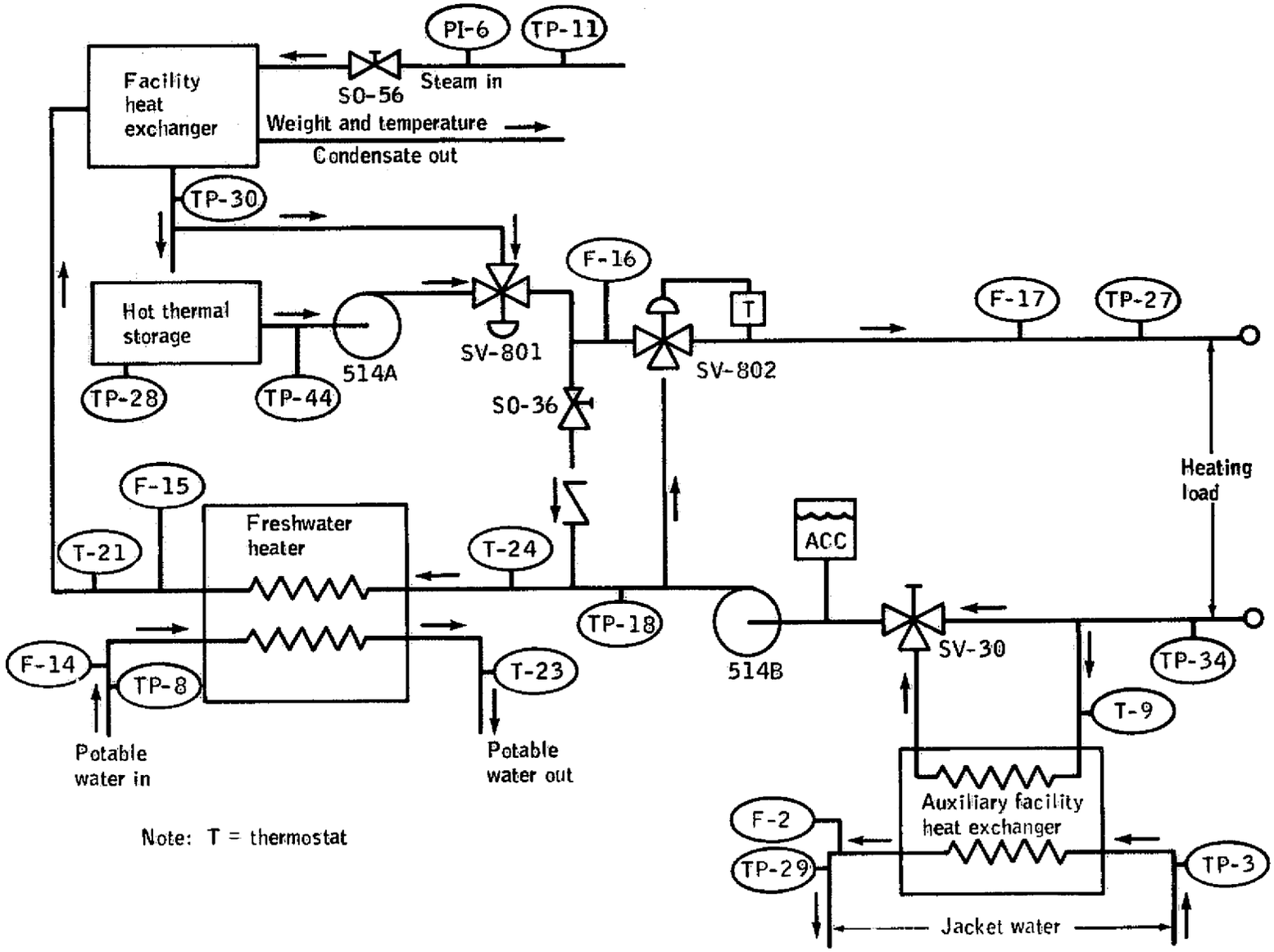

Figure 16.—Space-heating-loop schematic

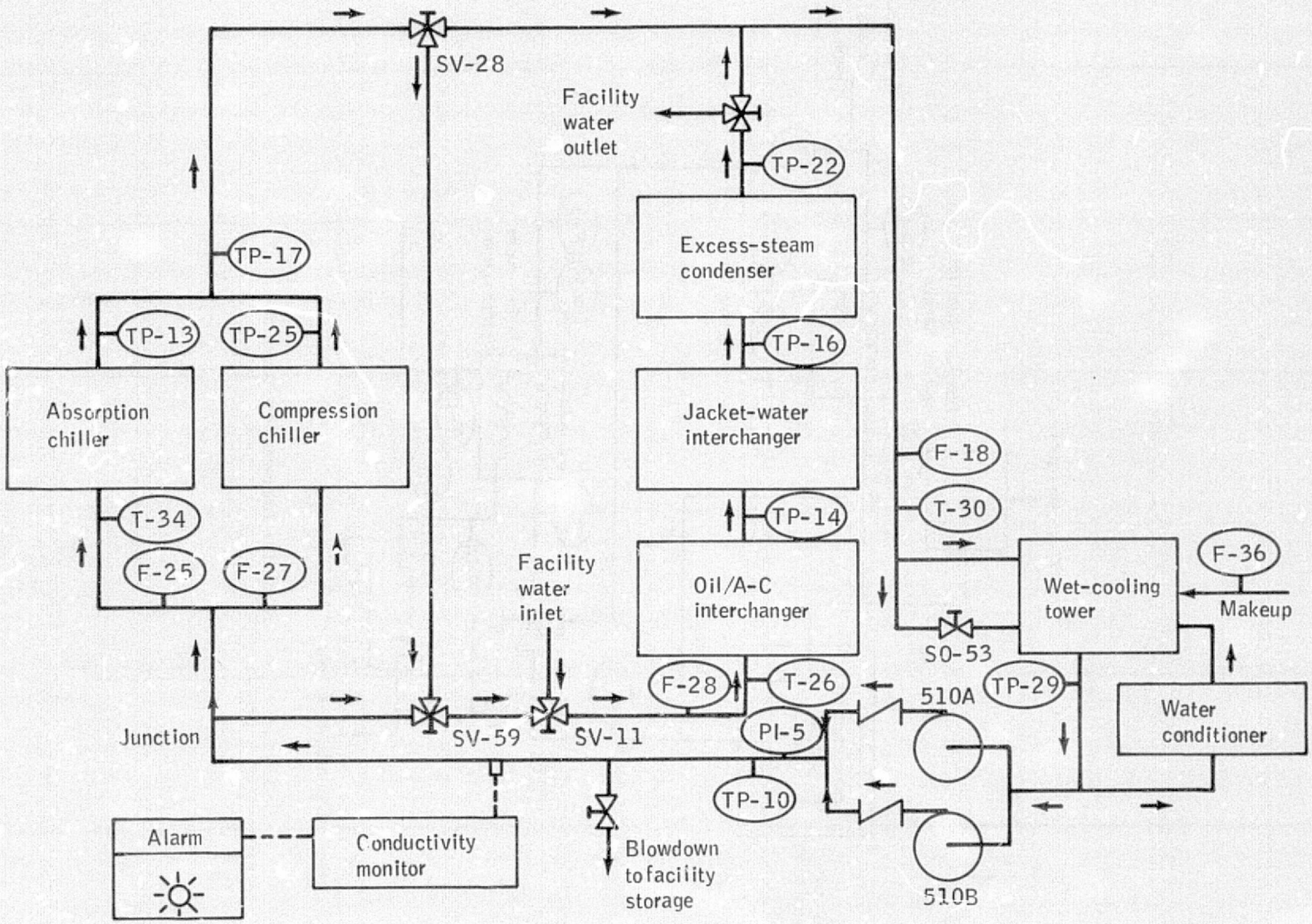

Figure 17.—Cooling-water-loop schematic.

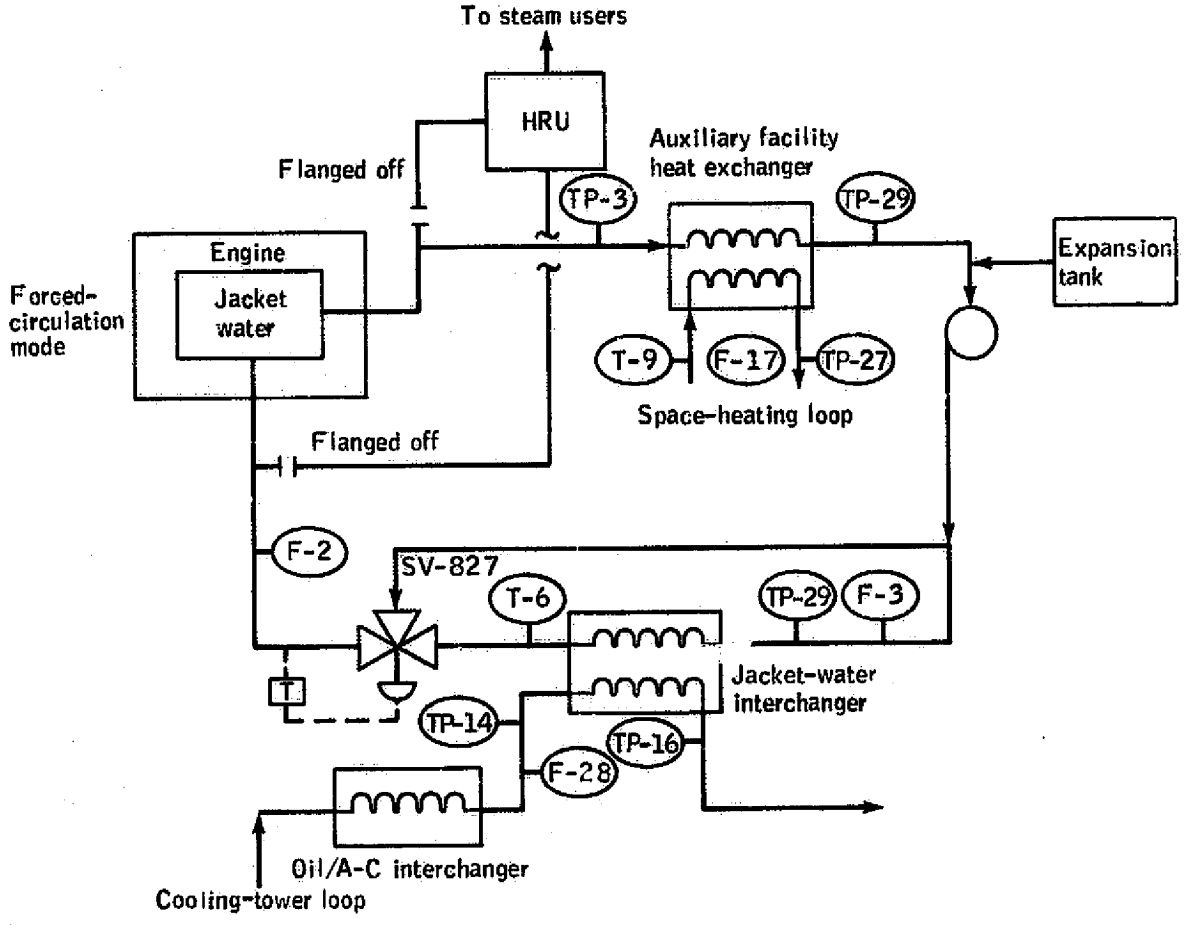

Figure 18.—Jacket-water-loop schematic.

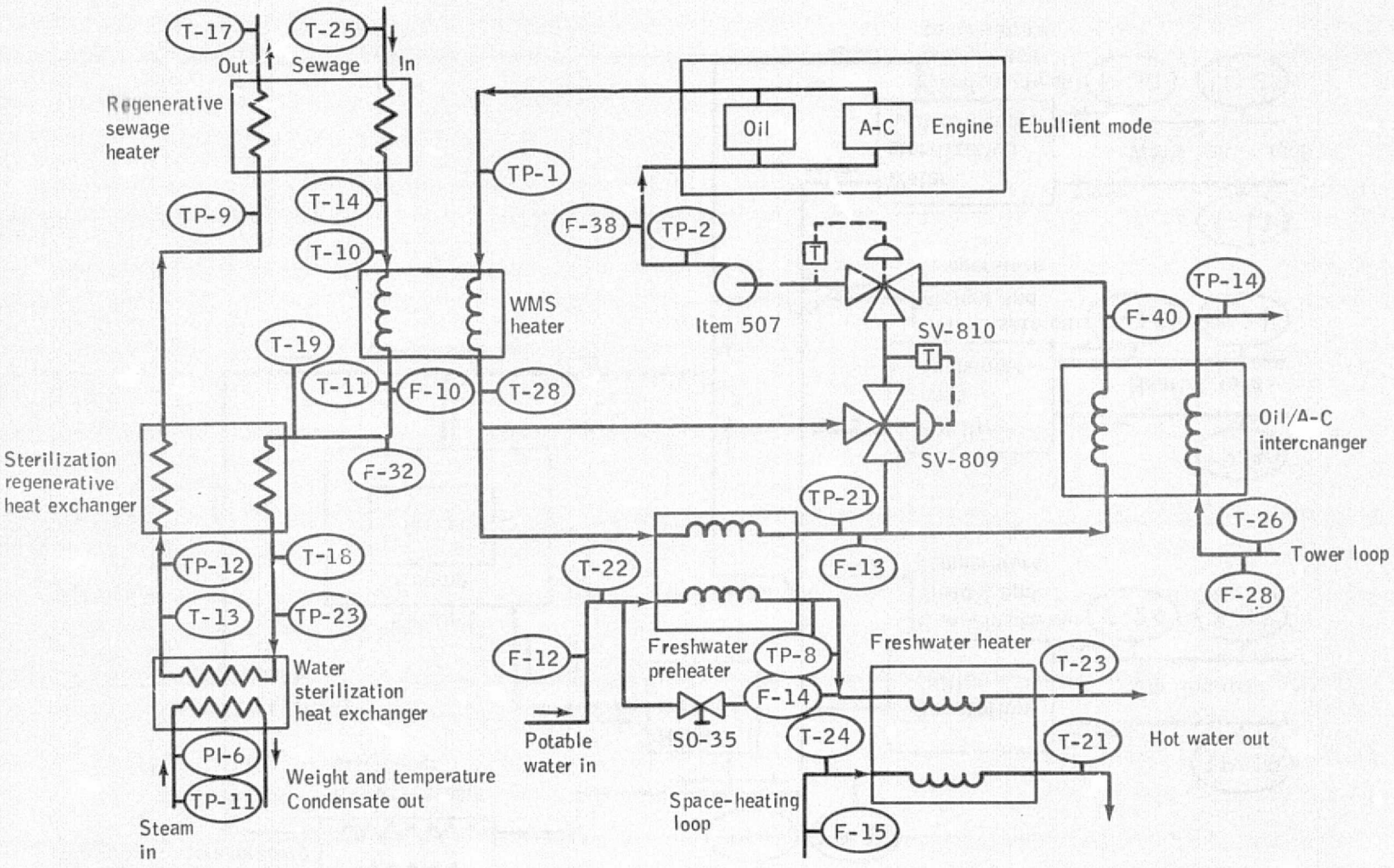

Figure 19.—Oil-coolant-loop schematic.

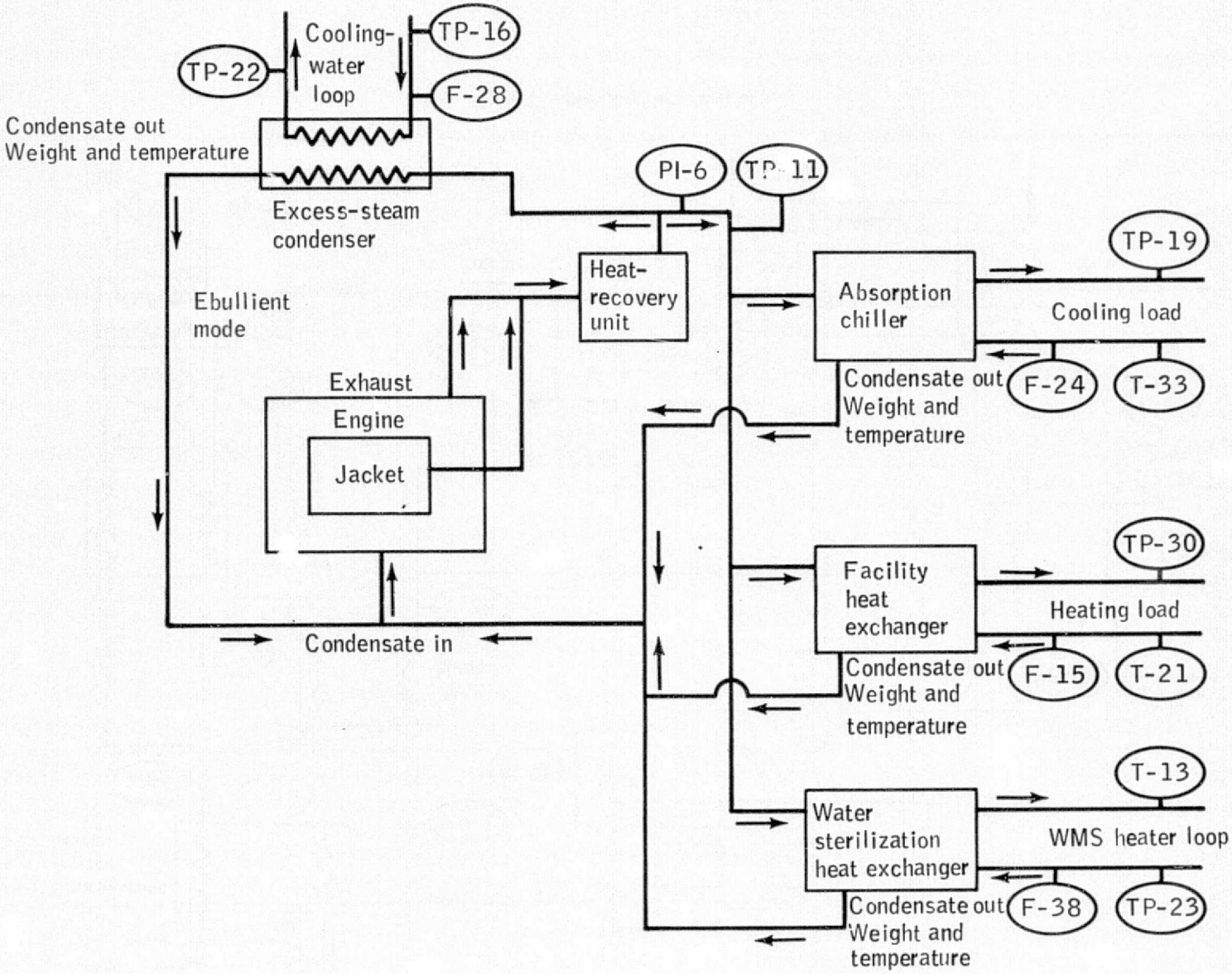

Figure 20.—Steam-loop schematic.

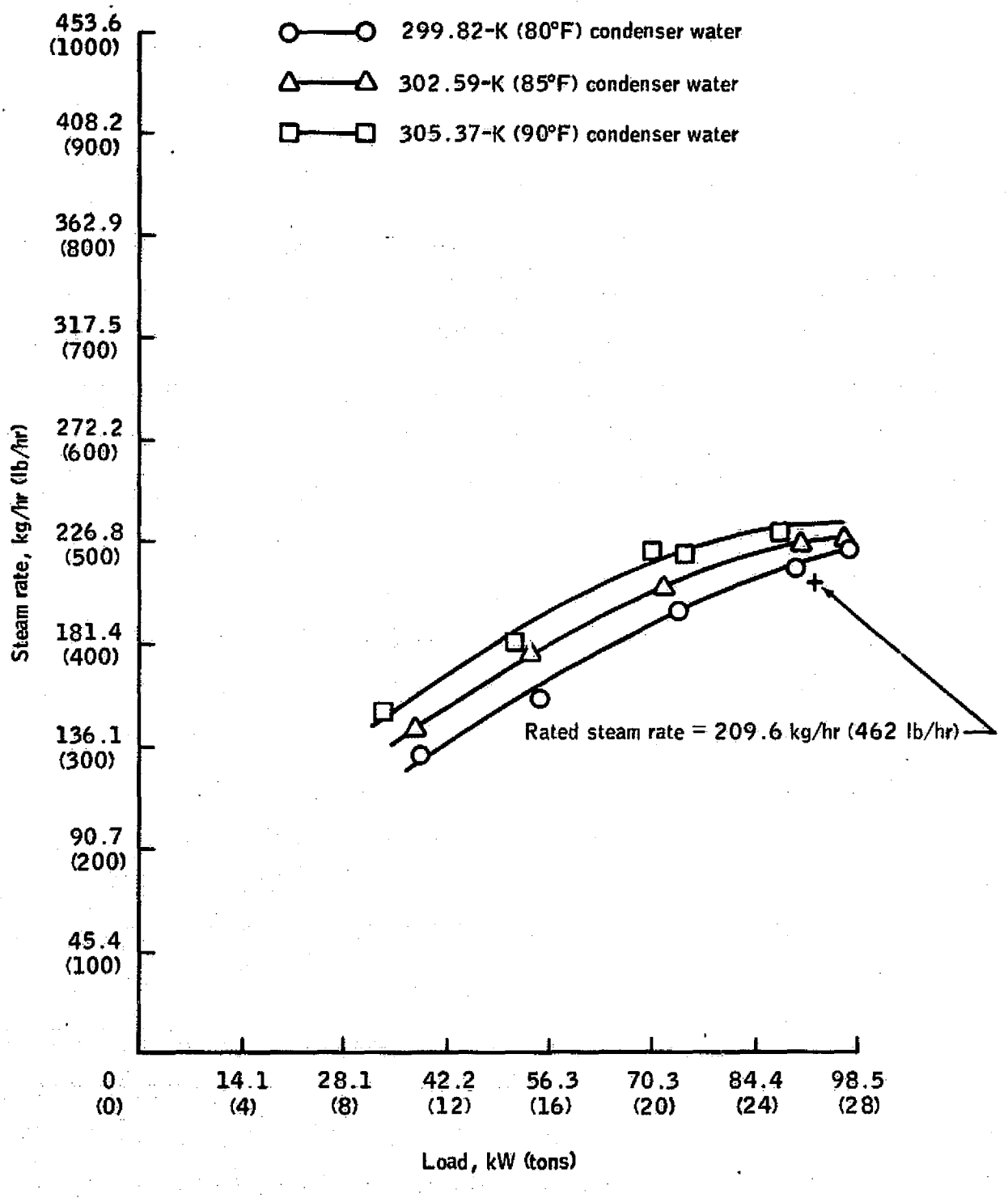

(a) Steam rate as a function of unit capacity.

Figure 21.—MIST series I test—absorption chiller.

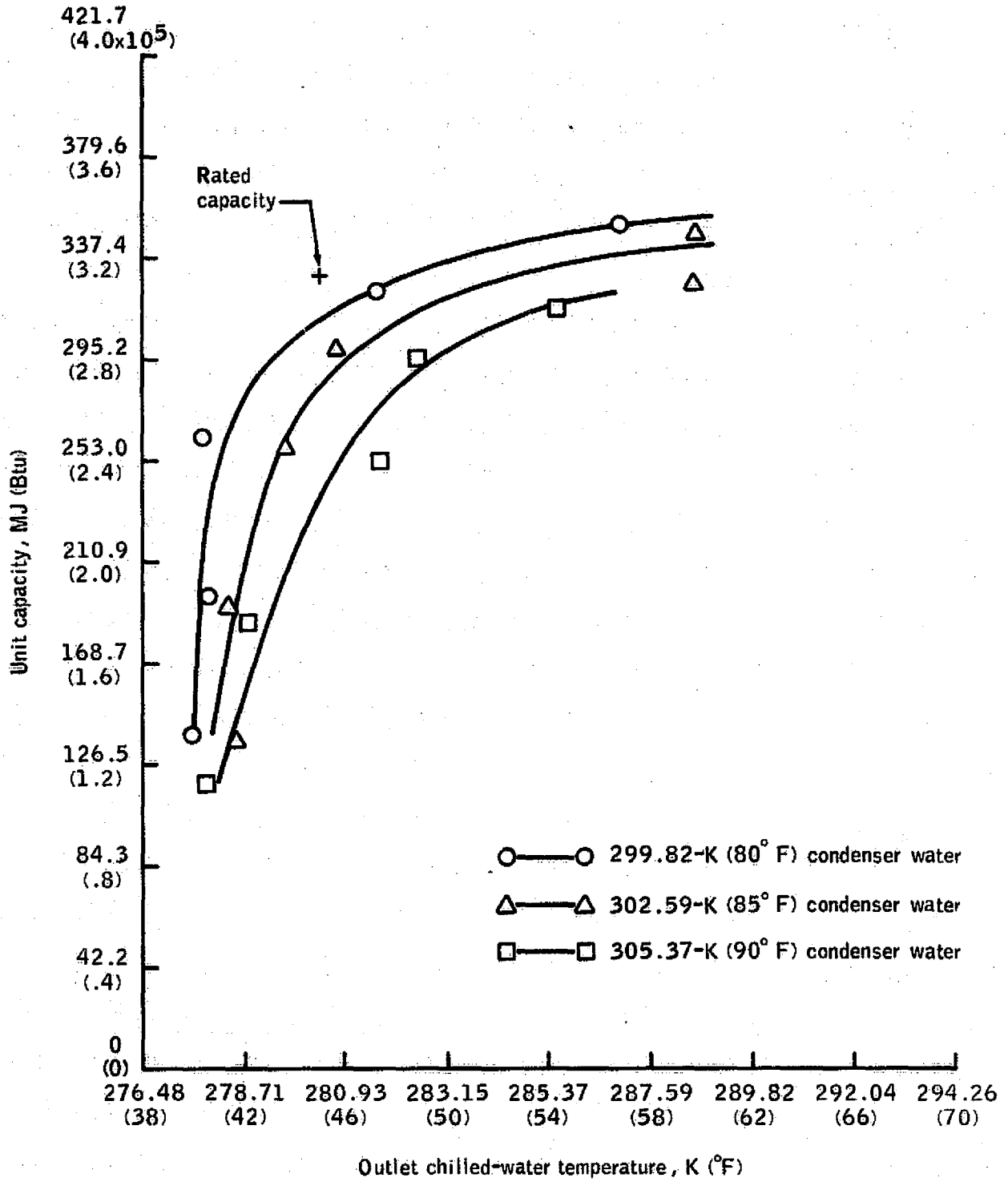

(b) Unit capacity as a function of chilled-water temperature.

Figure 21.—Continued.

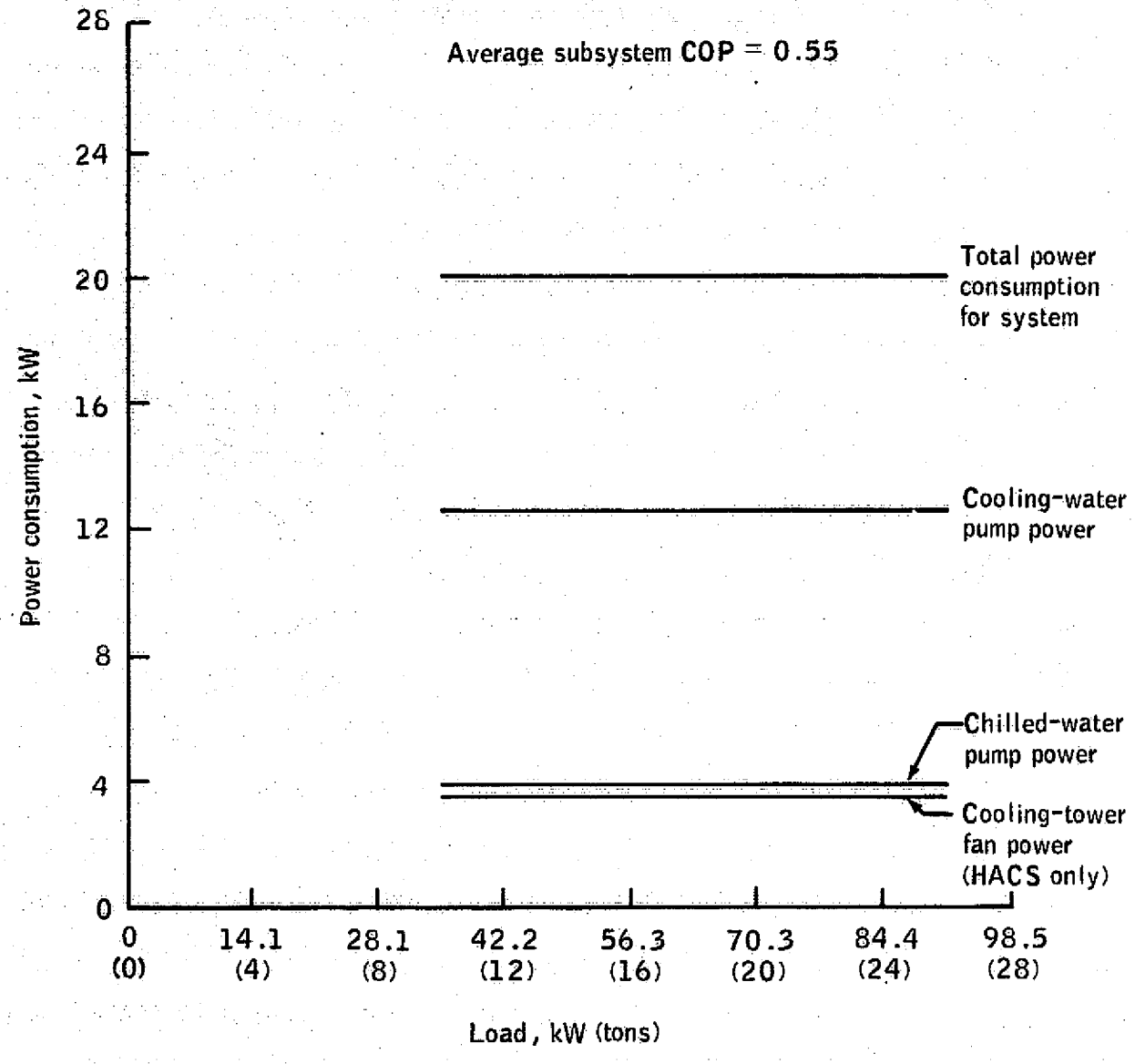

(c) Subsystem power consumption as a function of load.

Figure 21.—Continued.

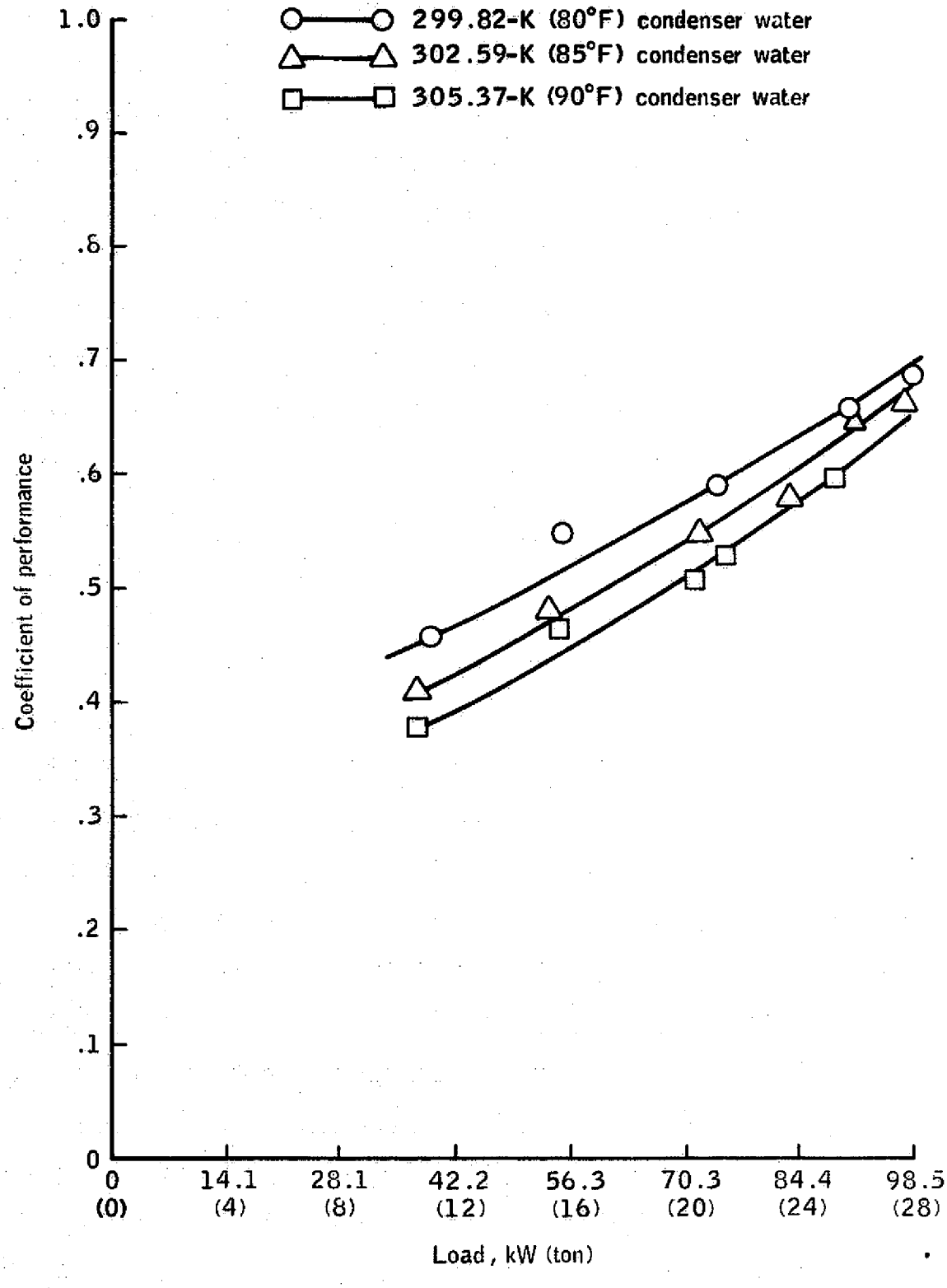

(d) Coefficient of performance as a function of load.

Figure 21.—Concluded.

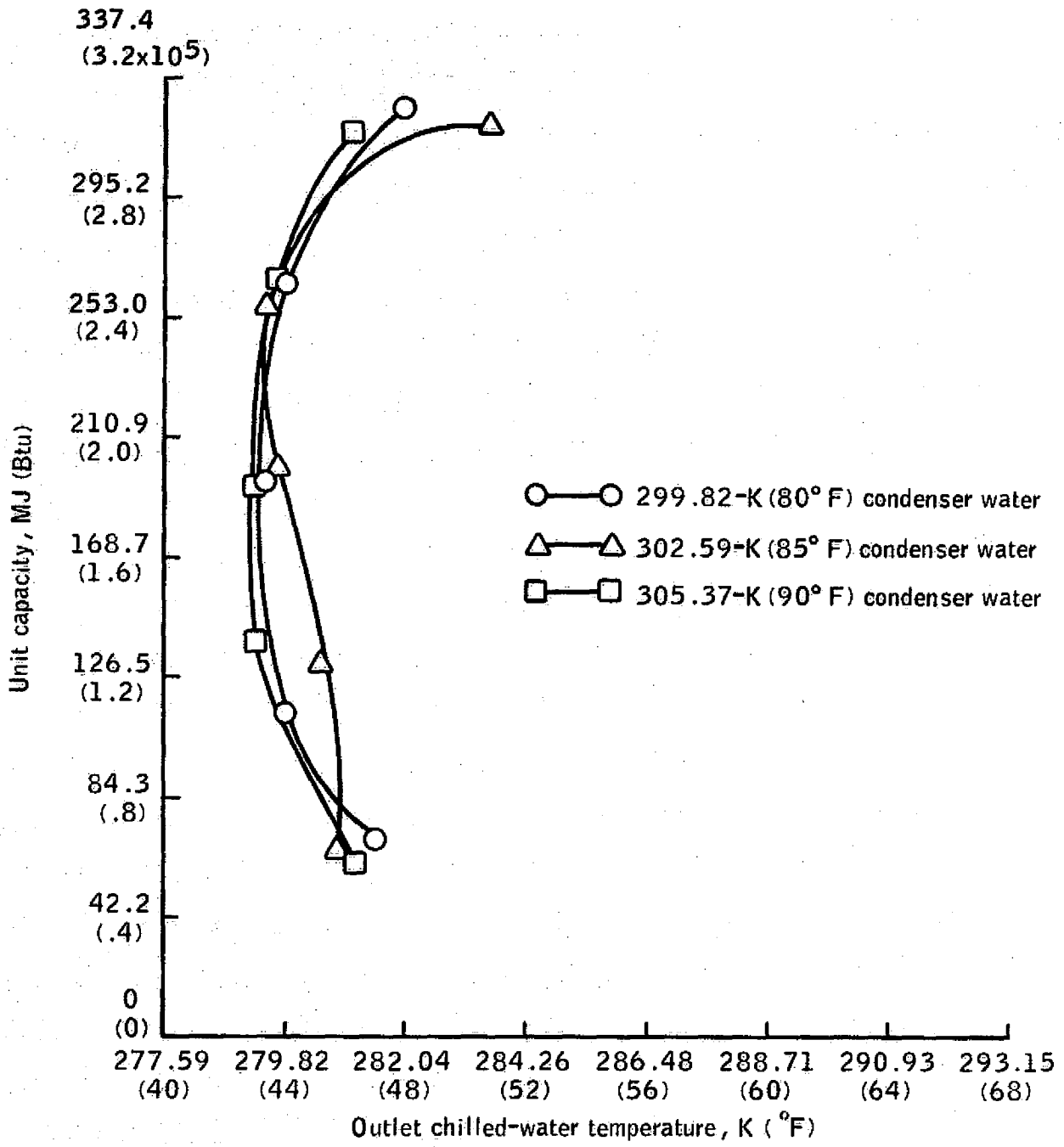

(a) Unit capacity as a function of chilled-water temperature, 284.26-K (52° F) sensor set point.

Figure 22.—MIST series II test—compression chiller.

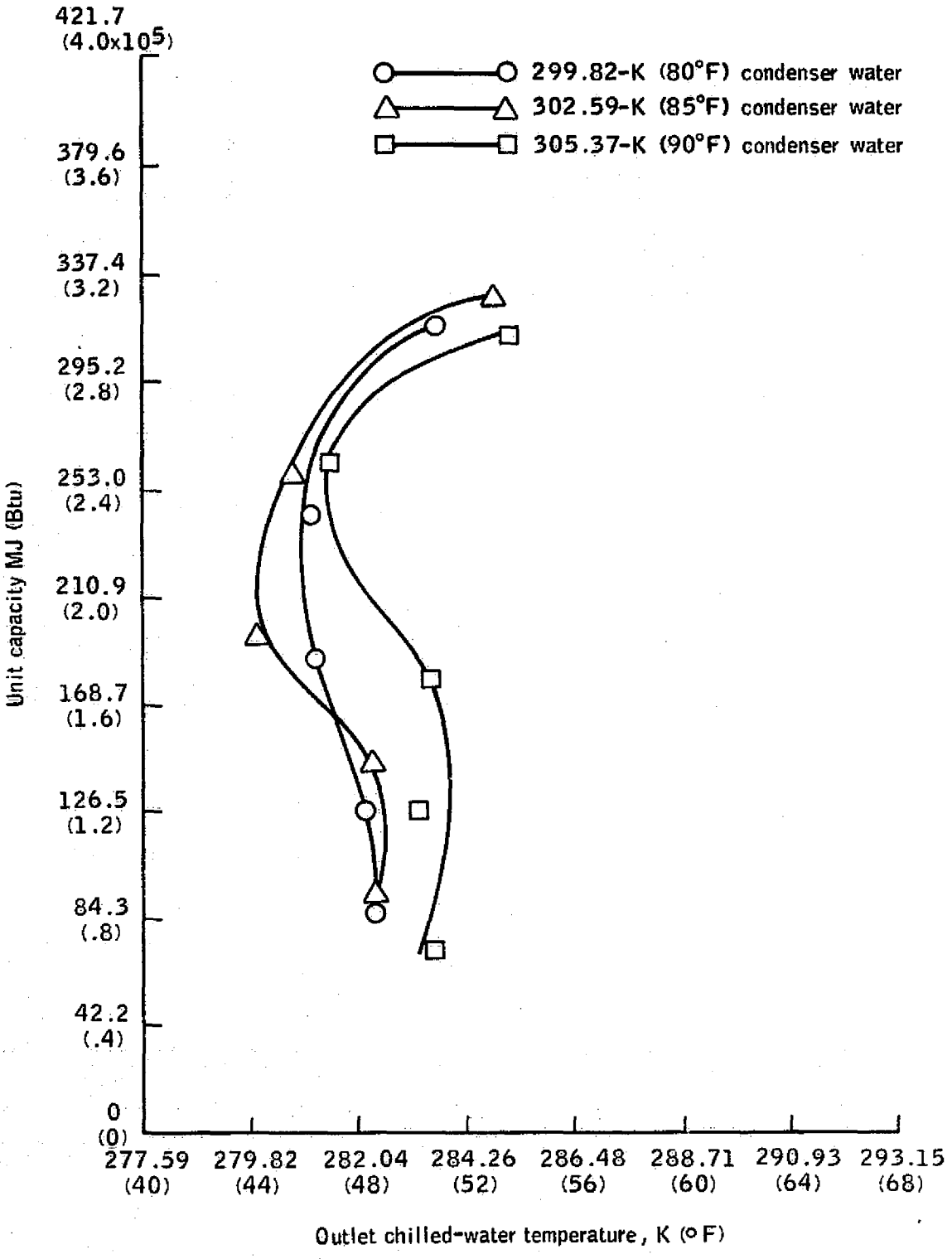

(b) Unit capacity as a function of chilled-water temperature, 285.93-K (55° F) sensor set point.

Figure 22.—Continued.

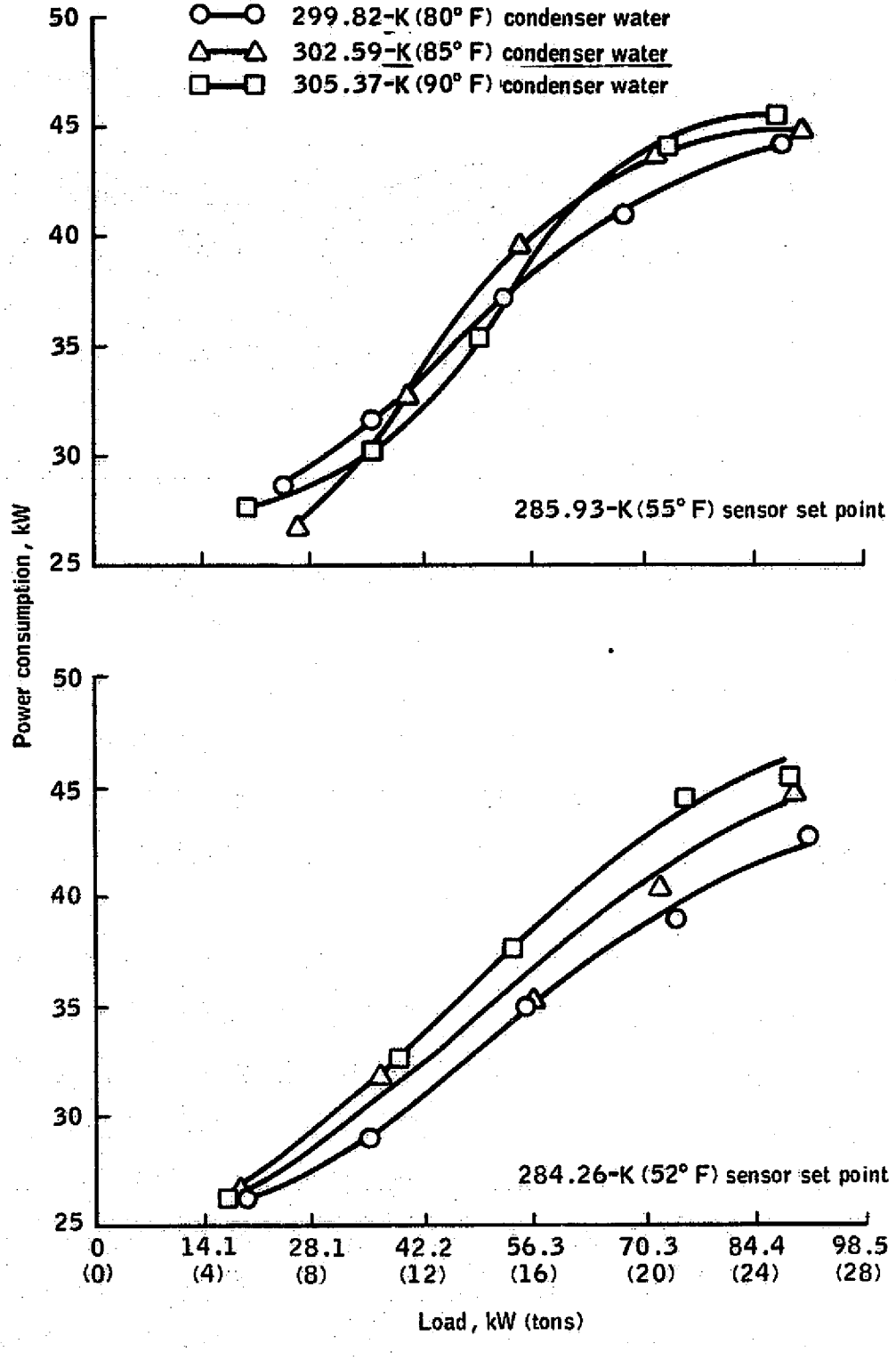

(c) Subsystem power consumption as a function of load.

Figure 22.—Continued.

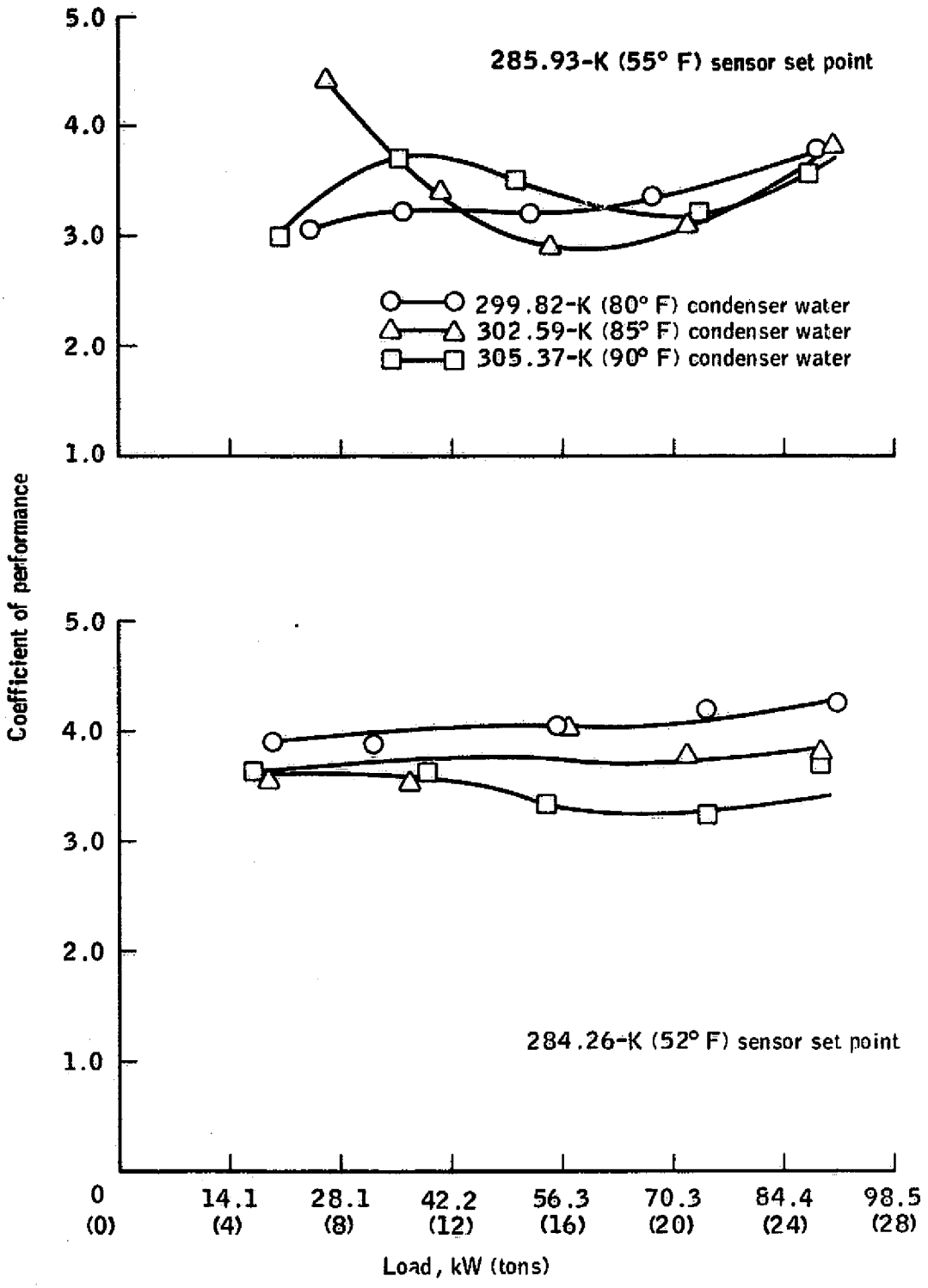

(d) Coefficient of performance as a function of load.

Figure 22.—Concluded.

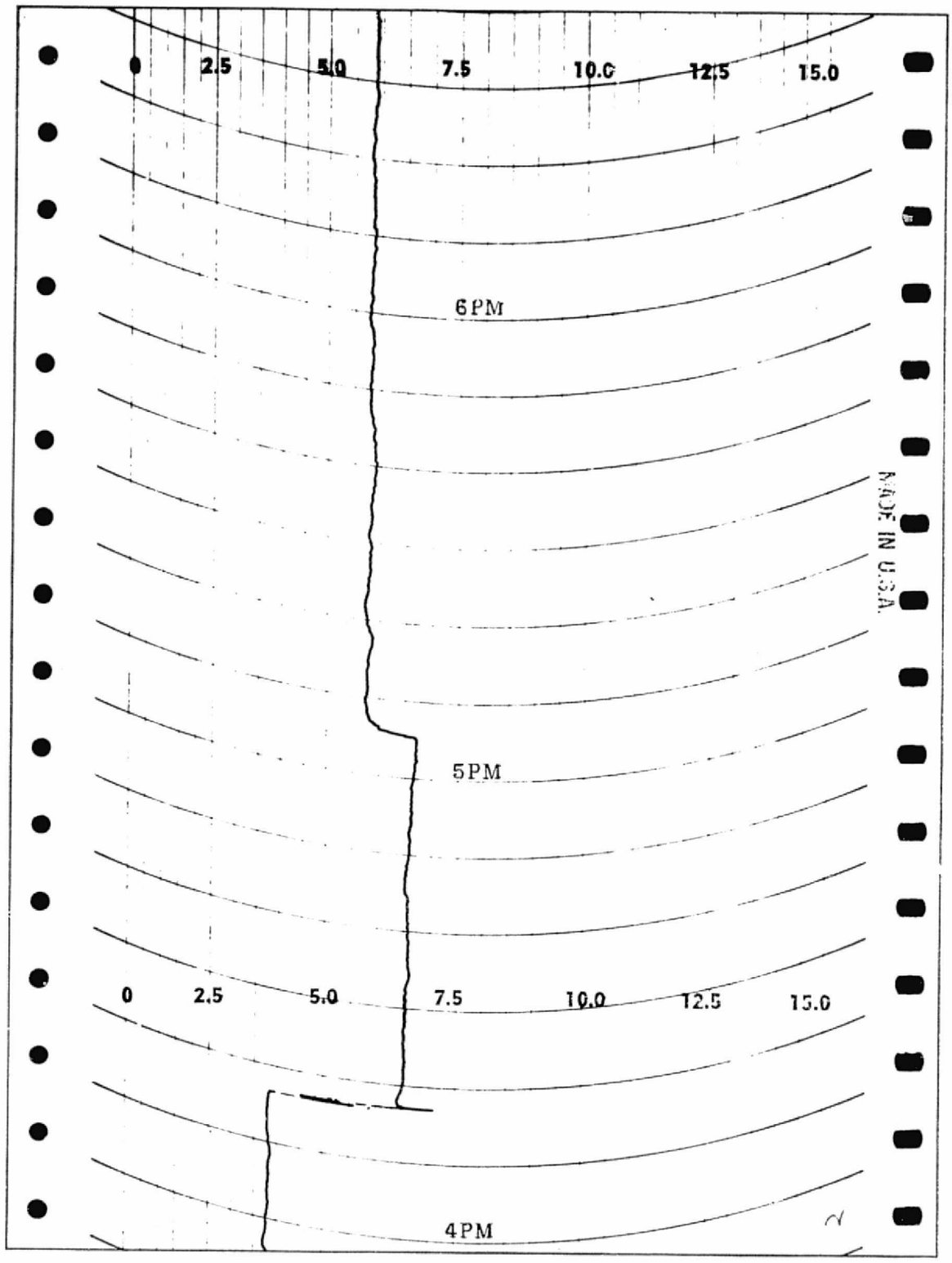

Figure 23.—Typical recording-ammeter strip chart.

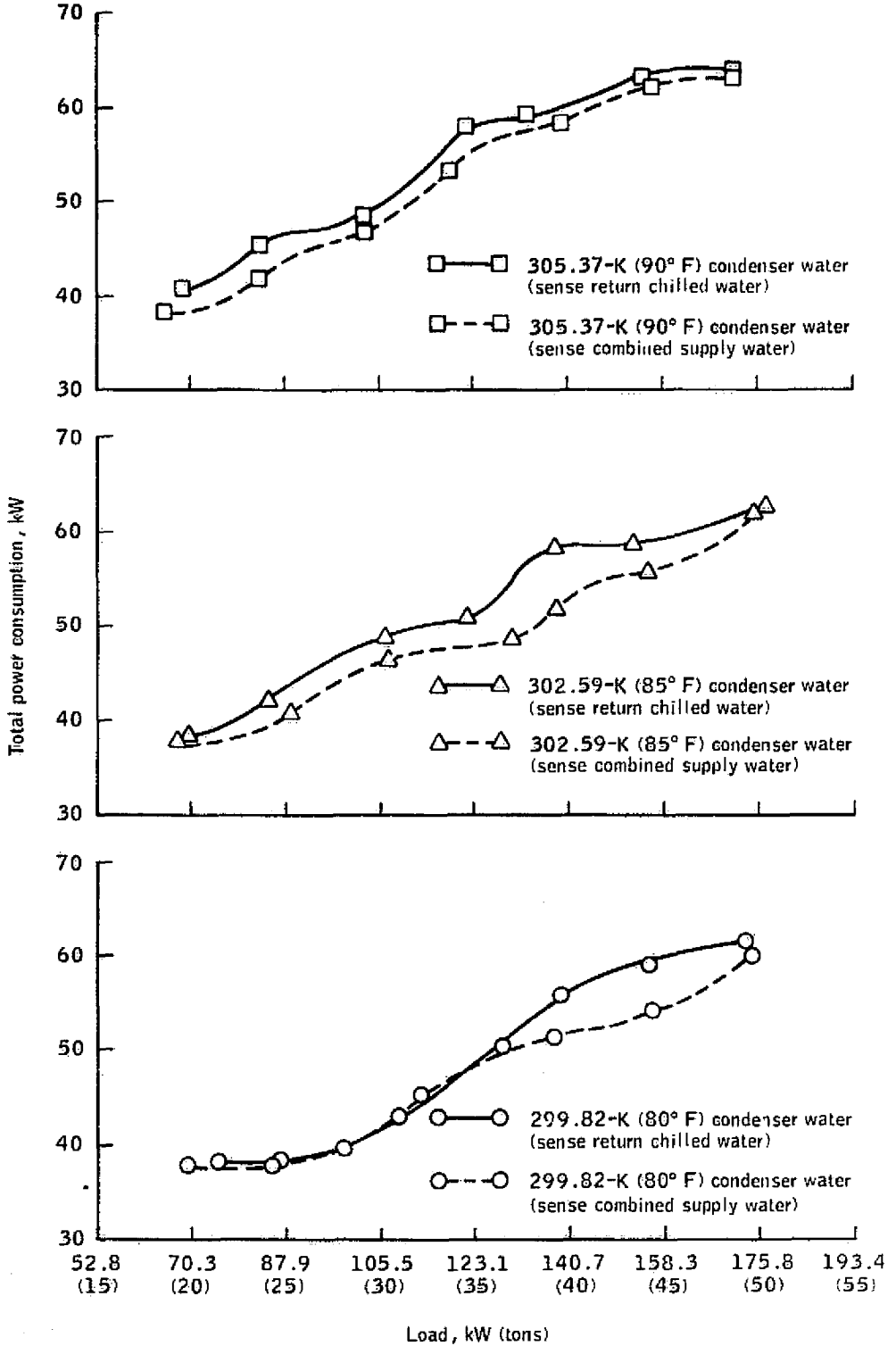

(a) Subsystem power consumption as a function of load.

Figure 24.—MIST series III test—combined chillers.

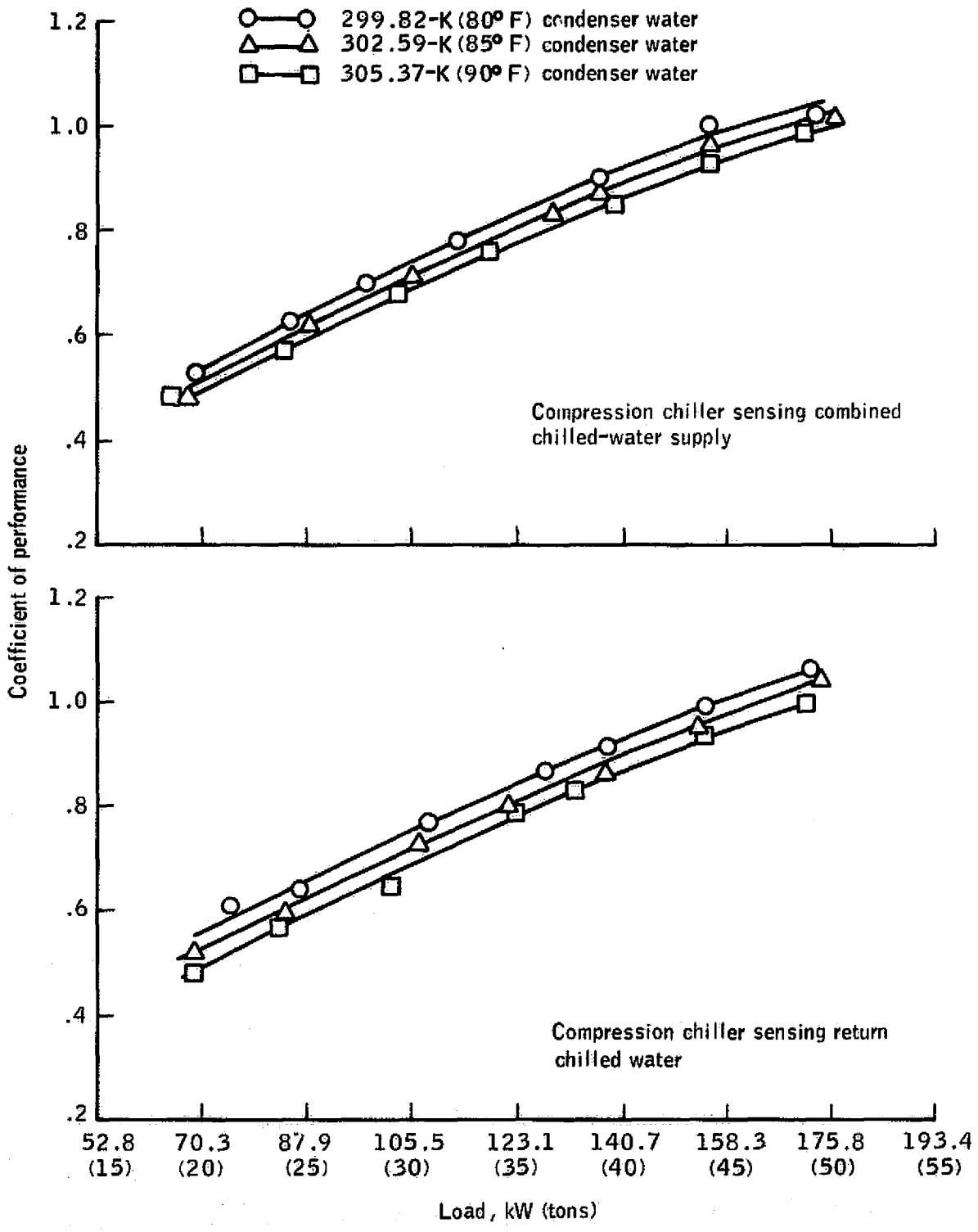

(b) Coefficient of performance as a function of load.

Figure 24.—Concluded.

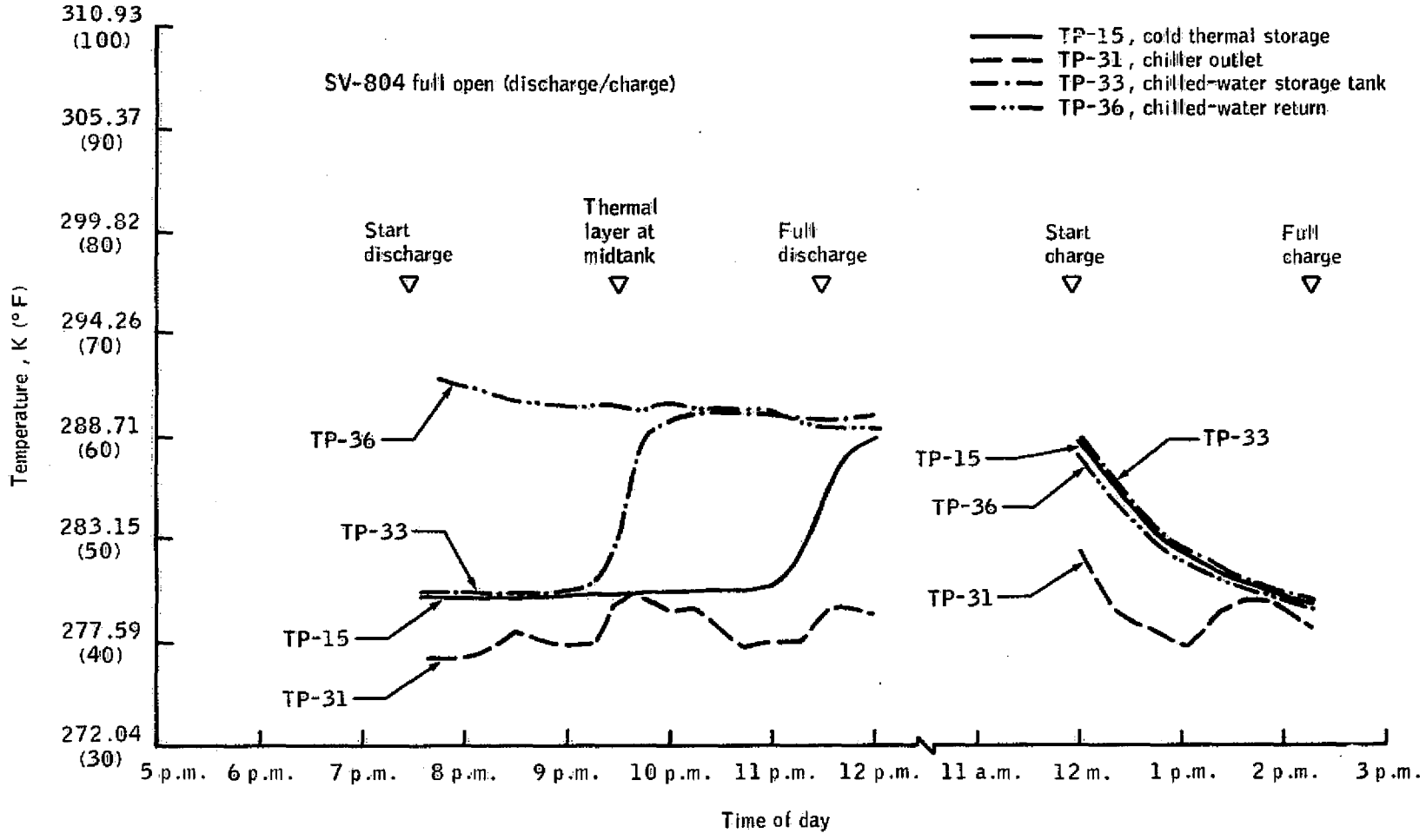

(a) Cold thermal storage discharge/charge profiles.

Figure 25.—MIST series IV test—thermal storage tanks.

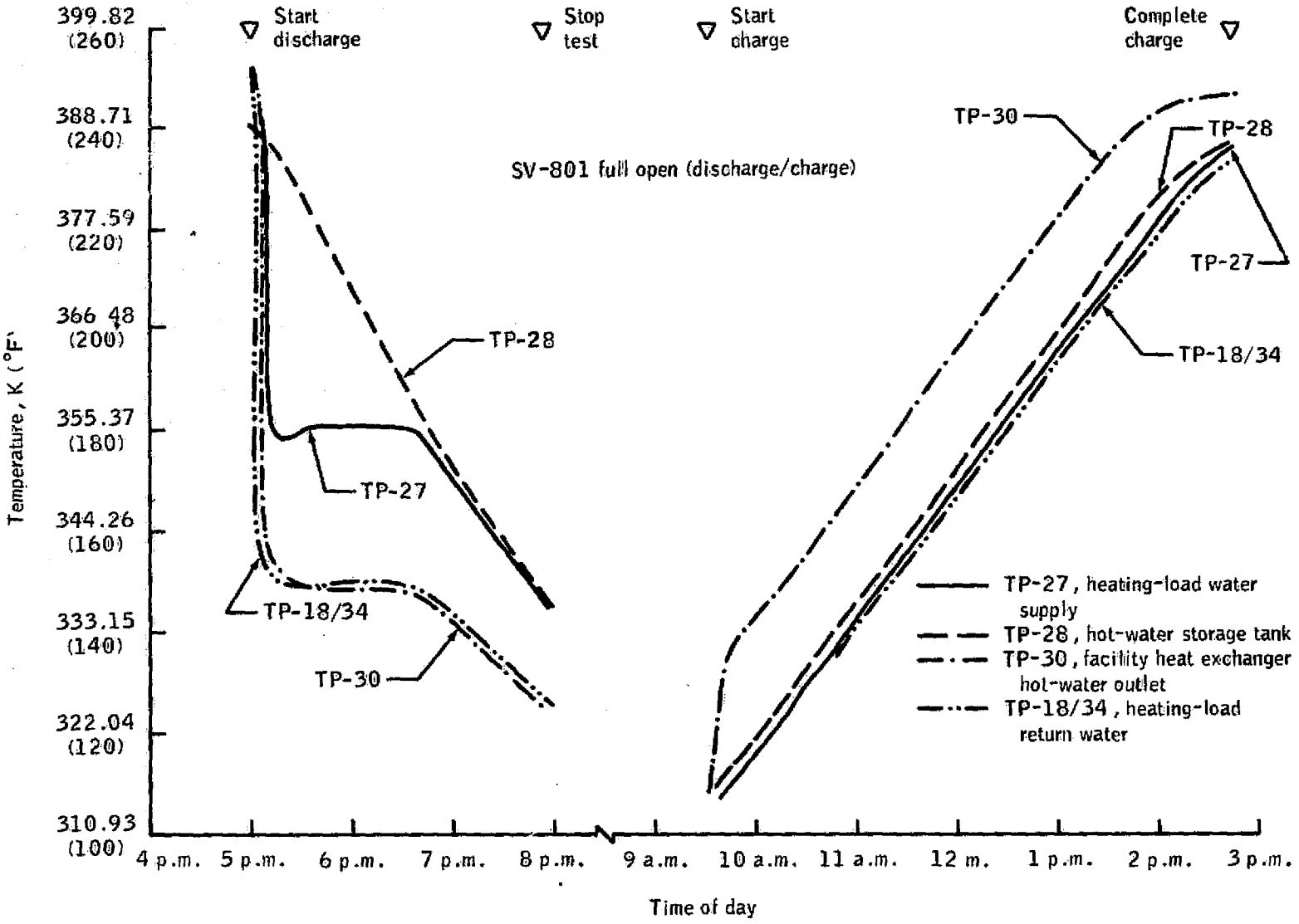

(b) Hot thermal storage discharge/charge profiles.

Figure 25.—Concluded.

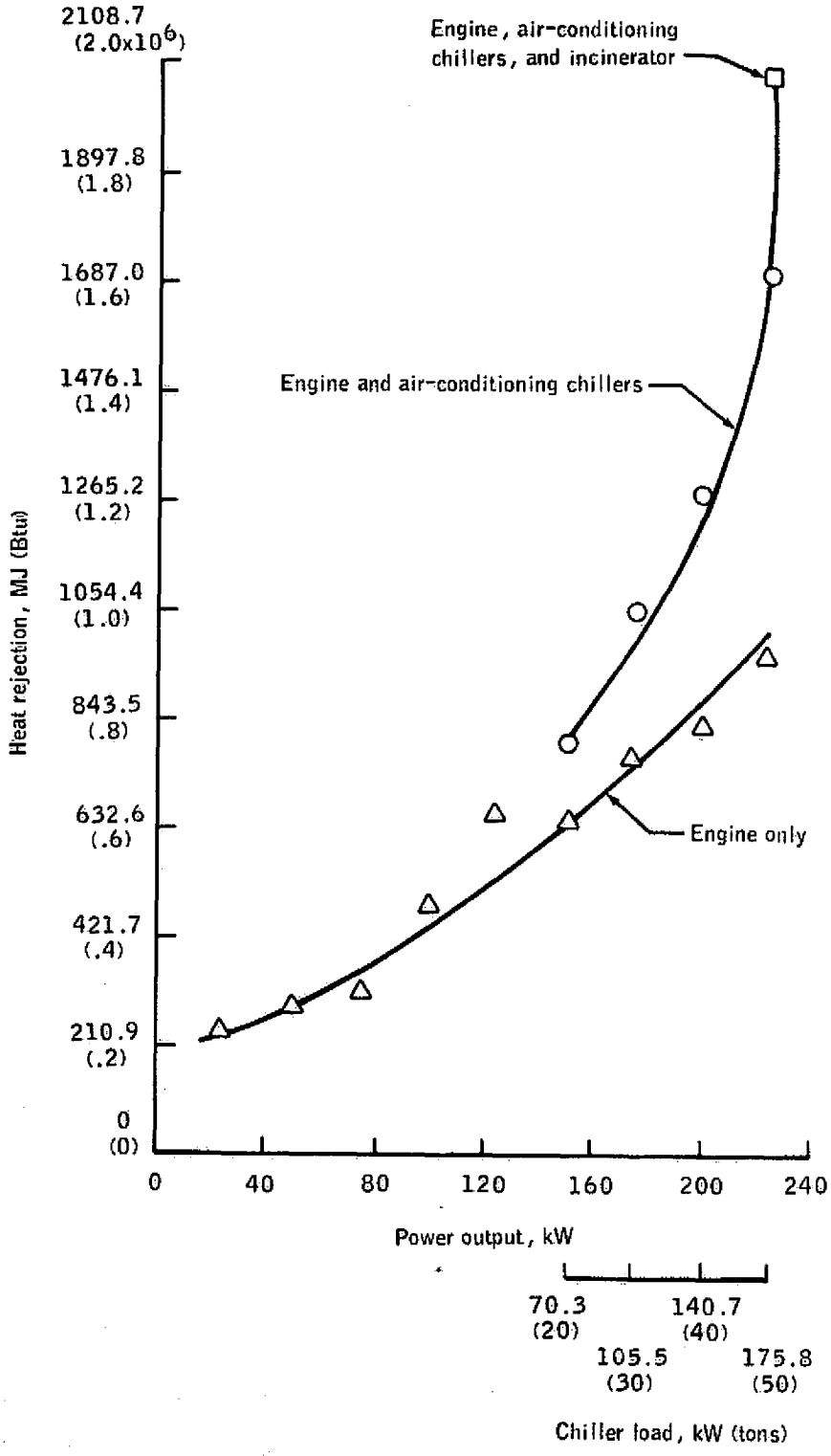

(a) Cooling-tower heat-rejection curve.

Figure 26.—MIST series V test—heat-rejection/heat-transfer network.

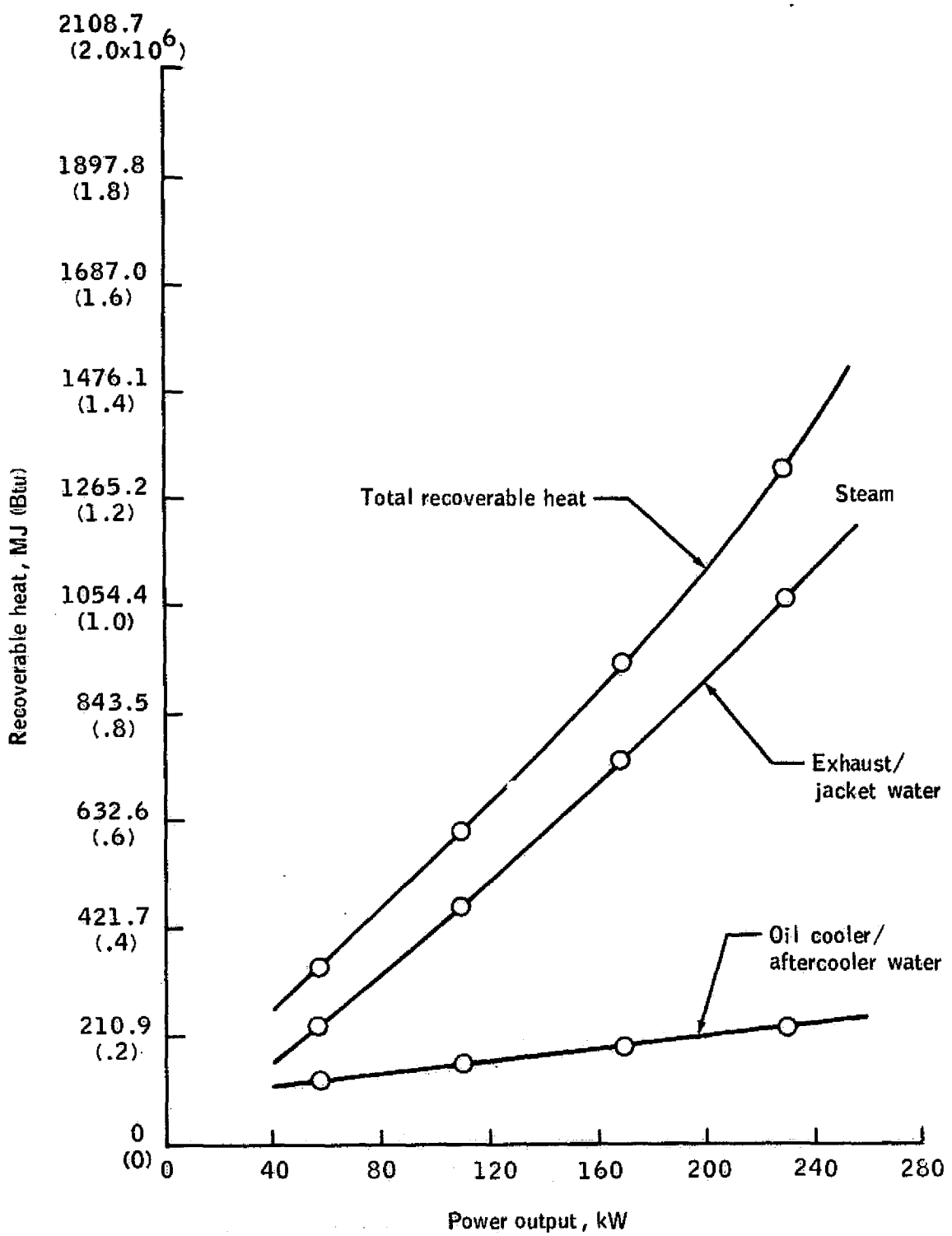

(b) Engine available recoverable heat as a function of output power (manufacturer's catalog data, ebullient-cooling mode).

Figure 26.—Continued.

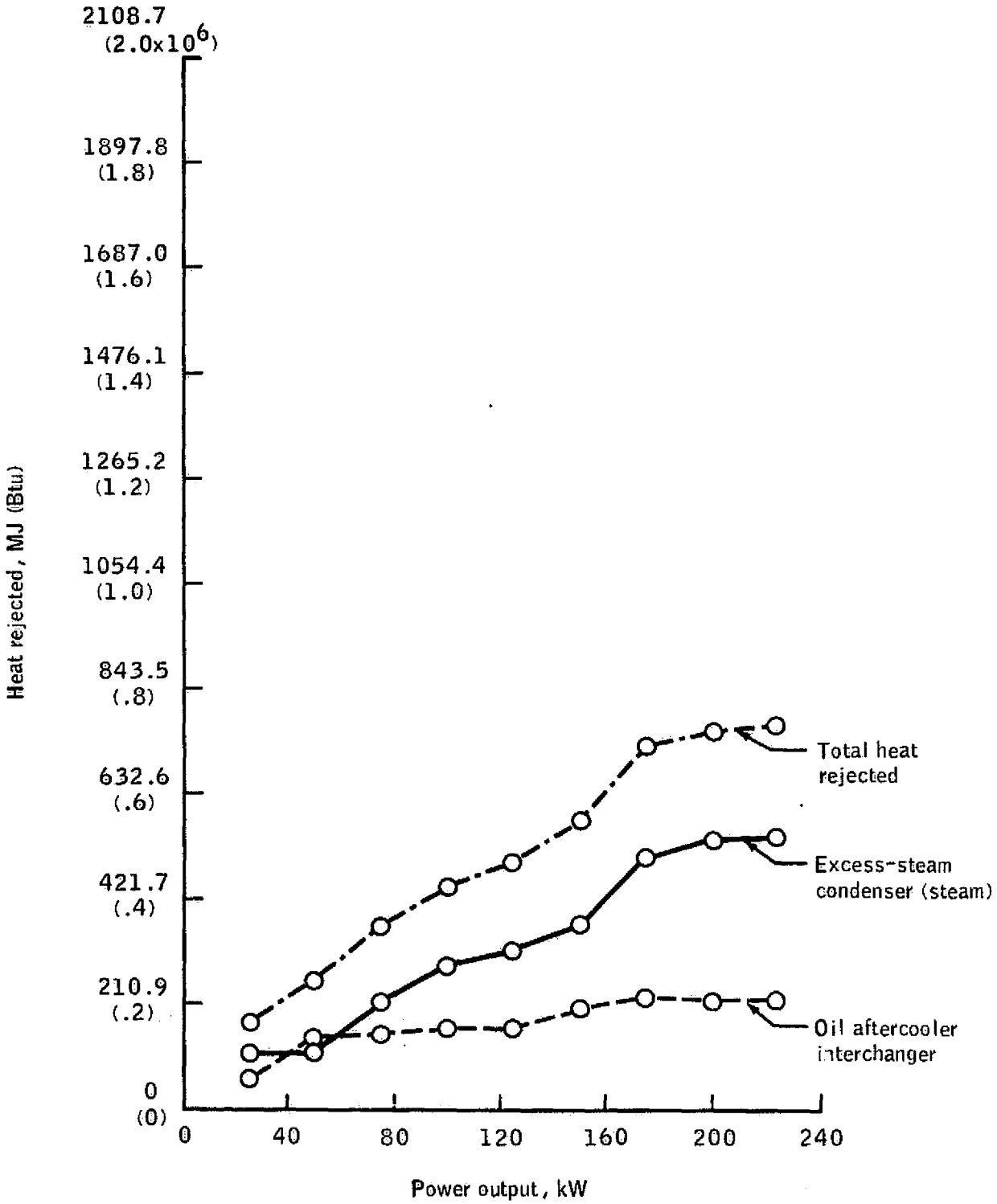

(c) Engine heat rejected to cooling loop (engine only; results based on exchanger performance).

Figure 26.—Continued.

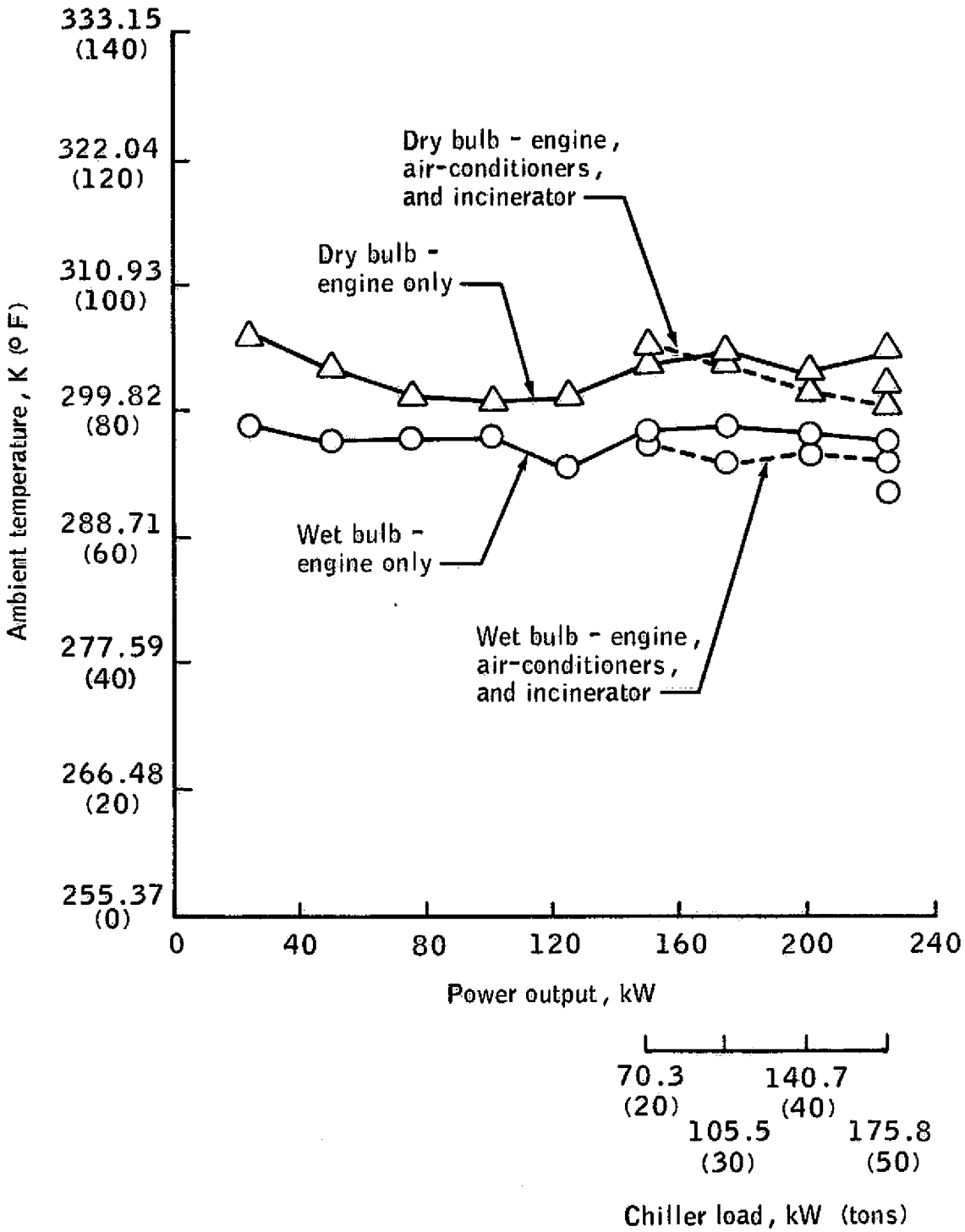

(d) MIST ambient conditions as a function of load.

Figure 26.—Continued.

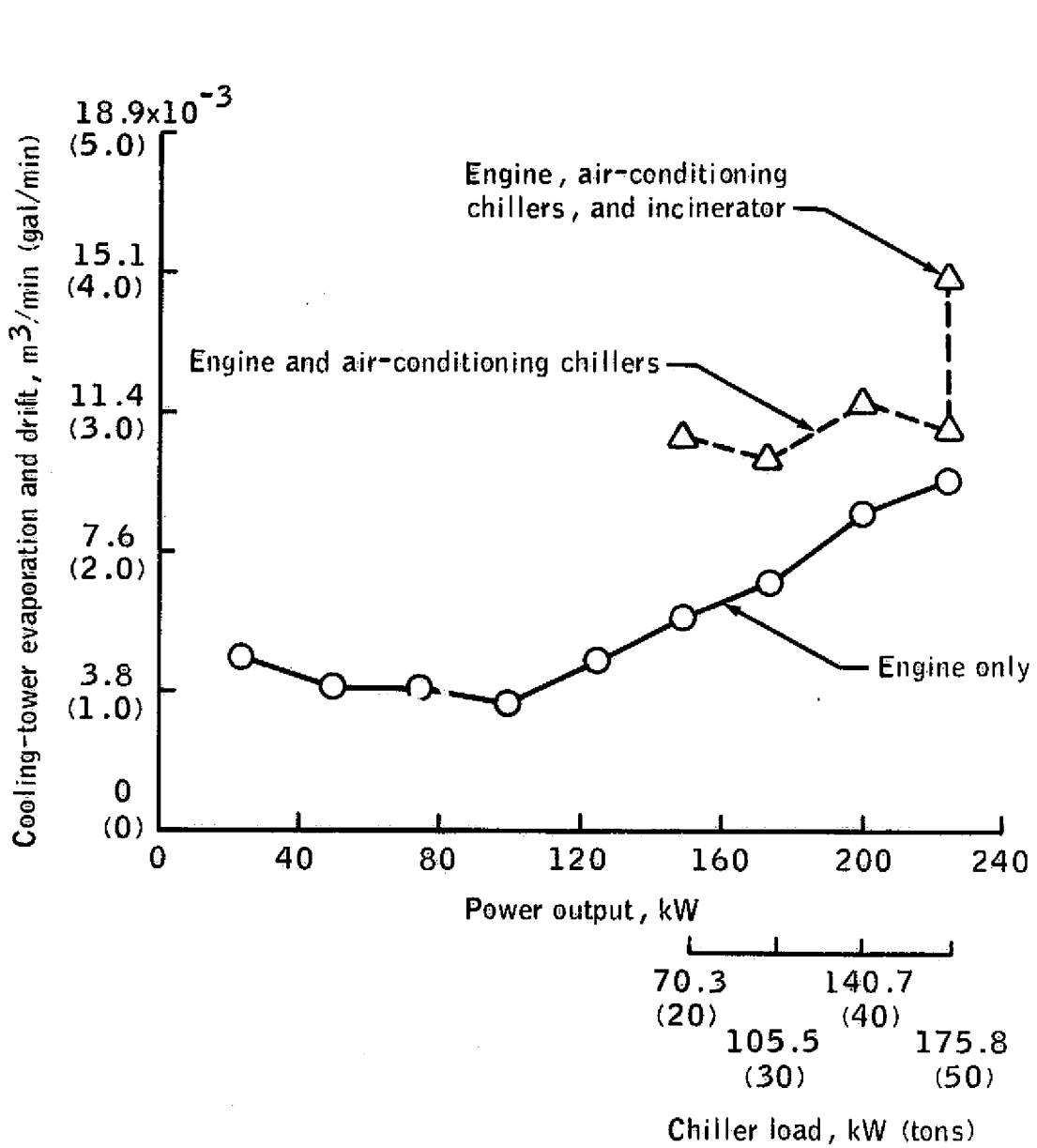

(e) Cooling-tower makeup as a function of load.

Figure 26.—Continued.

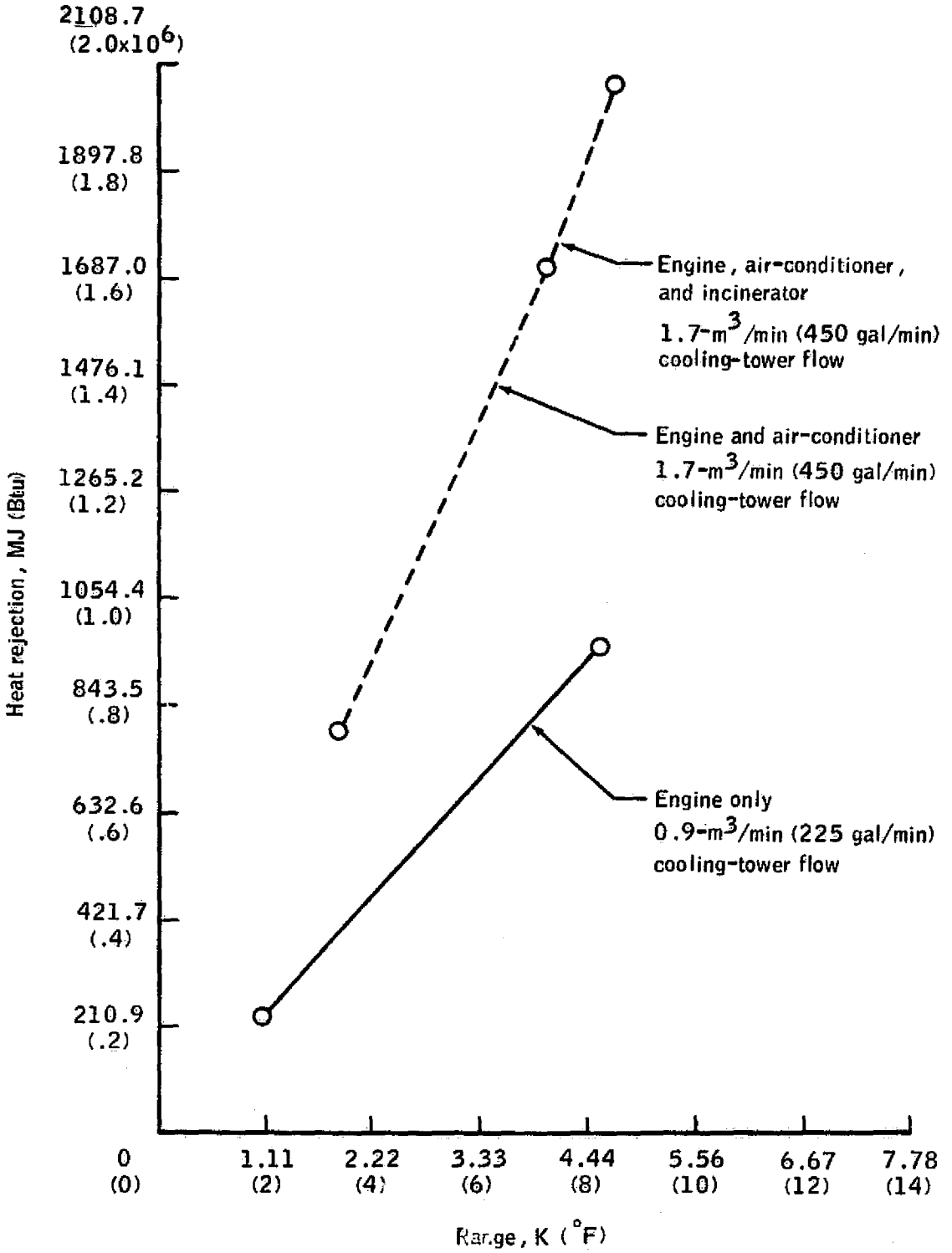

(f) Heat rejection as a function of cooling-tower range.

Figure 26.—Continued.

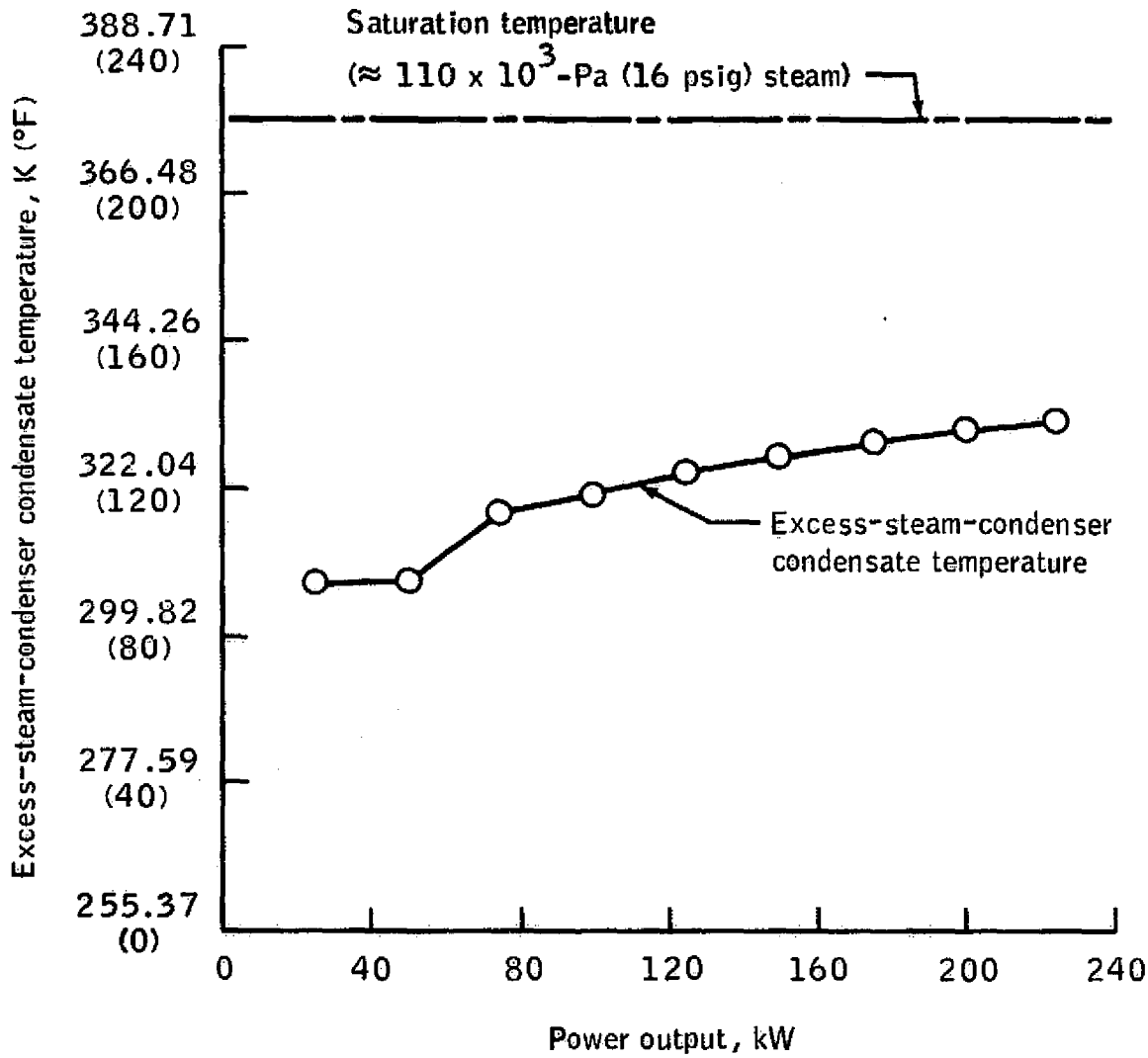

(g) Condensate temperature as a function of engine load.

Figure 26.—Concluded.

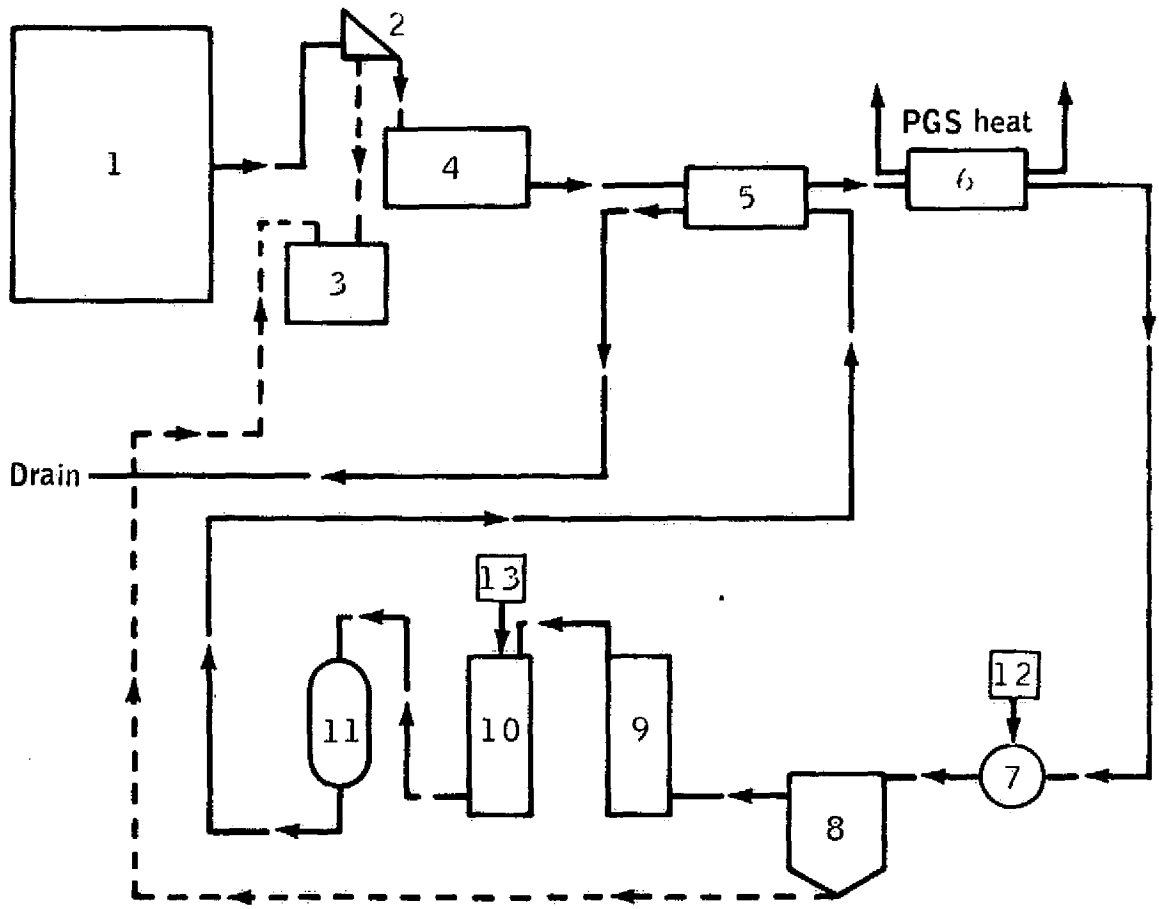

Key:

1. Wastewater supply tank
2. Primary separator
3. Sludge tank
4. Holding tank
5. Sewage regeneration, heat exchanger
6. WMS heater, heat exchanger
7. Flash mixer
8. P-C clarifier
9. Carbon column
10. Chlorine contact tank
11. Multimedia filter
12. Coagulant tank
13. Chlorine tank

Figure 27.—Physical-chemical WMS.

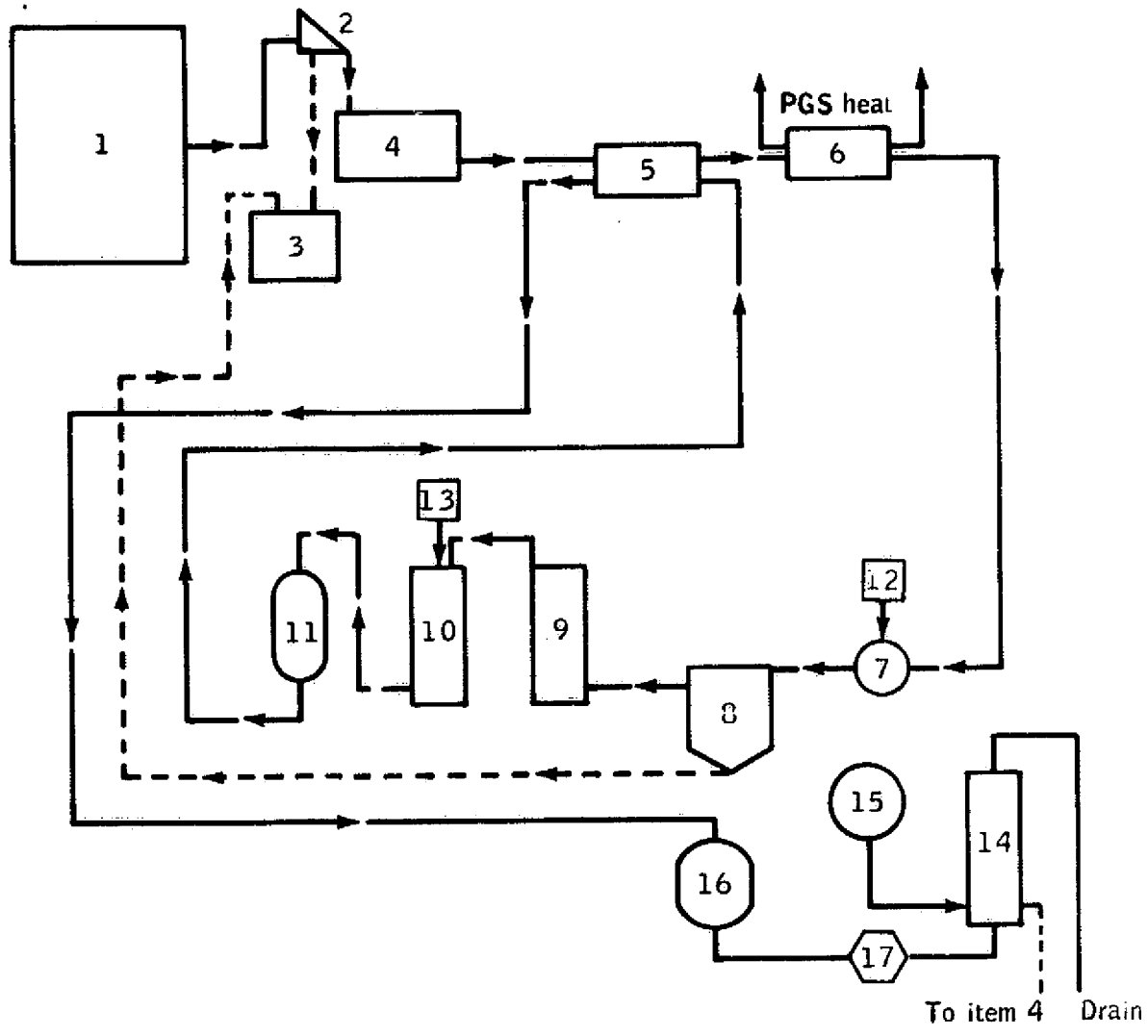

Key:

1. Wastewater supply tank
2. Primary separator
3. Sludge tank
4. Holding tank
5. Sewage regeneration, heat exchanger
6. WMS heater, heat exchanger
7. Flash mixer
8. P-C clarifier
9. Carbon column
10. Chlorine contact tank
11. Multimedia filter
12. Coagulant tank
13. Chlorine tank
14. RO separation module
15. Acid tank
16. RO sand filter
17. High-pressure pump

Figure 28.—Reverse-osmosis WMS.

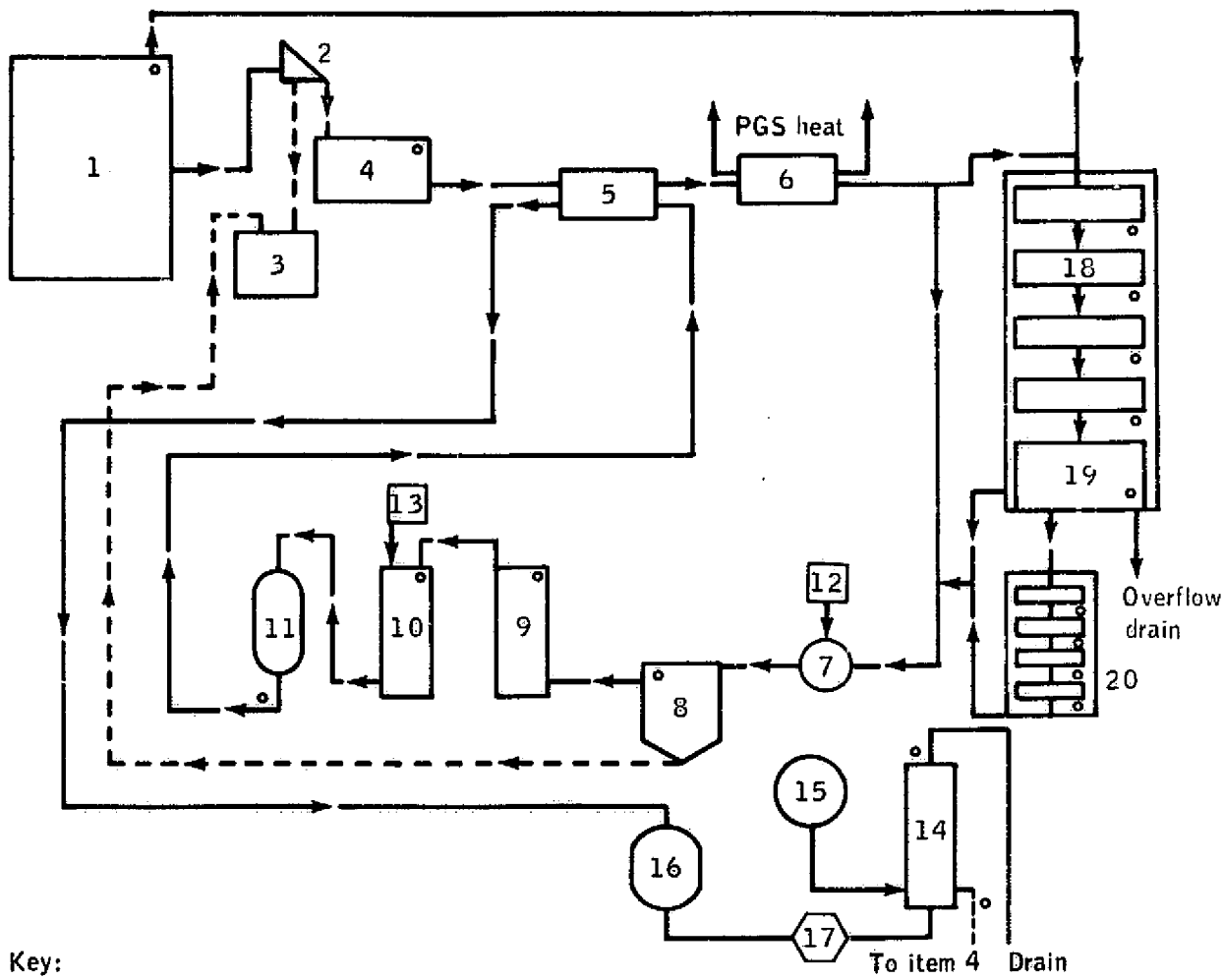

Key:

1. Wastewater supply tank
2. Primary separator
3. Sludge tank
4. Holding tank
5. Sewage regeneration, heat exchanger
6. WMS heater, heat exchanger
7. Flash mixer
8. P-C clarifier
9. Carbon column
10. Chlorine contact tank
11. Multimedia filter
12. Coagulant tank
13. Chlorine tank
14. RO separation module
15. Acid tank
16. RO sand filter
17. High-pressure pump
18. Bio-surf
19. Biological clarifier
20. Denitrifier

o Sampling points

Figure 29.—Biological-tertiary WMS.

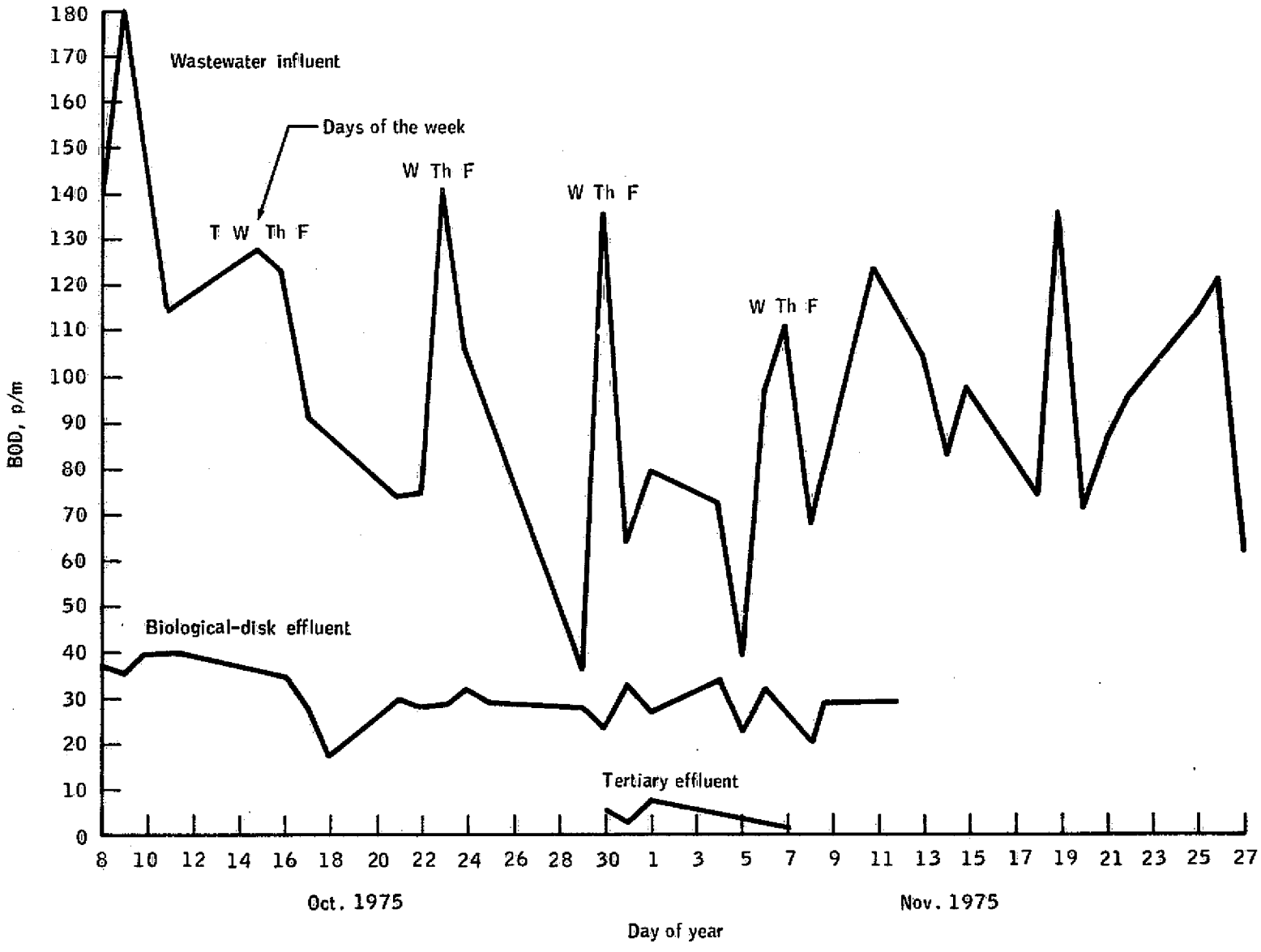

Figure 30.—Biological-oxygen-demand reduction.

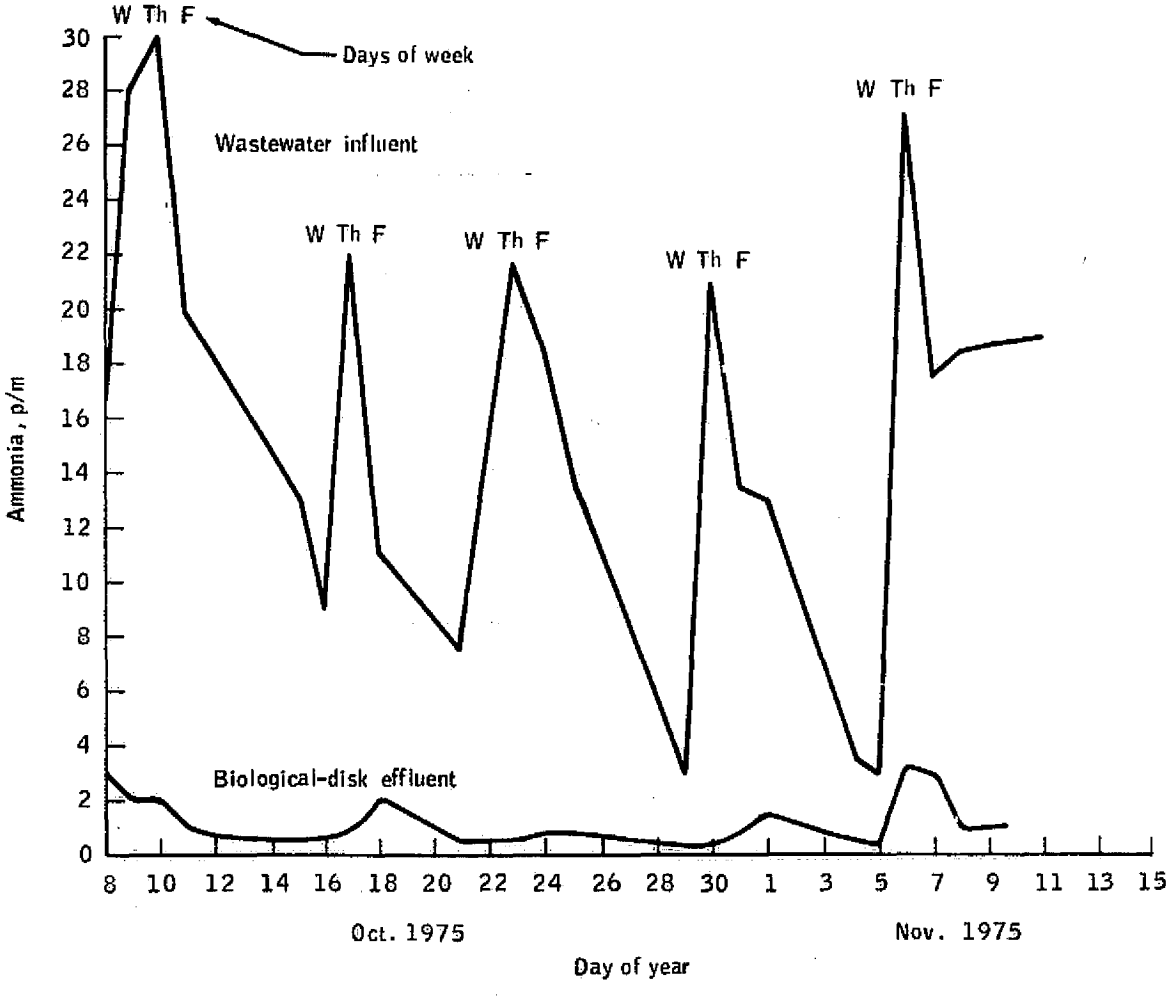

Figure 31.—Ammonia reduction.

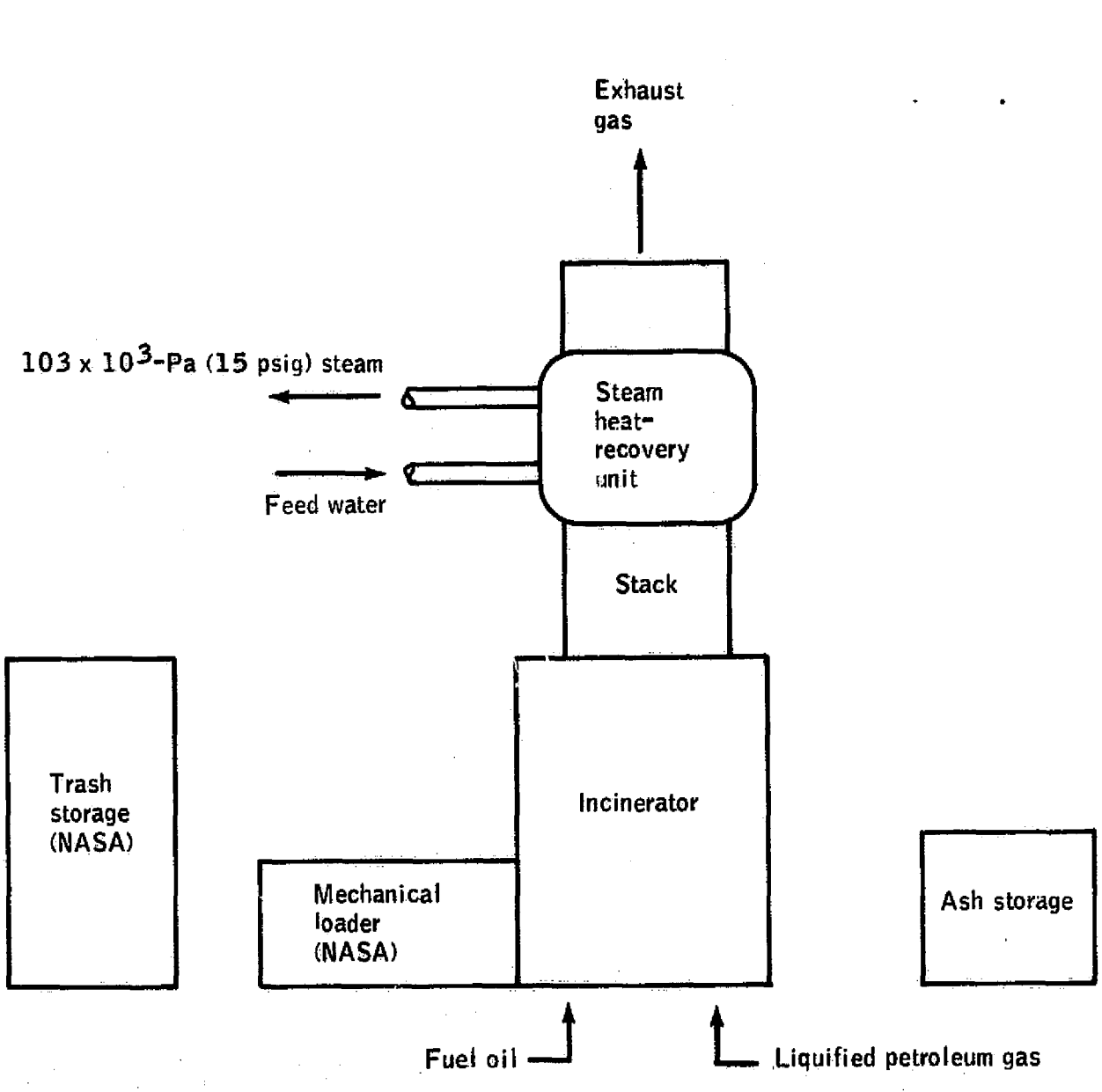

Figure 32.—Solid-waste-management schematic.

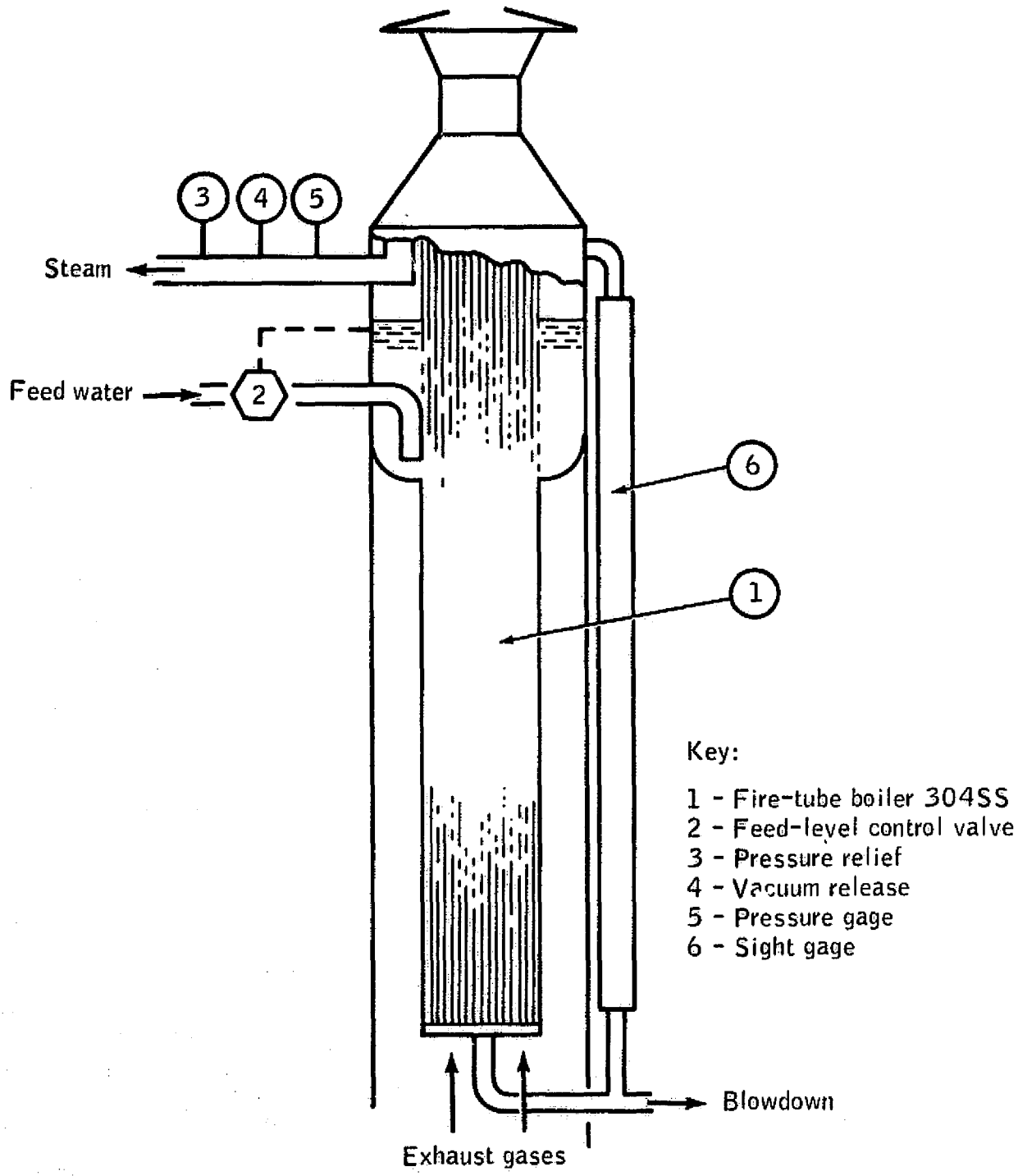

Figure 33.—Heat-recovery unit.

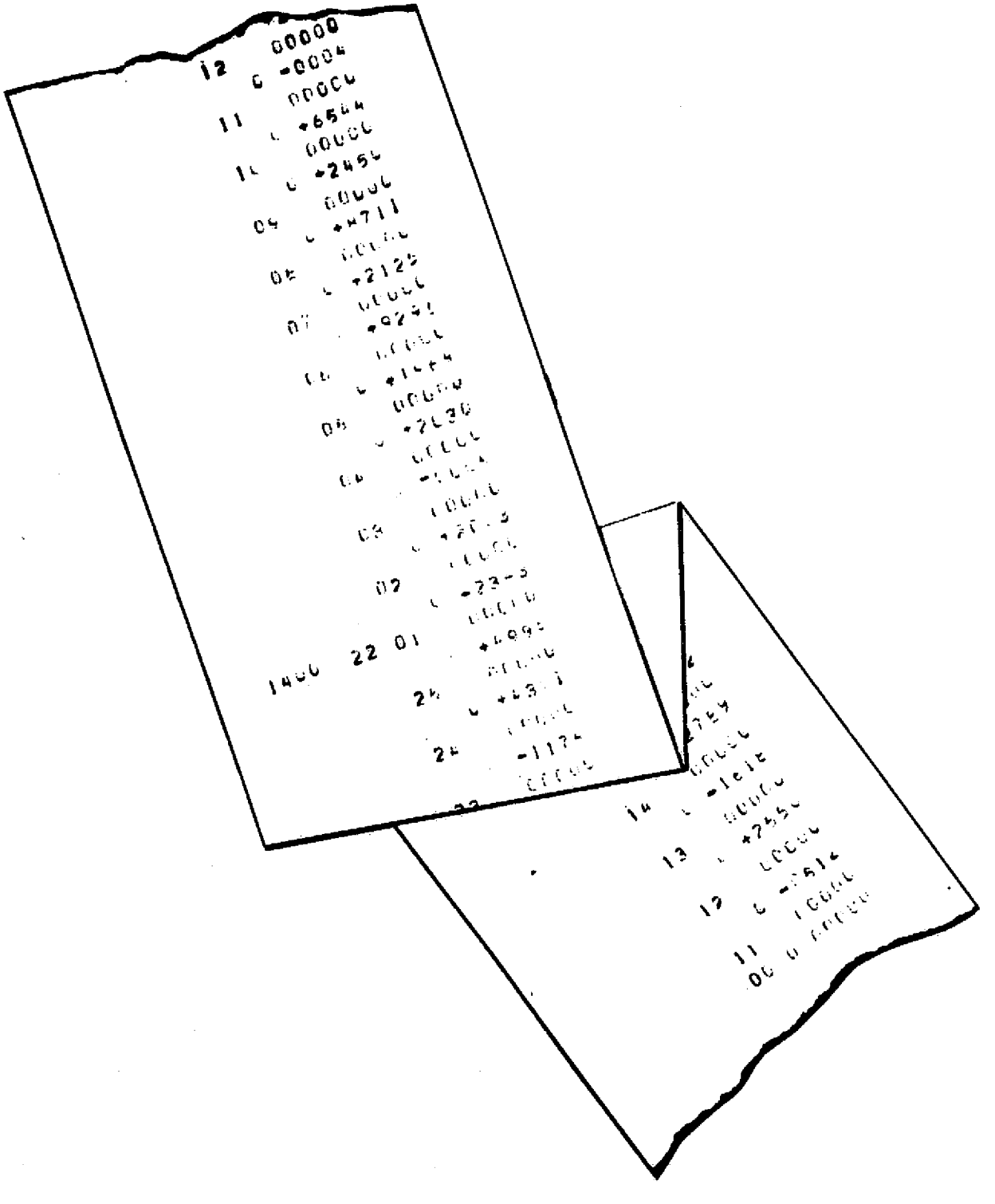

Figure 34.—A DEXTIR real-time printout.

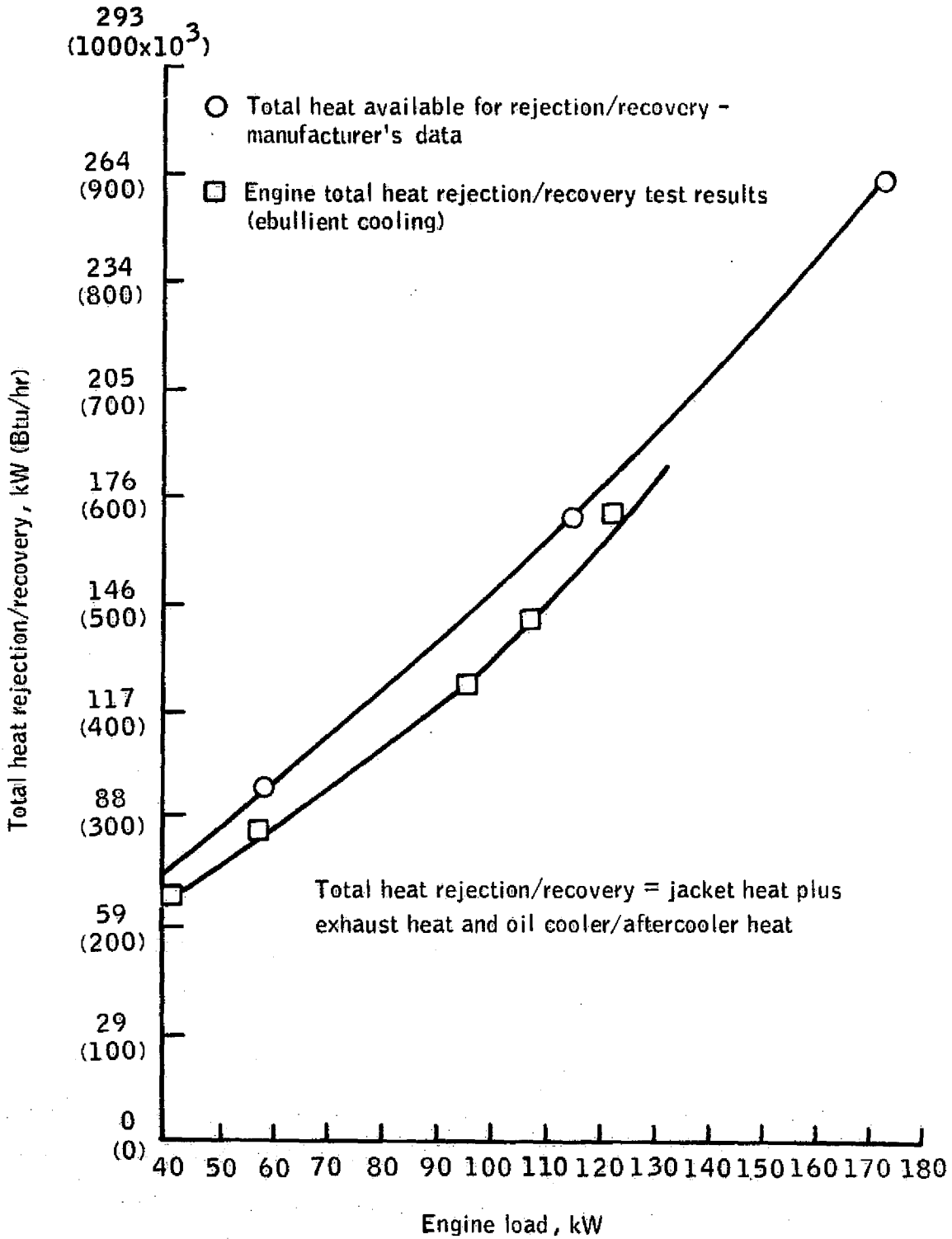

(a) Engine heat rejection/recovery as a function of engine load (time averaged).

Figure 35.—MIST series I integrated tests.

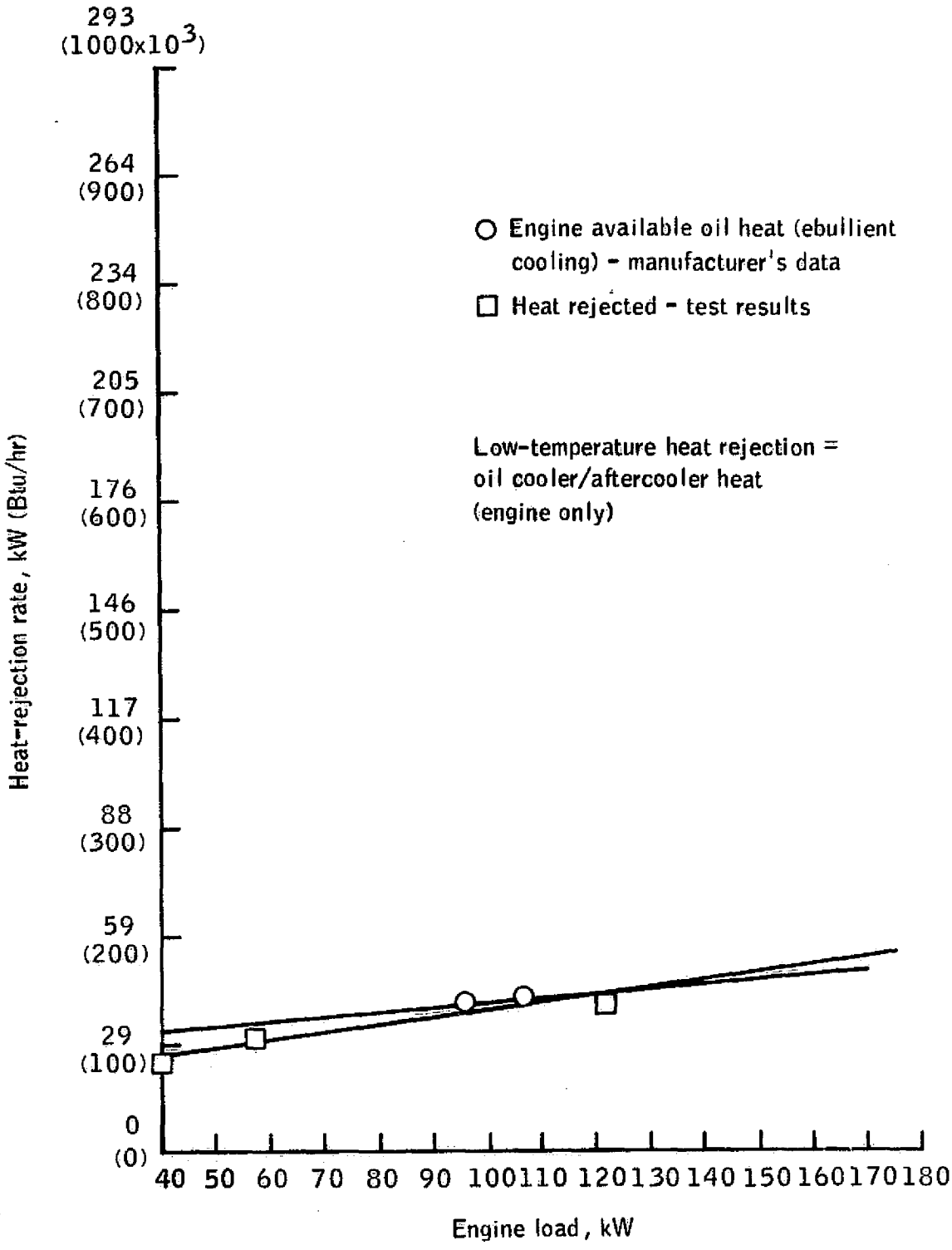

(b) Engine-oil-rejected heat as a function of engine load (time averaged).

Figure 35.—Continued.

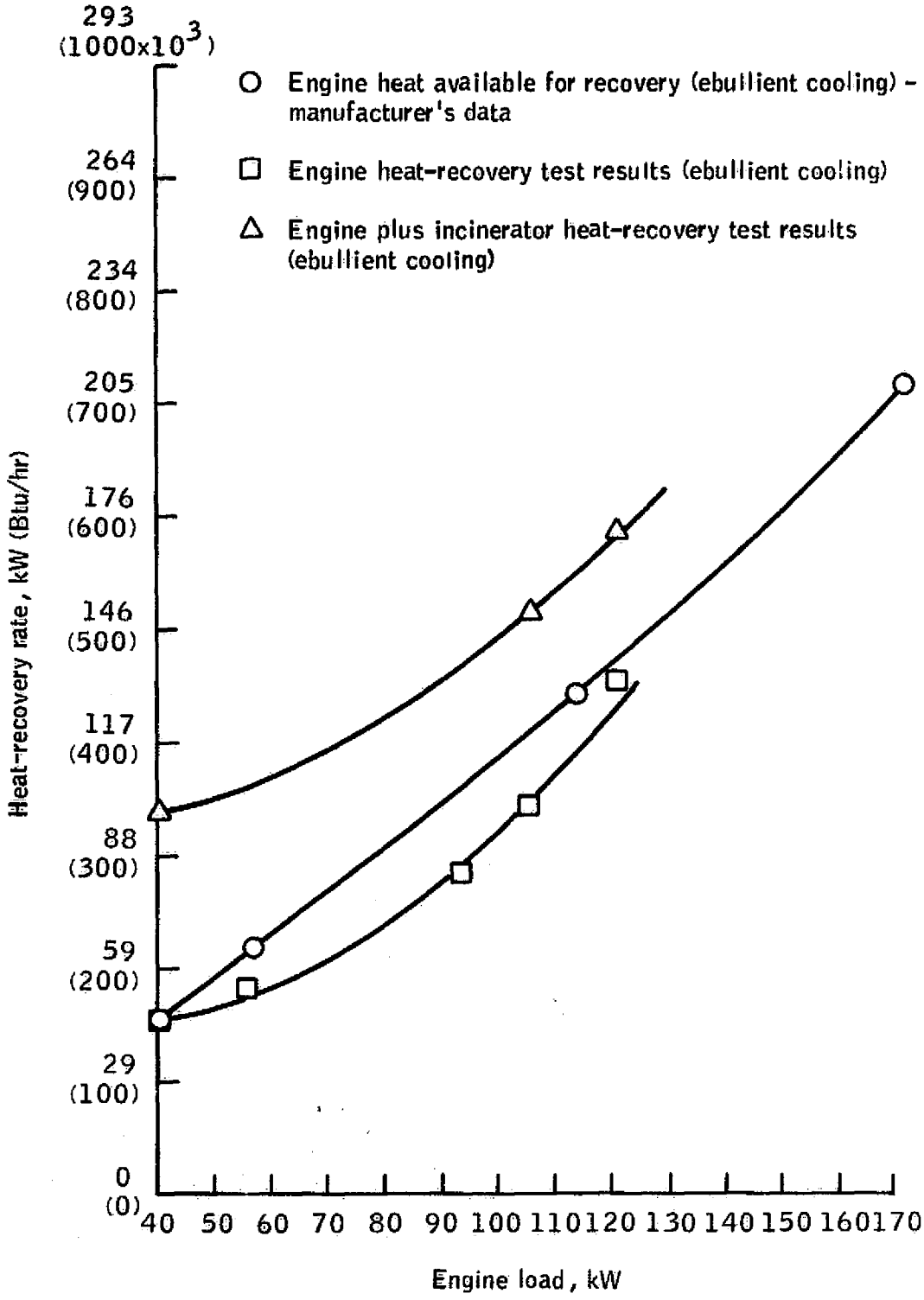

(c) Engine/incinerator-recovered high-grade heat as a function of engine load (time averaged; steam heat recovery at 103 kilopascals (15 psia)).

Figure 35.—Continued.

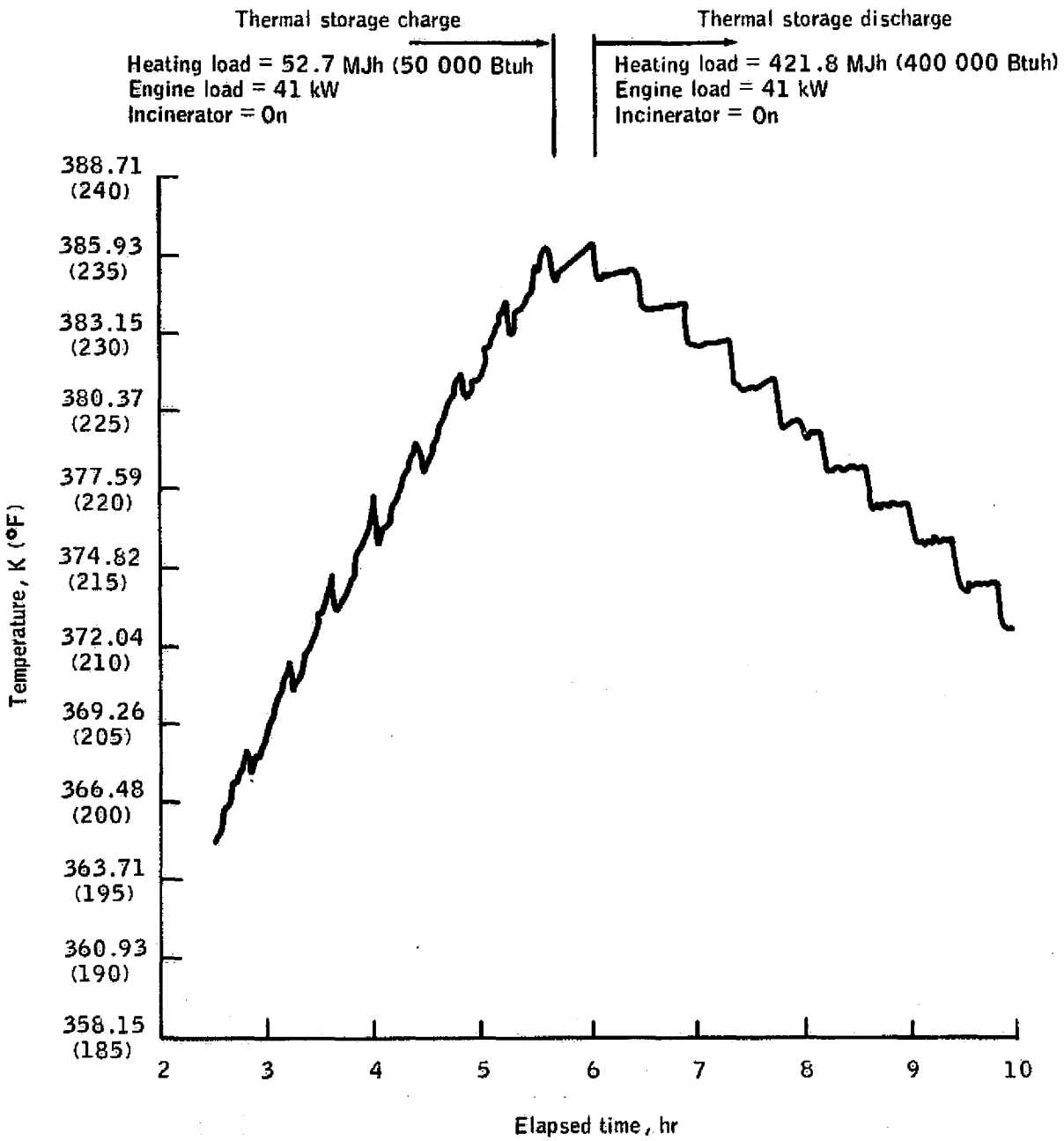

(d) Hot thermal storage charge/discharge temperature profile.

Figure 35.—Continued.

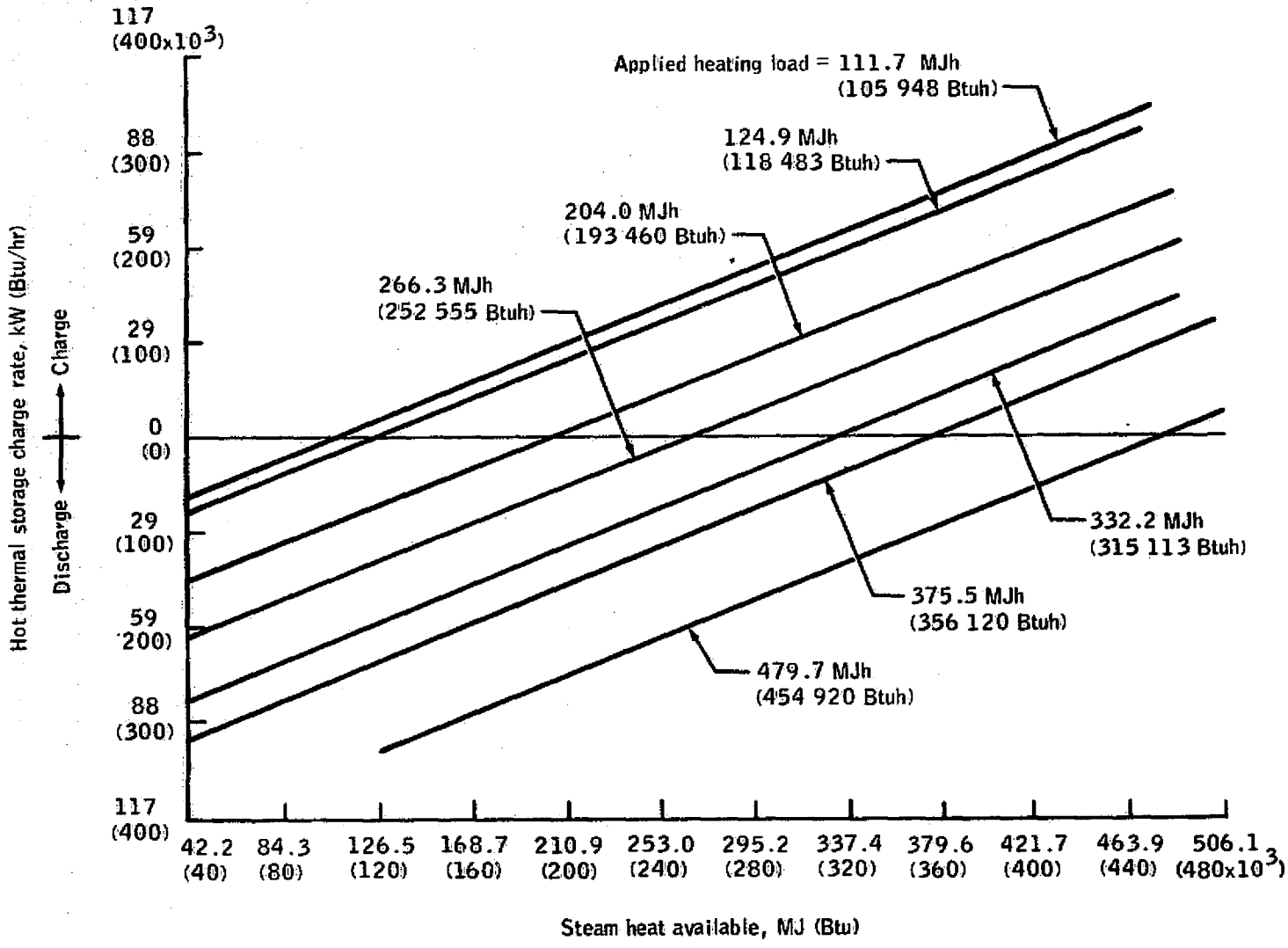

(e) Hot thermal storage charge/discharge rate as a function of steam-heat availability.

Figure 35.—Continued.

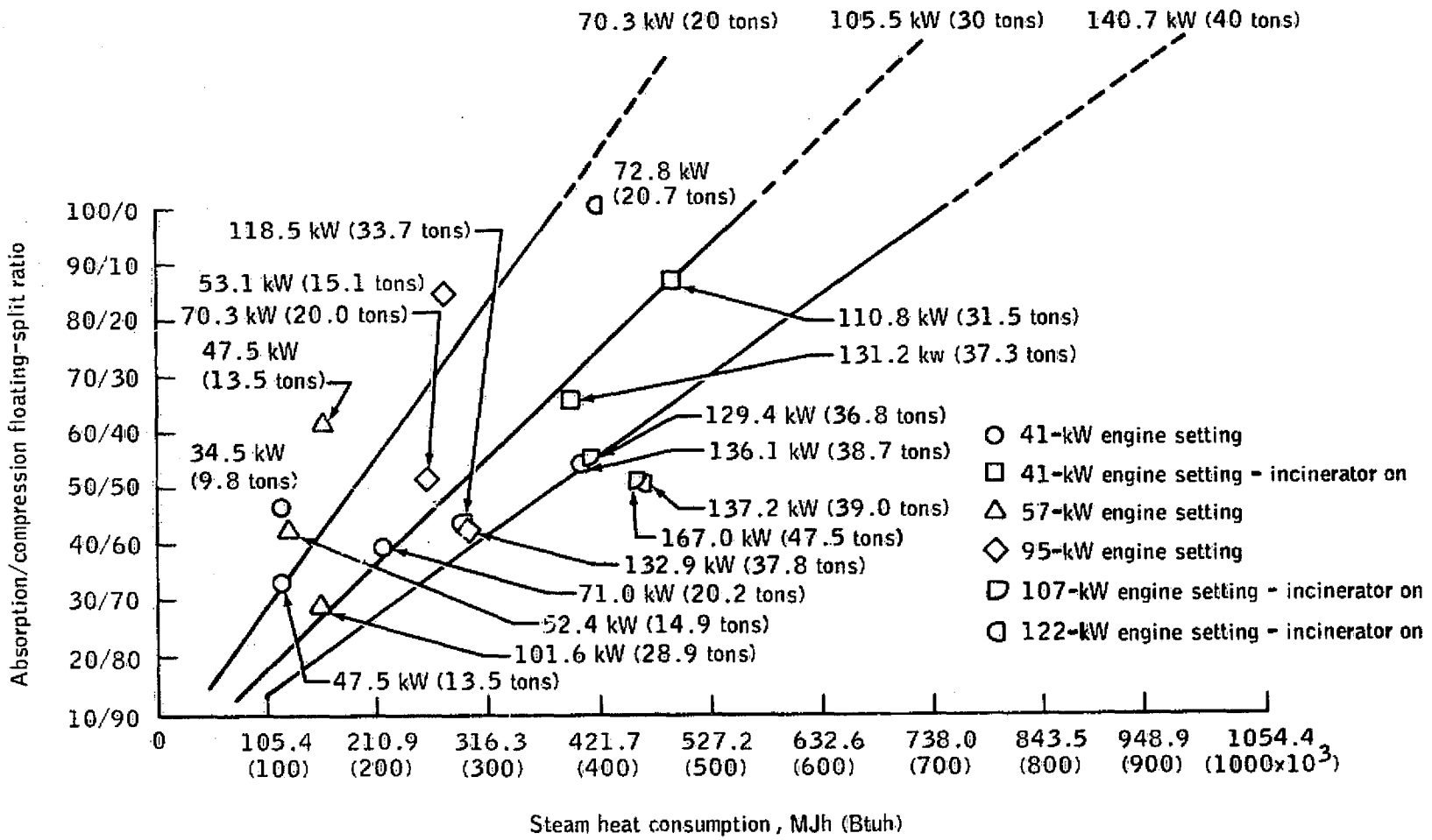

(f) Floating-split ratio as a function of steam-heat consumption.

Figure 35.—Continued.

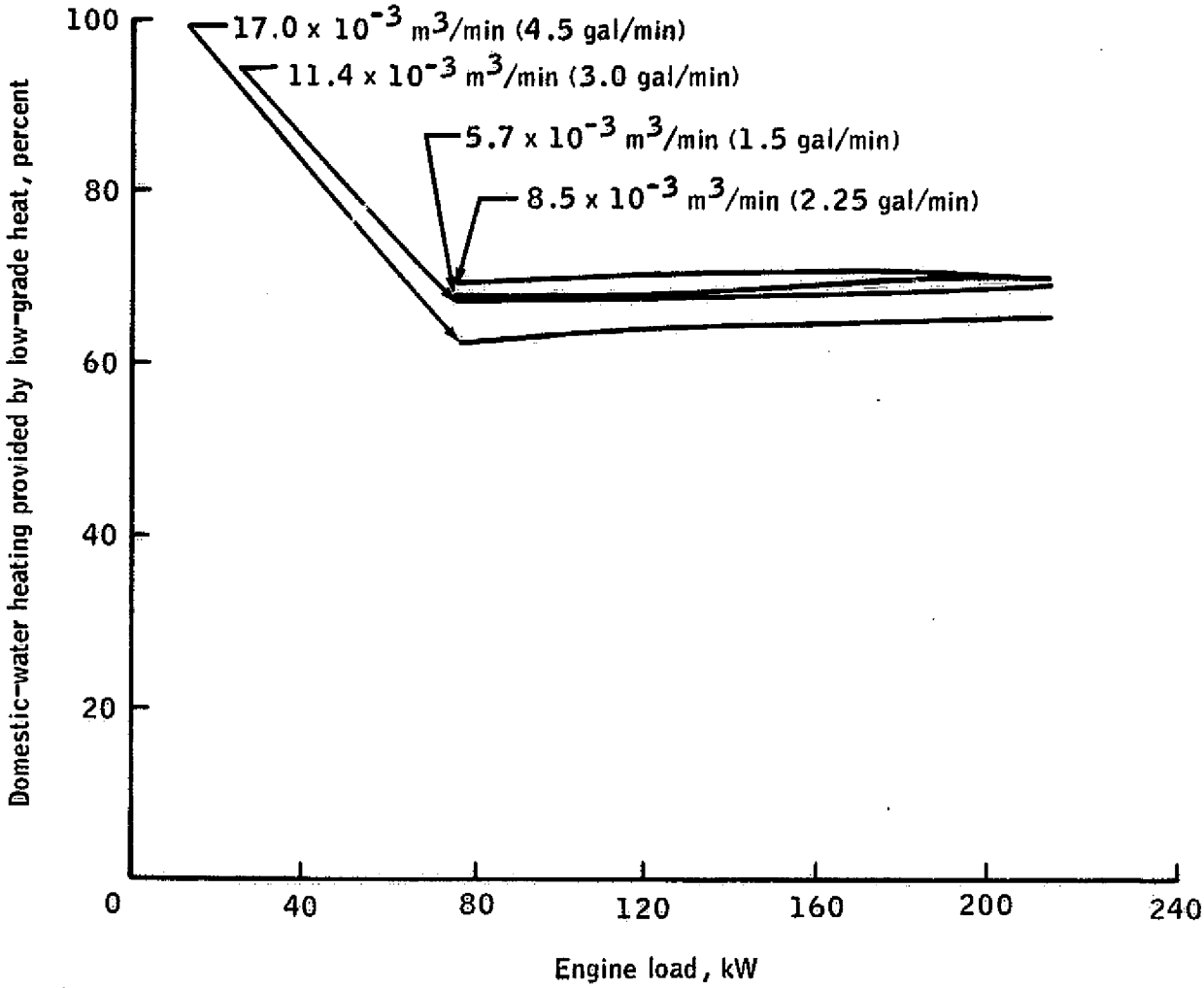

(g) Domestic-hot-water preheating as a function of engine load.

Figure 35.—Continued.

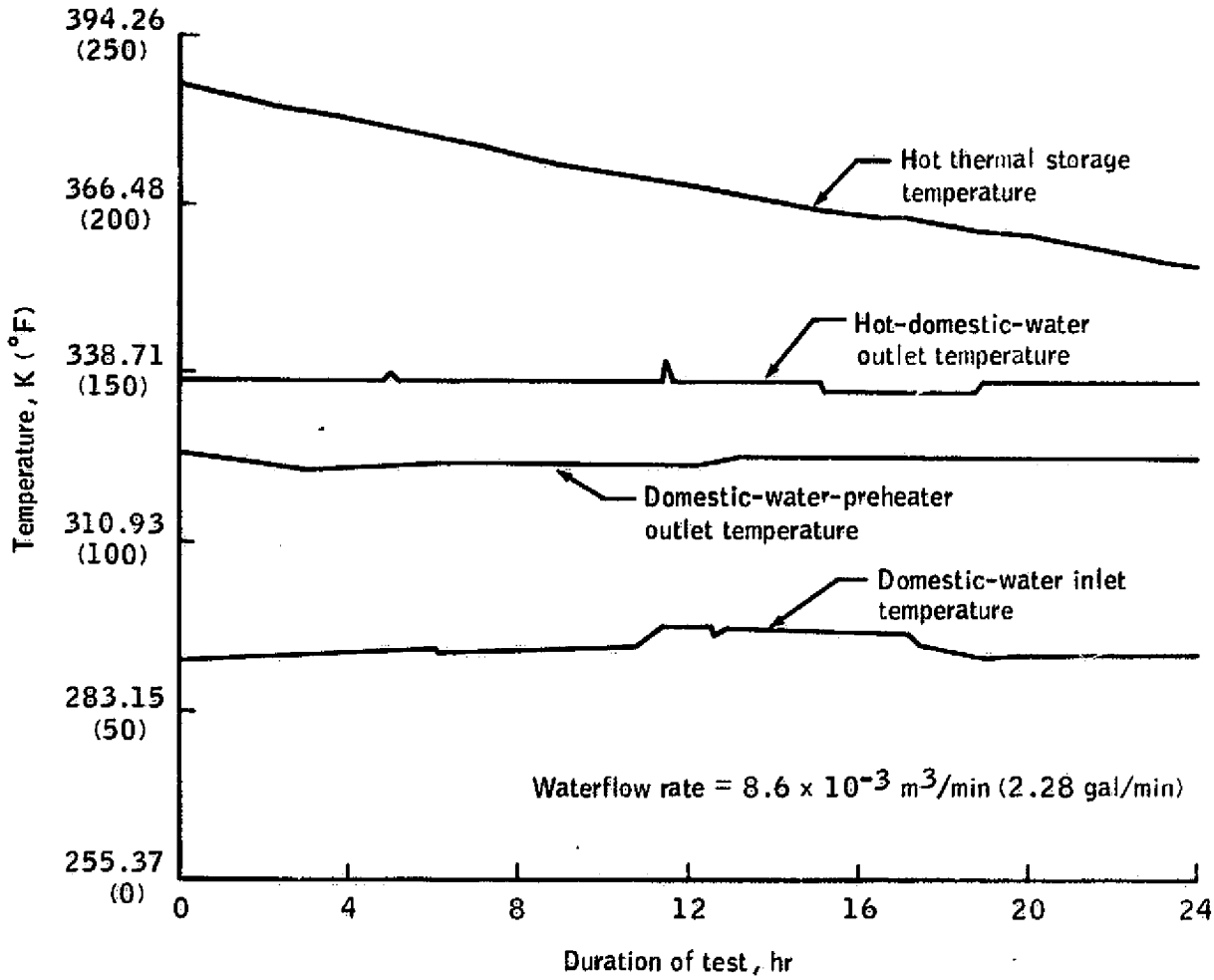

(h) Domestic-hot-water-heating temperature as a function of time—low-grade heat and thermal storage used.

Figure 35.—Concluded.

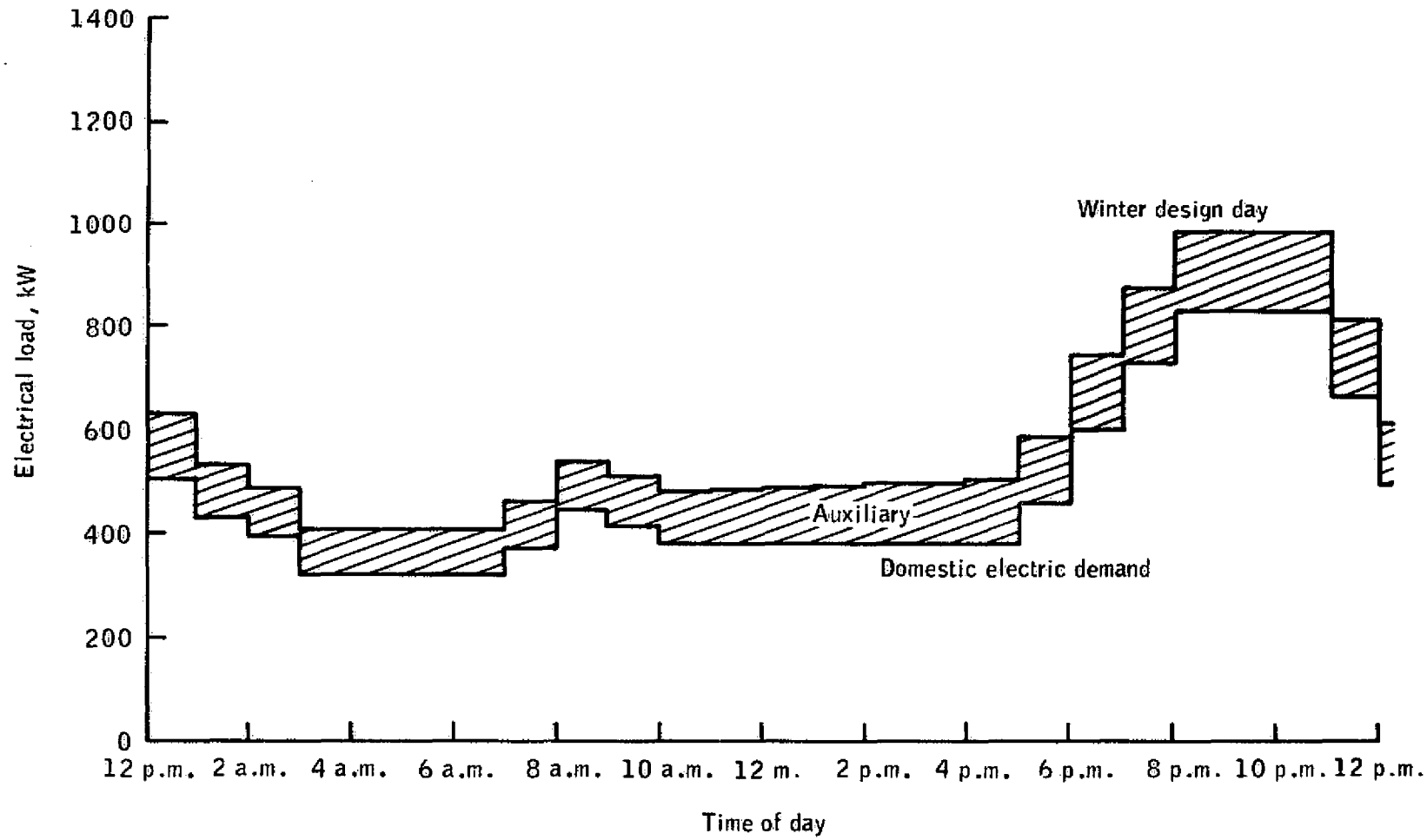

Figure 36.—MIUS power profile—less space cooling.

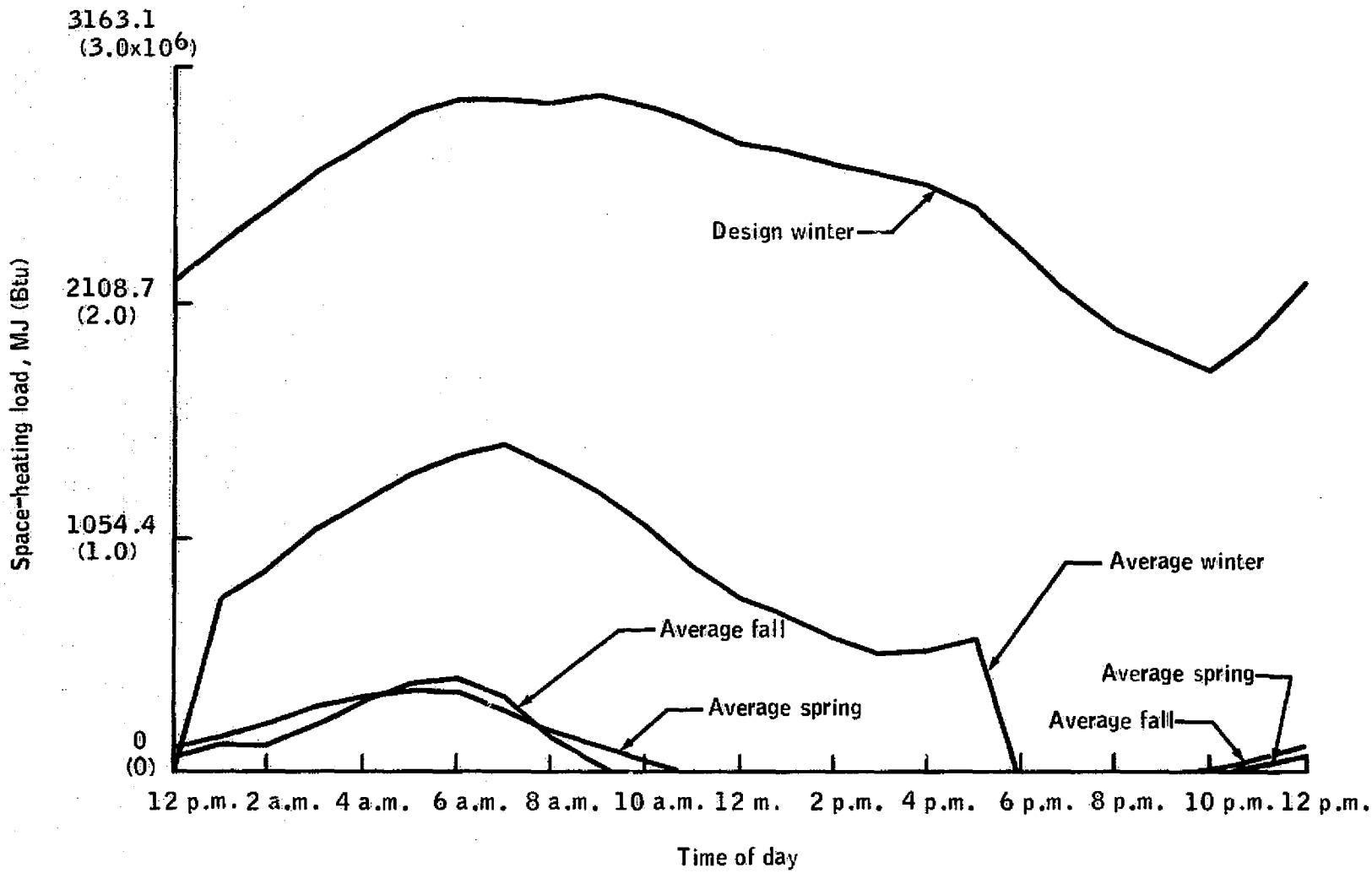

Figure 37.—MIUS space-heating-load profile.

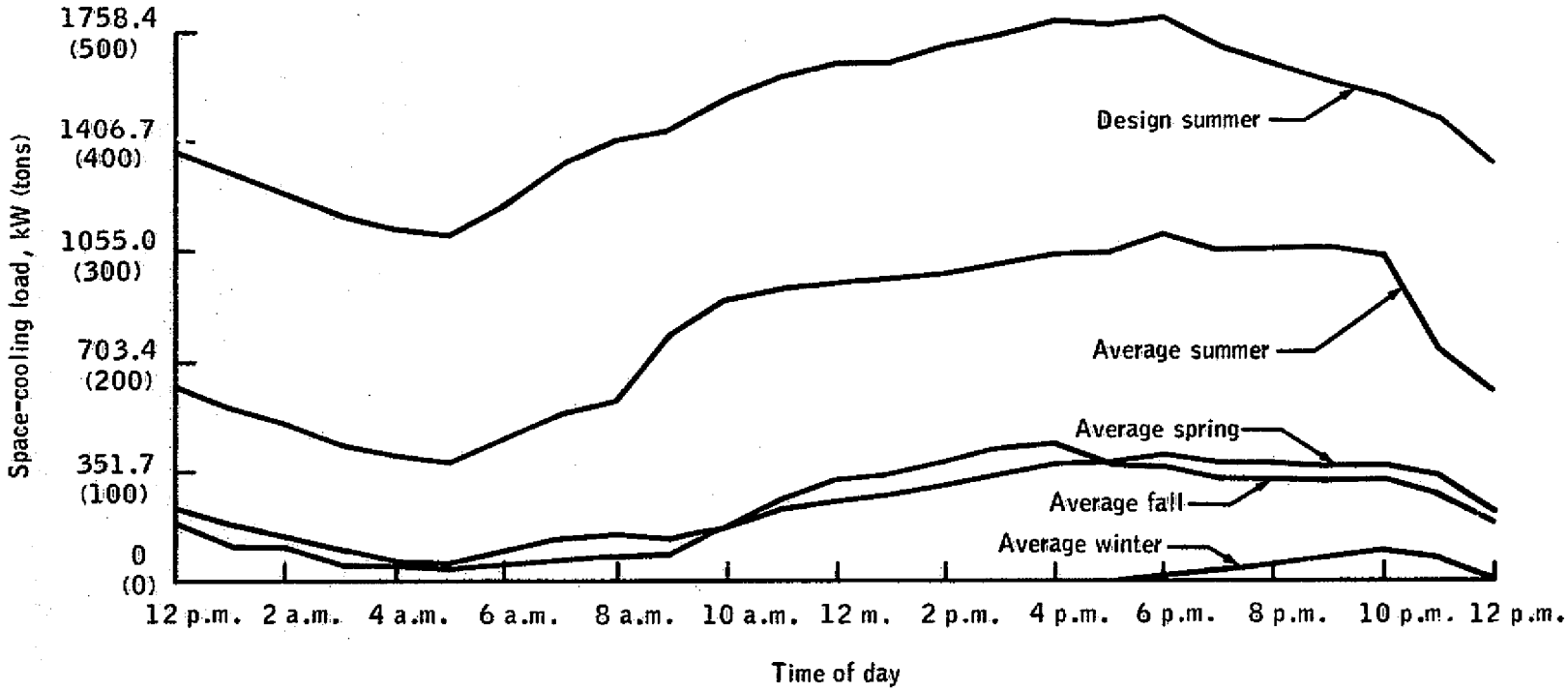

Figure 38.—MIUS space-cooling-load profile.

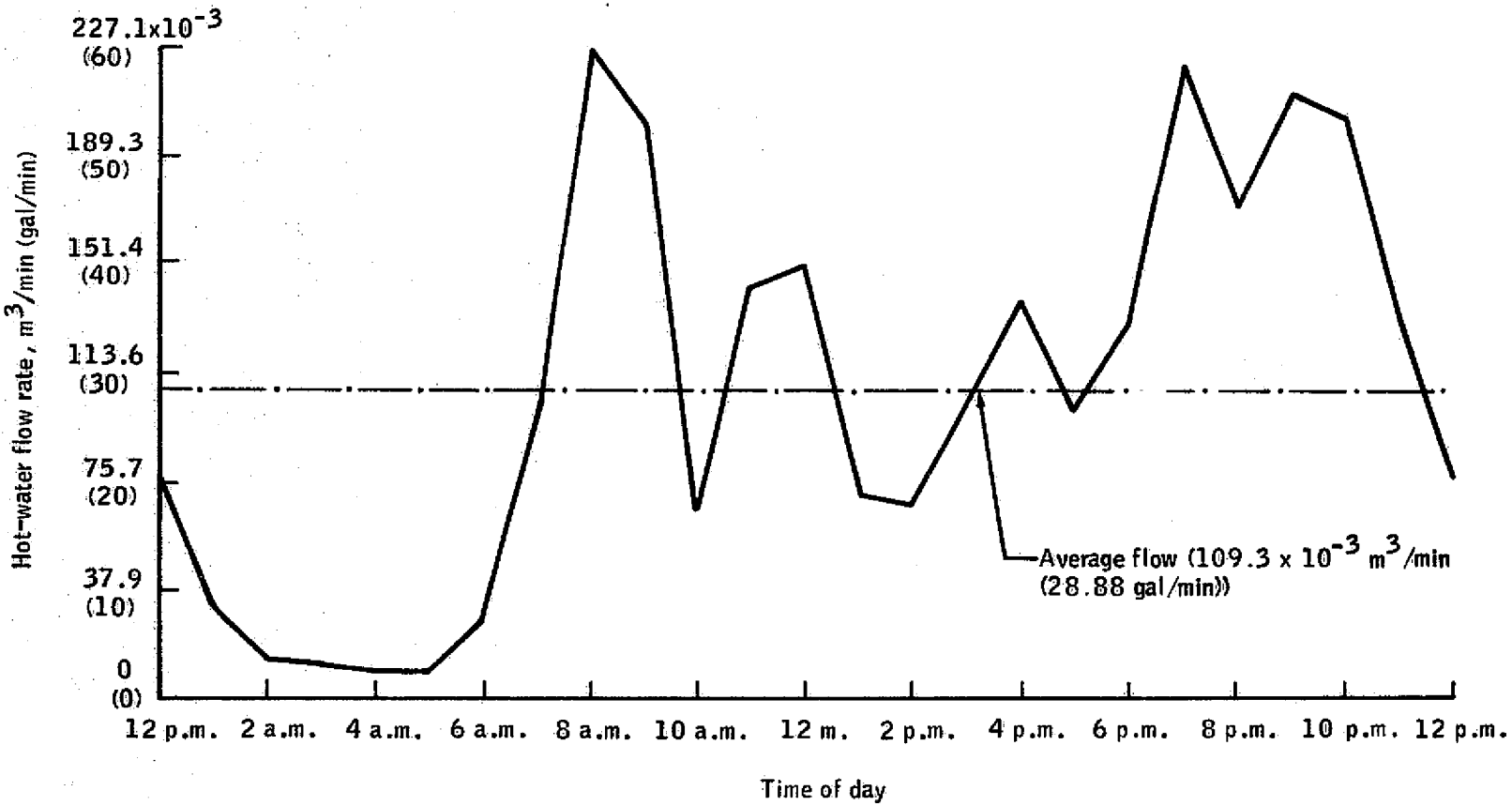

Figure 39.—MIUS domestic-hot-water-flow profile.

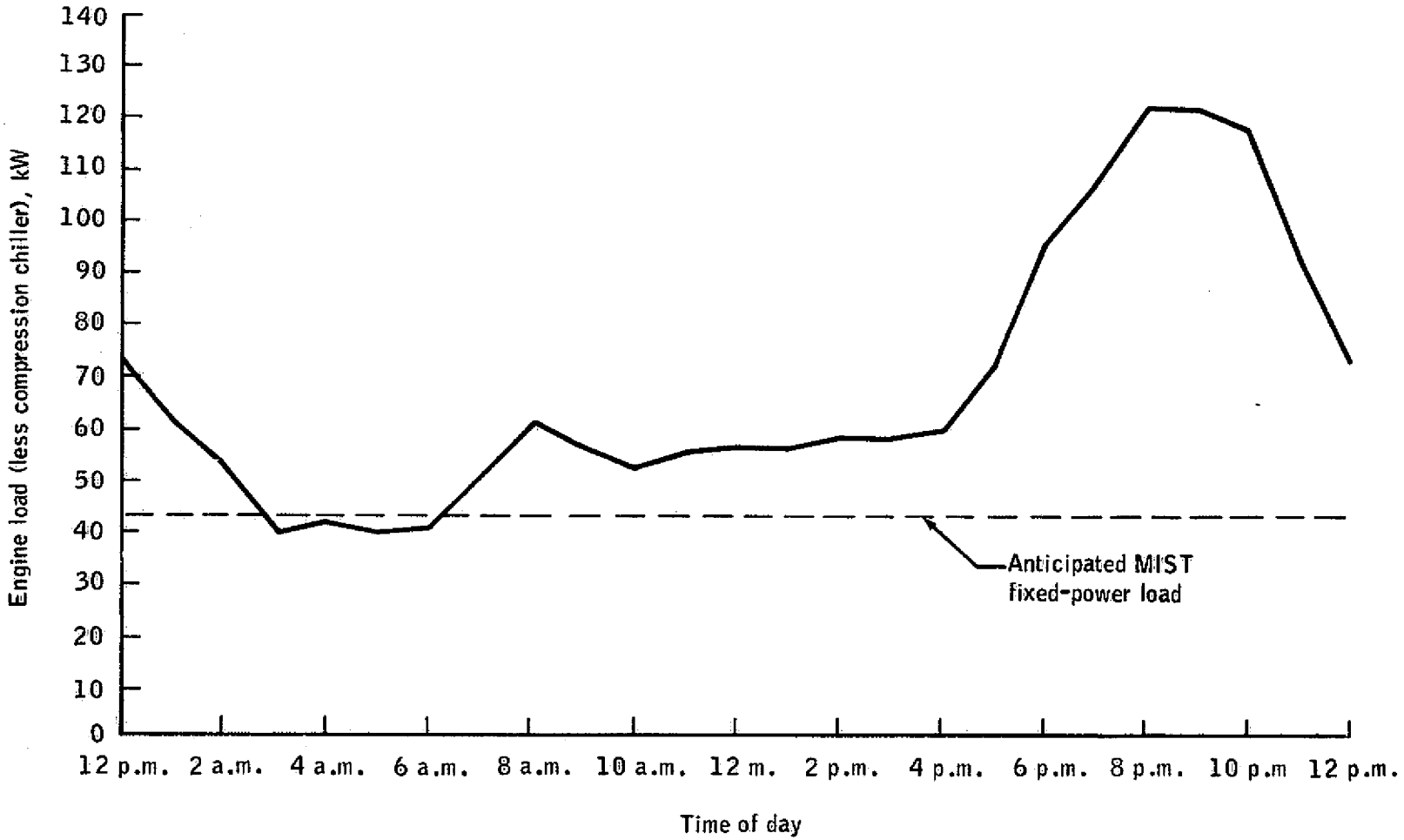

Figure 40.—MIST power profile.

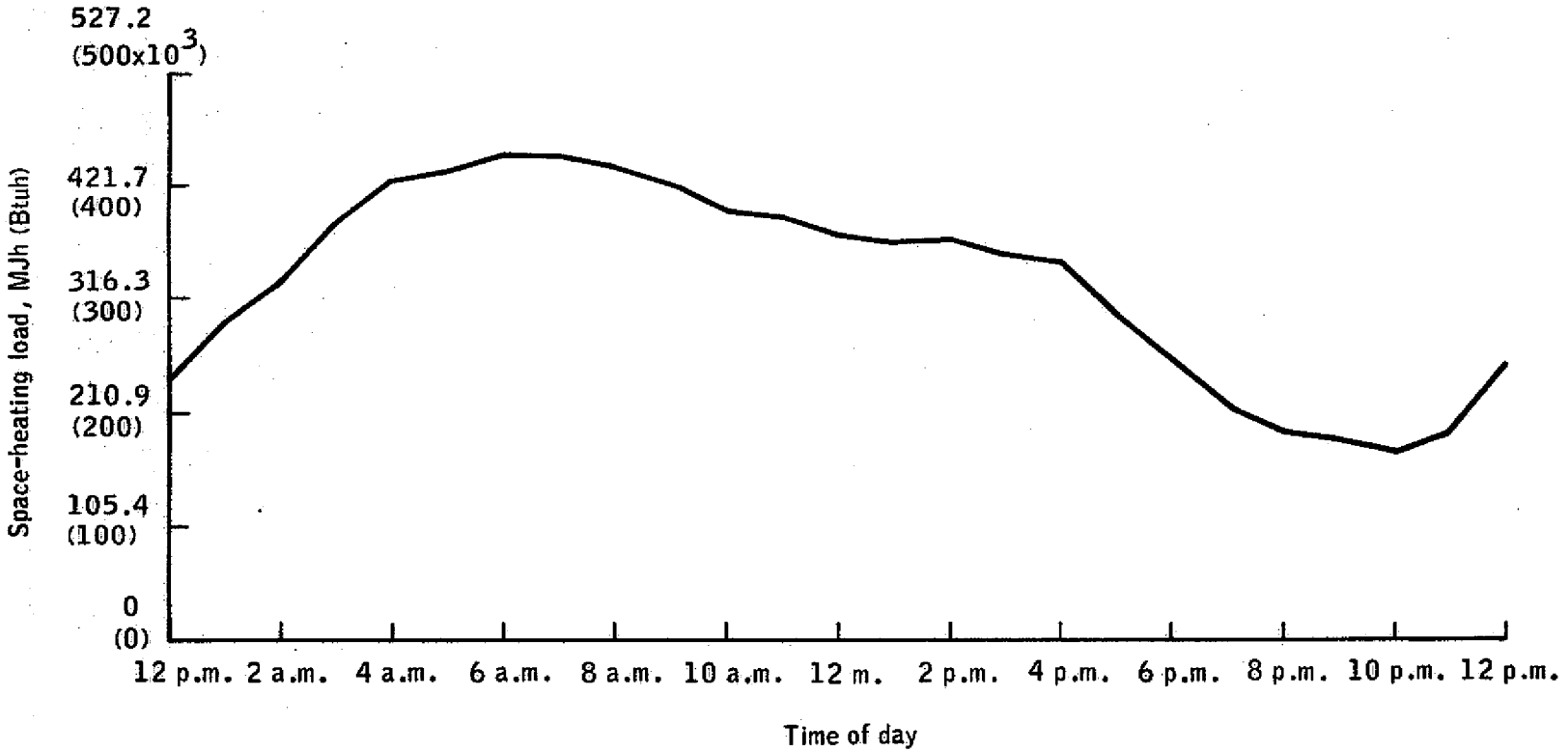

(a) Design winter day.

Figure 41.—MIST space-heating profile.

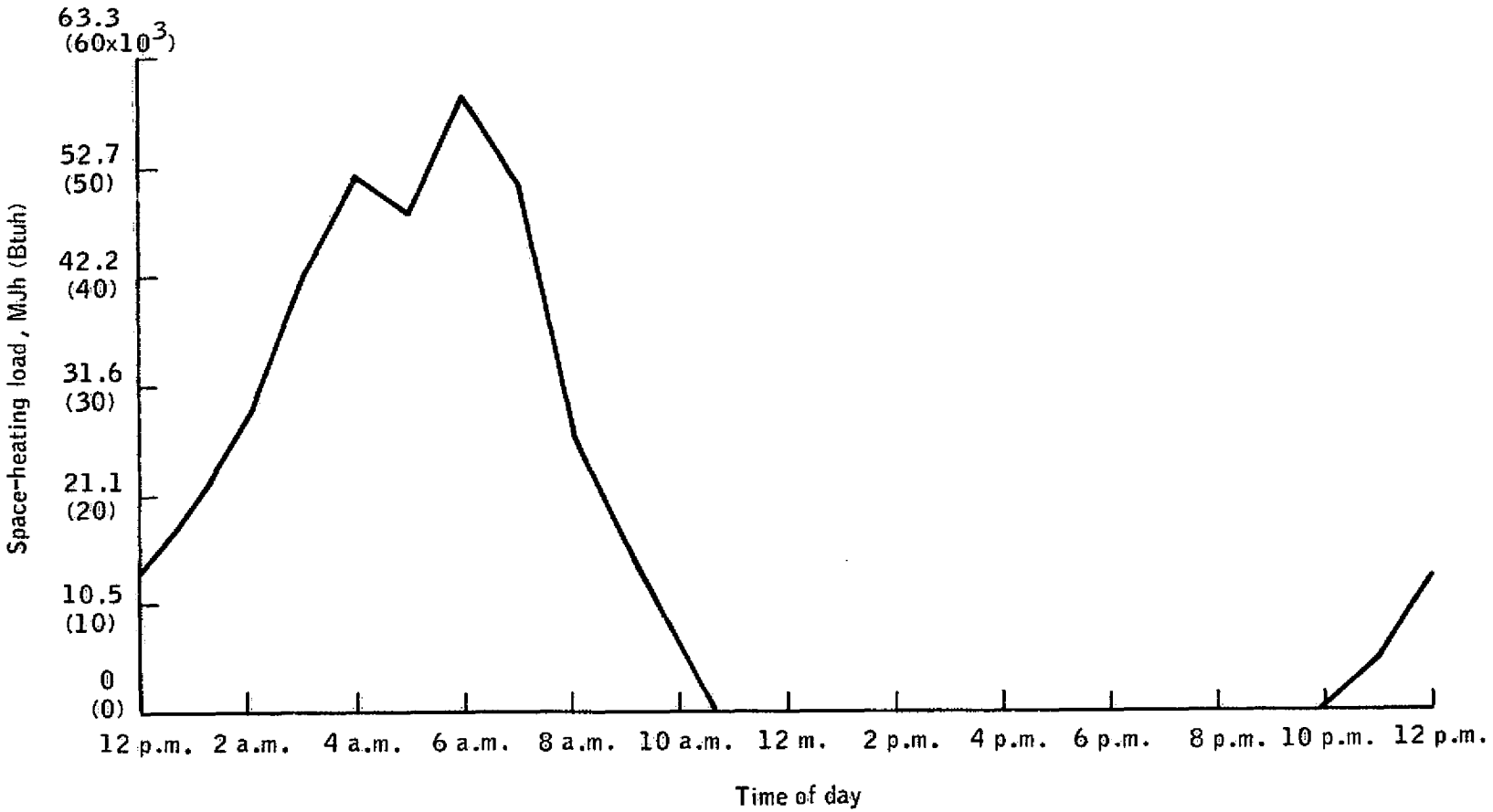

(b) Average spring/fall day.

Figure 41.—Concluded.

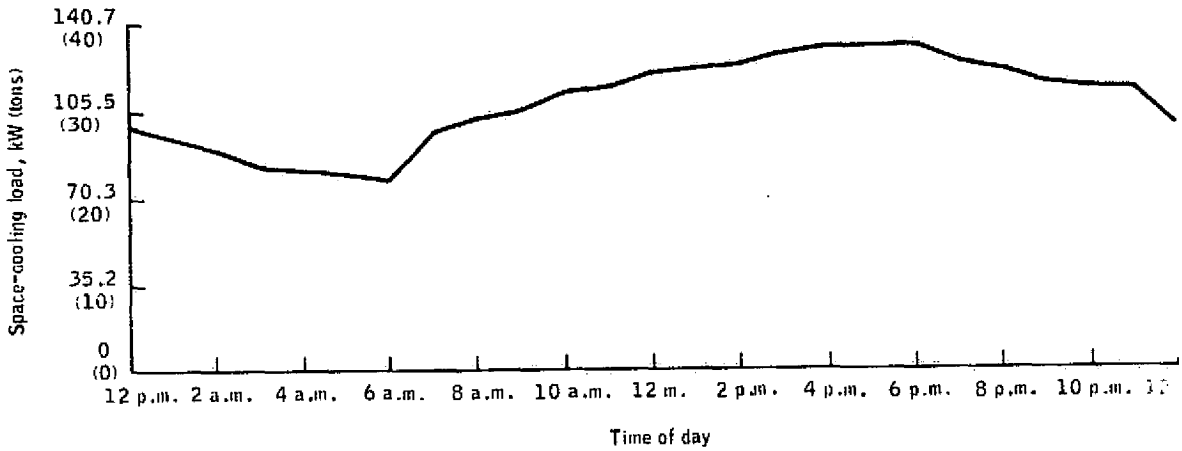

(a) Design summer day.

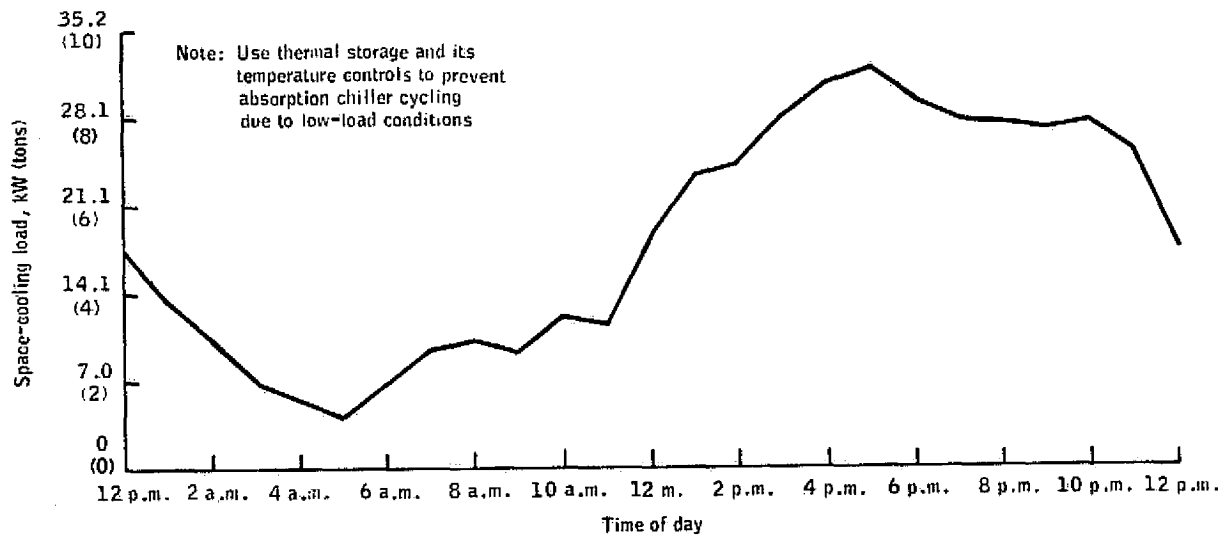

(b) Average spring/fall day.

Figure 42.—MIST space-cooling profile.

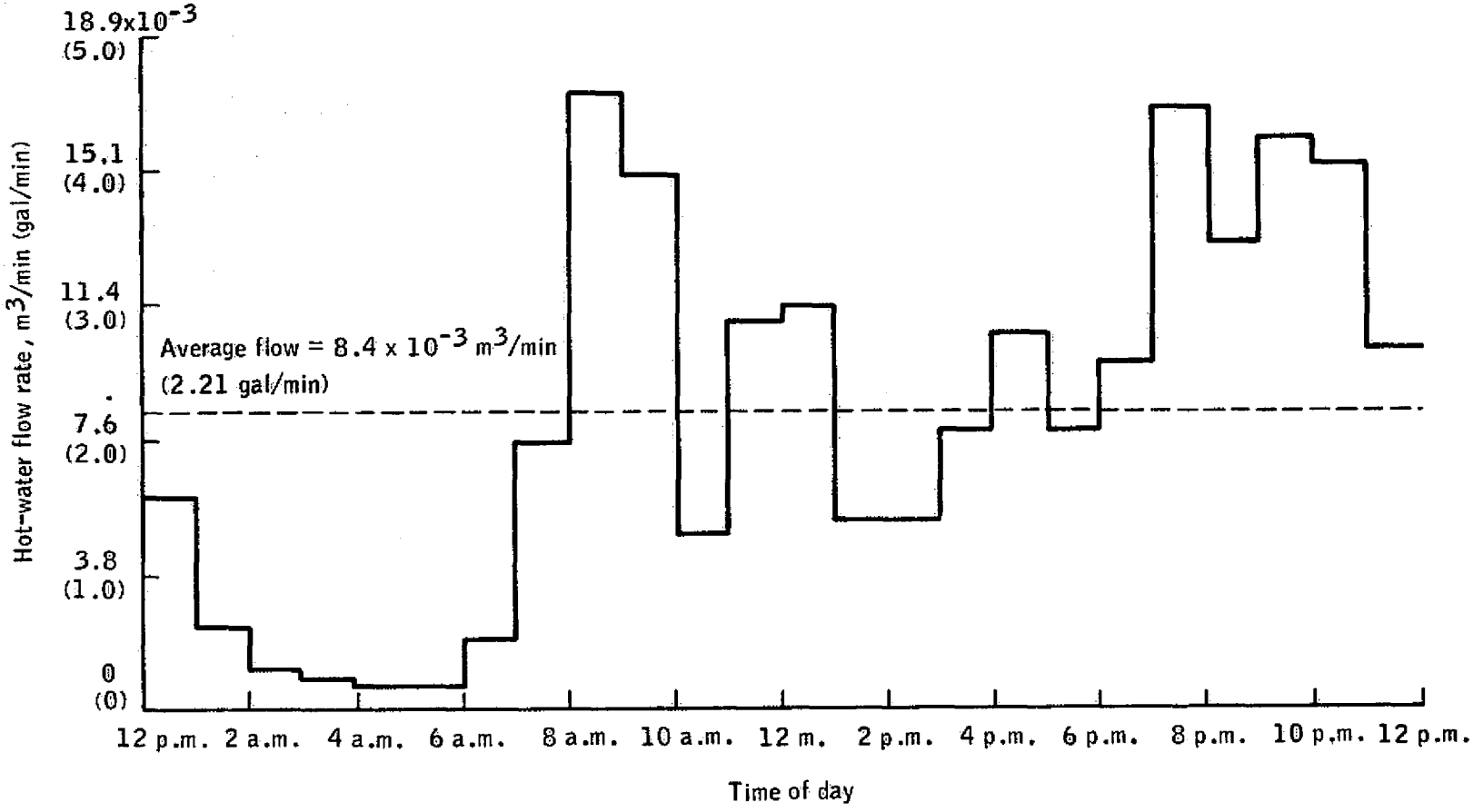

Figure 43.—MIST domestic-hot-water-flow profile.

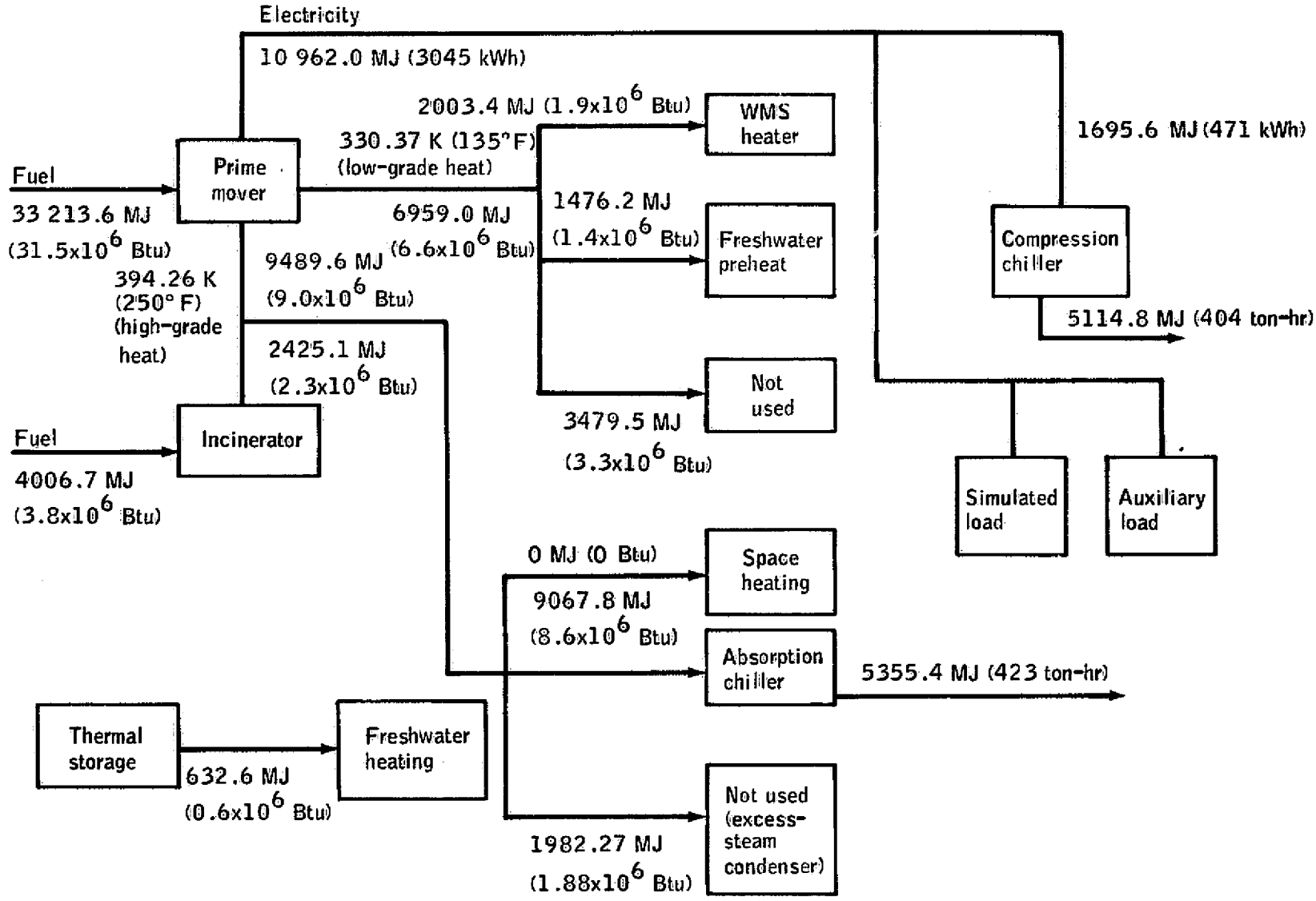

Figure 44.—Test IIA-1: summer design day with thermal storage

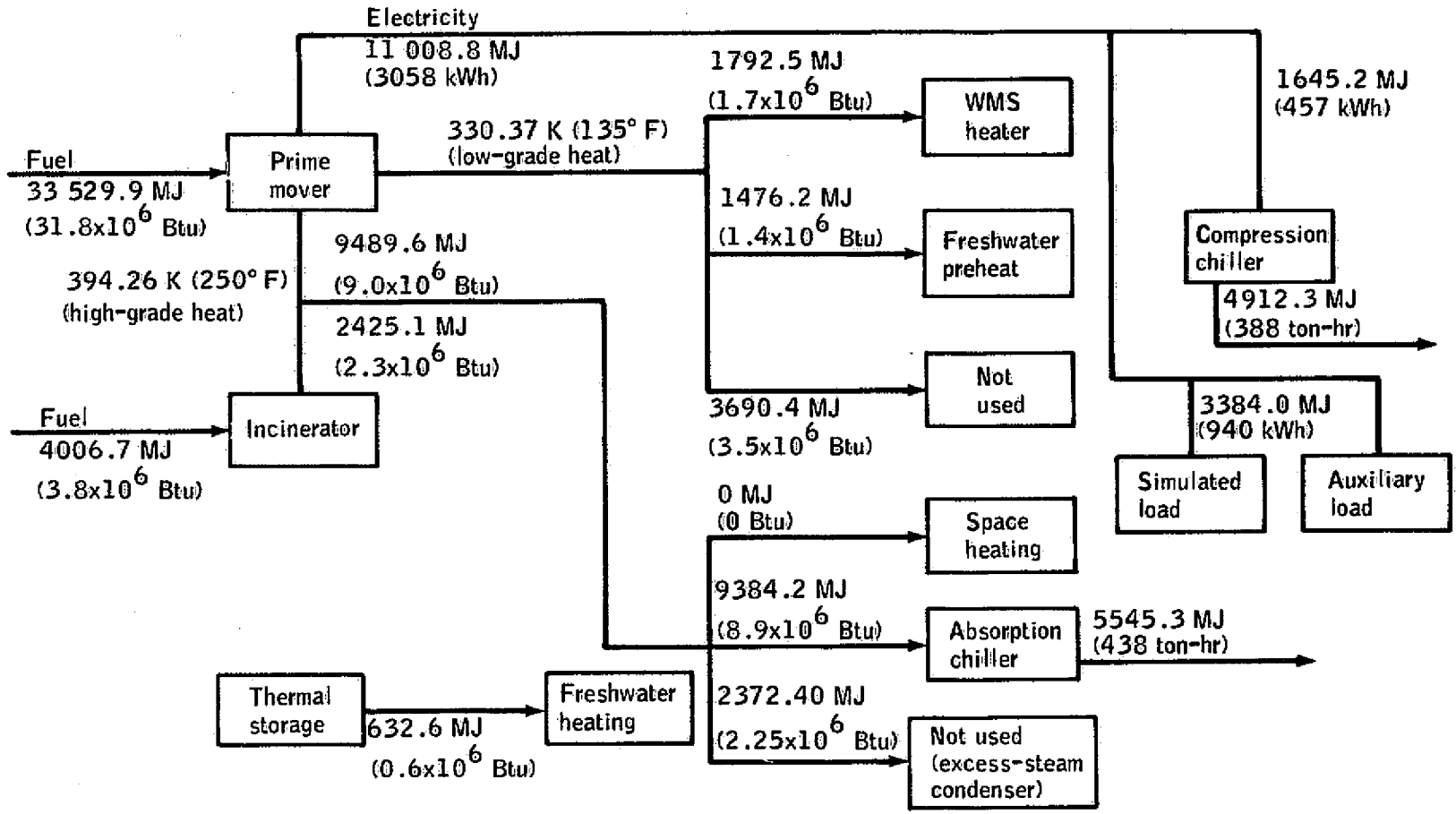

Figure 45.— Test IIA-2: summer design day without thermal storage.

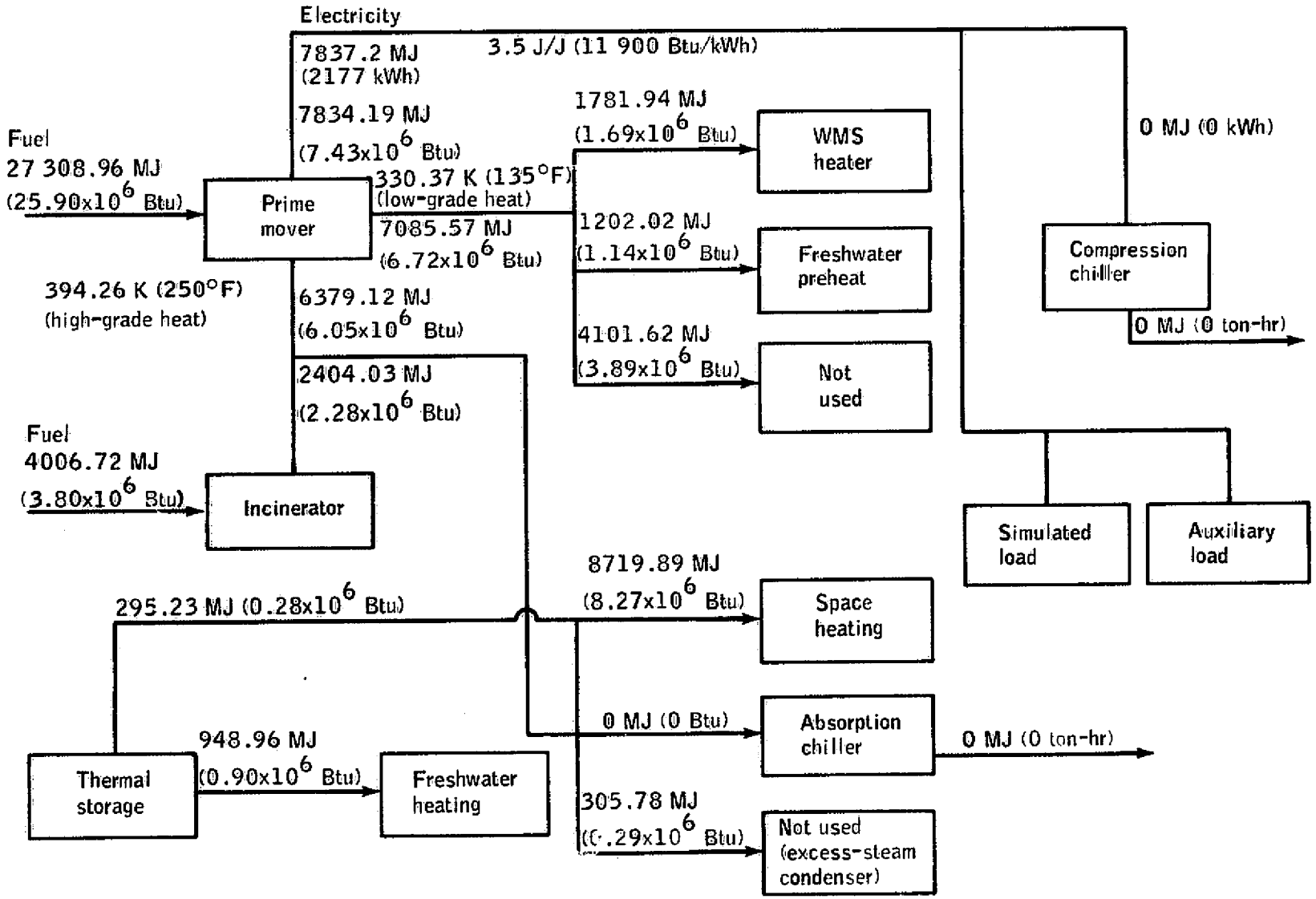

Figure 46.—Test IIB-1: winter design day with thermal storage

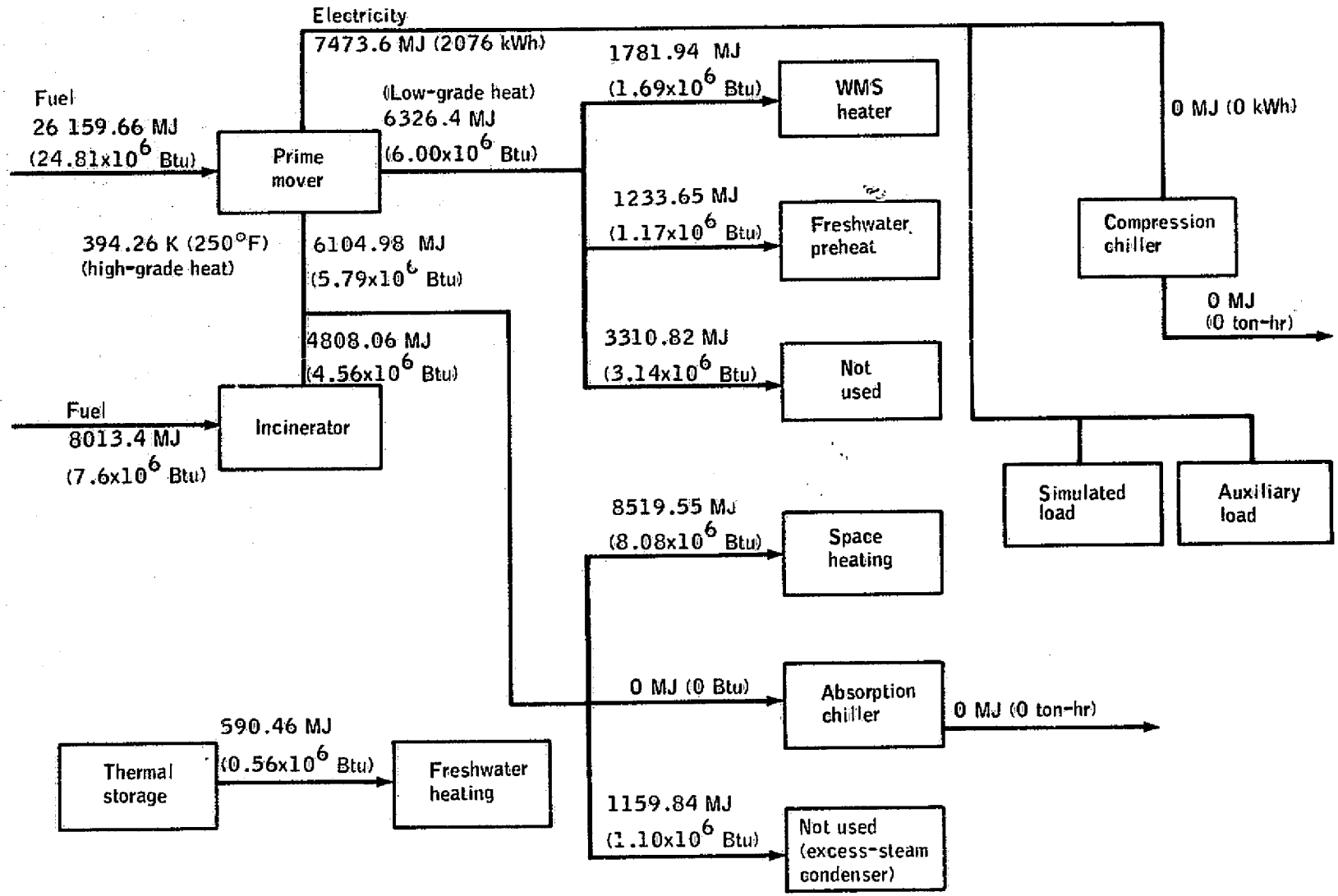

Figure 47.—Test IIB-2: winter design day without thermal storage.

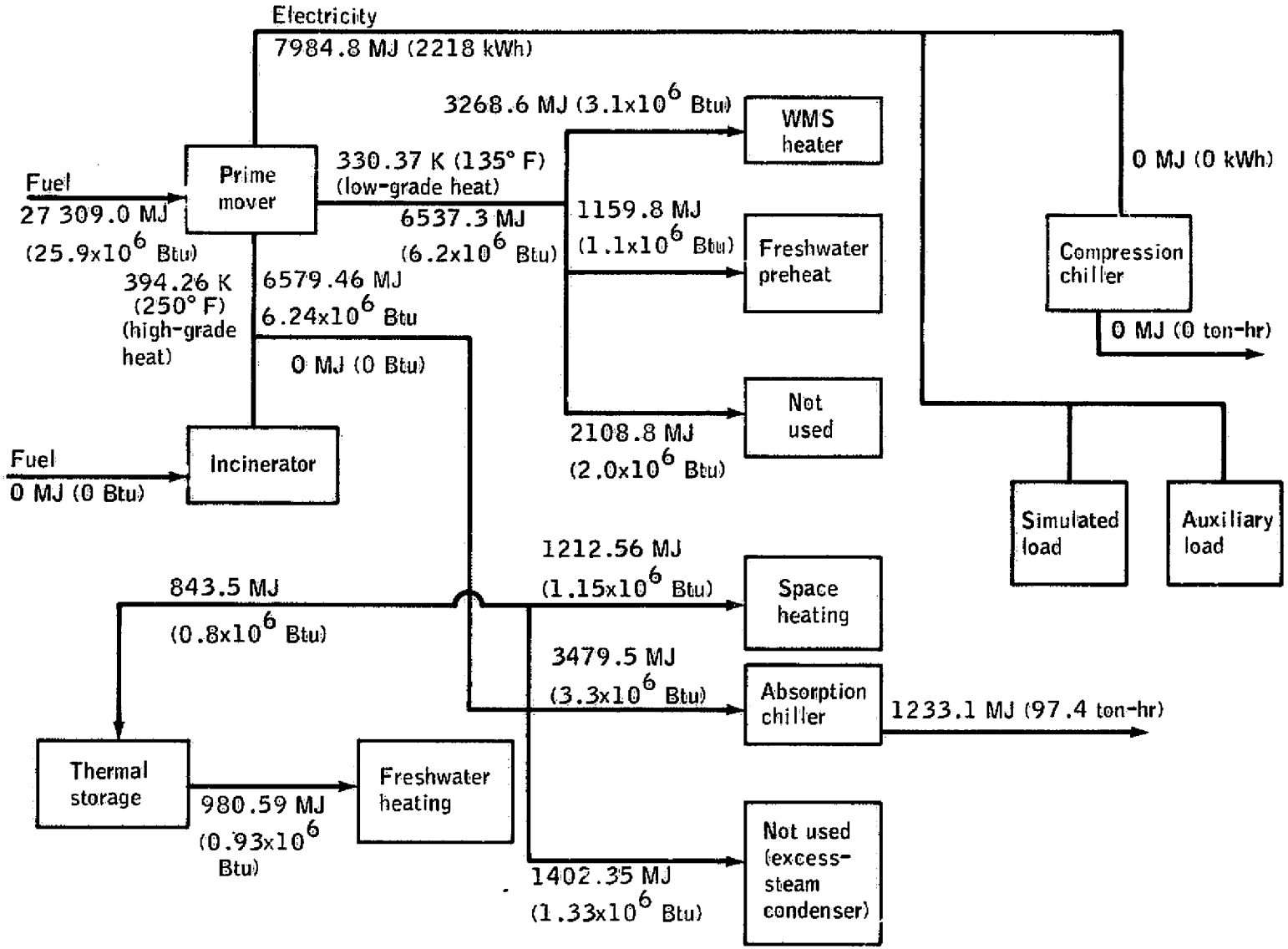

Figure 48 - Test HC-1, spring/fall average day

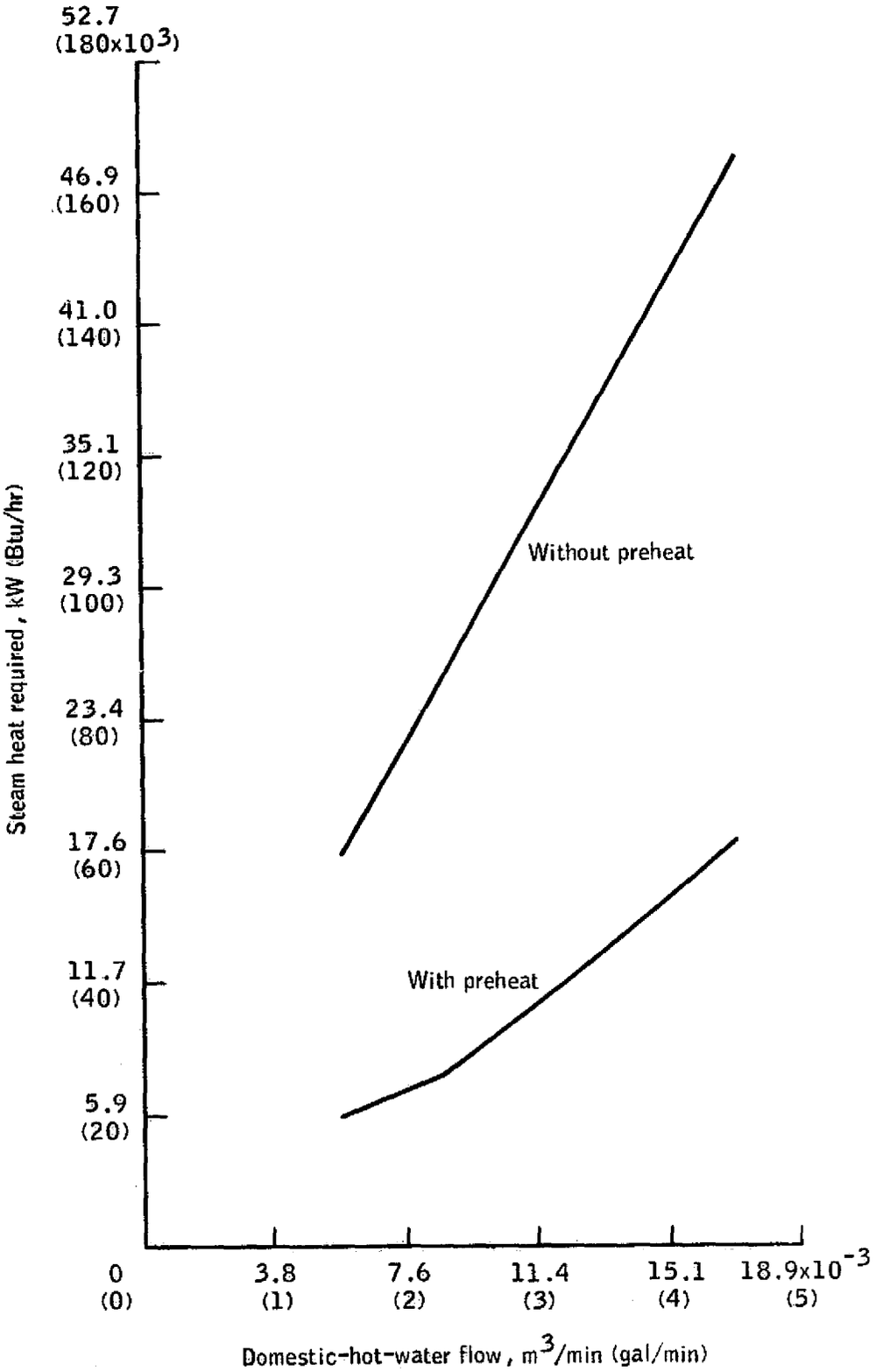

Figure 49.—Domestic-hot-water-heating steam heat required as a function of flow rate.

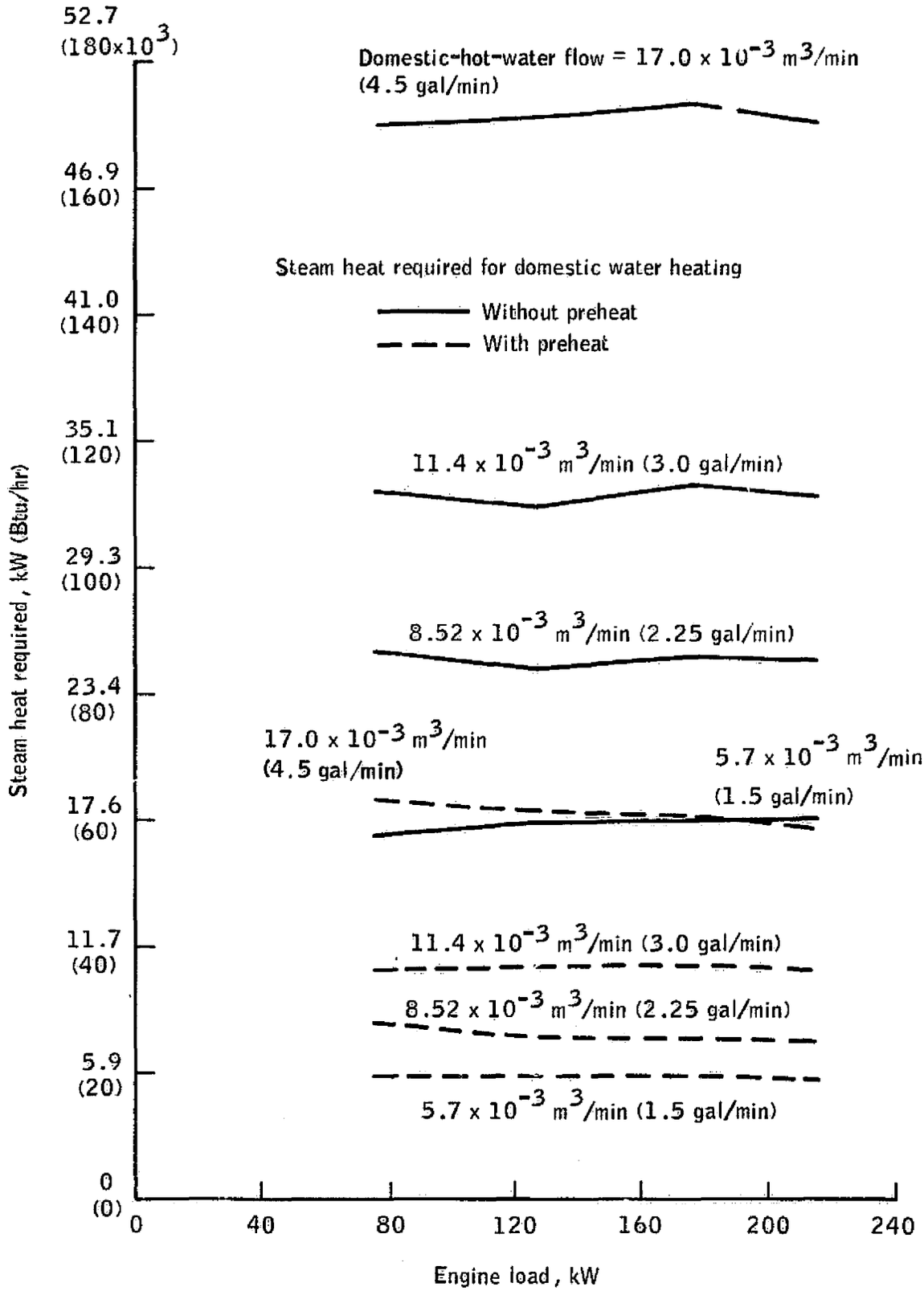

Figure 50.—Domestic-hot-water-heating steam heat required as a function of engine load.

APPENDIX

MIST FACILITY DESCRIPTION

GENERAL SYSTEM

The MIST facility combines all normal utility functions into a single, integrated plant. The objective of the MIST design was to maximize the use of waste products of one functional subsystem to enhance the performance of another subsystem function. This approach tends to minimize both the total input energy requirements and the polluting effluents.

The basic system is composed of four major functional elements: (1) power generation, (2) heating and air-conditioning, (3) wastewater treatment, and (4) solid-waste treatment. These major functional elements are represented in figure A-1, which is a block diagram of the basic relationships involved. Figure A-2 is a simplified schematic of the system. Table A-I contains maximum performance parameters of the system.

LOAD SIMULATORS

The MIST load simulators enable the imposition on the system of any desired utility time/load profile. Climatic conditions independent of the actual existing conditions or seasons can be simulated and compressed test schedules, as well as the investigation of worst-case conditions, are possible at any time. Loads for the wastewater and solid waste managment subsystems are actual waste streams and refuse delivered to these subsubsystems for processing.

POWER LOAD SIMULATOR

The electrical load simulator is an immersion probe device wherein a pair of metal probes is positioned in a tank of water; the load imposed is a direct function of the depth of immersion. The probes are winch driven and are manually positioned. Response time of the drive system is such that, for all practical purposes, an instantaneous load/time profile can be imposed.

COOLING-LOAD SIMULATOR

The cooling-load simulator is an air-to-water heat exchanger with a staged bypass. The MIST provides environmental cooling in the form of chilled water delivered at a temperature of 278.71 to 280.93 K (42° to 46° F). The load imposed on the MIST equipment is the temperature increment ΔT created between the 278.71- to 280.93-K (42° to 46° F) cooling water and the warmer water returning from the load. This ΔT load can be controlled for any desired condition by diverting a portion of the flow around the heat exchanger through the bypass. The bypass valves are pneumatically controlled for rapid, accurate load imposition. The unit can impose loads ranging to a maximum of 175.7 kilowatts (600 000 Btu/hr).

HEATING-LOAD SIMULATOR

The heating-load simulator is a 146.4-kilowatt (500 000 Btu/hr) air-to-water heat exchanger connected and controlled in the same fashion as the cooling-load simulator described in the previous paragraph. The load is measured as a ΔT between the 355.37-K (180° F) supply water and the return from the simulator.

SUBSYSTEMS DESCRIPTION

The major subsystems of the MIST facility are described in the following subsections.

MIST Data Subsystem

The MIST data subsystem provided engineering evaluation data for the integrated test efforts and performed the following functions.

1. Recording of all operational and engineering instrumentation signals on magnetic tape (Each parameter was acquired and recorded in a digital representation of the measured analog value once every 90 seconds (data cycle).)
2. Readout of a single parameter at each data cycle
3. Printout of the digital value of all parameters (The data subsystem selected parameters as they were being acquired and recorded.)

Complete analysis of the data required processing of the computer-compatible-magnetic-tape data. These data were converted to engineering units (temperature in degrees Fahrenheit, pressure in pounds per square inch, etc.) by the standard programs used for NASA Apollo spacecraft data processing. Tabulations, plots, and microfilms of the processed data were provided as outputs.

Power Generation Subsystem

The power generation subsystem (PGS) generates, regulates, and controls electrical power for the simulated and internal loads of the MIST. The PGS consists of a diesel engine-generator set with waste-heat-recovery units on the engine exhaust stack, the engine lubrication oil cooling circuit, and the engine water-jacket cooling circuit. Figure A-3 is a simplified schematic of the PGS showing interfaces to other subsystems. Figure A-4 depicts the power distribution network.

To enable the evaluation of alternate operating modes, the PGS is configured such that it can be cooled in a forced-water-circulation mode or in an ebullient mode. Appropriate heat-recovery units are installed in each of the cooling loops to enable reclamation and use of the thermal energy.

Tables A-II, A-III, and A-IV contain the PGS thermal, mechanical, and electrical parameters, respectively.

Heating, Ventilation, and Air-Conditioning Subsystem

The heating, ventilation, and air-conditioning (HVAC) subsystem provides heating and cooling to the using facility. It has the capability to store and use thermal energy recovered from the power generation subsystem and the incinerator. Figure A-5 is a simplified schematic of the subsystem and its interfaces.

Cooling is provided by means of chilled water produced by an 87.9-kilowatt (25 ton) absorption unit supplied with 103×10^3 pascals (15 psig) and an 82.6-kilowatt (23.5 ton) electric compression reciprocating unit. The baseload is satisfied by the absorption machine; peak demands, by the compression unit. The cooling loop is equipped with a 9.8-cubic-meter (2600 gallon) cold-water storage tank capable of storing 303.7 megajoules (288 000 British thermal units). To evaluate multiple modes of operation, the storage tank output can be switched to either the inlet or the outlet side of the chillers. This capability enables the load on the chillers to be minimized under all operating conditions, and the recovery capacity of the storage tank is expanded. Chilled-water delivery to the simulated cooling load is controlled to 279.82 $\pm$1.1 (44° $\pm$ 2° F). Total cooling capacity of the system is dependent upon available waste energy from the engine and the incinerator, but the simulator is designed to impose loads as great as 175.7 kilowatts (600 000 Btu/hr) on the system.

Steam and/or hot water recovered through the heat exchangers interfacing with the engine and the incinerator is used to satisfy a 146.4-kilowatt (500 000 Btu/hr) space-heating requirement, plus the simulated domestic-hot-water demands of the using facility. In addition, thermal energy is used to enhance the operation of the wastewater treatment plant. The heating circuit contains a hot thermal storage tank of 9.8 cubic meters (2600 gallons), capable of storing 1370.7 megajoules (1 300 000 British thermal units).

The inclusion of thermal storage tanks in the system enables a closer matching of the load-demand profiles imposed on the various subsystems by reducing the energy usage during peak electrical loading for meeting space heating and cooling and thereby reducing the size, the quantity, and the cost of power generation equipment.

A 615-kilowatt (175 ton) capacity wet-cooling tower is provided to meet equipment operating limits and to enable portions of the MIST to be operated independently for flexibility. The blowdown water from the cooling tower is processed in the wastewater management subsystem (WMS) and returned as makeup water.

The performance data for the HVAC subsystem are shown in table A-V.

Wastewater Management Subsystem

The WMS can process as much as 26.5 m^3/day (7000 gal/day) of municipal sewage and subsystems blowdown water. The effluents are purified water and sludge. The sludge is burned with trash in the incinerator. The effluent water is intended to have a quality approaching that of potable water but is to be used only as subsystem makeup water. Figure A-6 is a simplified schematic of the WMS and its interfaces.

Principal elements of the subsystem include a physical-chemical treatment plant, a biological treatment plant, and a reverse-osmosis unit. For test purposes, the units are interconnected so that the waste stream can be processed by an individual unit or by any combination.

The subsystem has heat exchangers interfaced with the thermal loops so that the effects of various controllable temperature levels can be evaluated. The output steam, of essentially potable quality, can be sterilized by chemical and/or thermal means.

Performance parameters for the subsystem are as follows.

1. Potable water — Heat 0.01 m^3/min (2.77 gal/min) to a temperature of 344.26 K (160° F).
2. Wastewater
   a. Treat 18.9 to 26.5 m^3/day (5000 to 7000 gal/day) of sanitary sewage.
   b. Process reclaimed water to potable quality through the reverse-osmosis unit.
   c. Use reclaimed water for subsystems makeup.

Solid Waste Management Subsystem

The solid waste management subsystem consists of an incinerator with its loader equipment, which burns solid waste and sludge. The thermal energy produced is exhausted out the stack through the heat-recovery unit to produce steam. Figure A-7 is a schematic representation of the subsystem and its interfaces.

The loader is a hydraulic ram that injects a premeasured load into the incinerator on command. At full load, 102.5 kilowatts (350 000 Btu/hr) of thermal energy in the form of steam at a pressure of 103×10^3 pascals (15 psig) can be recovered for use in the thermal loop.

The subsystem specification performance is summarized as follows.

1. Solid waste
   a. Refuse — 136.1 kg/day (300 lb/day) of type 2 trash
   b. Sludge — 56.7 kg/day (125 lb/day) of 20-percent solid sewerage sludge
2. Burn rate
   a. Design point — 31.8 kg/hr (70 lb/hr)
   b. Maximum — 45.4 kg/hr (100 lb/hr)

TABLE A-I.—Maximum Performance Parameters

Power generation, kW	230
Heating, kW (Btu/hr)	146.4 (500 000)
Air-conditioning, kW (tons)	175.8 (50)
Water processing, m^3/day (gal/day)	26.5 (7 000)
Solid-waste disposal, kg/hr (lb/hr)	31.8 (70)

TABLE A-II.—Power Generation Subsystem Thermal Properties

Circuit	*Energy form*	*Max. energy recovery, kW (Btu/hr)*	*Max. temperature, K (°F)*
Forced-circulation cooling			
Oil aftercooler	Water	63.3 (216 000)	327.59 (130)
Exhaust	Steam (103 kPa (15 psig))	135.0 (461 000)	394.26 (250)
Jacket	Water	163.4 (558 000)	[a]355.37 (180) [a]377.59 (220)
Ebullient cooling			
Oil aftercooler	Water	63.3 (216 000)	327.59 (130)
Exhaust/jacket	Steam (103 kPa (15 psig))	351.4 (1 200 000)	394.26 (250)

[a]Two set points are selectable for engine operation.

TABLE A-III.—Power Generation Subsystem Mechanical Properties

Engine stack exhaust	
Flow, m^3/min (ft^3/min)	0 to 67.4 (0 to 2380)
Pressure, Pa (in. H_2O)	4976.8 (20)
Temperature, K (°F)	505.37 to 713.71 (450 to 825)
Exhaust silencer	
Flow, kg/hr (lb/hr)	86.2 to 294.8 (190 to 650)
Pressure, kPa (psig)	103 to 124 (15 to 18)
Temperature, K (°F)	394.26 (250)
Jacket water	
Flow, m^3/min (gal/min)	0.6 (160)
Pressure, kPa (psig)	138 (20)
Temperature, K (°F)	355.37 to 388.71 (180 to 240)
Oil interchanger	
Flow, m^3/min (gal/min)	0.3 (80)
Pressure, kPa (psig)	276 (40)
Temperature, K (°F)	330.37 (135)
Fuel intake	
Flow, m^3/min (gal/min)	0.015 to 0.068 (4 to 18)
Pressure, kPa (psig)	6.9 to 13.8 (1 to 2)
Temperature	Ambient

TABLE A-IV.—Power Generation Subsystem Electrical Parameters

Peak demand, kW	230
Voltage, V ac (three phase)	480
Frequency, Hz	60
Power factor, min	0.8
Voltage regulation, percent	±1
Frequency regulation, percent	+0.5

TABLE A-V.—Heating, Ventilation, and Air-Conditioning Subsystem Thermal Parameters

Cooling	
Absorption (variable), kW (tons)	35.2 to 87.9 (10 to 25)
Compression (variable), kW (tons)	17.6 to 82.6 (5 to 23.5)
Storage in 9.8-m^3 (2600 gal) water tank at 279.82 K (44° F), MJ (Btu)	303.7 (288 000)
Heating	
Space, kW (Btu/hr)	0 to 146.4 (0 to 500 000)
Freshwater from 283.15 to 344.26 K (50° to 160° F), m^3/min (gal/min)	0.010 (2.77)
Wastewater from 283.15 to 310.93 K (50° to 100° F), m^3/min (gal/min)	0.018 (4.86)
Sterilization, K (°F)	≤373.15 (≤212)
Storage in 9.8-m^3 (2600 gal) water tank at 383.15 K (230° F), MJ (Btu)	1370.7 (1.3×10^6)

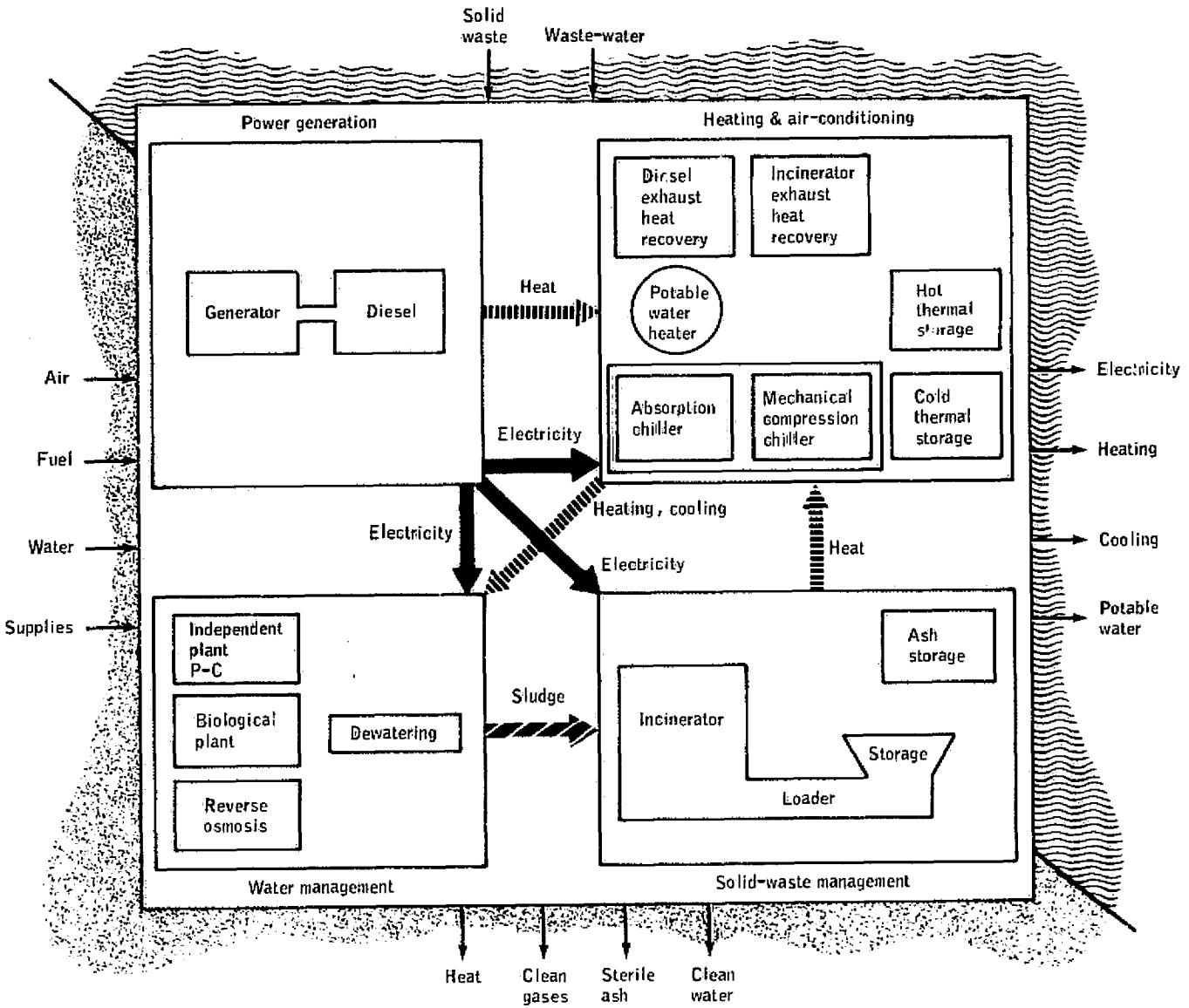

Figure A-1.—Baseline MIST system.

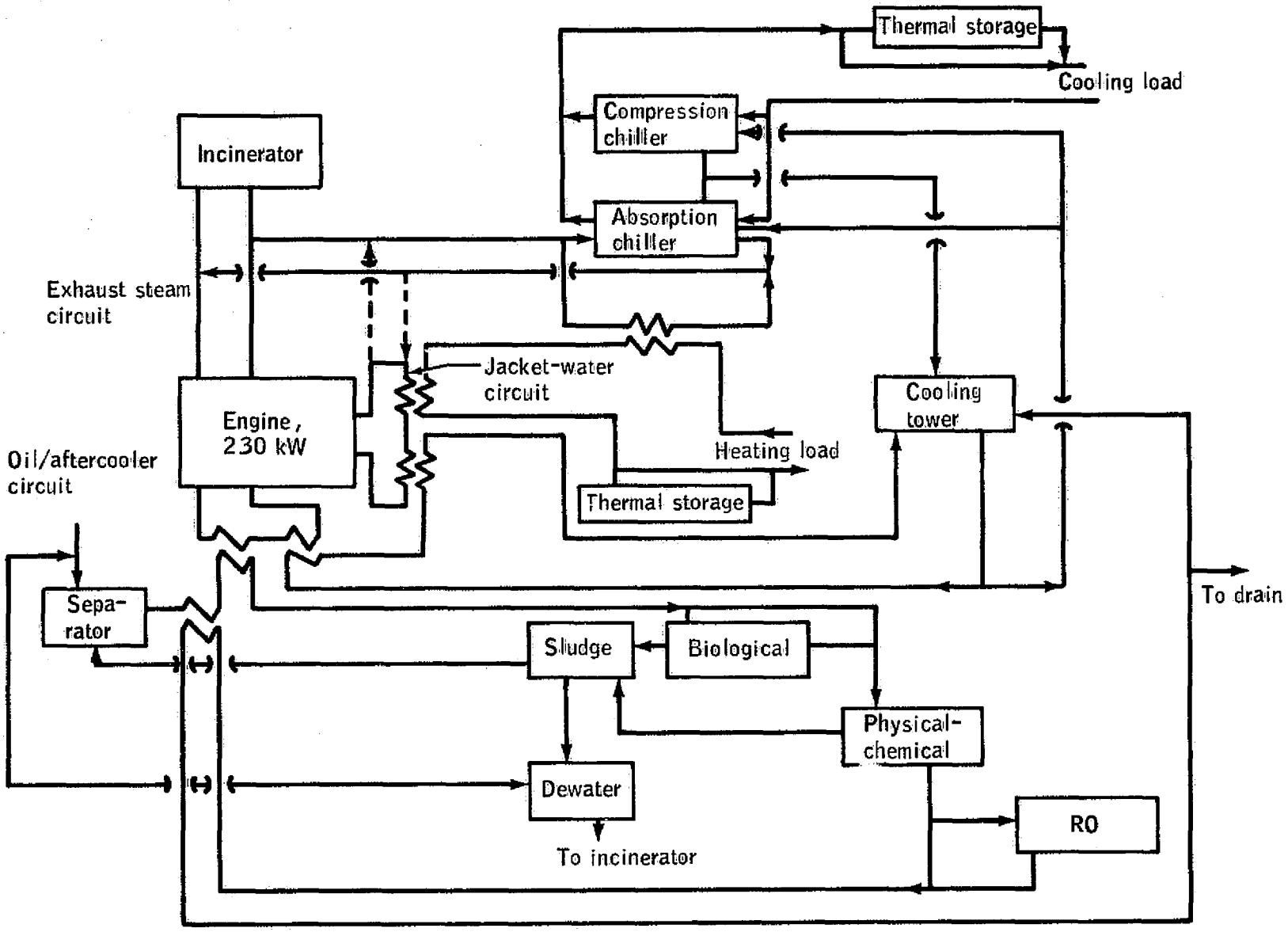

Figure A-2.—MIST system schematic.

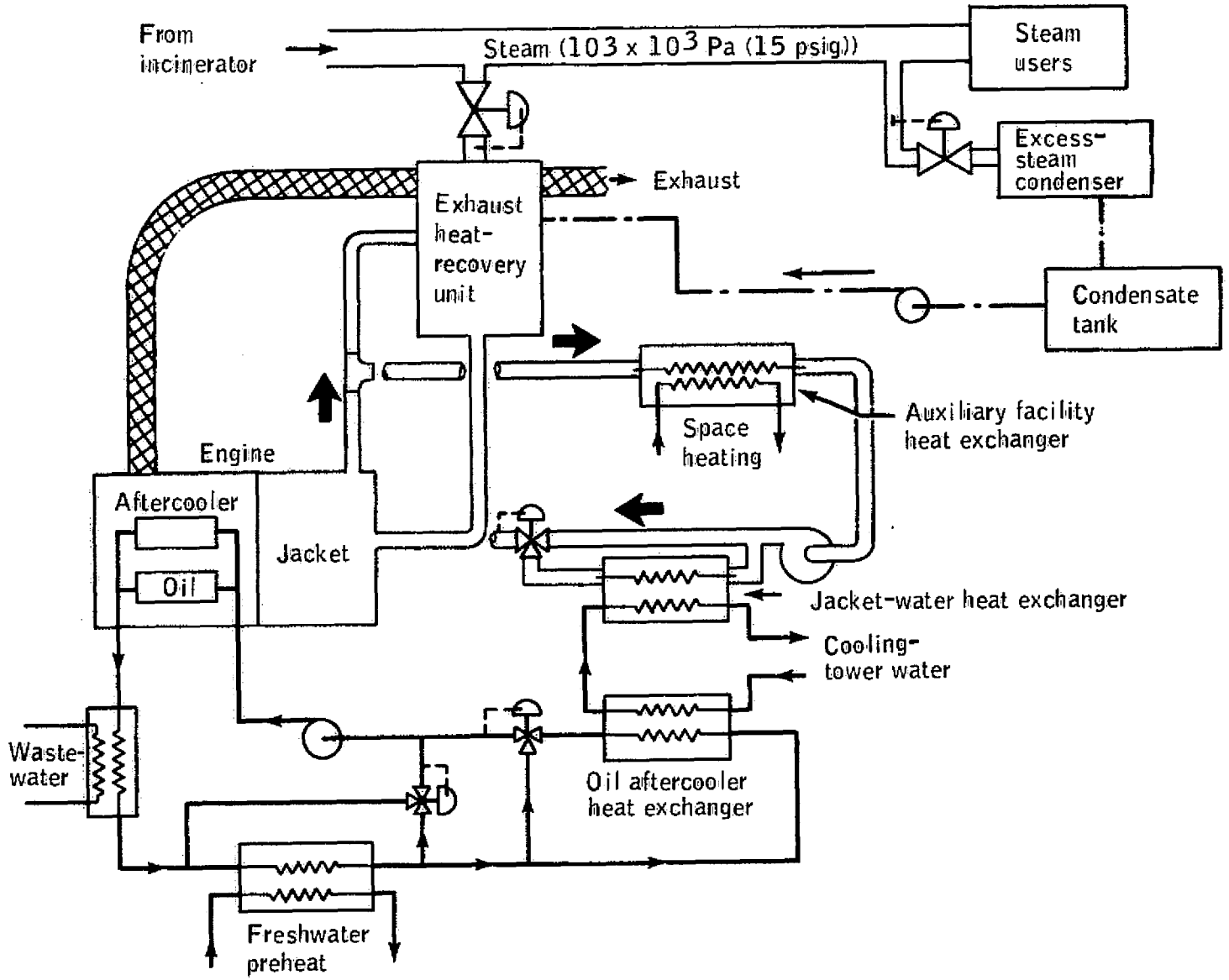

Figure A-3.—Thermal interface.

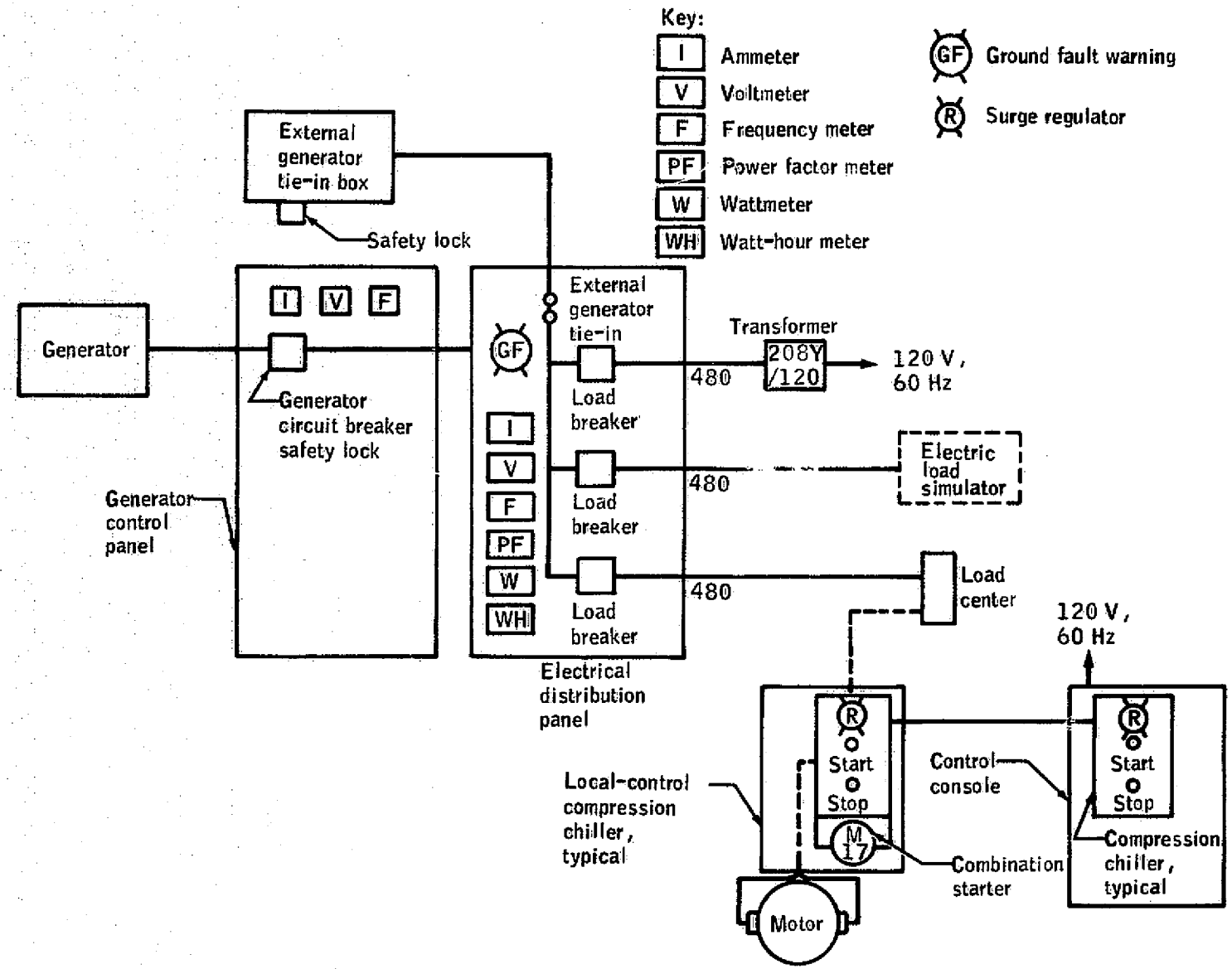

Figure A-4.—Electrical block diagram.

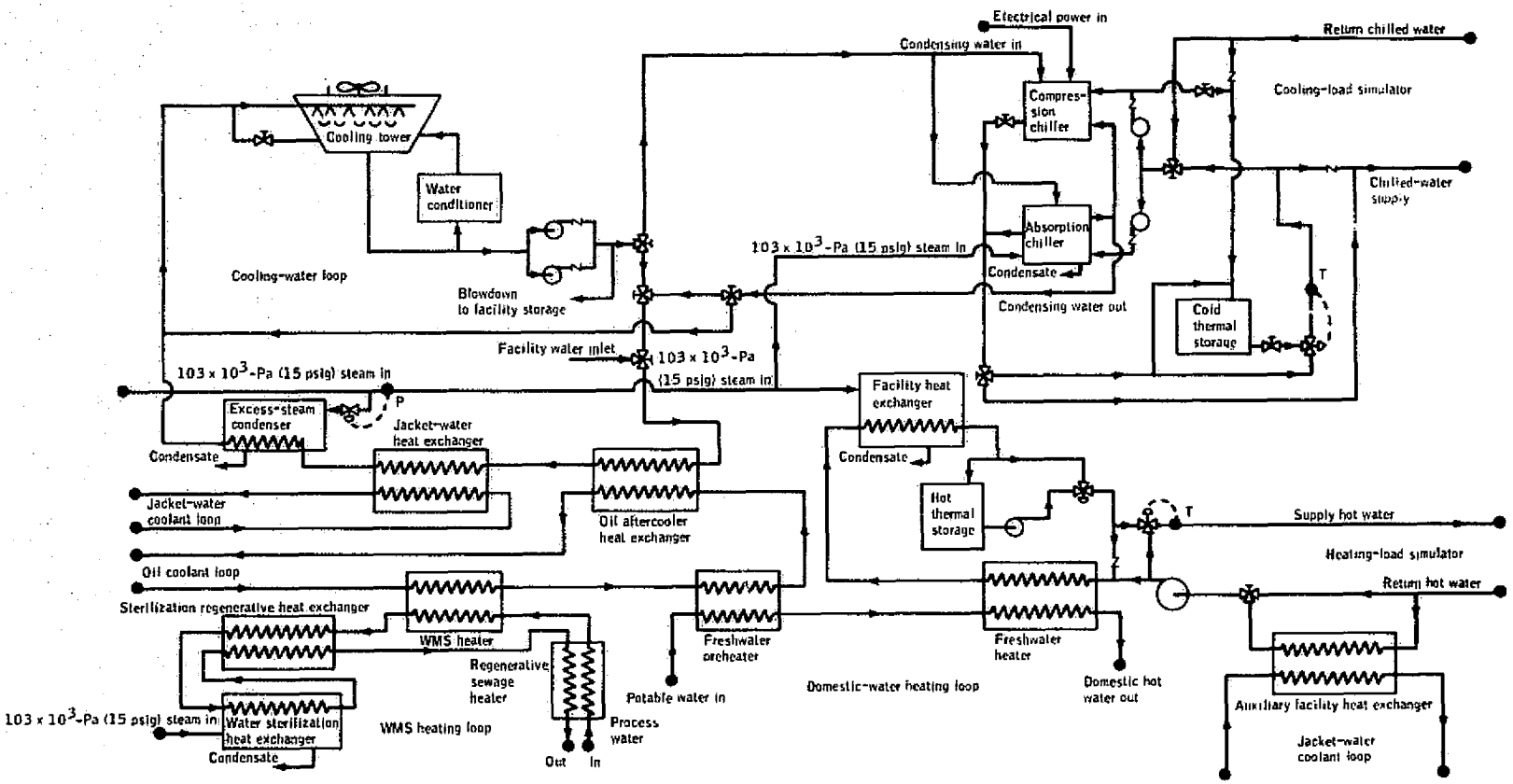

Figure A-5.—MIST heating and cooling subsystem.

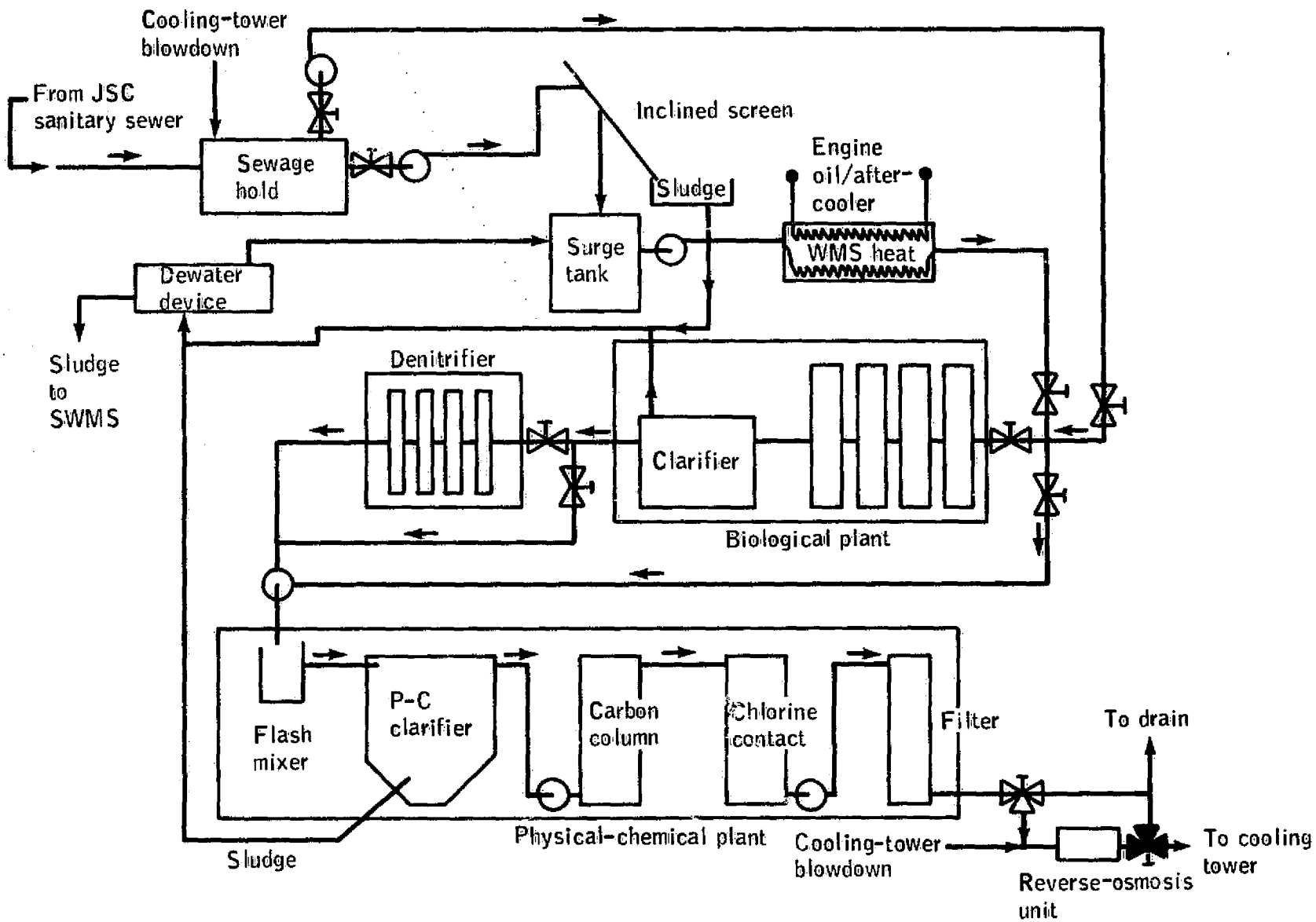

Figure A-6.—MIST wastewater management system.

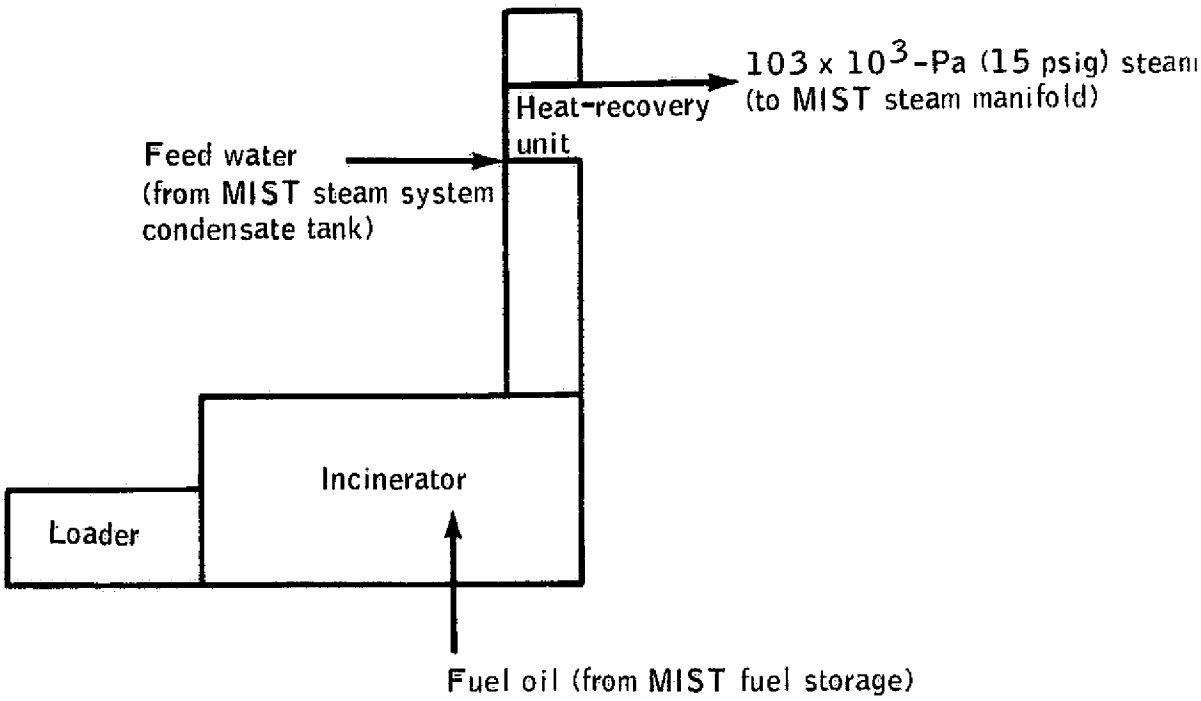

Figure A-7.—Solid-waste-interface schematic.